Novelty detection and context dependent processing of sky-compass cues in the brain of the desert locust *Schistocerca gregaria*

Novelty detection und die kontextabhängige Verarbeitung von Himmelskompasssignalen im Gehirn der Wüstenheuschrecke *Schistocerca gregaria*

D I S S E R T A T I O N

zur
Erlangung des Doktorgrades
der Naturwissenschaften
(Dr. rer. nat.)

---

dem Fachbereich Biologie
der Philipps-Universität Marburg
vorgelegt von

Tobias Bockhorst
aus Oldenburg (Oldb)

Marburg (Lahn) 2015

Vom Fachbereich Biologie der Philipps-Universität Marburg

als Dissertation am _____ angenommen.

Erstgutachter: Prof. Dr. Uwe Homberg

Zweitgutachter: Prof. Dr. Frank Bremmer

Tag der mündlichen Prüfung: 23.06.2015

CONTENTS ▪ INHALT

E R K L Ä R U N G

EIGENE BEITRÄGE UND VERÖFFENTLICHTE TEILE DER ARBEIT

Entsprechend §9 (1) der Promotionsordnung der Philipps-Universität Marburg in der Fassung vom 29.04.2009 werden im Folgenden die Anteile des Doktoranden an den einzelnen Teilleistungen der Dissertation (Kapitel 1-3) sowie an ihren allgemeinen Grundlagen detailliert dargelegt:

Kapitel I

- Formulierung der Fragestellung, d.h. Identifikation bisher nicht oder nicht detailliert untersuchter Merkmale von Antworten der Zentralkomplexneurone auf polarisiertes Licht
- Konzeption und Durchführung sämtlicher Experimente; jeweils ein Experiment (von 45) unter Beteiligung von Johannes Schuh und Jerome Beetz bzw. von Milosz Krala und Stefan Ries im Rahmen von Fachmodulen im Master-Studiengang
- Konzeption, Durchführung und Interpretation sämtlicher Auswertungen (histologische Aufbereitung von Präparaten und Auswertung von Fluoreszenzmarkierungen zur Identifikation der abgeleiteten Zellen erfolgten nach bereits etablierten Protokollen)
- hierbei insbesondere Entwicklung eines neuen Konzepts zur Auswertung von Antworten auf polarisiertes Licht, welches erstmals die Unterscheidung zwischen dem prinzipiellen Auftreten einer Antwort (Korrelation zwischen neuronaler Aktivität und Polarisationsebene) und der Stärke der Antwort (Modulationstiefe) erlaubt
- Erstellen sämtlicher Abbildungen, wobei die Abbildungen 1, 10*A*, 11*A* und 12*A* (z.T.) aus Teilabbildungen hervorgingen, welche von Dritten bereitgestellt wurden (s.a. Reproduktion in Abb. A6 im Anhang)
- Anfertigung des Manuskriptes in Zusammenarbeit (Korrektur) mit dem betreuenden Gutachter Prof. Dr. Uwe Homberg
- dieses Kapitel wurde wie vorliegend (von kleinen sprachlichen Änderungen abgesehen) im Journal of Neurophysiology publiziert (Bockhorst T and Homberg U. Amplitude and dynamics of polarization-plane signaling in the central complex of the locust brain. *J Neurophysiol*: in press, doi: 10.1152/jn.00742.2014.)

Kapitel II

- explorative Eingrenzung der Fragestellung (Vorgabe: Untersuchung der Antworten polarisations-empfindlicher Neurone auf objektähnliche Muster aus unpolarisiertem Licht)
- Konzeption und Durchführung sämtlicher Experimente; ein Experiment (von 14) unter Beteiligung von Milosz Krala und Stefan Ries im Rahmen eines Fachmoduls im Master-Studiengang
- Konzeption, Durchführung und Interpretation sämtlicher Auswertungen (histologische Aufbereitung von Präparaten und Auswertung von Fluoreszenzmarkierungen zur Identifikation der abgeleiteten Zellen erfolgten nach bereits etablierten Protokollen)
- Erstellen sämtlicher Abbildungen, wobei Abbildung 1 aus Teilabbildungen besteht, welche von Dritten bereitgestellt wurden (siehe Abbildungslegenden)
- Anfertigung des Manuskriptes in Zusammenarbeit (Korrektur) mit dem betreuenden Gutachter Prof. Dr. Uwe Homberg
- dieses Kapitel wurde wie vorliegend nach einer presubmission inquiry beim Online-Journal *PLOS Biology* eingereicht (Bockhorst T Homberg U (2015) Head-direction cells in the brain of an insect are sensitive to novel events in the visual world.)

Kapitel III

- Konzeption und Durchführung sämtlicher Experimente
- Konzeption, Durchführung und Interpretation sämtlicher Auswertungen (histologische Aufbereitung von Präparaten und Auswertung von Fluoreszenzmarkierungen zur Identifikation der abgeleiteten Zellen erfolgten nach bereits etablierten Protokollen)
- Erstellen sämtlicher Abbildungen, wobei die Abbildungen 1*A* und 2*A* aus Teilabbildungen hervorgingen, welche von Dritten bereitgestellt wurden (siehe Abbildungslegenden)
- Anfertigung des Manuskriptes in Zusammenarbeit (Korrektur) mit dem betreuenden Gutachter Prof. Dr. Uwe Homberg
- dieses Kapitel wurde zur Einreichung bei einem Fachjournal vorbereitet

Anteil an kapitelübergreifenden Beiträgen

Alle hier eingeflossenen Experimente wurden an einem Messstand durchgeführt, welchen der Autor in Teilen entworfen, in Zusammenarbeit mit den Technischen Werkstätten des Fachbereiches gefertigt und eigenständig optimiert bzw. kalibriert hat (s. Anhang).
Ein erheblicher methodologischer Anspruch der vorliegenden Arbeit lag in der Erstellung eines Software-Paketes (bestehend aus MATLAB-Skripten und -Funktionen) für die Steuerung, Dokumentation und Auswertung der Experimente. Auf Beiträge Dritter wurde hierbei nur in geringem Ausmaß zurückgegriffen; der Autor möchte diese im Folgenden genauer benennen. Als Orientierungshilfe für erste Schritte in der Programmierung des Stimulators ´ViSaGe´, waren Einblicke in Skripte von Dr. Stanley Heinze hilfreich. Eine für extrazelluläre Ableitungen und niedriges Signal-Rausch-Verhältnis entwickelte MATLAB-Funktion zur Bestimmung von Aktionspotential-Zeitpunkten wurde für den Autor im Rahmen seiner Diplomarbeit freundlicherweise von Dr. Naoya Itatani (Universität Oldenburg) erstellt. Der Autor hat diese zur Erstellung einer für die hier erhobenen Daten geeigneten Variante herangezogen und eine graphische Benutzeroberfläche hinzugefügt. Für ´raster plots´ (Kapitel I, Teilabbildungen 10*C* sowie 11*C*; Kapitel II, Teilabbildungen 3*D*,*D‘*,*D‘‘*, *D‘‘‘* und 5*A‘‘*,*B* sowie 6*A* und Abbildung 7; Kapitel III, Abbildung S1; Anhang Abb. A6*C*,*D*) wurde eine MATLAB-Funktion verwendet, welche auf www.mathworks.com zur freien Nutzung bereitgestellt ist (rasterplot.m, Rajiv Narayan, Boston University). Zur Erstellung von inter-spike-interval Histogrammen (Kapitel II, Teilabbildungen 3B,B‘,B‘‘,B‘‘‘; Anhang, Abb. A1*C*), spike-count Verteilungen (Kapitel II, Teilabbildungen 3*B*,*B‘*,*B‘‘*,*B‘‘‘*) und Auftragungen von spike-counts gegen den Beobachtungsindex (Kapitel I, Teilabbildungen 10*B* sowie 11*B;* Anhang, Abb. A1*C* und A6*B*) hat der Autor Quelltext von Funktionen verwendet, die von Prof. Dr. Sonja Grün (Research Center Jülich, RWTH Aachen University) im Rahmen einer Fortbildung (NWG-Kurs ´Analysis and Models in Neurophysiology‘, 16.-21.10.2011, Bernstein Center Freiburg) bereitgestellt wurden.

Für die Richtigkeit obenstehender Erklärung:

_____	_____
Prof. Dr. Uwe Homberg	Tobias Bockhorst

ZUSAMMENFASSUNG

VORWORT

NERVENSYSTEME erleichtern es Tieren, mit ihrer Umgebung in gezielte Interaktion zu treten – basierend auf Sinneswahrnehmung, Kognition und höherer motorischer Kontrolle. Durch zielgerichtetes Verhalten versucht das Tier hierbei, Vorteile zu erlangen und Nachteile zu vermeiden. So kann etwa die Wüstenheuschrecke davon profitieren, ihre Wanderflüge zur Suche nach neuen Habitaten kurz halten zu können, um körperliche Ressourcen zu schonen und das Risiko des Verhungerns oder Todes durch Feindfraß im Flug zu verringern. Dieser Anforderung ‚effizienter' Bewegung durch den Raum lässt sich besser entsprechen, wenn eine ausgeprägte Fähigkeit zur räumlichen Orientierung gegeben ist. Dasselbe gilt für so simple Herausforderungen aus dem Alltag des Menschen wie die Zurücklegung eines Arbeitsweges und für solch außerordentliche Phänomene wie die Futtersuche von Honigbienen oder die saisonalen Wanderflüge des Monarchfalters. Hierbei lassen sich diese Verhaltensleistungen hinsichtlich der überbrückten Distanzen und der zur Orientierung genutzten ´Hinweise´ klassifizieren. Lokal können visuelle **Landmarken**, d.h. Objekte an stabilen Positionen, einem Orts- oder Wegegedächtnis dienen, indem sie beispielsweise einen direkten Weg zu einer entfernten oder schlecht sichtbaren Futterquelle basierend auf einer *´egozentrischen´ Orientierung* relativ zu den Landmarken vermitteln. **Kompasssignale** können hingegen eine *´allothetische´ Orientierung* in einem globalen Bezugssystem vermitteln und somit eine anhaltende Bewegung in gleichbleibender Richtung ermöglichen – sei diese Richtung zum Zwecke der Flucht quasi beliebig oder bei Wanderungsflügen gezielt gewählt. Während räumliche Orientierung eine Voraussetzung derartiger ´geplanter´ Aktionen ist, hängt das Überleben eines Tieres gleichermaßen von der Fähigkeit ab, angemessen auf das Ungeplante, ja Unerwartete zu reagieren – etwa das Auftauchen eines Fressfeindes oder eine unverhoffte Paarungsgelegenheit. Dies setzt die Fähigkeit zur **novelty detection** voraus, d.h. zum Erkennen von Ereignissen, die auf der Grundlage vorherigen Geschehens nicht vorhersehbar waren und in diesem Sinne ´neu´ (engl. novel) sind. Allerdings ist hierbei die Definition von ´Neuheit´ auch an Wichtigkeit gebunden, also kontextabhängig: je nach Situation und Absichten des Tieres mögen manche Veränderungen unwichtig erscheinen und ignoriert werden.

Die vorliegende Dissertation beschreibt neuronale Repräsentationen von Kompassrichtungen sowie Korrelate von novelty detection und Interaktionen zwischen beiden im Gehirn eines Insekts, der Wüstenheuschrecke *Schistocerca gregaria*. Aus praktischen Gründen wurden sämtliche Experimente in immobilisierten, flügel- und beinlosen Männchen durchgeführt. Diese befanden

sich in der ´gregären´, d.h. vergemeinschafteten, in hoher Populationsdichte auftretender Phase, in welcher sie in Nordafrika und dem mittleren Osten Schwärme bilden (siehe Phasentheorie, Uvarov 1966). Die Aktivität einzelner Neurone im Hirn wurde elektrophysiologisch gemessen, während dem Tier der verwendete Kompassreiz (Kapitel I), bzw. Ereignisse in der visuellen Szenerie (Kapitel II) oder Kombinationen beider Reiztypen (Kapitel III) gezeigt wurden. Anschließend wurde die jeweilige Zelle durch Injektion eines Tracers markiert, so dass nach Kopplung an einen Fluoreszenzfarbstoff die Morphologie der Zelle visualisiert und ggf. bekannten Typen zugeordnet werden konnte. Die Experimente wurden an Zellen im **Zentralkomplex** durchgeführt, einem Areal des Insektenhirnes, welches an der visuell vermittelten Kontrolle von zielgerichteter Fortbewegung beteiligt ist. Die Experimente zeigten, dass die Repräsentation von Kompassrichtungen durch Zellen des Zentralkomplexes auf verschiedene Weisen für ihre Verwendung bei der Bewegungssteuerung ´aufbereitet´, d.h. in einen Kontext zu bisherigem Verhalten oder Ereignissen in der Umgebung gebracht wird. Letzteres basiert auf einer Interaktion zwischen zwei Sinnen der Außenwahrnehmung, nämlich Kompasssinn und Objektsehen, wobei novelty detection (Objektsehen) die Antworten auf den Kompassreiz moduliert. Die Ergebnisse verbessern das Verständnis des Kompassnetzwerkes im Hirn der Heuschrecke und zeigen überdies Parallelen zu höherer Verarbeitung sensorischer Informationen im Cortex des Wirbeltiergehirns.

EINLEITUNG

Kompasssignale am Tageshimmel und ihre Bedeutung für räumliches Orientierungsverhalten von Insekten

Viele adaptive Verhaltensweisen von Wirbeltieren und Wirbellosen fußen auf einer allothetischen Orientierung im Raum (Mouritsen 2001, Frost and Mouritsen 2006). Kompasssignale wie der Vektor des Erdmagnetfeldes sind über die Dauer von evolutionsbiologisch relevanten Zeiträumen stabil und praktisch allgegenwärtig verfügbar – auch dort, wo es an prägnanten Landmarken mangelt. Dies umfasst karge Umgebungen wie die Wüste ebenso wie einheitlich erscheinende Umgebungen, wie sie eine Wiese aus Sicht eines bodennahen Insekts darstellt. Diese beständige, breite Verfügbarkeit von Kompasssignalen erlaubt die Evolution von vererbten Verschaltungsmustern für ´fest verdrahtete´ Netzwerke von ´Kompassneuronen´. Diese können analog zu ´head direction cells´ in Wirbeltiergehirnen (Ranck 1984) Bewegungsrichtungen signalisieren und somit verschiedenste Verhaltensweisen lenken, so z.B. ein simples Ausweichen in gerader (wenn auch quasi beliebiger) Richtung oder aber anhaltende Navigation über weitere Distanzen. Insbesondere nutzen Insekten, welche die Umgebung ihrer Heimstätten zur Futtersuche erkunden (wie Honigbienen und Wüstenameisen) oder über lange Strecken wandern (Wüstenheuschrecken und Monarchfalter) sogenannte ***Himmelskompasssignale*** zur Mittel- und Langstreckenorientierung (Srinivasan 2011, Merlin et al. 2011, Cheng et al. 2012, Collett et al. 2013, Chapman et al. 2015). Das markanteste Kompasssignal am Tageshimmel liefert die Position der Sonne, genauer gesagt ihr Azimut (Horizontalwinkel), d.h. der gedachte Schnittpunkt von Sonnenbahn und Horizont

(Abb. 1*A*). Die Position der Sonne entlang ihrer Bahn ist zwar über den Tagesverlauf nicht ´stationär´ wie das Erdmagnetfeld, ändert sich jedoch auf zyklische, vorhersehbare Weise. Häufig jedoch ist die Sonne aufgrund von Bewölkung oder aus der Sicht eines von hohem Bewuchs umgebenden Insektes nicht direkt sichtbar. Dann sind Tiere welche den Sonnenkompass nutzen darauf angewiesen, indirekt auf die Position der Sonne zu schließen. Zu den indirekten Sonnenkompasssignalen zählt das Polarisationsmuster des blauen Himmelslichtes, welches durch Streuung von direktem Sonnenlicht an atmosphärischen Partikeln entsteht (Rayleigh Streuung; Strutt 1871a, 1871b). Das polarisierte Streulicht weist im Gegensatz zum direkten Sonnenlicht überwiegend Wellen mit *einem* bestimmten elektrischen Feldvektor (*E*-Vektor) auf (Abb. 1*B*). Die *E*-Vektoren bilden ein den Tageshimmel überstreckendes Muster, welches achsensymmetrisch zur Sonnenbahn ist und so auf den Sonnenazimut schließen lässt (Abb. 1*C, C´*) (Bech et al. 2014). Insbesondere sind *E*-Vektor-Winkel an Positionen, welche direkt auf der Sonnenbahn selber liegen – einschließlich des Zenits – stets *senkrecht* zur Sonnenbahn orientiert. Die Symmetrie des Polarisationsmusters erlaubt es, auch dann auf den Verlauf der Sonnenbahn zu schließen, wenn das Muster nicht in Gänze sichtbar ist (allerdings ist dieses recht robust gegenüber dem Einfluss von Bewölkung), sondern beispielsweise nur der Winkel des zenitalen *E*-Vektors bestimmt werden kann. Allerdings erlaubt dieser im Gegensatz zur Sicht auf das gesamte Polarisationsmuster noch nicht die Bestimmung des Sonnenazimuts, denn hierzu ist neben dem Verlauf der Sonnenbahn noch zu bestimmen, auf welcher Seite dieser Bahn sich die Sonne gegenwärtig befindet. Gegebenenfalls kann diese Uneindeutigkeit mittels zweier weiterer, ´gröberer´ Sonnenkompasssignale aufgelöst werden: Zwischen der sonnenzugewandten und der sonnenabgewandten Hälfte des Tageshimmels besteht neben dem Helligkeitsunterschied ein Gradient in der ´Färbung´ des Himmelslichtes (Abb. 1*C, C´*) (Pfeiffer and Homberg 2007, Heinze and Reppert 2011, el Jundi et al. 2014*B*).

Ein Orientierungsverhalten, bei welchem sich das Tier relativ zu einem Polarisations-Kompasssignal ausrichtet, wird als **Polarotaxis** bezeichnet. Es erlaubt - wie oben ausgeführt - auch dann eine zielgerichtete Bewegung relativ zur Sonne, wenn Letztere nicht direkt sichtbar ist. Polarotaxis wurde in zahlreichen Insektenspezies nachgewiesen, darunter Bienen (von Frisch 1949, Wehner 1984), Fliegen (Wolf et al. 1980, von Philipsborn and Labhart 1990, Weir and Dickinson 2012), Ameisen (Wehner 1984, 2003), Grillen (Brunner and Labhart 1987), Heuschrecken (Mappes and Homberg 2004), Monarchfalter (Reppert et al. 2004, Sauman et al. 2005) und Mistkäfer (Dacke et al. 2003, 2011; el Jundi et al. 2014*A*). Die polarisationsabhängige Rezeption von Himmelslicht wird durch spezialisierte Dorsale, also gen Himmel orientierte, Randregionen des Facettenauges (dorsal rim area, DRA) vermittelt (Abb. 2*B***;** Labhart and Meyer 1999, Eggers and Gewecke 1993, Dacke et al. 2002, Homberg and Paech 2002, Reppert et al. 2004, Stalleicken et al. 2006, Wernet et al. 2012). Polarotaxis dient verschiedensten Verhaltensweisen (siehe weiter oben aufgeführte Studien) von gerichteter Flucht (Mistkäfer) über Weg-Lernen bei der Futtersuche (Bienen, Ameisen) bis hin zur Orientierung bei Wanderungsbewegungen über lange Strecken (höchstwahrscheinlich bei Wüstenheuschrecken). Im Windkanal fliegende Heuschrecken zeigten das Bestreben, sich relativ zu einem von dorsal gegebenem Polarisationsreiz auszurichten. Hierbei wurden Änderungen der Bewegungsrichtung simuliert, indem ein Polarisator zwischen dem Kopf des Tieres und einer darüber positionierten Lichtquelle rotiert wurde (Mappes and Homberg 2004). Diese polarotaktische Ausrichtung der Flugrichtung fiel bei Verdeckung der dorsalen Randregionen beider Augen weg.

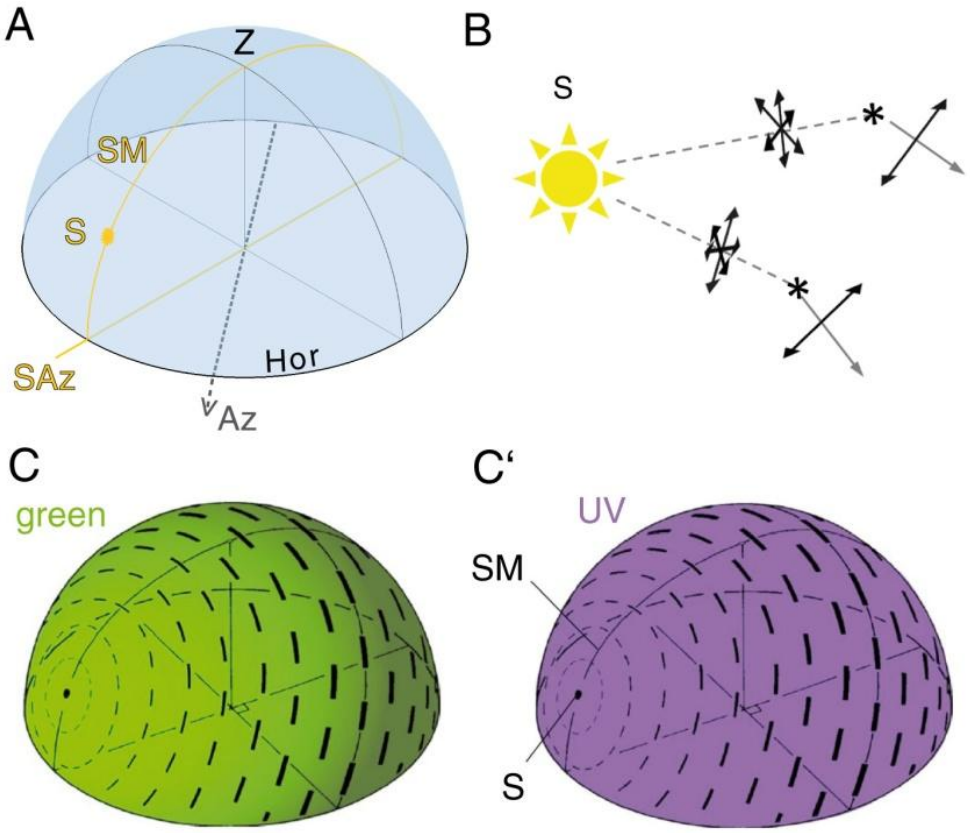

Abb. 1. Sonnenkompasssignale am Tageshimmel. ***A*** Durch Orientierung relativ zur Position der Sonne (S) wird eine gerichtete Fortbewegung (gestrichelter grauer Pfeil in der Horizontalebene) entlang eines ´Kompasskurses´ möglich. Der Horizontalwinkel der Sonnenposition, der Sonnenazimut (SAz), ist als Schnittpunkt von Sonnenbahn (Sonnenmeridian, SM) und geometrischem Horizont (Hor) definiert. Der 'Kompasskurs' wird durch den Winkelabstand zwischen dem SAz und dem Azimut der Wegstrecke (Az) definiert. Z: Zenit. ***B*** Ist die Sonne nicht sichtbar, so lassen indirekte Sonnenkompasssignale, hier das Polarisationsmuster des Himmelslichtes, auf ihre Position schließen. Direktes Sonnenlicht (gestrichelte graue Linien) ist unpolarisiert, die Lichtwellen haben elektrische Feldvektoren (*E*-Vektoren, Doppelpfeile) mit verschiedensten Winkelorientierungen. Bei Streuung an atmosphärischen Partikeln (Sternchen) geht diese gleichmäßige Verteilung von *E-V*ektor-Winkeln über in die Dominanz eines bestimmten Winkels; es entsteht linear polarisiertes Licht (graue Pfeile). ***C, C'*** Hierbei hängt dieser dominante *E*-Vektor-Winkel (schwarze Balken) von der Position am Himmel ab, wobei ein Muster mit Achsensymmetrie zur Sonnenbahn (Sonnenmeridian, SM) entsteht. Der Polarisationsgrad, d.h. der Grad der Dominanz des jeweiligen Winkels (Balkendicke) ist abhängig vom Winkelabstand von der Sonne. Er ist maximal entlang eines gedachten Kreises bei 90° Abstand zur Sonne sowie symmetrisch zu diesem Kreis verteilt. Eine grobe Unterscheidung von sonnenzugewandter und sonnenabgewandter Himmelshälfte ist basierend auf einem Helligkeitsunterschied und anhand eines Farbgradienten des Himmelslichtes möglich. Während die Intensität von grünem Licht mit wachsendem Abstand zur Sonne abnimmt (***C***), hat kurzwelliges UV-Licht eine gleichmäßige Intensitätsverteilung (**C'**). Darstellung in *A* basierend auf einem MATLAB-Skript von Dr. Keram Pfeiffer. *B* nach Marshall und Cronin (2011). *C*, *C'* verändert aus el Jundi et al. (2014*B*).

Abb. 2. Morphologie der Wüstenheuschrecke *Schistocerca gregaria*. *A* Neben Unterschieden in Neuroanatomie und Verhalten (nicht dargestellt) sind vereinzelt lebende Tiere (solitäre Phase) größer und weniger auffallend gefärbt als vergemeinschaftete Artgenossen (gregäre Phase). Letztere wurden in der vorliegenden Dissertation verwendet. ***C*** Bei Tieren beider Phasen weisen die Facettenaugen deutlich ausgebildete dorsale Randregionen (Pfeile, Ansicht von oben) zur polarisationsabhängigen Rezeption von blauem Himmelslicht auf. Maßstabsbalken 1 mm. *A* und *B* verändert aus Ott and Rogers (2010) bzw. Homberg und Paech (2002).

Der Zentralkomplex des Insektengehirns: ein Zentrum für höhere Reizverarbeitung mit besonderer Bedeutung für zielgerichtete Fortbewegung

Abbildung 3 zeigt die grobe Anatomie des Insektengehirns am Beispiel der Heuschrecke. Eingehender dargestellt sind beidseitig der Mittellinie angelegte Neuropile (d.h. Hirnregionen) des Sehsystems sowie der mittig angelegte Zentralkomplex, welcher multimodal ist bzw. – je nach Spezies - Eingänge aus verschiedenen Wahrnehmungssinnen verarbeitet (Pfeiffer and Homberg 2014). Der Zentralkomplex umfasst die obere und untere Einheit des Zentralkörpers (upper and lower unit of the central body, CBU bzw. CBL), die Noduli (paarig beiderseits der Mittellinie angelegt), und die Protocerebralbrücke (PB) (Abb. 3*A,B*). Diese sind feinanatomisch in vertikale Säulen, die sog. *Kolumnen* untergliedert (bei PB, CBU, CBL) und / oder weisen eine horizontale Schichtung (bei CBU, CBL, Noduli) auf. Diese regelmäßige Anatomie liegt auch der Bezeichnung von Neuronentypen des Zentralkomplexes zugrunde: Kolumnäre Neurone verbinden einzelne Kolumnen (engl. columns, C) der PB mit solchen von CBU (CPU-Neurone) und CBL (CL-Neurone). Zudem verzweigen sie in den Lateralen Komplexen, den wesentlichen Ein- und Ausgangsregionen des Zentralkomplexes (Heinze and Homberg 2008). Tangentialzellen hingegen verbinden mehrere oder sämtliche Kolumnen von CBL (TL-Neurone) oder PB (TB-Neurone) mit Bereichen der Lateralen Komplexe (TL-Neurone) bzw. der Posterioren Optischen Tuberkel (TB-Neurone) (Müller et al. 1997, Heinze and Homberg 2007). Abbildung 3*B* zeigt die Morphologie dieser bereits in früheren Arbeiten beschriebene Neuronentypen des Zentralkomplexes der Heuschrecke, welche in der vorliegenden Dissertation funktionell weiter charakterisiert wurden.

Bisherige Erkenntnisse zur Funktion des Zentralkomplexes stammen im Wesentlichen aus Läsionsstudien an Fliegen, d.h. der Beobachtung von Verhaltensleistungen oder neuronalen Antworten auf äußere Reize nach dauerhafter oder vorübergehender Inaktivierung von Teilen des Zentralkomplexes. Diese Studien identifizierten den Zentralkomplex als höheres Verarbeitungszentrum für Sinnesinformationen mit Bedeutung für die Bewegungssteuerung (Strauss 2002, Strauss and Heisenberg 1993; bei Schaben: Ritzmann et al. 2012), für ein visuelles Muster- und Arbeitsgedächtnis (Liu et al. 2006, Pan et al. 2009, Neuser et al. 2008), für ein visuell vermitteltes Ortsgedächnis (Ofstad et al. 2011), und für die homöostatische Kontrolle von

Schlafperioden (Donlea et al. 2014). Darüber hinaus ist der Zentralkomplex des Fliegenhirnes beteiligt an einer differenzierten Repräsentation der ´Attraktivität´ von Duftquellen (Beshel and Zhong 2013), welche sowohl die Qualität des Duftes (bzw. der damit assoziierten Nahrung) als auch seine Konzentration ´berücksichtigt´ und diese Größen zwischen mehreren gleichzeitig dargebotenen Quellen ´vergleicht´. Die so enkodierte Wertigkeit des Duftsignals hängt zudem vom gegenwärtigen Sättigungsgrad des Tieres ab und spiegelt sich im Verhalten der Tiere, d.h. der Annäherung oder Vermeidung einer jeweiligen Duftquelle wider.

Hinweise auf eine Rolle des Zentralkomplexes bei Himmelskompass-gestützter Orientierung wurden bei Grillen (Sakura et al. 2008) sowie bei zwei wandernden Spezies, nämlich der Wüstenheuschrecke (Heinze and Homberg 2007, Mappes and Homberg 2004) und dem Monarchfalter (Heinze and Reppert 2011) gefunden. Bei diesen fanden sich Zentralkomplexneurone, welche *E*-Vektor-Winkel von polarisiertem Licht repräsentieren, d.h. ihre Aktivität in Abhängigkeit vom *E*-Vektor änderten. Eine davon unabhängige Bevorzugung einer bestimmten Lichtfarbe und -richtung, und zwar die Bevorzugung blauen, von oben auf den Kopf des Tieres gerichteten Lichtes, spricht für eine Rolle bei der Himmelskompassorientierung. Anatomische und physiologische Studien (Homberg et al. 2011) haben zudem Pfade von polarisationsempfindlichen Neuronen identifiziert, welche ausgehend von den Dorsalen Randregionen der Facettenaugen Eingänge des Zentralkomplexes bilden (Abb. 3*A*). Abbildung 3*A´* zeigt, wie der bevorzugte, d.h. der von den Zellen durch gesteigerte Aktivität signalisierte *E*-Vektor-Winkel systematisch von der horizontalen Lage der Neurone im Zentralkomplex abhängt (Heinze and Homberg 2007). Diese **Polarotopie** bildet Bewegungsrichtungen unter dem Himmelszelt auf einer rechts-links-Achse im Zentralkomplex ab und wird daher als neuronales Substrat einer Himmelskompass-gestützten Orientierung oder als ´interner Kompass´ betrachtet. Ob hierbei jedoch eine eindeutige Signalisierung des Sonnenazimutes gegeben ist – etwa durch eine Repräsentation des gesamten Polarisationsmusters (Bech et al. 2014) – oder lediglich der dominante *E*-Vektor im Zenit die Polarisationsantworten der Neurone bestimmt, blieb bisher unklar. In letzterem Fall würde die Integration weiterer Sonnenkompasssignale erforderlich, wenn eindeutig auf die Position der Sonne geschlossen werden soll (siehe vorheriger Abschnitt). Eng verbunden mit der Frage, ob die Population der Kompassneurone die Position der Sonne oder nur den Winkel der Sonnenbahn repräsentiert ist eine zweite Frage: nämlich, ob die 2x180°-Redundanz der Polarotopie (Abb. 3*A´*) letztlich einer 360°-Repräsentation von Bewegungsrichtungen bzw. Sonnenpositionen entspricht oder nicht. Alternativ könnte diese ´doppelte Abbildung´ von *E*-Vektoren auch in der Notwendigkeit bestimmter Verschaltungsmuster zwischen den beteiligten Neuronen begründet sein, ohne dabei zwangsläufig einer ´echten 360°-Repräsentation´ zu entsprechen. Für diese Möglichkeit sprechen Erkenntnisse aus der vorliegenden Dissertation, die in Kapitel I dargestellt werden. Zudem zeigt das erste Kapitel, dass das ´bloße´ Kompasssignal von polarisationsempfindlichen Neurone auf der Eingangsebene des Netzwerkes (Abb. 3*B,* linke Teilabbildung) bereits in höheren Zellen des Zentralkomplexnetzwerkes (Abb. 3*B,* mittlere und rechte Teilabbildung) für seine Verwertung bei der Steuerung zielgerichteter Fortbewegung ´aufbereitet´ wird.

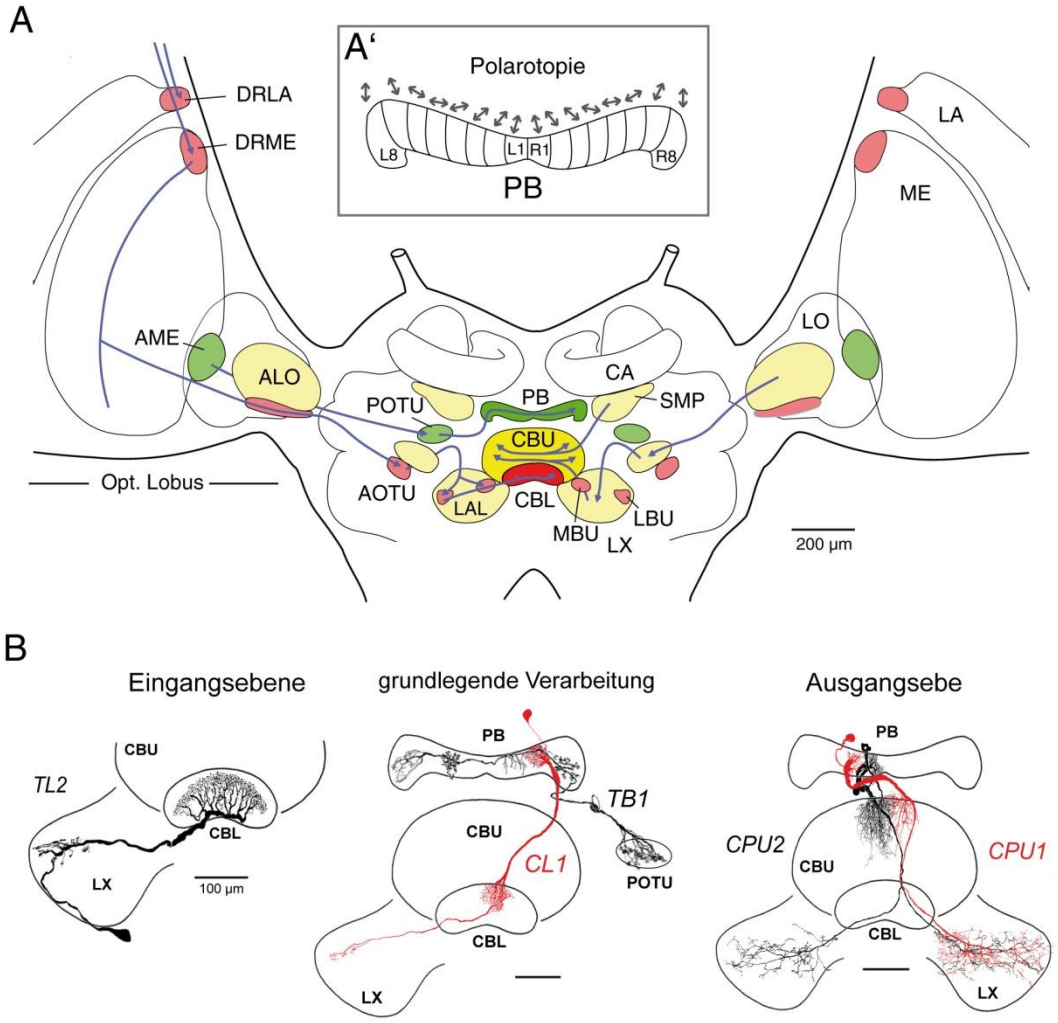

Abb. 3. Grobe Anatomie des Heuschreckengehirns mit Fokus auf das Sehsystem, den Zentralkomplex und relevante Neuronentypen in Frontalansichten. ***A*** Beidseitig angelegt sind die optischen Loben (Einzahl Opt. Lobus), welche die früheste Verarbeitung von Lichtreizen vollziehen. Sie umfassen jeweils die Neuropile Lamina (LA), Medulla (ME) und Lobula (LO). Ausgehend von den Optischen Loben ziehen Sehpfade aus ´lichtsensitiven´ Neuronen zu einem Netzwerk aus ´höheren´ Neuronen im Zentralkomplex. Rot (bzw. grün) dargestellte Neuropile sind Teil eines anterioren (bzw. posterioren) Pfades aus Interneuronen, welche auf Himmelskompasssignale reagieren. Weitere Pfade verlaufen durch die gelb dargestellten Neuropile und könnten etwa daran beteiligt seien, die scheinbare Bewegung der Umwelt während der Fortbewegung und / oder stationäre Objekte wie visuelle Landmarken in der Umwelt zu signalisieren. DRLA bzw. DRME: Dorsale Randregion der Lamina bzw. Medulla; ALO: anteriorer Lobus der Lobula; AME, Akzessorische Medulla; AOTU bzw. POTU: Anteriorer bzw. Posteriorer Optischer Tuberkel; MBU bzw. LBU: Medialer bzw. Lateraler Bulbus; LAL: Lateraler Akzessorischer Lobus. Zusammen mit dem LAL bilden MBU und LBU den jeweiligen Lateralen Komplex (LX). CBL bzw. CBU: unterer (engl. lower, L) bzw. oberer (engl. upper, U) Teil des Zentralkörpers (engl. central body, CB); PB: Protocerebralbrücke; SMP: Superiores Mediales Protocerebrum; CA: Calyx des Pilzkörpers. ***A'*** Polarotopie. Die von Neuronen der Protocerebralbrücke (PB) bevorzugten *E*-Vektor-Winkel (Doppelpfeile; hier für CPU-Neurone dargestellt) hängen systematisch von der horizontalen Position der vom jeweiligen Neuron durchzogenen Kolumne ab. Die so gebildete ´polarotope Achse´ ist spiegelsymmetrisch zur Mittellinie und deckt pro Gehirnhälfte einen *E*-Vektor-Winkelbereich von 180° ab. Dieser Bereich ist in jeweils 8 Schritten von etwa 22.5 ° abgedeckt, welche anatomisch den jeweils 8 Kolumnen der PB entsprechen (L1 bis L8 und R1 bis R8 für die linke bzw. rechte Hirnhälfte). Die polarotope Achse wird gemeinhin als kompassähnliche Repräsentation von Bewegungsrichtungen unter dem Himmelszelt verstanden. ***B*** Bekannte, hier weiter

untersuchte Zelltypen auf verschiedenen Hierarchiebenen des Kompassnetzwerkes im Zentralkomplex. Kolumnäre Neurone verbinden Kolumnen von PB und CBU (CPU-Neurone) bzw. von PB und CBL (CL-Neurone) und weisen weitere Verzweigungen in den Lateralen Komplexen auf. Tangentiale TB - Neurone verzweigen in mehreren Kolumnen der PB sowie in je einem Posterioren Optischen Tuberkel. Tangentiale TL-Neurone verbinden Regionen eines Lateralen Komplexes mit allen Kolumnen der CBL. *A:* verändert aus Pfeiffer und Homberg (2014), *B:* verändert aus Müller et al. (1997), Vitzthum et al. (2002), Heinze and Homberg (2007, 2009).

Allgemeine Fragestellung

Insgesamt widmet sich die vorliegende Arbeit der Frage, wie die Aktivität im internen Kompass des Zentralkomplexes in einen Kontext – etwa zur bisherigen Bewegungsrichtung oder unerwarteten Ereignissen - gebracht wird, durch welchen sie sich erst für ihre Verwertung zur zielgerichteten Bewegungssteuerung eignet.

GRUNDLEGENDE FACHBREGRIFFE

Die unten aufgeführten Fachbegriffe werden im weiteren Verlauf dieser Arbeit häufig auftreten. Da sich die Definitionen dieser Begriffe gelegentlich von Autor zu Autor unterscheiden, sollen die hier gültigen benannt werden:

Spike: lokales Maximum des gemessenen Membranpotentials, welches als Aktionspotential des abgeleiteten Neurons betrachtet wird.

(exterozeptive) neuronale Antwort: eine Veränderung der Aktivität (hier: Spike-Rate) eines Neurons, welche mit einem Ereignis in der Außenwelt zusammenfällt und dieses somit vermutlich ´repräsentiert´

exzitatorische Antwort: neuronale Antwort in Form einer Erhöhung der Spike-Rate

inhibitorische Antwort: neuronale Antwort in Form einer Verminderung der Spike-Rate

Falls nicht anders angemerkt, werden die Begriffe ´exzitatorsich´ und ´inhibitorisch´ verwendet, ohne damit bestimmte zugrunde liegende Mechanismen zu implizieren – d.h. eine hier als ´exzitatorisch´ klassifizierte Antwort könnte auf eine direkte Erregung eines Neurons und / oder auf das Wegfallen einer Hemmung zurückgehen.

KAPITEL I: AMPLITUDE AND DYNAMICS OF POLARIZATION-PLANE SIGNALING IN THE CENTRAL COMPLEX OF THE LOCUST BRAIN

(DYNAMIKEN DES ANTWORTVERHALTENS VON POLARISTATIONSEMPFINDLICHEN NEURONEN IM ZENTRALKOMPLEX DER WÜSTENHEUSCHRECKE)

Tobias Bockhorst and Uwe Homberg

Ziel war es zunächst, solche Eigenschaften von Antworten polarisationsempfindlicher Neurone zu identifizieren, die über ein bloßes *E*-Vektor-**Tuning**, d.h. die Bevorzugung eines bestimmten *E*-Vektor-Winkels pro Zelle hinausgehen. Um solche ´höheren Dynamiken´ zu identifizieren, wurden elektrophysiologische Ableitungen der Aktivität von TL-, CL-, TB- und CPU-Neuronen (Abb. 3*B*), also auf allen Hierarchieebenen des Netzwerkes (Heinze et al. 2009) durchgeführt. Die Auswertung der Messungen gründet auf der Bestimmung der Rate, mit welcher die Zellen Aktionspotentiale (im Folgenden **Spikes** bzw. **Spike-Rate** genannt) generierten.

Es wurde zum einen die ´Hintergrundaktivität´ der Zellen ohne Stimulation mit polarisiertem Licht bestimmt und zum anderen ihre Antworten auf den ´Kompassreiz´, d.h. von dorsal präsentiertes, blaues, linear polarisiertes Licht (im Folgenden kurz: polarisiertes Licht). Letzteres wurde mittels einer blaues Licht emittierenden Diode und eines zwischen der Diode und dem Kopf des Tieres positionierten Polarisators erzeugt und beleuchtete die Dorsalen Randregionen beider Facettenaugen. Durch Rotationen des Polarisators (360° bei 30°/s; im und gegen den Uhrzeigersinn) konnten stufenlose, gleichmäßige Änderungen des *E*-Vektor-Winkels (im Folgenden: ***E*-Vektor-Modulation**) erzeugt werden. Dieser Stimulus diente zur Untersuchung dreier Aspekte: (I) generelle **Responsivität** gegenüber *E*-Vektor Modulation, d.h. die Frage, ob die Zelle überhaupt auf Änderungen des *E*-Vektors mit Änderungen ihrer Aktivität antwortet, (II) Tuning der Antwort und (III) Stärke der Antwort.

Die Untersuchung dieser Aspekte erforderte zunächst die Entwicklung einer neuen Methode zur Auswertung von Antworten auf den rotierenden Polarisator. Im Folgenden werde ich diese in ihren wesentlichen Zügen beschreiben; für zusätzliche Details und Illustrationen sei auf den englischsprachigen Anhang unter APPENDIX: ADDENDUM TO CHAPTER I verwiesen. Um überhaupt einen möglichen Zusammenhang zwischen Spike-Rate und *E*-Vektor-Winkel untersuchen zu können, wurde zunächst (wie bei früheren Arbeiten) jedem Zeitpunkt, an dem ein Spike auftrat, die zu diesem Zeitpunkt gegebene Winkelorientierung des Polarisators (welche den *E*-Vektor-Winkel des Lichtes bedingt) zugeordnet. Hieraus ergibt sich einer Verteilung von ´**Spike-Winkeln**´, also sozusagen von durch je einen Spike beantworteten *E*-Vektor-Winkeln, welche bei Stimulation mit einer vollen Drehung des Polarisators alle Werte zwischen 0° und 360° haben können. Hierbei entsprechen aufgrund der ´axialen´ Natur von *E*-Vektoren Werte, die sich um 180° unterscheiden, demselben Winkel. Insbesondere entsprachen die Winkel 0°, 180° und 360° einem *E*-Vektor, der deckungsgleich bzw. parallel zur Längsachse des Tieres war.

In früheren Studien (Pfeiffer et al. 2005, siehe z.B. auch Heinze and Reppert 2011) wurde anschließend auf Responsivität getestet, indem die Spike-Winkel-Verteilung einem Rayleigh-Test (Fisher 1995) auf zirkuläre Gleichverteilung unterzogen wurde. Dieser Hypothesentest kann anzeigen, ob die Spike-Winkel gleichmäßig verteilt sind oder sich ´signifikant´ um einen mittleren Winkel konzentrieren, welcher dann dem bevorzugten *E*-Vektor-Winkel (Φ_{max}) der

Zelle (bzw. der jeweiligen Antwort) entspräche. Nur in letzterem Falle wurde in diesen Studien eine Responsivität gegenüber *E*-Vektor-Modulation angenommen. Zur Spezifikation des *E*-Vektor-Tunings wurde dann neben der Angabe von Φ_{max} – ohne physiologische Kriterien – ein Gegenwinkel von $\mathbf{\Phi_{min}} = \Phi_{max} + 90°$ als ´Vermeidungswinkel´ angegeben (nicht etwa von $\Phi_{max} + 180°$, weil *E*-Vektor-Winkel eine 180° Periodizität aufweisen und keine solche von 360°). Zusätzlich haben einige Studien die Stärke der Antwort mittels eines von Labhart (1996) vorgeschlagenen Maßes beschrieben. Dieses quantifiziert die *absolute* Amplitude der Antwort durch die aufsummierte Differenz zwischen der Spike-Rate bei verschiedenen *E*-Vektor-Winkeln und der über die gesamte Drehung berechneten mittleren Spike-Rate. Damit berücksichtigt dieses Maß jedoch nicht die *Höhe* dieser mittleren Spike-Rate. Es ist daher ´blind´ gegenüber dem Unterschied zwischen einer Änderung der Spike-Rate von 10 auf 15 Spikes pro Sekunde einerseits und 100 auf 105 Spike pro Sekunde andererseits (zudem ist hierbei nicht von Belang, wie die Spikes während der Drehung verteilt waren, was jedoch durch den Rayleigh-Test erfasst wird). Daher erschwert die Verwendung dieses Maßes Interpretationen und Vergleiche insbesondere dann, wenn Antworten auf *E*-Vektor-Modulation auf unterschiedlich starker Hintergrundaktivität ´reiten´.

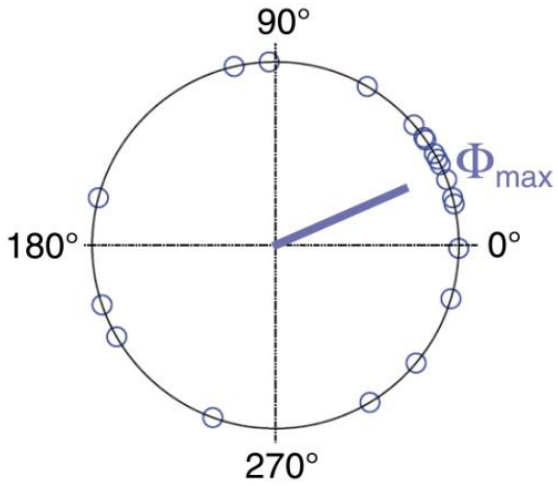

Abb. 4. Illustration des mittleren Winkels Φ_{max} eines zirkulären Datensatzes. Die hier gezeigten Daten sind zirkulär: ihre Verteilung hat einen einzigen Modus (häufigster Wert) auf der zirkulären (360°) Skala. Meßwerte sind als kleine blaue Kreise an den entsprechenden Winkelpositionen auf einem Einheitskreis dargestellt. Die blaue Linie zeigt den berechneten mittleren (´bevorzugten´) Winkel, $\Phi_{max.}$ Daten wie diese könnten etwa die Aktivität eines Neurons darstellen, welches auf die horizontale Position von Objekten in der Umgebung wie visuellen Landmarken oder der Sonne als Kompasssignal getuned ist (wobei die 0° - 180° Achse der Längsachse des Kopfes entsprechen würde). Im Falle eines Tunings auf *E*-Vektor-Winkel, d.h. bei einer axialen Größe (bei welcher 0° und 180° einander entsprechen), hätte die Verteilung einen zweiten Modus bei einem Winkel von Φ_{max} +180°. Verändert aus Berens (2009).

In der vorliegenden Arbeit sollte zunächst untersucht werden, wie *dynamisch* Antworten auf *E*-Vektor-Modulation bei Neuronen auf verschiedenen Ebenen des Netzwerkes im Zentralkomplex der Wüstenheuschrecke sind. Insbesondere strebte ich eine differenziertere Beschreibung der Antworten an, um etwa Antworten mit großer Amplitude (starker Veränderung der Spikerate) und engem Tuning (starker Konzentration der Aktivität um Φ_{max}) quantitativ von solchen mit geringerer Amplitude und breiterem Tuning unterscheiden zu können. Hierzu war es nötig, von der oben dargestellten Methodik abzurücken und neue Kriterien zur Beschreibung von Antworten zu erdenken.

Der neue Test auf Responsivität führt keinen Vergleich der Spike-Winkel-Verteilung mit einer zirkulären Gleichverteilung durch, sondern prüft, ob sich die Spike-Rate tatsächlich systematisch *mit dem E-Vektor-Winkel ändert*, d.h. ob beide kovariieren. Dies wird anhand einer (zirkulär-linearen) Korrelationsanalyse geprüft (Berens 2009); Responsivität wird demnach im Falle einer signifikanten ($p<0.05$) Korrelation zwischen der momentanen Spike-Rate und dem im jeweiligen ´Moment´ präsentierten *E*-Vektor-Winkel angenommen. Die Stärke dieser

Korrelation (welche nicht mit der Amplitude der Antwort zu verwechseln ist) wurde hier als **correlation strength** (**CS**) bezeichnet und mittels des Bestimmtheitsmaßes (**R^2**) quantifiziert. Diese Stärke ist proportional zur Breite des *E*-Vektor-Tunings, d.h. zur Größe des dynamischen Bereiches, über welchen die Spike-Rate des Neurons sich tatsächlich mit dem *E*-Vektor-Winkel ändert. Im Gegensatz zum Rayleigh-Test fragt die Korrelationsanalyse also nicht, wie eng Spikes um einen Φ_{max} Wert konzentriert sind, um zu entscheiden, ob ein Neuron überhaupt sensitiv gegenüber *E*-Vektor-Winkeln ist. Stattdessen prüft sie, ob die Aktivität des Neurons während der Drehung eines Polarisators generell geeignet ist, den *E*-Vektor-Winkel wiederzugeben – sei es durch enges oder breites Tuning, mit geringerer oder stärkerer Änderung der Spike-Rate. Zugleich liefert die Korrelationsanalyse mit R^2 ein Maß für die Tuningbreite, welches von der Amplitude der Antwort unabhängig ist. Zusätzlich zur Korrelationsanalyse wurde der Gehalt an Information berechnet, welchen der einzelne Spike bezüglich des *E*-Vektor Winkels liefern kann (Skaggs et al. 1993, 1996).

Zur Messung der Antwortamplitude wählte ich das Maß **vector strength** (**VS**) (Ashida et al. 2010), welches sensitiv gegenüber der Steilheit des Tunings ist. Quantifiziert wird die VS mittels **|r|**, der Länge des resultierenden (´mittleren´) Vektors der Spike-Winkel-Verteilung (Abb. 5, 6). Der oben erwähnte Φ_{max}-Wert entspricht dem *Winkel* dieses Vektors. Seine Länge, |r|, kann Werte zwischen 0 und 1 annehmen und ist 1 falls (und nur falls) alle Spike-Winkel identisch sind. Bei konstanten Levels von Hintergrundaktivität (und einer konstanten maximalen Änderung der Spikerate während der Antwort) spiegelt |r| im Wesentlichen die Breite des *E*-Vektor-Tunings wider: je breiter das Tuning, d.h. je breiter die Spike-Winkel um Φ_{max} verteilt sind, desto kleiner |r| (Abb. 5, 6). Wenn hingegen eine Antwort mit fester absoluter Amplitude auf unterschiedlich hohen Hintergrundaktivitäten ´reitet´, so gibt |r| die *relative* Amplitude wider, d.h. das Verhältnis der absoluten Höhe der Spike-Raten-Änderung zur Höhe der Hintergrundaktivität. Da Erkenntnisse aus der vorliegenden Arbeit implizieren, dass *E*-Vektor –Antworten der hier untersuchten Neurone tatsächlich von verschieden hohen Hintergrundaktivitäten überlagert werden, ist insbesondere diese Eigenschaft von |r| hier von Vorteil.

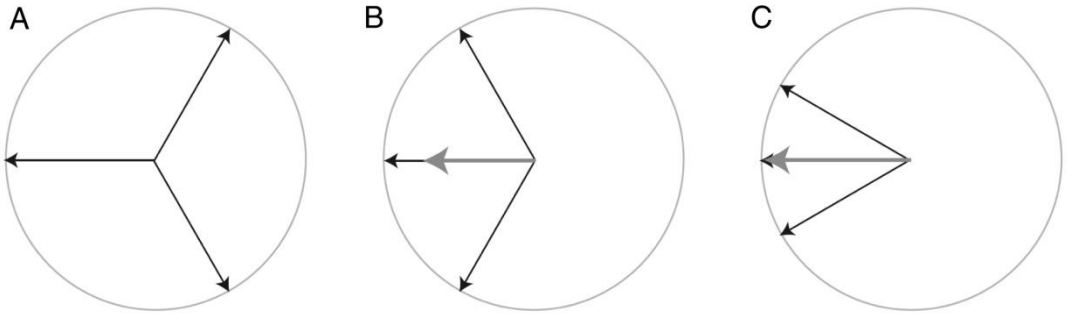

Abb. 5. Illustration des resultierenden Vektors. ***A-C*** zeigen unterschiedliche Verteilungsmuster für drei Ereignisse – etwa Aktionspotentiale eines visuellen Neurons während der Drehung eines Objektes um den Kopf eines Tieres. Diese sind durch zirkuläre Daten repräsentiert (schwarze Pfeile). Graue Pfeile zeigen den jeweiligen resultierenden Vektor (r) der Verteilung, welcher durch Addition der Vektoren berechnet werden kann. In ***A*** sind die Ereignisse gleichmäßig, d.h. ohne eine einzelne bevorzugte Richtung über den Kreis (also die 0°-360° Achse) verteilt: der Winkelabstand zwischen ihnen ist konstant (120°) und die Länge des resultierenden Vektors (|r|) beträgt Null. Im Gegensatz hierzu sind die Daten in ***B*** und ***C*** um eine 'bevorzugte' Richtung angeordnet, welche durch den Winkel von r (Φ_{max}) definiert ist. Hierbei verhält sich |r| negativ zur Breite dieses ´Tunings´: Das engere ´Tuning´ in ***c*** entspricht einem längeren resultierenden Vektor. Verändert aus Berens (2009).

Die Zielsetzung erforderte es häufig, Daten von mehreren Antworten einer Zelle bzw. mehreren Zellen kombiniert auszuwerten, um einen Eindruck von der ´durchschnittlichen´ Merkmalsausprägung zu erhalten. Vor diesem Schritt wurde die während der Drehung des Polarisators gemessene Spike-Rate auf die Hintergrundaktivitätsrate der jeweiligen Zelle normalisiert (durch Division). Um hierbei ausgeprägter Variabilität der Hintergrundaktivität Rechnung zu tragen, habe ich eine differenzierte Normalisierung eingeführt, bei welcher einmal unter Verwendung eines mittleren Levels der Hintergrundaktivität (Median) und zusätzlich mit Bezug auf Zustände geringer und hoher Hintergrundaktivität (2.5^{tes} und 97.5^{tes} Perzentil der Spike-Raten-Verteilung) derselben Zelle normalisiert wird.

Falls die Spike-Rate einer Zelle bei Φ_{max} höher als im Zustand hoher Hintergrundaktivität war, und zugleich die Spike-Rate bei Φ_{min} niedriger als im Zustand niedriger Hintergrundaktivität, so betrachtete ich dies als einen Fall echter ´**polarization opponency**´ (´Gegenpolreaktion´). Dieser Begriff wurde von Labhart (1988) eingeführt, das ursprüngliche Konzept beinhaltete jedoch keine Berücksichtigung von Hintergrundaktivitätsraten.

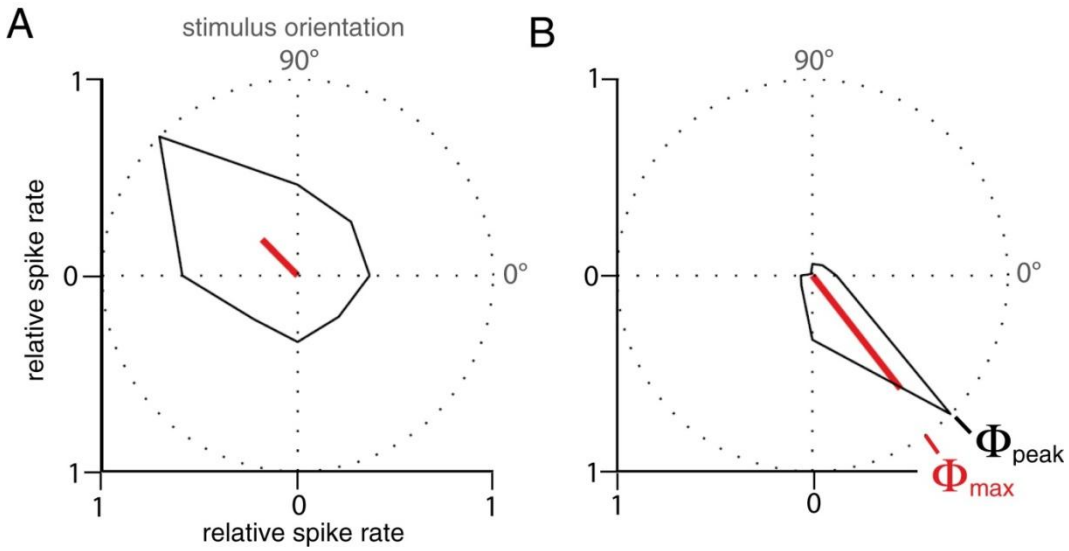

Abb. 6. Beispiele für breites und enges Tuning auf Winkelorientierungen. ***A*** und ***B*** zeigen Tuningkurven für Tuning auf die Winkelorientierung eines visuellen Objektes. Diese basieren auf Spike-Raten, welche im primären visuellen Cortex eines wachen Makaken gemessen wurden, während dem Tier Streifenmuster mit acht verschiedenen Winkelorientierungen gezeigt wurden. Die schwarzen Konturen geben die relative Spike-Rate wider. Stimulus-Orientierungen sind in Grad angegeben und der Radius des Kreises entspricht dem Maximum der während der Antwort gemessenen Spike-Rate. Rote Linien zeigen den jeweiligen resultierenden Vektor. Dessen Winkel, der mittlere (´bevorzugte´) Winkel Φ_{max} muss nicht dem 'besten' oder am stärksten beantworteten Winkel Φ_{peak} entsprechen, wie in *B* klar ersichtlich. Verändert aus Berens (2009).

Basierend auf dieser neuen Methodik habe ich analysiert, wie sich Antworten auf *E*-Vektor-Modulation zwischen Zelltypen, Zellen desselben Typs sowie im Laufe eines Experimentes, d.h. zwischen verschiedenen Stimulationen derselben Zelle unterschieden. Nach den Ableitungen wurde in die jeweilige Zelle ein Marker injiziert, welcher später zur mikroskopischen Visualisierung der Zelle an einen Fluoreszenzfarbstoff gekoppelt wurde. Die so identifizierten Zellen, welche in die endgültige Analyse aufgenommen wurden, umfassten 4

TL2-, 10 CL1-, 11 TB1-, 12 CPU1- und 6 CPU2-Neurone (s. Abb. 3), sowie zwei weitere, bisher unbekannte Neurone von außergewöhnlich komplexer Morphologie.

Die Hintergrundaktivität aller Neurone wies zelltypspezifische Eigenschaften auf. Diese hatten Einfluss auf die Amplitude von *E*-Vektor-Antworten und konnten zudem herangezogen werden, um im Falle einer nur schwach markierten Zelle oder mehrerer im Präparat markierter Zellen auf den Zelltyp der untersuchten Zelle zu schließen (siehe hierzu APPENDIX: ADDENDUM TO CHAPTER I). Der Median der Spike-Rate der Hintergrundaktivität schwankte gravierend zwischen Zellen desselben Typs. Hierbei tendierte die Spike-Rate der Hintergrundaktivität dazu, entlang der ´Hierarchie´ des Neuronalen Netzwerkes (TL-CL-TB-CPU), also von ´früheren´ zu ´späteren´ Stufen der Informationsverarbeitung größer und zugleich variabler zu werden.

TL2-Neurone der CBL, d.h. an der Eingangsebene des Netzwerkes, antworteten zuverlässig und mit engem Tuning auf ihren Φ_{max}. Die Antworten hoben sich deutlich von der regelmäßig-niedrigen Hintergrundaktivität dieses Zelltypes ab und der berechnete Informationsgehalt pro Spike war relativ konstant. Diese Antworteigenschaften von TL2-Neuronen sollten zu einer zuverlässigen Repräsentation von ´bevorzugten´ *E*-Vektor-Winkeln an der Eingangsebene des Netzwerkes beitragen.

Homberg et al. (1999) zeigten, dass TL2-Neurone GABA-immunoreaktiv sind, d.h. sich mit Antikörpern gegen den hemmenden Neurotransmitter Gamma-Aminobuttersäure (GABA) markieren lassen. Dies deutet auf eine hemmende Verschaltung auf nachfolgende Neurone, d.h. hier CL1-Zellen, hin. Damit übereinstimmend schien bei CL1-Neuronen die *Abwesenheit* von Spikes diejenige Größe zu bilden, welche zuverlässige *E*-Vektor-Information barg. Antworten auf den rotierenden Polarisator wiesen eine stärkere Variabilität (und somit geringere Zuverlässigkeit) bei Φ_{max} als bei Φ_{min} auf; dies galt insbesondere für stark antwortende Zellen. Dieser Effekt könnte auf das Fehlen echter polarization-opponency (´spiegelbildlich´ zu TL-Neuronen nun bei Φ_{max}) bei gleichzeitiger Überlagerung der Antworten durch variable Hintergrundaktivität zurückgehen. Letztere war bei CL1-Zellen gekennzeichnet von mehrere Sekunden anhaltenden Zuständen höherer bzw. niedrigerer Aktivität. Beim Vergleich mit diesen Zuständen erschien die Antwort um Φ_{min} robust, während sich jene bei Φ_{max} wenig von Zuständen erhöhter Hintergrundaktivität unterschied.

Hingegen waren die Antworten von TB1-Neuronen in der Protocerebralbrücke bei Φ_{min} *und* bei Φ_{max} robust, entsprachen also erstmals in der Hierarchie des Netzwerkes einem Fall echter polarization opponency. Dementsprechend war die Korrelation zwischen *E*-Vektor-Winkel und Spike-Rate stark und auch über die Gesamtheit der gemessenen Antworten von diesem Zelltyp betrachtet stabil. Dieses Antwortverhalten sollte die früher beschriebene kompassartige Repräsentation der bevorzugten *E*-Vektor-Winkel - *und* der zugehörigen Gegenwinkel - (Polarotopie, Heinze und Homberg 2007) in der Protocerebralbrücke stabilisieren. Es ließe sich erklären durch eine geeignete Verschaltung von CL1- und TB1–Neuronen sowie von TB1-Neuronen untereinander. Diese Verschaltung wäre so geartet, dass sie zu einer Kombination von Antworten zweier CL1-Neurone mit entgegengesetztem Tuning (Φ_{min} – Unterschied von 90°) führte, wobei einer der Eingänge indirekt, durch Hemmung zwischen TB1-Neuronen umgekehrt würde. Dieser putative Mechanismus und seine Annahme stützende morphologische Befunde sind in Abb. 7 dargestellt. Er könnte auch die in der Einleitung erwähnte 2x180°-´Redundanz´ der Polarotopie erklären: Die zweite, für das Kompasssignal ´redundante´ Repräsentation von vollen 180° würde dann aus den Verzweigungen von TB1-Neuronen bestehen, die die hemmende

Verschaltung auf das Partner-TB1-Neuron bilden.

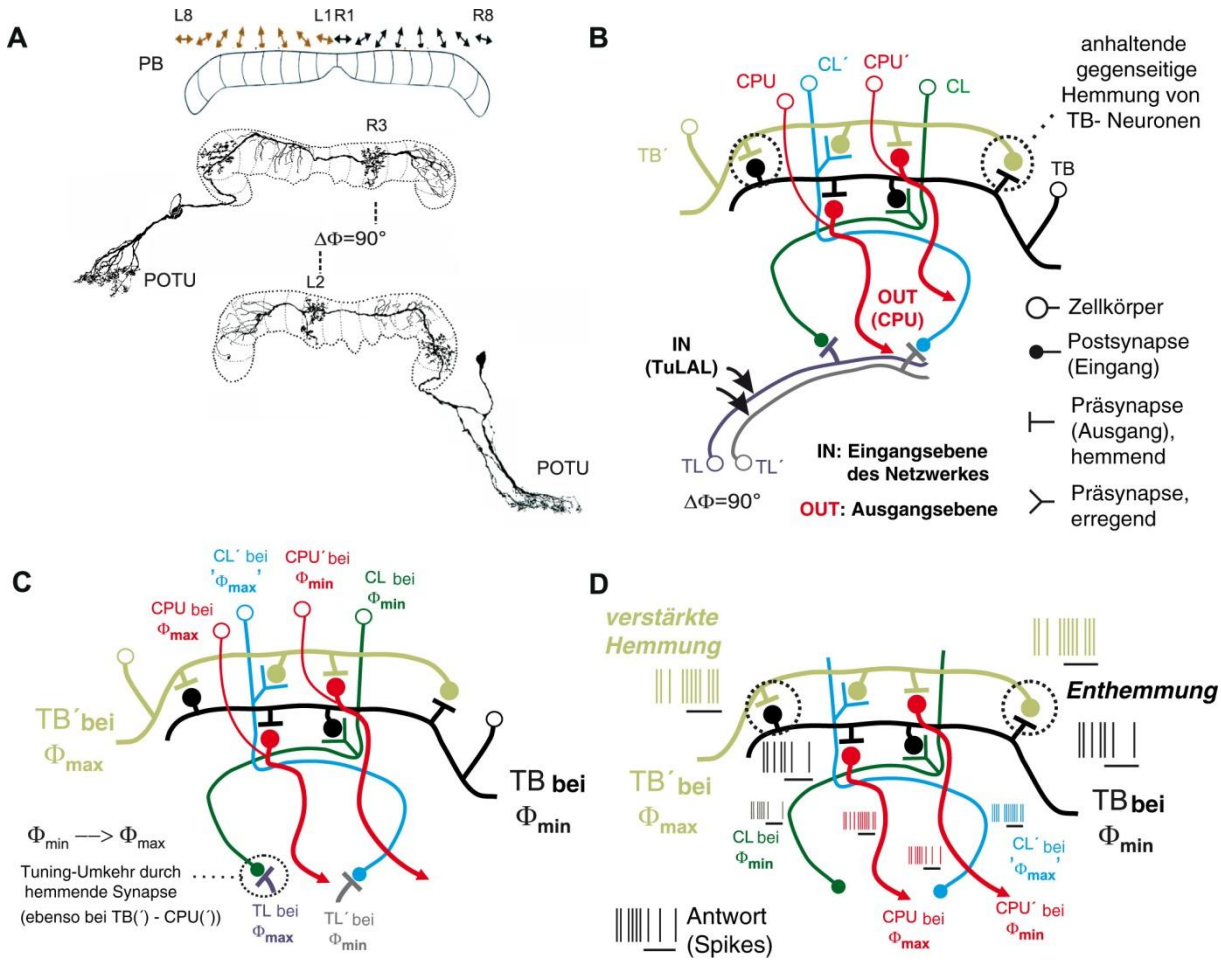

Abb. 7. Modell neuronaler Verschaltungen zur Erklärung von polarization-opponency bei *E*-Vektor Antworten von TB1-Neuronen. Robuste polarization-opponency und hohe Korrelationsstärke könnten aus gegenseitiger Hemmung zwischen TB1-Neuronen hervorgehen, welche ihrerseits Eingang von CL1-Neuronen mit gegensinnigem Tuning erhalten. ***A*:** Polarotopie in der Protocerebralbrücke (PB, obere Teilabbildung) und relevante morphologische Merkmale von TB1-Neuronen. Die PB birgt eine redundante polarotope Repräsentation von *E*-Vektor-Winkeln, welche über die Gesamtheit der 16 Kolumnen 2 x 180° abdeckt (je 180° und 8 Kolumnen pro Hemisphäre). Doppelpfeile: Φ_{max} –Werte (Vorzugswinkel) der TB–Neurone, welche in der jeweiligen Kolumne variköse und daher vermutlich präsynaptische Endigungen besitzen. Jedes TB1 hat zwei solche Ausgangs-Verzweigungen mit 8 Kolumnen Abstand, d.h. eine in jeder Hemisphäre der PB. Glatte und daher vermutlich postsynaptische Endigungen überspannen je drei benachbarte Kolumnen in jeder Hemisphäre. Dabei liegt die jeweils dem Zellkörper näher gelegene Seite dieser Eingangsbereiche eine Kolumne von einem Ausgangsbereich desselben Neurons entfernt. Die beiden hier gezeigten TB1 Neurone haben um 90° verschiedene Φ_{max} Werte. Entsprechend der oben beschriebenen Morphologie deckt sich pro Neuron ein Ausgangsbereich (Präsynapsen) mit einem Eingangsbereich (Postsynapsen) seines putativen ´Partner-´ Neurons. ***B***: vermutetes Muster der Verschaltungen zwischen grundlegenden Neuronentypen im Kompassnetzwerk des Zentralkomplexes der Heuschrecke. Input erhalten TL-Neurone der Eingangsebene ihrerseits von sog. TuLAL-Neuronen, welche die Anterioren Optischen Tuberkel (siehe Abb. 3) mit den Lateralen Akzessorischen Loben verbinden. Das Modell postuliert hemmende Synapsen von TL- auf CL-Neurone sowie zwischen TB-´Partner´-Neuronen und TB- und CPU-Neuronen, wodurch die synaptischen Partner jeweils entgegengesetzte Vorzugswinkel aufweisen (Φ_{max} – Unterschied von 90°) wie in ***C*** dargestellt. ***D***: Hypothetische Antwort des Netzwerkes auf Präsentation eines *E*-Vektors, welcher dem Φ_{max} des einen TL-Neurons (nicht mehr dargestellt) und somit dem Φ_{min} des anderen (TL´ in *C*) entspricht. Schwarze waagerechte Linien unter den symbolisierten Aktionspotentialspuren sollen die Dauer des Stimulus markieren (Adaptation auf anhaltende Stimulation

hin ist nicht dargestellt). Jenes TB-Neuron, für welches der Stimulus-*E*-Vektor dem Φ_{min} entspricht, erhält verminderten erregenden Input ´seines´ CL-Neurons und erfährt eine verstärkte Hemmung durch sein Partner-TB-Neuron (TB´). Für letzteres entspricht der Stimulus-*E*-Vektor dem Φ_{max}. Es erhält aufgrund der Hemmung seines Partner-TB-Neurons seinerseits weniger Hemmung über die TB-TB´-Synapse und zudem weiterhin erregenden Input seitens ´seines´ CL-Neurons (CL´). Anzumerken ist hierbei, dass die Aktivität von CL´ bei seinem ´Φ_{max}´ zwar vergleichsweise hoch ist, sich jedoch nicht von Zuständen hoher Hintergrundaktivität dieses Neurons unterscheidet. Dagegen etabliert der Mechanismus der gegenseitigen Hemmung / Enthemmung von TB-Neuronen im Modell eine echte ´polarization opponency´ in TB- und somit auch in CPU-Neuronen.

Die Erhöhung der Korrelationsstärke (CS) beim Übergang von CL- zu TB-Neuronen wird begleitet von einer *Abnahme* der vector strength (VS), entspricht jedoch einer Verbreiterung des dynamischen Bereiches des *E*-Vektor-Tunings und bewirkt eine Stabilisierung des Informationsgehaltes pro Spike. Dies legt nahe, dass eine Art Kompromiss zwischen erhöhter CS und verminderter VS ein essentieller Schritt auf dem Weg von der bloßen, über mehrere Zellen verteilten Repräsentation von Vorzugswinkeln zum Ziel eines in die Aktivität weniger prämotorischer Zellen gebündelten Kompasssignales sein könnte.

Im weiteren Verlauf der Verarbeitung kommt es zwischen TB1- und CPU-Neuronen zu einer erneuten ´Umkehr´ der Antworten. Diese basiert vermutlich auf weiteren hemmenden Synapsen (Abb. 7B-D) und äußert sich auch in empirisch gefundenen Unterschieden zwischen Φ_{max} Werten beider Neuronentypen, welche bei Heinze und Homberg (2007) häufig etwa 90° betrugen. Das Antwortverhalten von CPU-Neuronen – welche die Ausgangsebene des Netzwerkes bilden – war zudem von besonderer Variabilität geprägt. Dies gilt sowohl für die generelle Responsivität gegenüber *E*-Vektor-Modulation (CS) als auch für die Antwort-amplitude (VS) und den Informations-gehalt pro Spike. Auffallend ist hierbei, dass Zellen mit höherer Hintergrundaktivität geringere Antwort-amplituden zeigten. Dieses deutet auf eine ´Maskierung´ von Antworten durch Hintergrundaktivität hin, wobei diese Effekte offenbar mindestens für die Dauer eines Experimentes (15-45 min) anhielten (da die Unterschiede i.d.R. zwischen verschiedenen Zellen und nicht so sehr zwischen Stimulationen derselben Zelle auftraten). Im Falle von CPU2-Neuronen ergab sich hierbei eine Gesamtspanne, welche von fehlender Responsivität (keine Antwort) bis hin zu ausgeprägter polarization opponency, also ´vollständiger´ *E*-Vektor-Enkodierung reichte. Dieses Antwortverhalten ähnelt jenem von polarisationsempfindlichen absteigenden Neuronen (Träger and Homberg 2011) und deckt sich mit der Variabilität der Polarotaxis, welche in Verhaltensstudien bei Heuschrecken (Mappes and Homberg 2004) und Grillen (Brunner and Labhart 1987) beobachtet wurde. Desweiteren ist eine Ähnlichkeit zum Einfluss der Hintergrundaktivität auf sensorische Antworten im Cortex des Wirbeltiergehirns zu nennen (Arieli et al. 1996). In Studien von Verhalten und neuronalen Antworten konnte bei Wirbeltieren ein Zusammenhang zwischen diesem Phänomen und Aufmerksamkeit oder Wachsamkeit bei der Reizwahrnehmung hergestellt werden (Supèr et al. 2003, Hesselmann et al. 2008, Boly et al. 2007). Dementsprechend ist Hintergrund-aktivität im hiesigen Kontext keine bloße ´Spontanaktivität´, sondern eine essentielle Determinante neuronaler Antworten, welche ´innere´ Zustände wie Aufmerksamkeit – oder im Falle der Kompasszellen möglicherweise den Willen, sich räumlich zu orientieren – widerspiegelt. Maskiert werden könnten die *E*-Vektor Antworten dann etwa in Ruhephasen oder bei Paarungsverhalten, während sie bei anhaltender Fortbewegung durch verminderte Hintergrund-aktivität demaskiert werden könnten. Natürlich erfordert jedoch polarization opponency auch ein Mindestmaß an Hintergrundaktivität, da andernfalls die

Grundlage einer hemmenden Antwort bei Φ_{min} fehlen würde, wie etwa bei TL-Neuronen.

Neben den oben beschriebenen Dynamiken zeigten die Antworten auf den rotierenden Polarisator eine Abhängigkeit von der Drehrichtung. Diese Abhängigkeit hatte einen antizipatorischen Charakter, d.h. die Antworten ´kündigten während der Drehung das baldige Aufkommen der bevorzugten Richtung Φ_{max} an´. Die Φ_{max}-Werte beider Drehrichtungen unterschieden sich - und zwar so, dass bei beiden Drehrichtungen der Φ_{max} der individuellen Antworten erreicht war, *bevor* der über beide Drehrichtungen gemittelte Vorzugswinkel ($\Phi_{max,\ pooled}$) passiert wurde. Im Mittel (Median) betrug diese ´Vorausschau´ 10° bis 20° bei einer Drehgeschwindigkeit von 30°/s. Der mittlere Φ_{max} –Unterschied zwischen beiden Drehrichtungen war hierbei am stärksten bei CPU-Neuronen (etwa 33°), was auf eine besonders starke Antizipation bevorstehender Bewegungsrichtungen an der Ausgangsebene des Kompassnetzwerkes hindeutet. Zudem fällt die Antizipation noch stärker aus (etwa 45° bei CPU-Neuronen), wenn man anstelle der Φ_{max} -Winkel die Φ_{peak} -Winkel (Abb. 6) betrachtet. Generell könnte sie dazu dienen, während der gezielten Kontrolle der Bewegungsrichtung die Latenz zwischen sensorischer Verarbeitung und motorischen Antworten auszugleichen.

Die Antizipation bevorstehender Bewegungsrichtungen stellt zudem eine weitere Parallele zwischen den Kompasszellen im Heuschreckenhirn und den sog. ´head direction cells´ dar, welche von Ranck bereits 1984 in Ratten entdeckte und die eingehend von Taube und Kollegen untersucht wurden (Taube 2007, Clark and Taube 2012). Allerdings ´nutzen´ diese zur Antizipation vermutlich Signale wie jene des Vestibularsystems, welche Kopfbewegungen signalisieren, während die Heuschrecken in der hier angewandten Präparation fixiert waren und somit keine tatsächlichen (Kopf-)Bewegungen vollziehen konnten. Im Falle der Kompasszellen im Zentralkomplex könnten Informationen über die Drehrichtung und Geschwindigkeit aus dem Stimulus selber, also aus der *E*-Vektor-Modulation stammen.

Die bisher dargestellten Dynamiken von *E*-Vektor-Antworten bezogen sich auf Stimulationen mittels eines rotierenden Polarisators. Diese simulierten eine Drehung des Tieres um seine Hochachse. Um ergänzend auch den Zeitverlauf von Antworten auf unveränderte *E*-Vektoren zu untersuchen, wurden Messungen mit festen Orientierungen des Polarisators durchgeführt. Dies entspräche in natura z.B. einer anhaltenden Bewegung in dieselbe Richtung oder einem Stillstand. Zur Messung wurde der Polarisator zunächst in eine Stellung gedreht, welche für die jeweilige Zelle deutlich erregend (bei / nahe Φ_{max}) oder deutlich hemmend (bei / nahe Φ_{min}) war. Diese Orientierung wurde für etwa 20 bis 30s beibehalten.

TL2-Neurone an der Eingangsebene des hierarchischen (TL-CL-TB-CPU) Netzwerkes antworteten hierauf mit tonischer Erregung bei Φ_{max}. Dies bestätigt Vermutungen, die auf früheren Messungen mit kürzerer Stimulationsdauer gründeten (Vitzthum et al. 2002). Nachgeschaltete Neurone dagegen zeigten eine schnelle, *E*-Vektor-spezifische Adaptation der Antwort. Im Durchschnitt waren hemmende (CL, TB, CPU) und erregende (TB, CPU) Antworten nach etwa 6 bis 10s auf 50% ihrer anfänglichen Stärke abgefallen. Nach etwa 16-20s war die Antwort auf ein konstantes Mittelmaß abgeklungen.

Bei Wirbeltieren ist Stimulus-spezifische Adaptation vor allem aus Studien zur höheren Verarbeitung von akustischen Reizen bekannt und wird als Korrelat der Habituation, d.h. des Abklingens von Verhaltensantworten auf wiederholte Reizung betrachtet (Netser et al. 2011, Gutfreund 2012). Eine *E*-Vektor-spezifische Adaptation könnte analog als Grundlage der anhaltenden Bewegung in dieselbe

Kompassrichtung dienen, wie sie bei fixiert fliegenden Heuschrecken beobachtet wurde (Mappes and Homberg 2004). Es würden hierbei nur *Veränderungen* der Bewegungsrichtung vom Kompassnetzwerk ´gemeldet´ werden. Eine Adaptation an unveränderliche Kopfausrichtung ist dem Autor aus Arbeiten zu den head-direction cells der Ratte nicht bekannt.

E-Vektor-spezifische Adaptation, Antizipation und bedingte Responsivität eignen sich dazu, das Ausgangssignal des Kompassnetzwerks im Zentralkomplex für seine Anwendung bei der Steuerung zielgerichteter Fortbewegung aufzubereiten. Damit ist die Aktivität in der ´polarotopen´ Neuronenpopulation nicht mit dem bloßen Ausschlagen eines (unbeschrifteten) Kompasses vergleichbar. Sie ist vielmehr stark kontextabhängig mit Blick auf die ´Geschichte´ zuvor aufgetretener Bewegungsrichtungen (Antizipation, Adaptation) und hängt möglicherweise von inneren Zuständen wie einer Motivation des Tieres zur Orientierung im Raum ab (bedingte Responsivität durch Maskierung).

Meine Beobachtungen stützen somit die Betrachtung des Zentralkomplexes als einem Areal für höhere Verarbeitungsprozesse, welche sensorischen Input mit Bedeutung versehen, um eine gezielte Fortbewegung im Raum zu vollziehen. Einige in der Heuschrecke gefundene Dynamiken von neuronalen Antworten (Antizipation, Adaptation, Maskierung durch Hintergrundaktivität) ähneln solchen, die von höherer Verarbeitung sensorischer Informationen im Cortex des Wirbeltiergehirns bekannt sind.

KAPITEL II: HEAD-DIRECTION CELLS IN THE BRAIN OF AN INSECT ARE SENSITIVE TO NOVEL EVENTS IN THE VISUAL WORLD

(KOMPASSNEURONE IM HIRN EINES INSEKTS ANTWORTEN ZUSÄTZLICH AUF VERÄNDERUNGEN IN DER VISUELLEN UMGEBUNG)

Tobias Bockhorst and Uwe Homberg

Im vorigen Kapitel wurden Dynamiken im Antwortverhalten von Kompassneuronen im Zentralkomplex des Heuschreckengehirns beschrieben. Diese sind geeignet, das Ausgangssignal des Kompassnetzwerks so zu kontextualisieren – es beispielsweise nur *Änderungen* der Bewegungsrichtungen anzeigen zu lassen – dass es zur Steuerung gezielt gerichteter Fortbewegung genutzt werden kann. Rosner und Homberg (2013) zeigten, dass diese Kompass- oder ´head direction´-Neurone im Hirn der Heuschrecke auch auf Stimulation mit visuellen Mustern aus unpolarisiertem Licht reagieren. Insbesondere antworteten die Zellen auf die simulierte Annäherung eines Objektes (Looming); zudem wurden einige Antworten auf kleine ´vorbeiziehende´ Objekte gezeigt. Derartige Reize können bei Heuschrecken Fluchtreaktionen (Wegspringen, Änderung der Flugrichtung) auslösen, welche über schnelle, periphere Pfade mit absteigenden Neuronen zur visuell vermittelten Bewegungssteuerung kontrolliert werden (Rind et al. 2008, Fotowat et al. 2011, McMillan and Gray 2012). Die Tatsache, dass zudem auch Neurone im Zentralkomplex (welcher nicht Teil dieser schnellen peripheren Pfade ist) auf derartige Reize antworteten, deutet auf eine weitere Ebene der Kontextabhängigkeit neuronaler Antworten im Kompassnetzwerk hin: die Berücksichtigung kritischer Ereignisse in der Außenwelt. Diese kritischen Ereignisse könnten etwa in der Annäherung eines Fressfeindes oder der drohenden Kollision mit einem Artgenossen in einem dichten Schwarm entsprechen. Bei der Fliege (*Drosophila*) haben Läsionsstudien gezeigt, dass die Funktionalität eines landmarkenbasierten Ortsgedächtnisses von Eingangsneuronen des Zentralkomplexes abhängt (Ring-Neurone, welchen den TL-Neuronen der CBL bei der Heuschrecke entsprechen; Ofstad et al. 2011). Zudem zeigten Seelig und Jayaraman (2013) bei Neuronen vom gleichen Grundtyp Antworten auf diesen Landmarken ähnelnde, balkenartige Objekte (Antworten auf polarisiertes Licht sind dagegen für Zentralkomplexneurone der Fliege bis dato nicht veröffentlicht worden). Hierbei zeigten die Neurone ein Tuning auf die Position der Objekte in der Umgebung der Fliege sowie auf die Winkelorientierung ihrer Kanten.

Vor diesem Hintergrund sollte an der Heuschrecke untersucht werden, ob die Kompassneurone im Zentralkomplex in Bezug auf visuelle Objekte generell auf deren Bewegung antworten – wie es im Falle der Looming-Antworten wahrscheinlich ist – oder zudem eine Repräsentation von Landmarken bieten. Hierzu wurden die polarisations-sensitiven Neurone auf Responsivität gegenüber verschiedensten Stimuli aus unpolarisiertem Licht hin untersucht. Dabei waren die grundlegenden Methoden für Ableitungen und histologische Aufbereitung der Präparate dieselben wie in Kapitel I; tatsächlich gingen viele Zellen in die Datensätze aller drei Kapitel der Dissertation ein. Zur Stimulation mit unpolarisiertem Licht diente ein 22“ CRT-Monitor, welcher einen Sehfeldbereich von -45° bis 60° in der Horizontalen und -32° bis 28° in der Vertikalen überdeckte. Zur Messung von

Hintergrundaktivität und als visuellen Hintergrund für Objektreize zeigte der Monitor eine einheitlich graue Fläche. Zu den Objektreizen zählten insbesondere stationär und in Bewegung (Rotation oder Translation, d.h. ´Vorbeiziehen´) präsentierte Streifenmuster oder Objekte, welche sich hinsichtlich Form, Größe, Position unterschieden.

In den endgültigen Datensatz gingen 17 Neurone aus 17 Tieren ein; darunter 3 CL1-, 4 TB1-, 5 CPU1- und 5 CPU2-Neurone. TL-Neurone, welche den in der Fliege untersuchten Zelltypen entsprächen wurden nicht getroffen – abgesehen von einer Zelle, welche jedoch nicht auf die Objektreize antwortete.

Bei den Antworten auf die Objektreize wurde weder eine Repräsentation von Objektpositionen, noch eine solche von Objektmerkmalen wie Kantenorientierung beobachtet. Allerdings antworteten die Neurone generell nur auf distinkte Objekte in Bewegung, während ´großflächige´ Bewegungsmuster (Streifenmuster) und stationäre Objekte unbeantwortet blieben. Alle Zelltypen antworteten auf Translationsbewegungen (70°/s) eines schwarzen Rechtecks von etwa 2° x 1.5° Größe (in Sehwinkel-Einheiten). Zur genaueren Charakterisierung des Antwortverhaltens wurden Bewegungsrichtung und die Trajektorie (Bewegungsbahn, d.h. der vom bewegten Rechteck ´durchzogene´ Bereich auf dem Monitor) systematisch variiert. Es wurden verschiedene Abfolgen von aufwärts- und abwärtsgerichtete Bewegungen entlang vertikaler Trajektorien sowie Vorwärts- und Rückwärtsbewegungen entlang horizontaler Trajektorien verwendet. Diese ´Stimulusbatterien´ beinhalteten sowohl wiederholte Präsentationen derselben Kombination aus Bewegungsrichtung und Trajektorie als auch unvermittelte Änderungen der Bewegungsrichtung und / oder der Trajektorie.

Antworten waren bei CL- und CPU-Neuronen stets inhibitorisch und bei TB-Neuronen stets exzitatorisch. Die Antworten auf den jeweils ersten Reiz in einer Stimulusbatterie waren unabhängig von Bewegungsrichtung und Trajektorie. Bei wiederholter Präsentation desselben Reizes nahmen die Antworten schnell ab. Allerdings konnte diese Adaptation gebrochen werden, wenn (mindestens) die Trajektorie gewechselt wurde, während eine bloße Änderung der Bewegungsrichtung entlang derselben Trajektorie für gewöhnlich nicht diesen Effekt hatte. Offenbar handelte es sich somit um einen Fall von ´region-specific adaptation´, also einer spezifischen Adaption mit Bezug auf den vom Reiz abgedeckten Bereich im Sehfeld.

Allerdings waren die Neurone keinesfalls ´blind´ für die Bewegungsrichtung des Objektes – sie antworteten nur in einer sehr kontextabhängigen Weise, genauer gesagt, nur unter bestimmten Bedingungen auf Richtungsänderungen. So etwa in Fällen bei welchen (an denselben Zellen) eine komplexere Reizsequenz verwendet wurde, die ein Hintergrundmuster aus schwarzen Rechtecken beinhaltete. Dieses wurde zunächst unbewegt eingeblendet und begann dann abrupt, sich zu bewegen. Nach einigen Bewegungszyklen ´trat ein einzelnes Rechteck aus der Masse heraus´, indem es seine Bewegungsrichtung von rückwärts, d.h. mit dem Hintergrundfluss zu vorwärts, d.h. gegen den Hintergrundfluss änderte. Dieser ´pop out´ eines distinkten Objektes aus dem visuellen Hintergrund löste bei den Neuronen Antworten aus, die jenen auf den ersten Reiz der zuvor beschriebenen einfachen Stimulusbatterien entsprachen. In eben diesen einfachen Reizfolgen aber hatte ein bloßer Richtungswechsel vor dem einheitlich grauen (´leeren´) Hintergrund keine Antwort ausgelöst (siehe oben).
Zwar wurde eine Detektion kleiner ´Zielobjekte´ vor einem visuellen Hintergrundmuster bereits eingehend in peripheren visuellen Neuronen der

Libelle beschrieben (siehe O´Carroll 1993). Jedoch wurden bei diesen ´Zielobjekte´ verwendet, die sich hinsichtlich Größe und Kontrast stark vom Hintergrundmuster abhoben, sodass das Detektionsvermögen der Libellenneurone als extrem größen- und kontrastselektive Bewegungsempfindlichkeit erklärbar ist. Im Falle der hier untersuchten Neurone der Heuschrecke gründet die Abgrenzung des distinkten Objektes gegen den Hintergrundfluss (aus identischen und ähnlichen Objekten) offenbar auf höheren Prinzipien der Gruppierung von physikalischen Objekten in verschiedene ´Wahrnehmungsobjekte´. Elementare Regeln dieser Gruppierung sind in den sog. Gestaltprinzipien der Wahrnehmungspsychologie formuliert (siehe z.B. Goldstein 2007). Der hiesige Fall könnte dem Prinzip des ´gemeinsamen Schicksals´ entsprechen: Was sich gemeinsam bewegt (oder andersartig verändert), wird zu einem Wahrnehmungsobjekt gruppiert. Was sich in andere Richtungen bewegt, bildet ein anderes Wahrnehmungsobjekt. Erwähnenswert ist hierbei noch, dass erneut keine Antwort auf den ´großflächigen´ Hintergrundfluss an sich auftrat.

Insgesamt deuten sowohl die Adaptation auf Reizpräsentation im selben Sehfeldbereich als auch die ´Gestalt-basierten´ Antworten bei komplexeren Objekt-Hintergrund-Szenarien darauf hin, dass die untersuchten CL-, TB- und CPU-Neurone spezifisch auf das *Neuauftreten eines bewegten Objekts* in der Außenwelt antworten. Ähnlich der Antworten auf Looming-Reize (Rosner and Homberg 2013) signalisierten sie somit ´kritische´ Ereignisse, ohne jedoch die Positionen oder Merkmale der beteiligten Objekte zu repräsentieren – d.h., sie leisteten eine Form von ´novelty detection´. Zusammen mit ihren Antworten auf Kompassreize ergibt sich das Bild einer visuellen Bimodalität (Kompasssinn und Objektsehen), welche dazu dienen könnte, die Information über das plötzliche Auftreten eines bewegten Einzelobjektes in die kompassgestützte Bewegungskontrolle einfließen zu lassen. Diese wiederum könnte der ´Vermittlung´ zwischen der Notwendigkeit, auf diese Ereignisse zu reagieren – etwa vor einem Feind zu fliehen – und dem dauerhaften Ziel der Fortbewegung in eine bestimmte Richtung dienen.

Der Unterschied zu den positions- und objektmerkmalsabhängigen Antworten von Neuronen bei *Drosophila* lässt sich möglicherweise im Sinne unterschiedlicher Lebensweisen bzw. verschiedener Schwerpunkte bei den Strategien räumlicher Orientierung erklären. Zwar wurde auch bei *Drosophila* im Laborversuch Polarotaxis demonstriert (Weir and Dickinson 2012), jedoch agieren Fliegen für gewöhnlich in Habitaten überschaubarer Größen, welche reich an geeigneten Landmarken sind. Hingegen legen Wüstenheuschrecken häufig größere Distanzen in karger Umgebung zurück, wobei höchstwahrscheinlich eine kompassgestützte Orientierung betrieben wird. Allerdings ist ebenso möglich, dass in beiden Tieren parallele neuronale Netzwerke für Kompass- und Landmarkenorientierung bestehen.

Neben der oben beschriebenen Kontextabhängigkeit der Antworten auf bewegte Objekte zeigte sich erneut ein Einfluss der Hintergrundaktivität auf die sensorischen Antworten der CL-, TB- und CPU-Neurone. Erhöhte Hintergrundaktivität kann die inhibitorischen Antworten von CL- und CPU-Neuronen maskieren und die relative Amplitude exzitatorischer Antworten (TB-Neurone) herabsetzen. Um diesen Effekt quantitativ zu erfassen, wurde die Korrelation zwischen Spike-Raten berechnet, welche kurz vor der Reizung bzw. während der Reizung gemessen wurden. Es zeigte sich eine hochsignifikante, starke Korrelation (70% erklärte Varianz). Aus statistischen Gründen war diese Analyse auf CPU-Neurone beschränkt. Allerdings beinhalteten die Hintergrundaktivitätsmuster aller Neuronentypen Zustände von solch hoher

bzw. niedriger Spike-Rate, dass eine vollständige Maskierung der Antworten auf bewegte Objekte möglich erscheint. Diese Maskierung könnte dazu dienen, novelty-Informationen von einer vom Zentralkomplex vermittelten Bewegungssteuerung auszuschließen, falls sie in der gegenwärtigen Situation unbedeutend sind. Wie bereits die analogen Dynamiken von *E*-Vektor-Antworten stellen die beobachtete Maskierung und Stimulus-spezifische Adaptation Parallelen zu höherer sensorischer Prozessierung im Cortex des Wirbeltiergehirns dar (siehe Kapitel I).

KAPITEL III: GAIN MODULATION OF COMPASS SIGNALING BY SALIENT OBJECT MOTION IN AN INSECT BRAIN

(GAIN MODULATION VON KOMPASSANTWORTEN DURCH SALIENTE BEWEGUNGSREIZE)

Tobias Bockhorst und Uwe Homberg

Die vorigen Kapitel widmeten sich der Charakterisierung von Antworten auf polarisiertes Licht (Kompassantworten) bzw. auf das Auftreten bewegter Objekte (Objektantworten) bei Neuronen des Zentralkomplexes der Heuschrecke. Beide Antworttypen wurden in denselben Zellen unter ´unimodaler´ Stimulation gemessen – es wurde also bei jeder Messung entweder ein Kompassreiz oder ein Objektreiz dargeboten. Durch eine dritte Reihe von Tests sollte ergründet werden, wie sich die Bimodalität dieser Zellen äußert, wenn tatsächlich Reize aus beiden Domänen zusammenfallen – wie es unter natürlichen Bedingungen etwa während des Fluges in einem Schwarm häufig der Fall sein dürfte. Zu diesem Zwecke wurde bei einigen CL1-, TB1-, CPU1- und CPU2-Neuronen zusätzlich zu den in Kapitel I und II beschriebenen Stimulationen eine kombinierte Stimulation mit stationären *E*-Vektor-Winkeln und bewegten Objekten durchgeführt. Bei allen zu echter polarization-opponency ´fähigen´ Zellen (also TB1, CPU1 und CPU2) umfasste dies sowohl erregende als auch hemmende *E*-Vektoren. Die Bewegungsreize wurden erst dargeboten, nachdem die Kompassantworten wie in Kapitel I beschrieben durch *E*-Vektor-spezifische Adaptation abgeklungen waren. Insgesamt kommt die Stimulation damit einem Szenario nahe, in welchem die Heuschrecke nach einigen Sekunden der Fortbewegung in dieselbe Richtung mit dem Erscheinen eines bewegten Objektes konfrontiert wird.

Um diesen Effekt zu quantifizieren, wurden während der kombinierten Stimulation auftretende Spike-Raten gemessen. Diese Spike-Raten wurden mit jenen der vorangehenden nicht-adaptierten (frühen) *E*-Vektor-Antwort verglichen (jeweils 5 Sekunden Fensterlänge). Beide Spike-Raten wurden hierbei zunächst auf einen gemeinsamen Vergleichswert, nämlich die Spike-Rate der adaptierten *E*-Vektor-Antwort, normalisiert.

CL1-Neurone antworteten auf kombinierte Stimulation wie bei alleiniger Präsentation des bewegten Objektes mit Inhibition. Dieses Antwortverhalten bringt mit sich, dass bei hemmenden *E*-Vektoren unter kombinierter Stimulation wiederum eine Antwort auftritt, welche der ursprünglichen, abgeklungenen *E*-Vektor-Antwort entspricht. Bei nicht-hemmenden *E*-Vektor-Winkeln führt diese lineare Integration (´Addition´) der abgeklungenen Kompassantwort und der hemmenden Objektantwort dagegen zu einem aus der Warte des Kompasssinnes ´widersprüchlichen´ Ergebnis: die kombinierte Antwort ist hemmend, während der neutrale *E*-Vektor eigentlich Hintergrundaktivität ´fordert´. Es kommt hier also zu einer Art destruktiver Interferenz durch lineare Integration von Kompass- und Objektantwort. Ein vergleichbares Antwortverhalten wurde auch bei zwei TB1-Neuronen und einem CPU1-Neuron beobachtet, welche im Gegensatz zu CL1-Zellen polarization opponency zeigten. Dementsprechend traten bei den TB-Neuronen (exzitatorische Objektantwort) bei hemmenden *E*-Vektoren und im Falle des CPU1-Neurons (hemmende Objektantwort) beim erregenden *E*-Vektor ´paradoxe´ Antworten auf kombinierte Stimulation auf.

Sechs weitere Neurone (3 TB1-Neurone, ein CPU1-Neuron und zwei CPU2-Zellen) zeigten ein völlig anderes Antwortverhalten. Bei diesen traten keine deutlichen Antworten auf alleinige Präsentation des bewegten Objektes auf; ihre Antworten auf hemmende und erregende *E*-Vektor-Winkel waren eher phasisch-tonisch als phasisch – sie klangen also nicht vollständig auf das Niveau der Hintergrundaktivität ab. Bei kombinierter Stimulation kam es zu einem *nicht*-linearen Effekt: Das Auftreten des bewegten Objektes führte zu einer Wieder-Verstärkung der residualen Kompassantwort. Hierbei hatte also *derselbe* Objektreiz einen *hemmenden* Effekt bei gleichzeitiger Darbietung eines hemmenden *E*-Vektors und einen *erregenden* Effekt bei gleichzeitiger Darbietung eines erregenden *E*-Vektors. Bei intermediären, also ´neutralen´ *E*-Vektor-Winkeln trat keine Antwort bei kombinierter Reizpräsentation auf.

Ich betrachte dieses Antwortverhalten als eine weitere Form kontextabhängiger Kompassaktivität neben *E*-Vektor-spezifischer Adaptation, Antizipation und Maskierung (Kapitel I) und als einen ungewöhnlichen Fall von ´**gain modulation**´. Dieser Begriff bezeichnet für gewöhnlich Prozesse, bei welchen Verhaltenszustände (z.B. ruhend im Gegensatz zu fliegend) einen Einfluss auf die Amplitude sensorischer Antworten haben (siehe unten). Diese Effekte waren länger anhaltend als die bei linearer Integration beobachteten Objektantworten. Genauer gesagt entsprach ihre Dauer etwa jener der starken, frühen (noch nicht-adaptierten) *E*-Vektor-Antwort.

Zur quantitativen Analyse wurde untersucht, ob eine Korrelation zwischen den Spike-Raten der nicht-adaptierten *E*-Vektor-Antworten und jenen der zugehörigen Antworten auf kombinierte Stimulation besteht. Dies wurde sowohl für jede einzelne Zelle als auch für den Gesamtdatensatz durchgeführt (Einschlusskriterium war eine Mindestzahl von 10 kombinierten Stimulationen der Zelle, welche sowohl erregende als auch hemmende *E*-Vektor-Winkel beinhalten musste). Bei 5 der 6 Zellen zeigten sich signifikante ($p<0.05$), starke Korrelationen mit 33 bis 85% erklärter Varianz. Eines der CPU2-Neurone zeigte zwar keine signifikante Korrelation, jedoch einen entsprechenden Trend. Der Gesamtdatensatz der fünf übrigen Zellen (101 Messungen) ergab erneut eine signifikante Korrelation, welche insgesamt etwa 34% der Varianz erklärte.

Die durch gain modulation sozusagen wieder-erweckten Kompassantworten erschienen stark und langanhaltend genug, um mit den nicht-adaptierten Kompassantworten zu Beginn der Präsentation eines stationären *E*-Vektors vergleichbar zu sein. Sie sollten also eine ´adäquate´ Repräsentation von Kompassinformation bieten. Diese könnte etwa der Planung von Ausweichmanövern unter gleichzeitiger Berücksichtigung einer weiterhin angestrebten Bewegungsrichtung dienen. Eine kurz vor einem Ausweichmanöver erneut auftretende Repräsentation der bisherigen Bewegungsrichtung könnte die Grundlage für eine Art Gedächtnisspur dieser Richtungsinformation bilden. Nach einem Ausweichmanöver könnte diese dann mit der veränderten Bewegungsrichtung verglichen werden, um sich wieder ´auf Kurs begeben´ zu können, sobald die Gefahr gebannt ist. Sollte tatsächlich ein Ausweichmanöver stattfinden, so würde dieses zu einer Bewegung der Heuschrecke relativ zum Himmelspolarisationsmuster führen. Die dabei ausgelösten Antworten auf sich verändernde *E*-Vektor-Winkel (s. Kapitel I) könnten dann mit der hypothetischen Gedächtnisspur verglichen werden. Dies würde zu einer bereits bei Fliegen gezeigten Rolle des Zentralkomplexes für das visuell-räumliche Arbeitsgedächtnis passen (Neuser et al. 2008).

Eine lineare Integration von Kompass- und Objektantworten muss nicht zwangsläufig zu einer Störung der Kompassorientierung führen. Antworten – oder Hintergrundaktivitäten – die

keinen Bezug zu *E*-Vektoren haben, könnten durch hemmende Verschaltungen zwischen ´Ausgangskanälen´ des Zentralkomplexes ausgeglichen werden (siehe Anhang ADDENDUM TO CHAPTER III). Wenn hierbei die hemmend verschalteten Ausgänge entgegengesetzte *E*-Vektor Vorzugsrichtungen haben, so könnte die *E*-Vektor Information diesen Ausgleich ´überleben´, da sie in beiden Kanälen gegensinnig wäre – während die übrige, in beiden Kanälen gleichsinnige Aktivität ´weggehemmt´ werden könnte.

Mit Blick auf mögliche neuronale Mechanismen vermute ich weiterhin, dass sich sowohl lineare Integration als auch gain modulation mittels des in Kapitel I eingeführten Verschaltungsmusters erklären lassen könnten. Sie würden dann auf zwei unterschiedliche ´Betriebszustände´ des Kompassnetzwerks zurückgehen und nicht etwa zwei verschiedenen Zellpopulationen entsprechen. Wie in Abbildung 8 gezeigt, würde gain modulation dann auftreten, wenn die Antworten auf stationäre *E*-Vektoren phasisch-tonisch und nicht rein phasisch sind. Tatsächlich ging die beobachtete gain modulation oft mit solchen phasisch-tonischen Antworten einher.

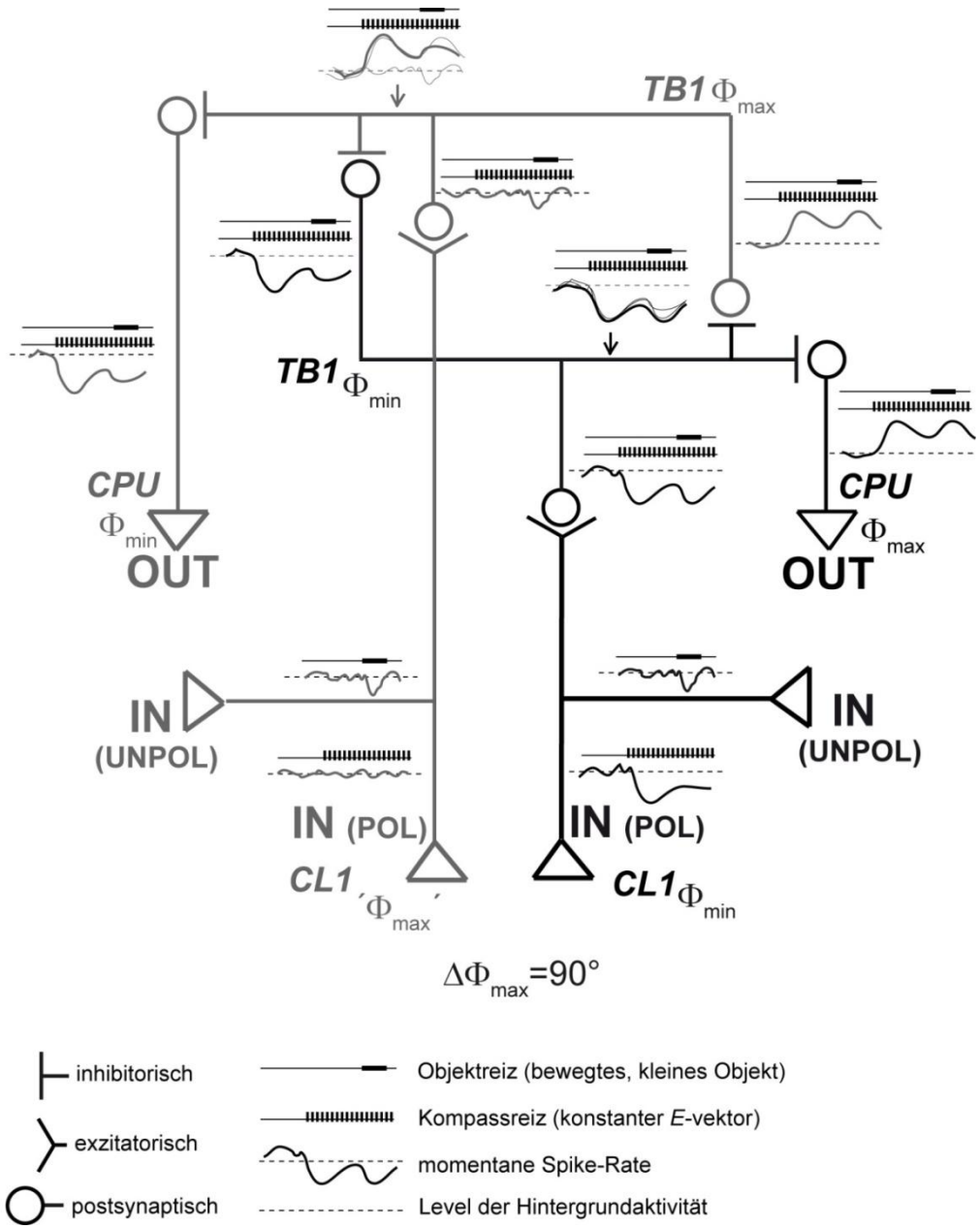

Abb. 8. Ein erweitertes Verschaltungsmodell des Zentralkomplexes erklärt Antworten auf kombinierte Reizung mit polarisiertem Licht und bewegten Objekten. Gezeigt ist ein putatives Muster von Verschaltungen und resultierenden Antworten von CL-, TB- und CPU-Zellen im Zentralkomplex (siehe Abbildung 7 für Details). Das Schlüsselelement bildet die gegenseitige (Ent-)Hemmung zweier TB-Neurone, welche Eingänge von CL1-Neuronen mit entgegengesetztem *E*-Vektor-Tuning erhalten (Φ_{max}=90°). Diese 'antagonistische Integration' erklärt, wie es bei TB-Neuronen zu echter ´polarization-opponency´ - d.h. zu erregenden *und* hemmenden *E*-Vektor-Antworten - kommt, während die vorgeschalteten CL1-Zellen lediglich eine hemmende Antwort bei ihrem jeweiligen Φ_{min} zeigen, nicht jedoch eine Erregung bei einem entsprechenden Gegenvektor (s. Kapitel I). CL1-Neurone wurden ebenso bei alleiniger Präsentation bewegter Objekte und bei Kombinationen von Kompass- und Objekt-Reizen gehemmt; unabhängig vom *E*-Vektor-Winkel. Verläuft die hemmende Kompassantwort des CL1-Neurons auf seinen Φ_{min} (schwarze Bahn) nicht rein phasisch, sondern phasisch-*tonisch*, so sollte die kombinierte Antwort dieses Neurons stärker ausfallen als jene der CL-Zelle mit entgegengesetztem *E*-Vektor-Tuning (graue Bahn), welche auf ihren 'Φ_{max}' neutral ´antwortet´. Durch die gegenseitige (Ent-)Hemmung der nachgeschalteten TB-Neurone bewirkt dieser Unterschied zwischen den Amplituden der CL1-Antworten die bei TB1- und CPU-Zellen beobachtete *gain modulation*. Dünne (dicke) Graphen symbolisieren die Antworten auf getrennte (kombinierte) Stimulation durch Kompass- und Bewegungsreize, 'gemessen' an den durch die kleinen Pfeile markierten Bereichen der Neurone. IN, OUT: Ein- bzw. Ausgänge des Schaltkreises; (UN)POL: Antworten auf (un-)polarisiertes Licht. Nicht dargestellt ist die Situation bei rein phasischer Kompassantwort der CL1-Neurone. Eine solche würde durch das vollständige Abklingen der Antwort auf das Niveau der Hintergrundaktivität zu gleich hoher Amplitude der kombinierten Antworten der CL-Neurone führen. Somit würde die Grundlage der gain modulation wegfallen und auch bei TB- und CPU-Zellen eine rein lineare Integration auftreten. Eine gewisse Variabilität der gain modulation könnte auf die ausgeprägte Dynamik der Hintergrundaktivität der vorgeschalteten CL1-Neurone zurückgehen (nicht dargestellt).

Hier gründet die gain modulation auf der Integration des Inputs von zwei verschiedenen Sinnen der Außenwahrnehmung: Kompasssinn und Objektsehen. Dies unterscheidet sich von Effekten des Bewegungszustandes auf die Höhe von Hintergrundaktivität und / oder visuellen Antworten von Zentralkomplexneuronen (Weir et al. 2014, Seelig and Jayaraman 2013, Homberg 1994). Unter Verwendung von Duftreizen konnte ebenfalls an Zentralkomplexneuronen der Fliege gezeigt werden, dass sensorische Antworten von *internen* Zuständen (Sattheit bzw. Hunger), sowie vom *(unimodalen) exterozeptiven Kontext* – etwa der gleichzeitigen Anwesenheit verschieden wertiger Duftquellen – abhängen (Beshel and Zhong 2013). Ferner ist eine Bedeutung des Zentralkomplexes für das visuelle Objekt-, Arbeits- und Orts-Gedächtnis von Fliegen belegt (Liu et al. 2006, Pan et al. 2009, Neuser et al. 2008, Ofstad et al. 2011). Zusammen mit den hier gewonnenen Erkenntnissen ergibt sich ein Bild des Zentralkomplexes als höheres Prozessierungszentrum des Insektengehirns, welches Verhaltensziele, interne Zustände des Tieres und Reizeingänge der Außenwahrnehmung vereint, um zielgerichtete Fortbewegung zu steuern.

FAZIT

EINE VIELZAHL von Studien an unterschiedlichen Insektenspezies identifizierte den Zentralkomplex des Insektengehirns als ein höheres Integrationszentrum mit besonderer Bedeutung für die Kontrolle zielgerichteter Fortbewegung. Über rein sensorische (taktile, visuelle, olfaktorsiche) Antworten hinaus wurden solche gezeigt, die zusätzlich vom Bewegungszustand der Tiere (z.B. ruhend oder fliegend) bzw. von inneren Zuständen (etwa Sattheit oder Hunger) abhingen. In ihrer Summe deuten diese Phänomene darauf hin, dass die Rolle des Zentralkomplexes bei der Kontrolle zielgerichteter Fortbewegung auf einer ´Kontextualisierung´ sensorischer Antworten gründet, welche Eingänge aus der Innen- und Außenwahrnehmung integriert.

Die vorliegende Dissertation stützt dieses Konzept durch Erkenntnisse zu Antworten von Zentralkomplexneuronen der Heuschrecke auf Kompassreize und visuelle Objekte. Insbesondere konnte gezeigt werden, dass Kompassantworten durch das Auftreten sich bewegender Objekte im Umfeld des Tieres mitbestimmt werden. Eine derartige Interaktion zwischen zwei Modalitäten der Außenwahrnehmung (Kompasssinn und Objektsehen) ist unseres Wissens nach bisher nicht für Neurone im Zentralkomplex berichtet worden. Weitere Kontextualisierungen von Kompassantworten durch Antizipation, Adaptation und konditionale Maskierung erscheinen besonders dazu geeignet, die sensori-motorische Transformation voranzutreiben – d.h. die Umwandlung von rein sensorischen Antworten in motorische Kommandos zur Steuerung polarotaktischer Fortbewegung.

Über den Forschungsgegenstand hinaus belegt die vorliegende Arbeit wie einige vor ihr die besondere Eignung des Insektengehirns für die Untersuchung der Fragestellung: Wie selektiert das Nervensystem sensorische Eingänge, wie gewichtet es diese und wie integriert es sie zum Zwecke der Kontrolle von gezielter Interaktion zwischen Individuum und Umgebung? Im Falle des Zentralkomplexes der Heuschrecke umfasst die Antwort wie hier gezeigt einige Parallelen zur aufmerksamkeitsabhängigen Verarbeitung von Sinnesreizen im Cortex des Wirbeltiergehirns.

QUELLEN

Arieli A, Sterkin A, Grinvald A, Aertsen A. Dynamics of ongoing activity: explanation of the large variability in evoked cortical responses. *Science* 273: 1868-1871, 1996.

Ashida G, Wagner H, Carr CE. Processing of phase-locked spikes and periodic signals. In: *Analysis of Parallel Spike Trains*, edited by Grün S and Rotter S. Springer, 2010. p. 59-74.

Bech M, Homberg U, Pfeiffer K. Receptive fields of locust brain neurons are matched to polarization patterns of the sky. *Curr Biol* 24: 2124-2129, 2014.

Berens P. CircStat: A MATLAB toolbox for circular statistics. *J Stat Soft* 31: 10, 2009.

Beshel J, Zhong Y. Graded encoding of food odor value in the *Drosophila* brain. *J Neurosci* 33: 15693–15704, 2013.

Boly M, Balteau E, Schnakers C, Degueldre C, Moonen G, Luxen A, Phillips C, Peigneux P, Maquett P, Laureys S. Baseline brain activity fluctuations predict somatosensory perception in humans. *Proc Natl Acad Sci U.S.A. (PNAS)* 104: 12187-12192, 2007.

Brunner D, Labhart T. Behavioural evidence for polarization vision in crickets. *Physiol Entomol* 12: 1-10, 1987.

Chapman JW, Reynolds DR, Wilson K. Long-range seasonal migration in insects: mechanisms, evolutionary drivers and ecological consequences. *Ecology Letters* 18: 287-302, 2015.

Cheng K, Middleton EJT, Wehner R. Vector-based and landmark-guided navigation in desert ants of the same species inhabitating landmark-free and landmark-rich environments. *J Exp Biol* 215: 3169-3174, 2012.

Clark BJ, Taube JS. Vestibular and attractor network basis of the head direction cell signal in subcortical circuits. *Front Neural Circuits* 6, 2012.

Collett M, Chittka L, Collett TS. Spatial memory in insect navigation. *Curr Biol* 23: R789-R800, 2013.

Dacke M, Nordström P, Scholtz CH, Warrant EJ. A specialized dorsal rim area for polarized light detection in the compound eye of the scarab beetle *Pachysoma striatum*. *J Comp Physiol A* 188: 211- 216, 2002.

Dacke M, Nordström P, Scholtz C. Twilight orientation to polarised light in the crepuscular dung beetle *Scarabaeus zambesianus*. *J Exp Biol* 206: 1535-1543, 2003.

Dacke M, Byrne MJ, Baird E, Scholz CH, Warrant EJ. How dim is dim? Precision of the celestial compass in moonlight and sunlight. *Philos Trans R Soc Lond B Biol Sci* 366: 697-702, 2011.

Donlea JM, Pimentel D, Miesenböck G. Neuronal machinery of sleep homeostasis in *Drosophila*. *Neuron* 81: 860–872, 2014.

Eggers A, Gewecke M. The dorsal rim area of the compound eye and polarization vision in the desert locust (*Schistocerca gregaria*). In: *Sensory Systems of Arthropods*, edited by Wiese K, Gribakin FG, Popov AV, and Renninger G. Birkhäuser, 1993. p. 101-109.

elJundi B, Smolka J, Baird E, Byrne M, Dacke M. Diurnal dung beetles use the intensity gradient and polarization pattern of the sky for orientation. *J Exp Biol* 217: 2422-2429, 2014*A*.

elJundi B, Pfeiffer K, Heinze S, Homberg U. Integration of polarization and chromatic cues in the insect sky compass. *J Comp Physiol A* 200: 575-589, 2014*B*.

Fisher NI. Statistical Analysis of Circular Data. Revised edition. Cambridge University Press, 1995.

Fotowat H, Harrison RR, Gabbiani F. Multiplexing of motor information in the discharge of a collision detecting neuron during escape behaviors. *Neuron* 69: 147-158, 2011.

Frost BJ, Mouritsen H. The neural mechanisms of long distance animal navigation. *Curr Opin Neurobiol* 16: 481-488, 2006.

Goldstein EB. Perceiving objects. In: Goldstein EB, editor. Sensation and Perception (7th edition). Belmont, CA: Thomson-Wadsworth; 2007. pp. 93-119.

Gutfreund Y. Stimulus-specific adaptation, habituation and change detection in the gaze control system. *Biol Cybern* 106: 657-668, 2012.

Heinze S, Homberg U. Maplike representation of celestial *E*-vector orientations in the brain of an insect. *Science* 315: 995-997, 2007.

Heinze S, Homberg U. Neuroarchitecture of the central complex of the desert locust: intrinsic and columnar neurons. *J Comp Neurol* 511: 454-478, 2008.

Heinze S, Homberg U. Linking the input to the output: new sets of neurons complement the polarization vision

network in the locust central complex. *J Neurosci* 29: 4911–4921, 2009.

Heinze S, Reppert SM. Sun compass integration of skylight cues in migratory monarch butterflies. *Neuron* 69: 345-358, 2011.

Heinze S, Gotthardt S, Homberg U. Transformation of polarized light information in the central complex of the locust. *J Neurosci* 29: 11783–11793, 2009.

Hesselmann G, Kell CA, Eger E, Kleinschmidt A. Spontaneous local variations in ongoing neural activity bias perceptual decisions. *Proc Natl Acad Sci U.S.A. (PNAS)* 105: 10984–10989, 2008.

Homberg U. Flight-correlated activity changes in neurons of the lateral accessory lobes in the brain of the locust *Schistocerca gregaria*. *J Comp Physiol A* 175: 597-610, 1994.

Homberg U, Paech A. Ultrastructure and orientation of ommatidia in the dorsal rim area of the locust compound eye. *Arthropod Struct Dev* 30: 271-280, 2002.

Homberg U, Vitzthum H, Müller M, Binkle U. Immunocytochemistry of GABA in the central complex of the locust *Schistocerca gregaria*: identification of immunoreactive neurons and colocalization with neuropeptides. *J Comp Neurol* 409: 495–507, 1999.

Homberg U, Heinze S, Pfeiffer K, Kinoshita M, el Jundi B. Central neural coding of sky polarization in insects. *Philos Trans R Soc B* 366: 680-687, 2011.

Labhart T. Polarization-opponent interneurons in the insect visual system. *Nature* 331: 435-437, 1988.

Labhart T. How polarization-sensitive interneurones of crickets perform at low degrees of polarization. *J Exp Biol* 199: 1467–1475, 1996.

Labhart T, Meyer EP. Detectors for polarized skylight in insects: a survey of ommatidial specializations in the dorsal rim area of the compound eye. *Microsc Res Tech* 47: 368-379, 1999.

Liu G, Seiler H, Wen A, Zars T, Ito K, Wolf R, Heisenberg M, Liu L. Distinct memory traces for two visual features in the *Drosophila* brain. *Nature* 439: 551–556, 2006.

Mappes M, Homberg U. Behavioral analysis of polarization vision in tethered flying locusts. *J Comp Physiol A* 190: 61-68, 2004.

Marshall J, Cronin TW. Polarisation vision. *Curr Biol* 21: R101-R105, 2011.

McMillan GA, Gray JR. A looming-sensitive pathway responds to changes in the trajectory of object motion. *J Neurophysiol* 108: 1052-1068, 2012.

Merlin C, Heinze S, Reppert SM. Unraveling navigational strategies in migratory insects. *Curr Opin Neurobiol* 22: 1-9, 2011.

Müller M, Homberg U, Kühn A. Neuroarchitecture of the lower division of the central body in the brain of the locust (*Schistocerca gregaria*). *Cell Tissue Res* 288: 159-176, 1997.

Mouritsen H. Navigation in birds and other animals. *Image Vision Comput* 19: 713-731, 2001.

Netser S, Zahar Y, Gutfreund Y. Stimulus-specific adaptation: can it be a neural correlate of behavioral habituation? *J Neurosci* 31: 17811–17820, 2011.

Neuser K, Triphan T, Mronz M, Poeck B, Strauss R. Analysis of a spatial orientation memory in *Drosophila*. *Nature* 453: 1244–1247, 2008.

O'Carroll D. Feature-detecting neurons in dragonflies. *Nature* 362: 541 - 543, 1993.

Ofstad TA, Zuker CS, Reiser MB Visual place learning in *Drosophila melanogaster*. *Nature* 447: 204–207, 2011.

Ott SR, Rogers SM. Gregarious desert locusts have substantially larger brains with altered proportions compared with the solitarious phase. *Proc R Soc B* 277: 3087-3096, 2010.

Pan Y, Zhou Y, Guo C, Gong H, Gong Z, Liu L. Differential roles of the fan-shaped body and the ellipsoid body in *Drosophila* visual pattern memory. *Learn Mem* 5: 289–295, 2009.

Pfeiffer K, Kinoshita M, Homberg U. Polarization-sensitive and light-sensitive neurons in two parallel pathways passing through the anterior optic tubercle in the locust brain. *J Neurophysiol* 94: 3903–3915, 2005.

Pfeiffer K, Homberg U. Coding of azimuthal directions via time-compensated combination of celestial compass cues. *Curr Biol* 17: 960–965, 2007.

Pfeiffer K, Homberg U. Organization and functional roles of the central complex in the insect brain. *Annu Rev Entomol* 59: 165–184, 2014.

Ranck JB, Jr. Head-direction cells in the deep cell layers of dorsal presubiculum in freely moving rats. *Soc Neurosci Abstr* 10: 599, 1984.

Reppert SM, Zhu H, White RH. Polarized light helps monarch butterflies navigate. *Curr Biol* 14: 155–158, 2004.

Rind FC, Santer RD, Wright GA. Arousal facilitates collision avoidance mediated by a looming sensitive visual neuron in a flying locust. *J Neurophysiol* 100: 670-680, 2008.

Ritzmann RE, Harley CM, Daltorio KA, Tietz BR, Pollak AJ, Bender JA, Guo P, Horomanski AL, Kathman ND; Nieuwoudt C, Brown AE, Quinn RD. Deciding which way to go: how do insects alter movements to negotiate barriers? *Front Neurosci* 6: 97, 2012.

Rosner R, Homberg U. Widespread sensitivity to looming stimuli and small moving objects in the central complex of an insect brain. *J Neurosci* 33: 8122-8133, 2013.

Sakura M, Lambrinos D, Labhart T. Polarized skylight navigation in insects: model and electrophysiology of e-vector coding by neurons in the central complex. *J Neurophysiol* 99: 667-682, 2008.

Sauman I, Briscoe AD, Zhu H, Shi D, Froy O, Stalleicken J, Yuan Q, Casselman A, Reppert SM. Connecting the navigational clock to sun compass input in monarch butterfly brain. *Neuron* 46: 457–467, 2005.

Seelig JD, Jayaraman V. Feature detection and orientation tuning in the *Drosophila* central complex. *Nature* 503: 262-266, 2013.

Skaggs WE, McNaughton BL, Gothard KM, Markus EJ. An information-theoretic approach to deciphering the hippocampal code. *NIPS* 5: 1030-1037, 1993.

Skaggs WE, McNaughton BL, Wilson MA, Barnes, CA. Theta phase precession in hippocampal neuronal populations and the compression of temporal sequences. *Hippocampus* 6: 149-172, 1996.

Srinivasan MV. Honeybees as a model for the study of visually guided flight, navigation, and biologically inspired robotics. *Physiol Rev* 91: 413-460, 2011.

Stalleicken J, Labhart T, Mouritsen H. Physiological characterization of the compound eye in monarch butterflies with focus on the dorsal rim area. *J Comp Physiol A* 192: 321–331, 2006.

Strauss R. The central complex and the genetic dissection of locomotor behaviour. *Curr Opin Neurobiol* 12: 633-638, 2002.

Strauss R, Heisenberg M. A higher control center of locomotor behavior in the *Drosophila* brain. *J Neurosci* 13: 1852-1861, 1993.

Strutt JW. On the light from the sky, its polarization and colour. *Philos Mag* 41: 107-120, 274-279, 1871a.

Strutt JW. On the scattering of light by small particles. *Philos Mag* 41: 447-454, 1871b.

Supèr H, van der Togt C, Spekreijse H, Lamme VAF. Internal state of monkey primary visual cortex (V1) predicts figure–ground perception. *J Neurosci* 23: 3407–3414, 2003.

Taube JS. The head direction signal: origins and sensory-motor integration. *Annu Rev Neurosci* 30: 181-207, 2007.

Träger U, Homberg U. Polarization-sensitive descending neurons in the locust: connecting the brain to thoracic ganglia. *J Neurosci* 31: 2238 –2247, 2011.

Uvarov B. Phase Polymorphism. In: **Uvarov B.** *Grasshoppers and Locusts (Vol. 1)*. Cambridge Univ Press, London, U.K., 1966, p. 332-386.

Vitzthum H, Müller M, Homberg U. Neurons of the central complex of the locust *Schistocerca gregaria* are sensitive to polarized light. *J Neurosci* 22: 1114–1125, 2002.

von Frisch K. Die Polarisation des Himmelslichtes als orientierender Faktor bei den Tänzen der Bienen. *Experientia* 5: 142 – 148, 1949.

von Philipsborn A, Labhart T. A behavioral study of polarization vision in the fly, *Musca domestica*. *J Comp Physiol A* 167: 737-743, 1990.

Wehner R. Astronavigation in insects. *Annu Rev Entomol* 29: 277-298, 1984.

Wehner R. Desert ant navigation: how miniature brains solve complex tasks. *J Comp Physiol A* 189: 579-588, 2003.

Weir PT, Dickinson MH. Flying *Drosophila* orient to sky polarization. *Curr Biol* 22**:** 21-27, 2012.

Weir PT, Schnell B, Dickinson MH. Central complex neurons exhibit behaviorally gated responses to visual motion in *Drosophila. J Neurophysiol* 111: 62-71, 2014.

Wernet MF, Velez MM, Clark DA, Baumann-Klausener F, Brown JR, Klovstad M, Labhart T, Clandinin TR. Genetic dissection reveals two separate retinal substrates for polarization vision in *Drosophila*. *Curr Biol* 22: 12-20, 2012.

Wolf R, Gebhardt B, Gademann R, Heisenberg M. Polarization sensitivity of course control in *Drosophila melanogaster. J Comp Physiol* 139: 177-191, 1980.

SYNOPSIS

PREFACE

NERVOUS SYSTEMS facilitate purposeful interactions between animals and their environment, based on the perceptual powers, cognition and higher motor control. Through goal-directed behavior, the animal aims to increase its advantage and minimize risk. For instance, the migratory desert locust should profit from being fast in finding a fresh habitat, thus minimizing the investment of bodily resources in locomotion as well as the risk of starvation or capture by a predator en route. Efficient solutions to this and similar tasks – be it finding your way to work, the daily foraging of worker bees or the seasonal long-range migration of monarch butterflies - strongly depend on spatial orientation in local or global frames of reference. Local settings may include visual landmarks at stable positions that can be mapped onto *egocentric* space and learned for orientation, e.g. to remember a short route to a source of benefit (e.g. food) that is distant or visually less salient than the landmarks. **Compass signals** can mediate orientation to a global reference-frame (*allothetic orienation*), e.g. for locomotion in a particular compass direction or to merely ensure motion along a straight line. Whilst spatial orientation is a prerequisite of doing the *planned* in such tasks, animal survival in general depends on the ability to adequately respond to the *unexpected*, i.e. to unpredicted events such as the approach of a predator or mate. The process of identifying relevant events in the outside world that are not predictable from preceding events is termed **novelty detection**. Yet, the definition of 'novelty' is highly contextual: depending on the current situation and goal, some changes may be irrelevant and remain ´undetected´.

The present thesis describes neuronal representations of a compass stimulus, correlates of novelty detection and interactions between the two in the minute brain of an insect, the migratory desert locust *Schistocerca gregaria*. Experiments were carried out in tethered locusts with legs and wings removed. More precisely, adult male subjects in the gregarious phase (see phase theory, Uvarov 1966) that migrates in swarms across territories in North Africa and the Middle East were used. The author performed electrophysiological recordings from single neurons in the locust brain, while either the compass stimulus (Chapter I) or events in the visual scenery (Chapter II) or combinations of both (Chapter III) were being presented to the animal. Injections of a tracer through the recording electrode, visualized by means of fluorescent-dye coupling, allowed the allocation of cellular morphologies to previously described types of neuron or the characterization of novel cell types, respectively. Recordings were focused on cells of the **central complex**, a higher integration area in the insect brain that was shown to be involved in the visually mediated control of goal-directed locomotion. Experiments delivered insights into how representations of the compass cue are

modulated in a manner suited for their integration in the control of goal-directed locomotion. In particular, an interaction between compass-signaling and novelty detection was found, corresponding to a process in which input in one sensory domain (object vision) modulates the processing of concurrent input to a *different exteroceptive* sensory system (compass sense). In addition to deepening the understanding of the compass network in the locust brain, the results reveal fundamental parallels to higher context-dependent processing of sensory information by the vertebrate cortex, both with respect to spatial cues and novelty detection.

INTRODUCTION

Diurnal sky-compass cues and their relevance for spatial orientation in insects

Allothetic orientation guides adaptive locomotor behavior both in vertebrates and invertebrates (Mouritsen 2001, Frost and Mouritsen 2006). Compass cues such as the vector of the Earth's magnetic field are stable even over evolutionarily relevant periods. In addition, they are virtually ubiquitous – readily available in environments as sparse as the desert or as indifferently structured as grassland can be, in particular as seen by an insect on the ground. They hence yield a basis for the evolution of capabilities for spatial orientation hard-wired in the neural circuitry. These may serve for tasks from sudden escape in a straight direction over initial orientation in preparation for migrations to ongoing navigation-like control of steering. In particular, a variety of insect central-place foragers and migrants rely on *sky*-compass cues (Fig. 1) for spatial learning in local settings or when bridging long distances (Srinivasan 2011, Merlin et al. 2011, Cheng et al. 2012, Collett et al. 2013, Chapman et al. 2015). The most distinctive diurnal sky-compass cue is the position of the Sun (Fig. 1*A*), which is not stationary but still reliable as it moves in a predictable, cyclic manner. Yet, direct view of the Sun is often obscured by clouds or objects in the nearby environment. As a consequence, Sun-compass users may have to conclude on the Sun's position from indirect cues such as the polarization-pattern of skylight. The scattering of direct, unpolarized sunlight in the atmosphere (Rayleigh scattering; Strutt 1871a, 1871b) results in linear polarization (Fig. 1*B*), i.e. in a transformation into light with a dominant electric field-vector angle (*E*-vector angle). The observed pattern of *E*-vector angles across the sky depends on the position of the Sun relative to the observer. It can thus signal one's bearing relative to the Sun, if a sufficient portion of the pattern is visible (Bech et al., 2014). Alternatively, the *E*-vector angle in the zenith which is always perpendicular to course of the Sun (the solar meridian) may be integrated with the chromatic or intensity gradient of skylight (Fig. 1*C,C'*) to distinguish between the solar and antisolar sky hemispheres and hence conclude on the azimuthal position of the Sun (Pfeiffer and Homberg 2007, Heinze and Reppert 2011, el Jundi et al. 2014*B*). The alignment of one's direction of locomotion to a polarization-based compass signal is termed **polarotaxis**. Under an open sky, polarotactic alignment allows the animal to steer a steady bearing to the Sun when the latter is not directly visible. Polarotaxis was demonstrated in several insect species, including bees (von Frisch 1949, Wehner 1984), flies (Wolf et al. 1980, von Philipsborn and Labhart 1990, Weir and Dickinson 2012), ants (Wehner 1984, 2003), crickets (Brunner and Labhart 1987), locusts (Mappes and Homberg 2004), monarch butterflies (Reppert et al. 2004, Sauman et al.

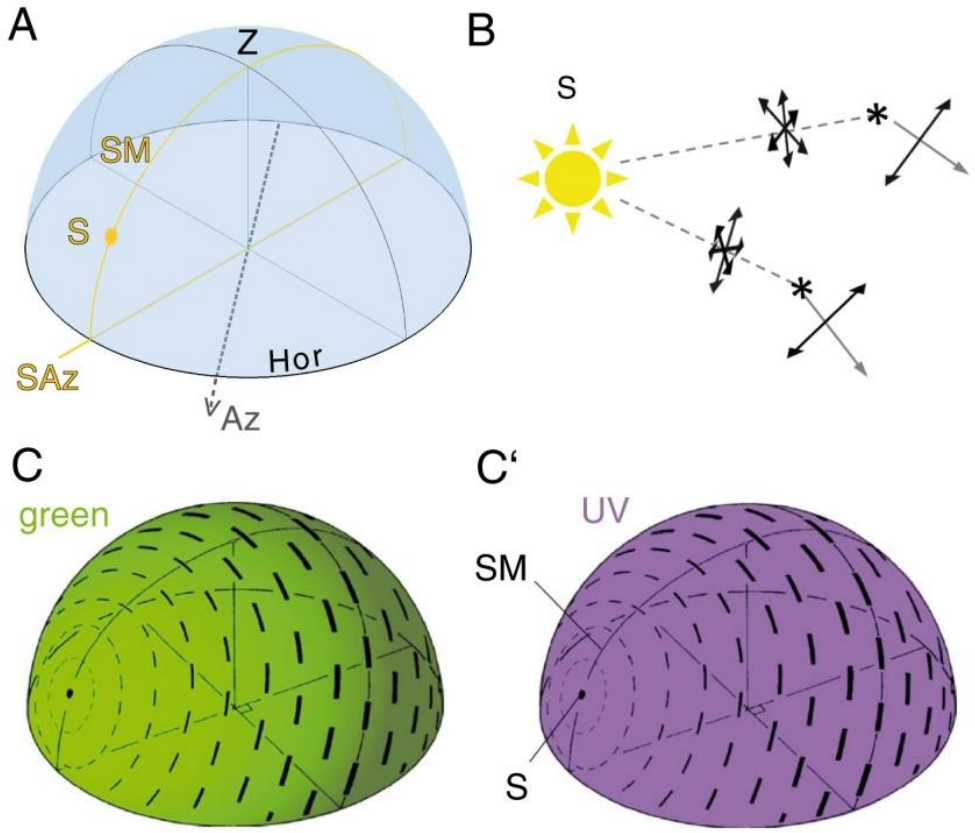

Fig. 1. Diurnal sky-compass cues. ***A*** Locomotion along a particular compass-course (dashed grey arrow in horizontal plane) can be mediated by orientation relative to the position of the Sun (S). The azimuthal component of the Sun's position, the solar azimuth (SAz), is defined as the intersection point of the geometrical horizon (Hor) and the solar meridian (SM) that depicts the diurnal course of the Sun. The angular distance between the solar azimuth and the azimuth of the path travelled (Az) gives a compass bearing for directed locomotion. Z: zenith. ***B*** If the Sun is not visible, its position can be deduced from indirect Sun-compass cues, e.g. the polarization pattern of skylight. Direct sunlight (dashed grey lines) is unpolarized, i.e. the orientations of its electric field vectors (*E*-vectors, double arrows) cover all angles in the plane perpendicular to the light beam's direction of travel. Scattering at atmospheric particles (asterisks) produces linearly polarized light (solid grey arrows) marked by a single dominant *E*-vector orientation (double arrows). ***C, C'*** The resultant dominant *E*-vector angle (black bars) depends on the position of scattering in the sky, which produces a pattern of angles mirror-symmetric to the solar meridian. The degree of polarization (bar thickness) is a function of angular distance from the Sun, being maximal along and symmetrical to a circle at 90° distance. Gross cueing of solar position is provided by the gradients in light intensity and spectrum that distinguish the solar hemisphere from the antisolar hemisphere. While the intensity of green light decreases with increasing angular distance from the Sun (***C***), short-wavelength UV light has a uniform intensity distribution (**C'**). Hemisphere plot in *A* based on a MATLAB script kindly provided by Dr. Keram Pfeiffer. *B* after Marshall and Cronin (2011). *C*, *C'* modified from el Jundi et al. (2014*B*).

2005) and dung-beetles (Dacke et al. 2003, 2011; el Jundi et al. 2014*A*). In general, polarization-dependent reception of skylight is mediated by specialized 'dorsal rim areas' of the compound eye (Fig. 2*B***;** Labhart and Meyer 1999, Eggers and Gewecke 1993, Dacke et al. 2002, Homberg and Paech 2002, Reppert et al. 2004, Stalleicken et al. 2006, Wernet et al. 2012). The tasks promoted by polarotaxis range from directed escape (in dung-beetles) over

route-learning in central-place foraging (in bees and ants) to – most likely – orientation during long-distance migrations (in locusts). Tethered flying locusts strive to attune their horizontal (azimuthal) direction of flight to slow rotations of a linear polarizer positioned in the ´zenith´ above the animal's head (Mappes and Homberg, 2004). This polarotactic steering is not longer present after occlusion of the dorsal rim areas.

Fig. 2. Morphology of the desert locust *Schistocerca gregaria*. *A* Along with neuroanatomical and behavioral differences, solitarious locusts are bigger and coloured less brightly than the gregarious animals used in the present study. ***C*** In both phases, the compound eye features a dorsal rim area (arrows, shown in top view) specialized for the polarization-plane dependent reception of blue skylight. Bar 1000 µm. *A* and *B* modified from Ott and Rogers (2010) and Homberg and Paech (2002), respectively.

The central complex: a higher integration area in the insect brain linked to goal-directed locomotion

Figure 3 illlustrates the gross anatomy of the insect (locust) brain, with emphasis on bilateral visual neuropils and the multimodal central complex (Pfeiffer and Homberg 2014). The central complex is a set of midline-spanning neuropils (Fig. 3*A,B*) that include the lower and upper divisions of the central body (CBU and CBL, respectively), the paired noduli and the protocerebral bridge (PB). These are structured into vertical slices (PB, CBU, CBL) and horizontal layers (CBU, CBL, noduli). This anatomical fine structure of the neuropils is the basis for the nomenclature of central-complex neurons. Columnar neurons connect distinct slices of the PB to the CBU (CPU-neurons) or CBL (CL-neurons). Additional branches invade the lateral complexes, the presumed main input- and output-relays of the central complex (Heinze and Homberg 2008). Tangential neurons invade many or all slices of the CBL (TL-neurons) or the PB (TB-neurons), with additional branches in the lateral complexes (TL-neurons) and the posterior optic tubercle (TB-neurons), respectively (Müller et al. 1997, Heinze and Homberg 2007). Figure 3*B* illustrates those morphologically well-described subtypes of locust central-complex neuron encountered in the present study (TL2, CL1, TB1, CPU1 and CPU2). Insights into the functional role of the central-complex are largely based on lesion studies in flies. These have identified the area as a higher integration center related to locomotor control (Strauss 2002, Strauss and Heisenberg 1993; in cockroaches: Ritzmann et al. 2012), visual pattern- and working memory (Liu et al. 2006, Pan et al. 2009, Neuser et al. 2008), visually mediated place learning (Ofstad et al. 2011), and homeostatic sleep-control (Donlea et al. 2014). Furthermore, the fly central-complex is involved in encoding food odor value, i.e. the olfactorily mediated, behaviorally expressed relative attractiveness of a food source (Beshel and Zhong 2013).

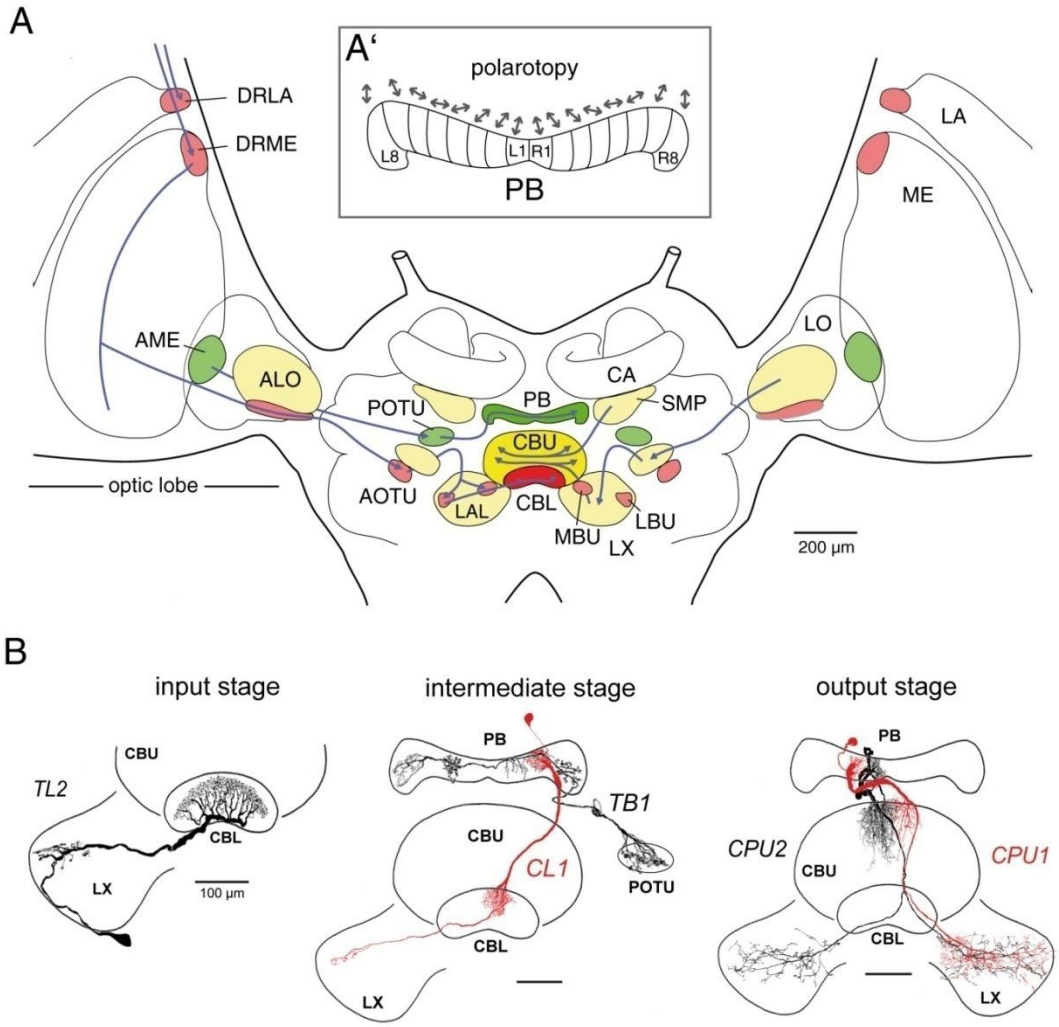

Fig. 3. Gross anatomy of the locust brain, visual pathways, and relevant types of central-complex neuron in frontal view. ***A*** Bilateral pathways of light-sensitive neurons from the optic lobes converge onto a network in the central complex. Stages of early visual processing include the lamina (LA), medulla (ME) and lobula (LO) of the optic lobe. Neuropils shaded red (green) are involved in an anterior (posterior) pathway of interneurons sensitive to sky compass signals. Additional pathways (yellow neuropils) might signal optic flow and / or represent features of the visual object-background scenery. DRLA (DRME), dorsal rim area of the lamina (medulla); (ALO), anterior lobe of the lobula; AME, accessory medulla; AOTU, anterior optic tubercle; POTU, posterior optic tubercle; MBU (LBU) medial (lateral) bulb; LAL, lateral accessory lobe; together with the LAL, the MBU and LBU make up the lateral complex (LX). CBL (CBU) lower (upper) division of the central body; PB, protocerebral bridge; SMP, superior medial protocerebrum; CA, calyx of mushroom body. ***A'*** Polarotopy. The preferred *E*-vector angles of polarization-sensitive neurons that invade the PB (double arrows; shown for CPU-neurons) change systematically along the horizontal axis of the neuropil. The resultant 'polarotopic axis' covers 2 x 180° mapped onto the 16 slices of the neuropil (L1 to L8 and R1 to R8 for the left and right brain-hemisphere respectively). It is considered a compass-like representation of heading directions under the open sky. ***B*** Relevant cell types of the central complex. Columnar neurons connect distinct slices of the PB to the CBU (CPU-neurons) or CBL (CL-neurons) of the central body and have additional arborizations in the lateral complexes. Tangential neurons invade slices within the PB and layers of one POTU (TB-neurons) or slices within the CBL and regions in one LX (TL-neurons). *A:* modified from Pfeiffer and Homberg (2014), *B:* modified from Müller et al. (1997), Vitzthum et al. (2002), Heinze and Homberg (2007, 2009).

Evidence for a role in sky-compass aided locomotion was obtained in crickets (Sakura et al. 2008), as well as in two migratory species, the desert locust (Heinze and Homberg 2007, Mappes and Homberg 2004) and monarch butterfly (Heinze and Reppert 2011). In these, certain types of central-complex neuron signal the *E*-vector angle of linearly polarized blue light (hereafter: polarized light) presented from above, suggestive of a role in sky-compass aided orientation. In line with this, anatomical and physiological approaches have identified bilateral pathways of polarization-sensitive interneurons that receive input from the respective dorsal rim area and converge onto a 'polarization vision network' or ´compass network´ in the central complex (Homberg et al. 2011) (Fig. 3*A*). At the central-complex stage, a co-variation between *E*-vector tuning and cell position along the horizontal brain-axis 'maps' the azimuthal space under the blue sky onto the columnar organization of neuropils (Heinze and Homberg 2007), as illustrated in Figure 3*A'*. This compass-like ´mapping´ is termed **polarotopy** and is reminiscent of the tonotopic axis in the vertebrate auditory system rather than of retinotopy. Polarotopy provides a neural substrate of polarotaxis. It has been argued that the *E*-vector in the zenith provides a compass cue of particular robustness, as it remains perpendicular to the bearing of the solar azimuth (i.e., the intersection point of the solar meridian and the horizon) throughout the solar day. Yet, this cue does not suffice to distinguish the solar hemisphere from the antisolar hemisphere, due to symmetry of the polarization pattern (see previous subsection). As a consequence, the mere representation of the zenithal *E*-vector would effectively correspond to "a compass with no labeling": it could signal the alignment of the animal to a global reference axis (the solar meridian) but not the actual heading direction, e.g. 'toward the Sun'. Related to this aspect is the unclear role of the midline-symmetry of the polarotopic axis (Fig. 3*A'*). It might correspond to a ´true´ 360° range of Sun-positions, if additional cues other than the zenithal *E*-vector were integrated to solve the ambiguity. Alternatively, it could correspond to a redundant (2 x 180°) representation of the solar meridian´s angle and might then stem from hitherto unknown wiring-patterns in the network. Moreover, it remained unclear where and how neuronal responses to sky-compass cues are integrated in the control of locomotion. Chapter 1 of this thesis addresses these aspects by characterization of responses to zenithally presented *E*-vectors with respect to context-dependent properties of the responses that go beyond the mere tuning to *E*-vector angle. A refined wiring model is proposed that links the 2x180°-redundancy of the polarotopic representation to the processing of the zenithal *E*-vector alone.

General subject

The present thesis aims to investigate whether the activity of the internal compass in the central complex depends on a context – e.g. previous heading direction or unexpected events en route – that is relevant for the control of goal-directed locomotion.

BASIC TERMS

The terms listed below will be frequently encountered throughout the rest of this thesis. As their definitions may differ depending on authors, the definitions valid in the present thesis are given here.

spike: a local maximum of the recorded membrane potential, corresponding to an action potential fired by the neuron

(exteroceptive) neuronal response: a change in the activity (here: spike rate) of a neuron that coincides with an event in the outside world and hence putatively ´represents´ it

excitatory response: a neuronal response that consist of an increase in spike rate

inhibitory response: a neuronal response that consist of a decrease in spike rate

Unless stated otherwise, the terms ´excitatory´ and ´inhibitory´, are being used without any assumption on particular mechanisms underlying the observed increase or decrease in spike rate – e.g., a response denoted as ´excitatory´ here may trace back to direct excitation of the respective neuron and / or to the ceasing of an inhibitory input.

CHAPTER I: AMPLITUDE AND DYNAMICS OF POLARIZATION-PLANE SIGNALING IN THE CENTRAL COMPLEX OF THE LOCUST BRAIN

Tobias Bockhorst and Uwe Homberg

To identify features of *E*-vector responses other than mere tuning to *E*-vector angle, I recorded background activity as well as responses to polarized light in identified neurons at all stages of the putative processing hierarchy in the compass network, TL-CL-TB-CPU (Heinze et al. 2009). The polarized-light stimulus was generated using a blue-light source and a rotatable linear polarizer, positioned in the zenith to fully cover the dorsal rim areas of both compound eyes. By rotation of the polarizer (360° range; 30°/s; clockwise and counterclockwise) a steady change (hereafter: modulation) of *E*-vector angle was produced for measurements of (I) general responsiveness to *E*-vector modulation, i.e. whether the recorded cell consistently changes its firing rate in response to changes of the *E*-vector (II) the tuning to *E*-vector angle, and (III) response amplitude in terms of modulation depth.

In the following paragraph, I will describe how the measurements of (I)-(III) were performed by means of a novel method for response analysis. Additional illustrations and details are provided in APPENDIX: ADDENDUM TO CHAPTER I. To relate spike rate and *E*-vector angle, spike times (the points in time, relative to the beginning of polarizer rotation, at which action potentials occurred) were converted into 'spike angles', i.e. into the corresponding angular orientations of the polarizer at the respective points in time (calculated based on the direction and velocity of polarizer rotation). The resultant distribution of spike angles that may range from 0° to 360°, where 360° (180°, 0°) corresponds to an angle congruent with the longitudinal body axis of the locust.

In previous studies (Pfeiffer et al. 2005, see e.g. also Heinze and Reppert 2011), responsiveness to *E*-vector modulation was rated by performing the Rayleigh test (Fisher 1995) for circular uniformity on the distribution of spike angles. This hypothesis test can indicate whether spike angles are uniformly distributed or significantly clustered around a common mean direction, which would then be the **preferred *E*-vector angle** ($\mathbf{\Phi_{max}}$) of that cell (or, to be more precise, of that very response). Only in that case, responsiveness to *E*-vector modulation was assumed and *E*-vector tuning was specified by the calculated Φ_{max} and an 'anti-preferred' *E*-vector angle (Φ_{min}) which was not identified physiologically but defined mathematically by $\Phi_{min} = \Phi_{max} + 90°$ (and not by $\Phi_{max} + 180°$, because *E*-vector angles are axial data, i.e. they have a periodicity of 180°, not the 360° periodicity that marks circular data). In addition, some studies included a quantification of response amplitudes using a measure introduced by Labhart (1996). In brief, Labhart's measure is intended to quantify the *absolute* amplitude of the response by the summed absolute difference between the spike rates at different *E*-vector angles and the mean spike rate. It is 'blind' for the relative response amplitude, i.e. the measure cannot distinguish between a change from 10 to 15 spikes per second and a change from 100 to 105 spikes per second). This is disadvantageous and hampers comparisons, especially if *E*-vector responses 'ride upon' different levels of background activity.

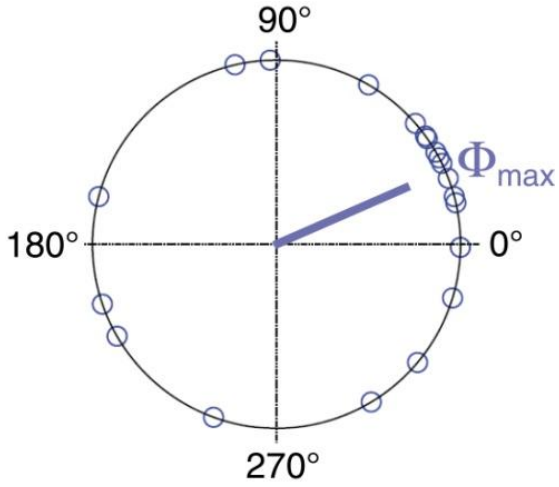

Fig. 4. Illustration of the mean angle Φ_{max} for a set of circular data. In this example, the data is circular, i.e. it has a single mode on the 360° range. Data points are shown as small blue circles plotted onto the unit circle. The angle indicated by the blue line is the calculated *mean* ('preferred') direction $\Phi_{max.}$ Such data could stem from a neuron tuned to the horizontal positions of objects in the outside world, such as visual landmarks or the Sun as a compass cue (whereas the 0° - 180° axis could correspond to the rostral-caudal axis). In case of *E*-vector tuning, i.e. axial data where 0° is equal to 180°, a second mode on the 360° range would be expected, occurring at Φ_{max} +180°. Modified from Berens (2009).

In the present study, I aimed at characterizing *dynamics* of responses to *E*-vector modulation at different stages of the network. In particular, I aimed at providing a more differentiated description of responses, e.g. to distinguish cases of high response amplitude and narrow tuning from cases of lower response amplitude but broader dynamic ranges. To this end, I conceived novel criteria for rating general responsiveness to *E*-vector modulation and response amplitude. The novel test for general responsiveness asks whether the spike rate *co-varies* consistently with the presented *E*-vector angle. This is rated by means of a linear-circular correlation analysis (Berens 2009): responsiveness to *E*-vector modulation was defined as the case of a significant correlation ($p<0.05$) between the instantaneous spike rate at a given point in time and the *E*-vector angle presented at that very point in time. The strength of this correlation (not to be confused with response amplitude) was termed **'correlation strength' (CS)** and quantified by the coefficient of determination, R^2. It is positively related to the broadness of *E*-vector tuning, i.e. the dynamic range over which the spike rate of a given neuron can actually signal the *E*-vector angle.

Hence the correlation analysis, in contrast to the formerly applied Rayleigh test, does not ask how tightly spikes are clustered around Φ_{max} to decide whether the cell is sensitive to *E*-vector angles at all. Instead it asks whether the activity of the neuron is suited to encode the *E*-vector in general, be it by narrow tuning to a single Φ_{max} or by broad sensitivity to the entire 180° periodicity-range of the *E*-vector angle. At the same time, it provides a measure of tuning broadness (R^2) that is independent from the particular amplitude of the response, i.e. from the *amount* by which the spike rate changes during polarizer rotation. In addition to correlation analysis, the average informational content (*E*-vector coding) per spike was calculated according to Skaggs and colleagues (Skaggs et al. 1993, 1996).

For the quantification of response amplitudes, I chose to use the vector strength (VS) statistic (Ashida et al. 2010) which is sensitive to the steepness of the tuning curve. VS is quantified by $|r|$, the length of the spike angle distribution's resultant ('mean') vector (Fig. 5, 6). Note that Φ_{max}.gives the *angle* of this vector. In simple terms, $|r|$ ranges from 0 to 1, and it becomes 1 if and only if all the spike angles are identical.

For a given level of background activity and a constant absolute response amplitude (the maximum absolute change in spike rate during polarizer rotation), $|r|$ reflects the broadness of *E*-vector tuning, being negatively related to it (Fig. 5, 6). If the same absolute change in spike rate ´rides´ upon *different* levels of background

activity, |r| reflects the *relative* steepness of the response, i.e. the ratio of the change in spike rate that occurs during polarizer rotation to the superimposed background activity. This behavior of |r| is advantageous here, because observations in the present study suggest that *E*-vector responses are indeed integrated with cell-type specific and variable levels of background activity.

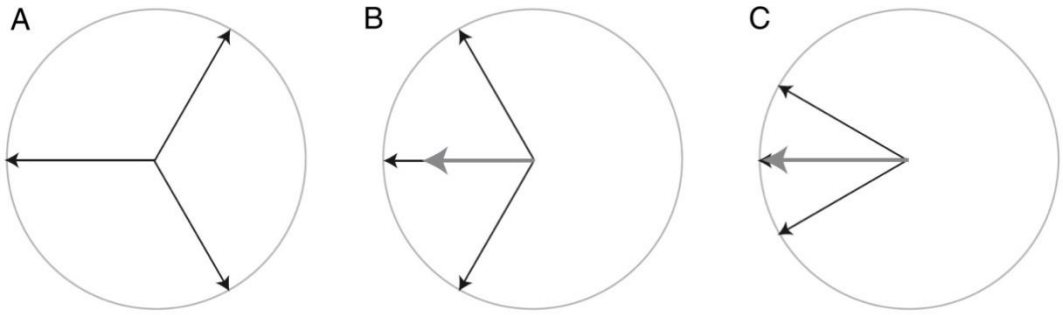

Fig. 5. Illustration of the resultant vector. ***A*-*C*** show different distributions of three events (black arrows), such as action potentials recorded from a visual neuron while an object was rotated around the head of an animal. Grey arrows indicate the respective resultant vector (r) which can be obtained by addition of the black 'event' vectors. In ***A***, the events are uniformly spaced around the circular scale, lacking tuning to a single preferred direction. The angular distance between the data points is constant (120°) and the length of the resultant vector, |r| is zero. By contrast, the three respective samples in ***B*** and ***C*** are clustered around a 'preferred' direction that is defined by the angle of r, i.e. Φ_{max}. At this, |r| is negatively related to the 'width' of this 'tuning': the tighter tuning in ***c*** corresponds to a longer resultant vector. Modified from Berens (2009).

Prior to pooling data across trials in an experiment or across cells of the same type, I normalized (by division) response spike-rates to the respective cell's background activity. To account for pronounced dynamics of background activity, I introduced a differentiated normalization to low, medium and high states of background activity – quantified in terms of the 2.5^{th} percentile, the median and the 97.5^{th} percentile of its spike count distribution.

If a neuron's spike rate at Φ_{max} was higher than high-state background activity *and* the same neuron's spike rate at Φ_{min} was lower than low-state background activity, I considered the response as a case of true '**polarization opponency**'. This term was introduced by Labhart (1988), but the original definition does not include a comparison to background activity. By means of the novel approach outlined above, I analyzed how responses to *E*-vector modulation varied between cell types, across cells of the same type and over the course of a recording from the same cell. Subsequent to recording, neurons were stained by injection of a tracer and coupling of the injected tracer to a fluorophore to visualize their morphology and identify described types of neuron. Data included in final analyzes originated from 4 TL2-cells, 10 CL1-cells, 11 TB1-cells, 12 CPU1-cells, 6 CPU2-cells and from two polarization-sensitive cells of previously not described, complex morphologies.

The background activities of all neurons showed cell-type specific characteristics. In addition to their effect on response amplitudes, the cell-type specific dynamics could be used to identify cell types in the rare case of faint or ambiguous cell staining (see APPENDIX: ADDENDUM TO CHAPTER I). Median spike-rates in background activity varied substantially between cells of the same

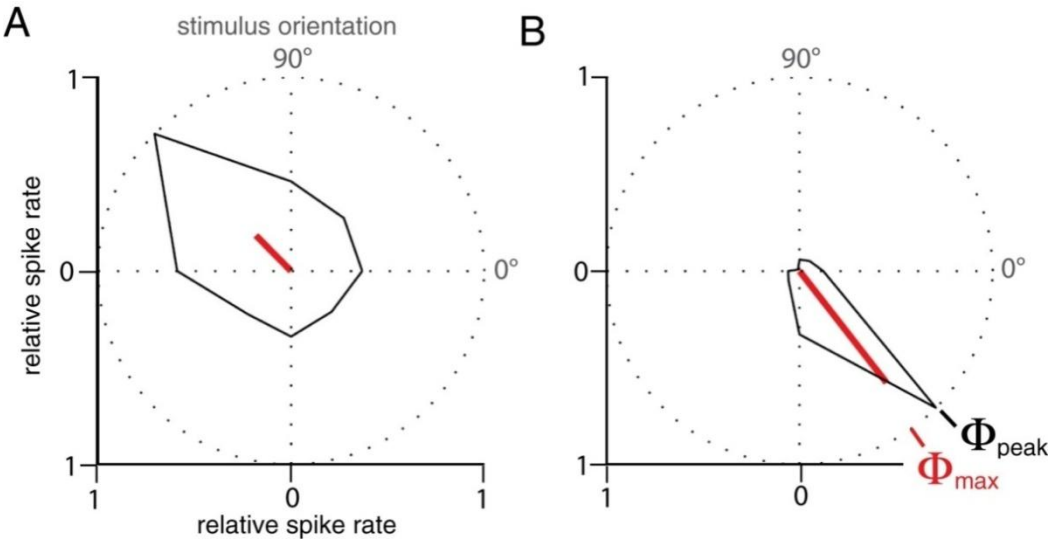

Fig. 6. Examples of broad and tight orientation-tuning. ***A*** and ***B*** show orientation tuning curves, based on spiking activity recorded in the primary visual cortex of an awake macaque monkey while grating-stimuli with eight different angular orientations were being presented to the animal. Black contours indicate the relative spike rate. Stimulus orientations are specified in degrees and the radius of the circle corresponds to the maximum spike rate obtained. Red lines show mean resultant vectors. Note that the angle of the resultant vector, i.e. the mean or 'preferred' angle Φ_{max} does not necessarily equal the 'best' or 'peak' angle Φ_{peak}. Modified from Berens (2009).

type, and lower bounds as well as ranges of the spike-count distributions tended to increase along the putative hierarchy of processing (TL-CL-TB-CPU).

In TL2-neurons of the CBL, i.e. at the input stage, robust responses to *E*-vector angles were confined to a narrow range around Φ_{max}. Responses were distinct from the rather low and regular background activity and relatively constant in informational content of the individual spike. This should establish a reliable representation of *E*-vector angles across the population of TL2-neurons at the input stage of the network.

Homberg et al. (1999) showed that TL2-neurons are GABA-immunoreactive, which suggests inhibitory synapses of TL2-neurons onto ascending subtypes of CL1-neurons. In line with this, it appears to be the *absence* of spiking that holds more reliable *E*-vector information in the CL1-neurons. Their responses to the rotating polarizer were marked by increased variability (and thus by lower reliability) at Φ_{max} as compared to Φ_{min}, particularly in strongly responding neurons. The increased response variability in CL1-neurons may trace back to the lack of true polarization opponency (with respect to Φ_{max}) and superimposition by more variable background activity. In particular, the background activity of CL1-neurons was marked by abrupt changes in spike rate, whereas the respective 'states' of increased or decreased spike rate often lasted for several seconds. When compared to background activity, responses at Φ_{min} were robust while those at Φ_{max} resembled high levels of the background activity.

Further downstream, tangential neurons of the PB (TB1) responded more robustly to both Φ_{min} and Φ_{max}, i.e. in a truly polarization opponent manner. Here, the association between the individual neuron´s spiking and the acute *E*-vector angle was strong and relatively stable for responses to the rotating polarizer. Both

phenomena – polarization opponency and a strong correlation - stabilize the compass-like polarotopic mapping of *E*-vector angles across the PB reported by Heinze and Homberg (2007). They may arise from antagonistic integration across CL1-neurons with opponent tuning (Fig. 7). In individual CL1-neurons, the difference between extreme states of background activity readily matches the difference in spike rate between *E*-vector responses at Φ_{max} and Φ_{min}. Thus, the mere observation of an individual CL1-neuron's spiking cannot suffice for unambiguous signaling of *E*-vector angles. In theory, this ambiguity could be resolved by inhibitory coupling within pairs of TB1-neurons, where each of two 'paired' TB1-neurons would receive input from a CL1-neuron via non-inverting synapses. If the two CL1-neurons are tuned to Φ_{min} angles 90° apart, the antagonistic integration of their outputs should result in the polarization opponency found in TB1-neurons. This antagonistic integration might also smooth out the pronounced state-like variability of background activity that interferes with polarization-signaling in CL1-neurons. In addition to explaining how polarization-opponency in TB-neurons arises, the model unravels the redundancy of the polarotopic representation across the width of the PB as a mere ´byproduct´ of the wiring which establishes mutual inhibition among TB-neurons (Fig. 7A). In other words, the second, from the perspective of compass-signaling demands ´redundant´ representation of another full 180° (see previous section "The central complex: a higher integration area in the insect brain linked to goal-directed locomotion") consists of those arborizations making up the inhibitory TB-TB´ connections (Fig. 7).

The enhancement in correlation strength (CS) at the transition from CL1- to TB1-neurons is accompanied by both a stabilization of informational content and a *reduction* of response amplitude in terms of overall vector strength (VS). This suggests that a CS-VS trade-off could be a crucial step in bundling a distributed representation of preferred *E*-Vector angles (TL- and CL-cells) into pooled pre-motor output (TB- and CPU-neurons) which is ´meaningful´ over the entire range of *E*-vectors - even if its overall VS is lower compared to that of the input stage.

A second inversion of responses presumably occurs at the transition from TB1- to CPU-neurons near the output stage of the network, as indicated by the near 90° phase shift in the polarotopy between TB1- and CPU-neurons that arborize in the same slice of the PB (Heinze and Homberg 2007). In CPU-neurons, the variability of responses was particularly high with respect to general responsiveness (i.e. correlation strength), response amplitude and informational content per spike. At this stage, the average response amplitudes are negatively related to the cells´ average levels of background activity: cells with relatively low background activity showed pronounced *E*-vector responses, while those with high overall levels of background activity hardly changed spiking in response to *E*-vector modulation. This is suggestive of a masking of polarization responses by high-level background activity that lasts throughout the 15 – 45 min period of a recording session. In CPU2-neurons, the resultant span of response strength ranges from effective unresponsiveness to a pronounced polarization opponency. This resembles tuning profiles of polarization-sensitive descending neurons (Träger and Homberg 2011) and is in concert with the variability of polarotactic responses to modulations of zenithal *E*-vector angle observed in tethered flying locusts (Mappes and Homberg 2004) and in crickets walking on a treadmill (Brunner and Labhart 1987). Moreover, this conditional responsiveness is reminiscent of the modulation of sensory responses by dynamic background activity in vertebrate cortex (Arieli et al. 1996), a phenomenon linked to attention or vigilance (as rated by signal detection performance) and to perceptual decisions on ambiguous stimuli (Supèr et al. 2003, Hesselmann et al. 2008, Boly et al. 2007).

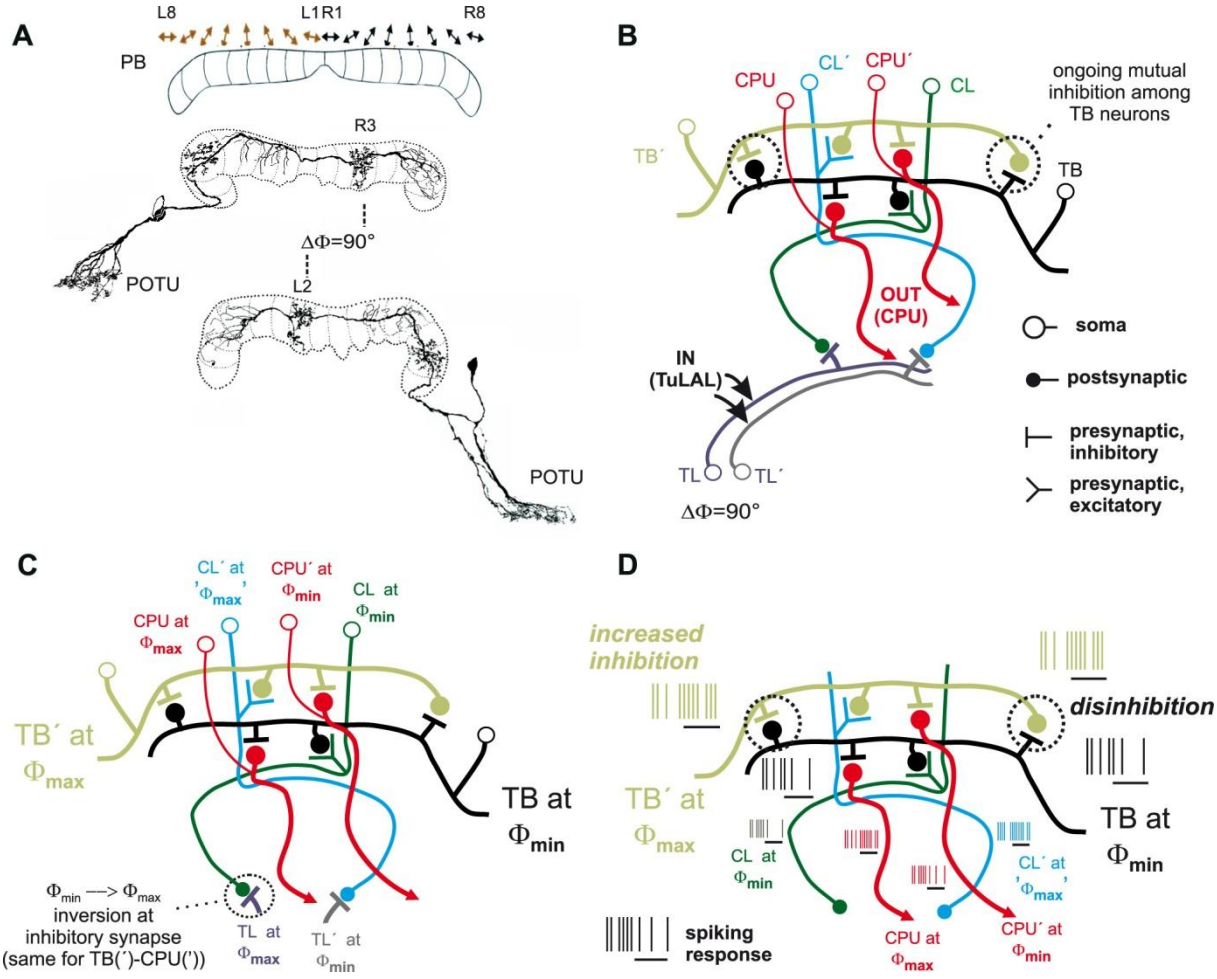

Fig. 7. A mutual inhibition model of polarization-opponent *E*-vector responses in TB1-neurons. Robust polarization-opponency of *E*-vector responses might arise from mutual inhibition among TB1-neurons that receive input from opponently tuned CL1-neurons. ***A*:** polarotopy in the protocerebral bridge (PB, upper subfigure) and relevant morphological features of TB1-neurons. The PB holds a redundant polarotopic representation of *E*-vector angles, covering 2 x 180° across the 16 vertical slices of the neuropil (corresponding to 180° across 8 slices per hemisphere). Double arrows symbolize the Φ_{max} values of TB-neurons that have varicose and hence putatively presynaptic terminals in the respective slices of the PB sketched beneath. Each TB1-neuron has two distinct columns of presynaptic arborizations lying 8 slices apart from one another and hence in different hemispheres of the PB. Smooth and thus presumably dendritic endings span three neighbouring slices in each hemisphere, with the proximalmost (relative to soma position) of the three lying one slice distal to the respective varicose column. The particular TB1-neurons shown here are tuned to Φ_{max} values 90° apart. According to the general morphology described above, their presynaptic columns lie four slices apart, being congruent with slices that hold dendritic columns of the putative partner TB-neuron. ***B***: presumed synaptic wiring among basic types of central-complex neuron involved in the model. Input to the network is provided onto TL-neurons by TuLAL-neurons connecting the anterior optic tubercles to the lateral accessory lobes (see Fig. **3**). The model posits inhibitory synapses between TL- and CL-neurons as well as within pairs of TB-neurons and between TB and CPU-neurons, with synaptic partners being tuned to Φ_{max} values 90° apart as sketched in ***C***. ***D***: Hypothetical network response, as expected from the wiring pattern and resultant tuning relationships depicted in *B* and *C*, to an *E*-vector that matches Φ_{max} for the input TL-neuron to the left in the diagram and Φ_{min} for the second one, labeled TL´. Black horizontal lines beneath the stylized spike trains mark stimulus time windows (adaptation to further ongoing stimulation not shown). In particular, the TB-neuron for which the stimulus *E*-vector angle matches Φ_{min} receives reduced excitatory input from its partner CL-neuron as well as increased inhibitory input from its partner TB-neuron (TB´) for which, in turn, the same stimulus *E*-vector angle corresponds to Φ_{max}. The reduced activity of the TB-neuron at its

Φ_{min} releases its partner TB´, from inhibition via the TB-TB´ synapse, thus adding enhancement to the excitatory input TB´ receives from its partner CL´. Note that the activity of CL´ at its ´Φ_{max}´ is comparatively high but not distinct from higher levels of its background activity whereas the mechanism of mutual inhibition / disinhibition among TB-neurons provides a basis for truly polarization-opponent responses downstream to CL-neurons.

Here, the state of background activity could reflect the motivation to either use compass information (moderate background activcity, allowing true polarization opponency and strong responses) or not to use it, e.g. while resting or mating (high background activity, masked response).

In addition to the dynamics outlined above, responses to the rotating polarizer depended on the direction of rotation in an 'anticipatory' manner. Mean spike angles (Φ_{max}-values) of the responses to clockwise (cw), resp. counterclockwise (ccw) rotations anteceded the $\Phi_{max,\ pooled}$-value calculated from pooling the responses across both directions.

Median deviations of $\Phi_{max\ cw/ccw}$ from $\Phi_{max,\ pooled}$ amounted to about 10° to 20° in absolute value at 30°/s rotation velocity, except for a far lower median value for clockwise rotations in CL1-neurons. The difference between median Φ_{max} values of both directions of rotation was highest in CPU1-and CPU2-neurons (about 33° both), pointing at a particularly pronounced anticipation of future *E*-vector angles near the output stage of the network. Moreover, spiking tended to *peak* even prior to the passage of the direction-specific $\Phi_{max\ cw/ccw}$ angle. This resulted in a further 'anticipatory' shift of the $\Phi_{peak\ cw/ccw}$ -angle (see Fig. 6) relative to the direction-averaged mean angle $\Phi_{max,\ pooled}$. In the most prominent cases, again obtained from CPU-neurons, the *E*-vector angle of peak spiking preceded $\Phi_{max,\ pooled}$ by about 45°, being equivalent to 1.5s at 30°/s rotation velocity. The anticipation might serve to compensate for sensory-motor delays in the control of heading direction.

This 'prediction' of upcoming compass-directions from recently encountered directions extends the analogy between polarization-sensitive neurons in the locust central complex and vertebrate head direction cells, that were discovered in rats by Ranck (1984) and studied in detail by Taube and colleagues (Taube 2007, Clark and Taube 2012). Yet, anticipation by head direction cells is believed to depend on idiothetic indicators of head motion, such as vestibular signals, which are not available to the locust in the preparation applied here. Anticipation by polarization-sensitive neurons might be controlled by a mechanism which infers the velocity and direction of (apparent) rotatory movements from the stimulus history per se, i.e., from the *E*-vector angles encountered in the near past and the time intervals between them.

To capture the time course of responses to *unmodulated* *E*-vector angles, additional rotations of the polarizer were stopped at orientations close to the (anti-)preferred angle of the respective neuron, and presentation of the respective constant *E*-vector angle was maintained for 20 to 30s. This corresponds to a condition of persistent alignment to the celestial *E*-vector pattern.

Responses of TL2-neurons, i.e. at the input stage of the TL-CL-TB-CPU hierarchy were tonic as suggested by earlier recordings using shorter stimuli (Vitzthum et al. 2002). Downstream, response behavior was marked by *E*-vector specific adaptation. On average, the adapting responses faded to 50% in normalized amplitude within 6-10s in CL1 and 8-12s in TB1 and CPU. Transitions to background-activity-like spiking occurred about 16-20s after stimulus onset.

In vertebrates, stimulus-specific adaptation is a prominent feature of higher-stage auditory processing and a presumed correlate of behavioral habituation (Netser et al. 2011, Gutfreund 2012). *E*-vector specific adaptation may correlate with a tendency to steer a steady

course previously observed in tethered flying locusts (Mappes and Homberg 2004). Adaptation to constant head orientation has not been reported for vertebrate (rat) head direction cells.

E-vector specific adaptation, anticipation of modulated input, and conditional responsiveness are features of polarization-plane signaling in the central complex suited to prepare for sensory-motor transformation of this sky-compass cue. Activity in the polarotopic population of central-complex neurons is thus far from being equivalent to the mere operation of an unlabeled compass. It is context-dependent with respect to both stimulus history (anticipation, *E*-vector specific adaptation) and precedent activity of the cells (conditional responsiveness) that might reflect operational network states. Such operational states of the neuronal network could be linked to internal states or behavior of the animal, e.g. the will to migrate (and the necessity to use compass information for doing so), or mating behavior which does not require compass information.

My observations support a view on the central complex as a substrate of higher-stage processing that assigns contextual meaning to sensory input for motor control in goal-driven behaviors. Some phenomena encountered - anticipation, stimulus-specific adaptation and modulation of responses by background activity - parallel the higher processing of sensory information in vertebrates.

CHAPTER II: HEAD-DIRECTION CELLS IN THE BRAIN OF AN INSECT ARE SENSITIVE TO NOVEL EVENTS IN THE VISUAL WORLD

Tobias Bockhorst and Uwe Homberg

In the previous chapter, I described response dynamics of polarization-plane sensitive neurons (hereafter "compass neurons") in the locust central complex. These dynamics are suited to promote the sensory-motor transformation of the head-direction signal for polarotactic locomotion. Rosner and Homberg (2013) showed that these compass neurons are also sensitive to looming stimuli, and the authors provided some initial observations of responses to moving small-field objects. Looming stimuli, such as expanding discs, mimic the rapid approach of an object and trigger escape maneuvers (jumping or flying away from the direction of approach) via fast peripheral pathways from early visual interneurons to descending neurons (Rind et al. 2008, Fotowat et al. 2011, McMillan and Gray 2012). Looming-responses of compass neurons could point to an additional kind of context-dependency in the signaling of heading direction: the consideration of critical events, such as the approach of a predator or impeding collision with a conspecific in a dense swarm. In *Drosophila*, lesion studies demonstrated that place learning based on visual landmarks depends on the integrity of 'ring neurons' at the input stage to the central complex (Ofstad et al. 2011). In line with this, Seelig and Jayaraman (2013) showed that ring neurons similar to those lesioned in the behavioral experiments are tuned to egocentric position and contour orientation of bar-shaped objects, with a preference for vertical features similar to those that constitute preferred landmarks in flies (whereas, to the author's knowledge, polarization-sensitivity has not been studied in central complex neurons of the fly).

In the light of these findings, I investigated whether the compass neurons in the locust central complex generally respond to visual objects in an event-related manner, as suggested by their responsiveness to looming, or also represent object-information suited for landmark-based orientation in local settings as found in flies. To this end, neurons were screened for responses to stationary and moving object-stimuli.

The histological and electrophysiological procedures were identical to those described in Chapter I; in fact, many cells contributed to the datasets in all three chapters of this thesis. Object stimuli were computer-generated and displayed on a 22" CRT screen which, for practical reasons, was positioned slightly tilted as to cover -45° to 60° in azimuth and -32° to 28° in elevation within the left antero-lateral visual field. A uniform grey background was displayed for measurement of background activity and for presentation of individual objects. Stimulus features that were varied in screening experiments include object size, vertical compactness, contour orientation, object position, and rotational as well as translational motion.

Data included in the final analysis here covered 17 neurons from 17 adult gregarious animals. Of these, 3 recordings were from CL1- neurons, 4 from TB1-neurons, 5 from CPU1-neurons and 5 from CPU2-neurons. Measurements of polarization-sensitivity were performed in the very same cells to confirm their role as compass-neurons, i.e. in essence, as head-direction cells. TL-neurons, which would be comparable to the ring neurons studied in the fly have not been

encountered in these experiments, except for a single cell that was polarization-sensitive but did not respond to those visual objects that drove the other types of neuron.

Neither selectivity for object position nor narrow tuning to object features were observed, apart from a preference of distinct objects over visual flow. In fact, none of the neurons encountered responded to wide-field motion. Across cell-types, neurons responded to the translatory motion (70°/s) of a black filled square (hereafter: patch) of about 2° x 1.5° size in visual angle, presented against the grey background. To investigate response behavior, horizontal (forward and backward) and vertical (upward and downward) motion in different regions of the mapping field were presented in different sequences, with several repetitions of the same combination as well as sudden changes in the direction of motion and / or region.

Responses were inhibitory in CL-and CPU-neurons but excitatory in TB-cells. Initial responses were independent of direction of motion but showed strong adaptation to the trajectory, i.e. the region of the visual field occupied by the course of the moving object. This region-specific adaptation could be broken by changing the elevation of horizontal trajectories and the azimuth of vertical ones, but it was unaffected by changing the direction of motion along an unchanged trajectory.

Yet, neurons were not generally blind to the direction of motion, but responded in a highly context-dependent manner: in additional tests performed in the same cells, changing the direction of motion *did* trigger responses if it made a single patch pop-out against a flow field of coherently moving others. Importantly, patches that constituted the background flow in these experiments had the same size and contrast as the individual patch that triggered a response by changing its direction of motion relative to the background patches. Hence, the observed response behavior is not explainable in terms of mere tuning to high-contrast small-field motion against a low-contrast background clutter of wide-field elements. This is a striking difference to the size- and contrast- dependent responses of peripheral small-target movement detectors described in the dragonfly (O'Carroll 1993). It is suggestive of object discrimination in terms of Gestalt principles (see Goldstein 2007). These principles describe the 'laws' of how physical objects and events in the outside world are grouped into perceptual objects, and in the present case, the principle of common fate predicts that objects moving in the same direction will be grouped together, thus distinguishing background flow from distinct 'target' objects. Note that thus the very same event, a change in the direction of motion, might signal a mere change in the behavior of the same object (in the 'blank grey background' regime) or the sudden emergence of a novel object (in the ´complex object-background´ regime).

Together with the region-specific adaptation to the motion of a single patch, the "Gestalt-based" responses strongly suggest that compass neurons in the locust central complex are capable of novelty detection in the visual object-background scenery. They signal salient events of object motion that are 'unpredictable' from the recent stimulus history, but responses do not precisely represent the features of the objects involved. This visual bimodality of locust central-complex neurons might serve to integrate novelty-event information in the control of compass-guided locomotion. This in turn might attune compass-aided locomotor control to unexpected events in the environment, such as the approach of a predator or impeding collision with a conspecific in a dense swarm.

The novelty-dependent responses to small field motion are in line with previous reports on responses to looming objects (Rosner and Homberg 2013), but strikingly different from data obtained in *Drosophila*. This difference in tuning properties of central-complex neurons might relate to lifestyle differences between the two species. Although *Drosophila* can orient

using the sky polarization pattern (Weir and Dickinson 2012), it largely lives in local, visually rich environments suited for landmark learning. In contrast, the desert locust is a long-range migrating species that might preferentially rely on compass navigation. It should finally be noted, that Seelig and Jayaraman (2013) studied ring neurons of the central body of *Drosophila*; these correspond to TL-neurons in the locust (Müller et al. 1997) which were not included in the present study. Hence, results do not rule out the existence of parallel neuronal networks for the two orientation strategies.

In addition to the context-dependency described above, the responses of locust central-complex neurons to small-field motion co-varied with the level of preceding background activity. High-level background activity can mask inhibitory responses (CL1, CPU) by superimposition and reduce the relative strength of excitatory responses (TB1) via framing of responses by response-like spiking. To characterize the effect quantitatively, I tested whether spike counts during stimulus presentation correlated with spike counts during the directly preceding stimulus-free period. The analysis revealed a highly significant and strong correlation that explains about 70% of the observed overall variability in spike count. For statistical reasons, this analysis was confined to CPU-neurons. Yet, across cell-types, the cell-specific ranges of background activity (i.e. variability over time) include levels suited to ´mask´ even the most pronounced responses observed here. This might serve to exclude any currently irrelevant novelty-event information from the higher locomotor control that is most likely promoted by the output of the central-complex.

The masking of object responses by background activity as well as their region-specific adaptation resembles the masking and *E*-vector specific adaptation of compass- responses in the same cells (Chapter I). This further widens the parallel to novelty- and attention-dependent processing of sensory input in the vertebrate cortex outlined in the previous chapter.

CHAPTER III: GAIN MODULATION OF COMPASS SIGNALING BY SALIENT OBJECT MOTION IN AN INSECT BRAIN

Tobias Bockhorst and Uwe Homberg

In the previous Chapters, responses of locust central-complex neurons to polarized light (**compass responses**) and moving small-field objects (**object responses**) were characterized. Both types of response were measured in the very same cells, but results hitherto described were obtained by presentation of either type of stimulus alone. To elucidate the possible role of the visual bimodality for these neurons' function as head direction cells, I investigated the responses to simultaneous presentation of polarized light *and* motion stimuli. Again, these tests were performed in CL1-, TB1-, CPU1-, and CPU2-cells that were also tested for responsiveness to either stimulus alone. The basic procedures were identical to those described in Chapter I and II. Experiments began with presentations of movement stimuli alone and measurements of tuning to *E*-vector angle by means of clockwise and counterclockwise rotations of the polarizer. Subsequent to tuning measurement, the polarizer was rotated to orientations that elicited prominent *E*-vector responses (close to Φ_{max} or Φ_{min}). Once the response to the stationary *E*-vector had declined, sequences of simple small-field motion stimuli were presented concurrent with the ongoing presentation of zenithal polarized light. This stimulus regime corresponds to a situation in which the locust aligns to a particular compass-course, keeps this course for a while and is then confronted with moving objects that most likely trigger escape.

To quantify phasic (early) compass-responses as well as responses to combined stimulation, spike rates in peri-stimulus time windows (5s) were compared to a sample (5s) of the declined (late) compass-response.

CL1-cells showed phasic inhibitions to anti-preferred *E*-vector angles and inhibitory novelty-dependent responses to the moving object alone, as described in the previous chapters. Responses to combined stimulation resembled those to presentation of the motion-stimuli alone: they were always inhibitory, even if the concurrently presented *E*-vector angle was maximally different (i.e., by 90°) from the inhibitory *E*-vector angle (Φ_{min}) of the respective cell. In the latter case, the combined responses were thus ´paradox´ in terms of compass-signaling. I consider these responses a **linear integration** of the novelty-event response with the fully adapted compass-response (the latter being effectively indistinguishable from background activity).

The same response behavior was observed in two TB1-neurons and one CPU1-neuron which showed the previously reported polarization-opponent compass-responses, i.e. phasic, excitatory responses to the preferred *E*-vector angle and phasic inhibition in response to the anti-preferred angle. As a consequence, their combined responses were paradox in terms of compass signaling for excitatory *E*-vector angles in CPU-cells and for inhibitory *E*-vector angles in TB-cells.

By contrast, six other cells (three TB1-neurons, one CPU1-neuron and two CPU2-cells) showed a substantially different response behavior. They were unresponsive to the moving object alone and showed compass-responses that tended to be phasic-tonic rather than merely phasic in time course. They responded to combined stimulation in a *nonlinear* manner that re-increased the gain of the residual compass-response during the small-field motion stimulus. Importantly, the very same events brought back a respective cell's excitatory compass-response to its preferred *E*-vector angle and its inhibitory compass-response to the anti-preferred *E*-

vector, while no effect was observed at neutral, intermediate *E*-vector angles. I consider this response behavior as context-dependent compass-signaling and classified it as an unusual case of '**gain modulation**'. This term was previously used for effects of behavior (e.g., resting vs. flying) on the strength of neuronal responses to visual input in insects (see further below). Noteworthy, the gain-modulation effects surpassed the duration of novelty-dependent responses to object motion that marked the abovementioned linear integration behavior.

To quantify gain-modulation, I performed correlation analyzes, for which each experiment contributed at least 10 measurements of responses to combined stimulation, including measurements at both excitatory and inhibitory *E*-vector angles. These measured the degree to which the response to combined stimulation co-varied with the initial, phasic compass-response. The results proved positive correlations significant at the 5% level, with explained variances ranging from 33% to 85% for a respective cell, except for one of the CPU2-neurons in which, nevertheless, a positive trend in line with the observed phenomenon was found. The analysis of pooled data was restricted to the five cells that showed a significant correlation each (three TB1-, one CPU1- and one CPU2-neuron; 101 measurements). As expected, it also revealed a highly significant positive correlation ($F(99,1)=50.55$, $p(F)<<0.0001$) with a strong associated effect that still explained about 34 % of the observed variability.

As rated from its strength and duration, the gain-modulating effect should provide suitable compass-signaling that could serve the planning of evasive maneuvers. Bringing back a brief representation of the original compass bearing – right before an escape maneuver – might provide a memory template for subsequent re-orientation. It could thus help the animal in getting re-aligned to this 'desired' compass course. This would be in line with previous implications on a role of the central complex for visuo-spatial working memory (see below).

The actual execution of an escape maneuver would result in an apparent drift or rotation of the skylight polarization pattern across the polarization-sensitive parts of the compound eyes. As responsiveness to changes in *E*-vector orientation was preserved throughout the entire course of experiments, this effect should provide compass signaling after the initiation of escape. Acute heading direction could then be compared to the abovementioned hypothetical memory template of the original compass course, thus controlling corrective yaw.

While gain modulation most likely promotes compass guidance of directed locomotion, linear integration does not necessarily have to hinder the same. Any *E*-vector unrelated response to object motion could be cancelled out by lateral inhibition between output channels of the compass network (i.e., neurons downstream to CPU-cells), and the same might hold for coincident background activity in the channels (see Appendix ADDENDUM TO CHAPTER III).

As for the underlying mechanisms of the two response behaviors, I presume that these represent different operational states of the central-complex compass-network rather than two functionally distinct cellular populations. The network wiring scheme introduced in Chapter I could also explain this functional dualism of compass cells if extended by a simple assumption, a conditional transition from phasic responses to polarized light to phasic-tonic responses that indeed often concurred with gain-modulation here (Fig. 8).

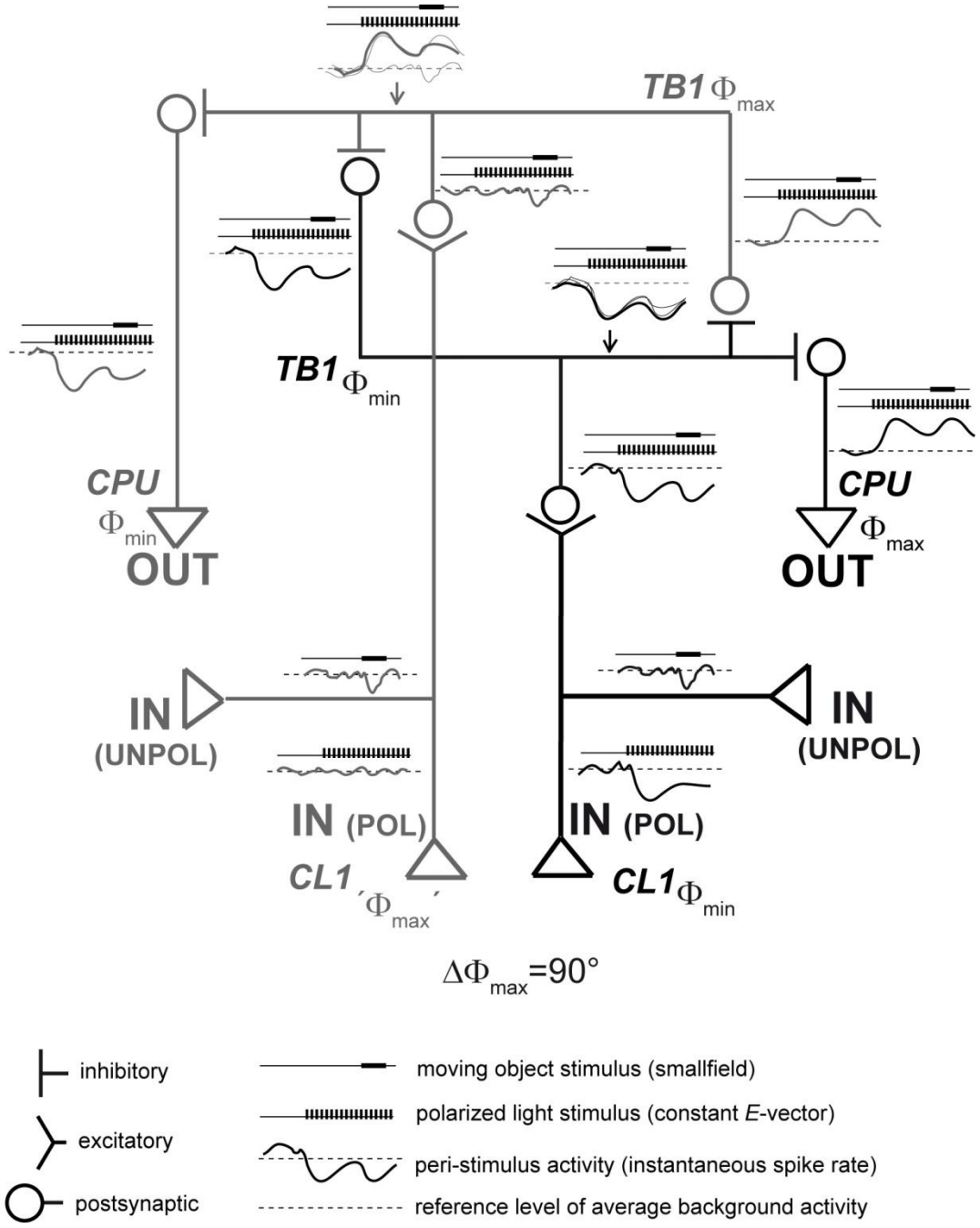

Fig. 8. A refined wiring model of the CX explains responses to combined stimulation by polarized light and moving objects. The scheme illustrates how CL-, TB- and CPU-cells are presumably connected and responding in the elementary circuit of the polarization-vision network. The key element is mutual (dis-)inhibition between two TB-cells that receive input from oppenently tuned CL-cells (Φ_{max}=90°), as shown in Figure 7 of the previous Chapter summary. This 'antagonistic integration' also explains how TB- and CPU-neurons can respond to preferred (Φ_{max}) *and* anti-preferred *E*-vector angles (Φ_{min}), while CL1-cells solely respond at their Φ_{min}. All responses of CL-cells to presentations of moving objects alone as well as to combinations with polarized light are inhibitory. A phasic-tonic response of CL at Φ_{min} (black path) should cause a stronger response to combined stimulation as compared to the partner CL-cell (grey path) which 'responds' neutrally to its 'Φ_{max}' –angle. Due to the mutual (dis-) inhibition among the TB-cells, this difference in amplitude of responses to combined stimulation results in the gain modulation observed in TB- and CPU-cells, concurrent with phasic-tonic compass-responses. Thin (thick) lines indicate responses to separate (combined) stimulation by compass- and motion stimuli, 'tapped' at the positions indicated by arrows. IN, OUT: input to and output of the circuit, respectively; (UN)POL: responses to presentation of

(un)polarized-light stimuli. Otherwise (not illustrated), a pure phasic response to polarized light would, once declined to the level of background activity, result in equal amplitudes of combined responses in CL. This in turn would cause linear integration for combined stimuli by TB- and CPU-cells. Variability of the gain-modulating effect (at the same *E*-vector) might trace back to dynamics of background activity in upstream neurons (CL1) that most likely provide input to TB1-cells.

In the experiments presented here, gain modulation results from integrated input from two different exteroceptive domains, as distinguished from previously demonstrated effects of locomotor state on background activity and visual responsiveness in central-complex neurons (Weir et al. 2014, Seelig and Jayaraman 2013, Homberg 1994). An integration of internal state (level of satiation) and complex exteroceptive input (quantity and quality of food odors) by cells that invade the central complex was shown to play a role in the graded encoding of food odor value in the fly brain (Beshel and Zhong 2013). In concert with evidence for a role of the central complex in visual pattern memory (Liu et al. 2006, Pan et al. 2009), visuo-spatial working memory (Neuser et al. 2008) and place learning (Ofstad et al. 2011), converging evidence so far suggests a role of the central complex as a higher processing site in the insect brain that integrates goals, internal states and exteroceptive input to control goal-driven locomotion.

CONCLUSION

A VARIETY of studies identified the central complex of the insect brain as a higher integration site involved in the control of goal-directed locomotion. In particular, some work has demonstrated that sensory (tactile, visual, olfactory) responses are modulated by behavior (locomotor activity) or internal states (satiety) of the animal. These phenomena suggest that the role of the central complex in higher locomotor control is based on a 'contextualization' of sensory responses that integrates interoceptive and exteroceptive input.

Here we provide further evidence supporting this idea and extending it to compass-signaling by central-complex neurons as well as to responses to object motion. In particular, we show that compass responses are linked to presumably salient, relevant events of object-motion in the outside world by means of a gain-modulating interaction. We are not aware of previous reports on gain-modulation between two exteroceptive senses in an insect brain as opposed to a modulation of an exteroceptive response by behavior or internal states. The novel insights indicate that activity in the population of central-complex neurons surpasses the role of a 'crystalline polarotopy' signal as it is highly contextualized in ways suited to promote sensory-motor transformation for polarotactic locomotion. In more general terms, this study adds to those that illustrate the suitability of the insect brain for investigations into how the nervous system selects, weighs and integrates sensory input to guide purposeful interactions between the animal and its environment. In case of the locust central-complex, the answer to this fundamental question includes parallels to higher sensory processing in the vertebrate cerebral cortex, as evidenced here.

REFERENCES

Arieli A, Sterkin A, Grinvald A, Aertsen A. Dynamics of ongoing activity: explanation of the large variability in evoked cortical responses. *Science* 273: 1868-1871, 1996.

Ashida G, Wagner H, Carr CE. Processing of phase-locked spikes and periodic signals. In: *Analysis of Parallel Spike Trains*, edited by Grün S and Rotter S. Springer, 2010. p. 59-74.

Bech M, Homberg U, Pfeiffer K. Receptive fields of locust brain neurons are matched to polarization patterns of the sky. *Curr Biol* 24: 2124-2129, 2014.

Berens P. CircStat: A MATLAB toolbox for circular statistics. *J Stat Soft* 31: 10, 2009.

Beshel J, Zhong Y. Graded encoding of food odor value in the *Drosophila* brain. *J Neurosci* 33: 15693–15704, 2013.

Boly M, Balteau E, Schnakers C, Degueldre C, Moonen G, Luxen A, Phillips C, Peigneux P, Maquett P, Laureys S. Baseline brain activity fluctuations predict somatosensory perception in humans. *Proc Natl Acad Sci U.S.A. (PNAS)* 104: 12187-12192, 2007.

Brunner D, Labhart T. Behavioural evidence for polarization vision in crickets. *Physiol Entomol* 12: 1-10, 1987.

Chapman JW, Reynolds DR, Wilson K. Long-range seasonal migration in insects: mechanisms, evolutionary drivers and ecological consequences. *Ecology Letters* 18: 287-302, 2015.

Cheng K, Middleton EJT, Wehner R. Vector-based and landmark-guided navigation in desert ants of the same species inhabitating landmark-free and landmark-rich environments. *J Exp Biol* 215: 3169-3174, 2012.

Clark BJ, Taube JS. Vestibular and attractor network basis of the head direction cell signal in subcortical circuits. *Front Neural Circuits* 6, 2012.

Collett M, Chittka L, Collett TS. Spatial memory in insect navigation. *Curr Biol* 23: R789-R800, 2013.

Dacke M, Nordström P, Scholtz CH, Warrant EJ. A specialized dorsal rim area for polarized light detection in the compound eye of the scarab beetle *Pachysoma striatum*. *J Comp Physiol A* 188: 211- 216, 2002.

Dacke M, Nordström P, Scholtz C. Twilight orientation to polarised light in the crepuscular dung beetle *Scarabaeus zambesianus*. *J Exp Biol* 206: 1535-1543, 2003.

Dacke M, Byrne MJ, Baird E, Scholz CH, Warrant EJ. How dim is dim? Precision of the celestial compass in moonlight and sunlight. *Philos Trans R Soc Lond B Biol Sci* 366: 697-702, 2011.

Donlea JM, Pimentel D, Miesenböck G. Neuronal machinery of sleep homeostasis in *Drosophila*. *Neuron* 81: 860–872, 2014.

Eggers A, Gewecke M. The dorsal rim area of the compound eye and polarization vision in the desert locust (*Schistocerca gregaria*). In: *Sensory Systems of Arthropods*, edited by Wiese K, Gribakin FG, Popov AV, and Renninger G. Birkhäuser, 1993. p. 101-109.

elJundi B, Smolka J, Baird E, Byrne M, Dacke M. Diurnal dung beetles use the intensity gradient and polarization pattern of the sky for orientation. *J Exp Biol* 217: 2422-2429, 2014*A*.

elJundi B, Pfeiffer K, Heinze S, Homberg U. Integration of polarization and chromatic cues in the insect sky compass. *J Comp Physiol A* 200: 575-589, 2014*B*.

Fisher NI. Statistical Analysis of Circular Data. Revised edition. Cambridge University Press, 1995.

Fotowat H, Harrison RR, Gabbiani F. Multiplexing of motor information in the discharge of a collision detecting neuron during escape behaviors. *Neuron* 69: 147-158, 2011.

Goldstein EB. Perceiving objects. In: Goldstein EB, editor. Sensation and Perception (7th edition). Belmont, CA: Thomson-Wadsworth; 2007. pp. 93-119.

Frost BJ, Mouritsen H. The neural mechanisms of long distance animal navigation. *Curr Opin Neurobiol* 16: 481-488, 2006.

Gutfreund Y. Stimulus-specific adaptation, habituation and change detection in the gaze control system. *Biol Cybern* 106: 657-668, 2012.

Heinze S, Homberg U. Maplike representation of celestial *E*-vector orientations in the brain of an insect. *Science* 315: 995-997, 2007.

Heinze S, Homberg U. Neuroarchitecture of the central complex of the desert locust: intrinsic and columnar neurons. *J Comp Neurol* 511: 454-478, 2008.

Heinze S, Homberg U. Linking the input to the output: new sets of neurons complement the polarization vision

network in the locust central complex. *J Neurosci* 29: 4911–4921, 2009.

Heinze S, Reppert SM. Sun compass integration of skylight cues in migratory monarch butterflies. *Neuron* 69: 345-358, 2011.

Heinze S, Gotthardt S, Homberg U. Transformation of polarized light information in the central complex of the locust. *J Neurosci* 29: 11783–11793, 2009.

Hesselmann G, Kell CA, Eger E, Kleinschmidt A. Spontaneous local variations in ongoing neural activity bias perceptual decisions. *Proc Natl Acad Sci U.S.A. (PNAS)* 105: 10984–10989, 2008.

Homberg U. Flight-correlated activity changes in neurons of the lateral accessory lobes in the brain of the locust *Schistocerca gregaria*. *J Comp Physiol A* 175: 597-610, 1994.

Homberg U, Paech A. Ultrastructure and orientation of ommatidia in the dorsal rim area of the locust compound eye. *Arthropod Struct Dev* 30: 271-280, 2002.

Homberg U, Vitzthum H, Müller M, Binkle U. Immunocytochemistry of GABA in the central complex of the locust *Schistocerca gregaria*: identification of immunoreactive neurons and colocalization with neuropeptides. *J Comp Neurol* 409: 495–507, 1999.

Homberg U, Heinze S, Pfeiffer K, Kinoshita M, el Jundi B. Central neural coding of sky polarization in insects. *Philos Trans R Soc B* 366: 680-687, 2011.

Labhart T. Polarization-opponent interneurons in the insect visual system. *Nature* 331: 435-437, 1988.

Labhart T. How polarization-sensitive interneurones of crickets perform at low degrees of polarization. *J Exp Biol* 199: 1467–1475, 1996.

Labhart T, Meyer EP. Detectors for polarized skylight in insects: a survey of ommatidial specializations in the dorsal rim area of the compound eye. *Microsc Res Tech* 47: 368-379, 1999.

Liu G, Seiler H, Wen A, Zars T, Ito K, Wolf R, Heisenberg M, Liu L. Distinct memory traces for two visual features in the *Drosophila* brain. *Nature* 439: 551–556, 2006.

Mappes M, Homberg U. Behavioral analysis of polarization vision in tethered flying locusts. *J Comp Physiol A* 190: 61-68, 2004.

Marshall J, Cronin TW. Polarisation vision. *Curr Biol* 21: R101-R105, 2011.

McMillan GA, Gray JR. A looming-sensitive pathway responds to changes in the trajectory of object motion. *J Neurophysiol* 108: 1052-1068, 2012.

Merlin C, Heinze S, Reppert SM. Unraveling navigational strategies in migratory insects. *Curr Opin Neurobiol* 22: 1-9, 2011.

Müller M, Homberg U, Kühn A. Neuroarchitecture of the lower division of the central body in the brain of the locust (*Schistocerca gregaria*). *Cell Tissue Res* 288: 159-176, 1997.

Mouritsen H. Navigation in birds and other animals. *Image Vision Comput* 19: 713-731, 2001.

Netser S, Zahar Y, Gutfreund Y. Stimulus-specific adaptation: can it be a neural correlate of behavioral habituation? *J Neurosci* 31: 17811–17820, 2011.

Neuser K, Triphan T, Mronz M, Poeck B, Strauss R. Analysis of a spatial orientation memory in *Drosophila*. *Nature* 453: 1244–1247, 2008.

O'Carroll D. Feature-detecting neurons in dragonflies. *Nature* 362: 541 - 543, 1993.

Ofstad TA, Zuker CS, Reiser MB Visual place learning in *Drosophila melanogaster*. *Nature* 447: 204–207, 2011.

Ott SR, Rogers SM. Gregarious desert locusts have substantially larger brains with altered proportions compared with the solitarious phase. *Proc R Soc B* 277: 3087-3096, 2010.

Pan Y, Zhou Y, Guo C, Gong H, Gong Z, Liu L. Differential roles of the fan-shaped body and the ellipsoid body in *Drosophila* visual pattern memory. *Learn Mem* 5: 289–295, 2009.

Pfeiffer K, Kinoshita M, Homberg U. Polarization-sensitive and light-sensitive neurons in two parallel pathways passing through the anterior optic tubercle in the locust brain. *J Neurophysiol* 94: 3903–3915, 2005.

Pfeiffer K, Homberg U. Coding of azimuthal directions via time-compensated combination of celestial compass cues. *Curr Biol* 17: 960–965, 2007.

Pfeiffer K, Homberg U. Organization and functional roles of the central complex in the insect brain. *Annu Rev Entomol* 59: 165–184, 2014.

Ranck JB, Jr. Head-direction cells in the deep cell layers of dorsal presubiculum in freely moving rats. *Soc Neurosci Abstr* 10: 599, 1984.

Reppert SM, Zhu H, White RH. Polarized light helps monarch butterflies navigate. *Curr Biol* 14: 155–158, 2004.

Rind FC, Santer RD, Wright GA. Arousal facilitates collision avoidance mediated by a looming sensitive visual neuron in a flying locust. *J Neurophysiol* 100: 670-680, 2008.

Ritzmann RE, Harley CM, Daltorio KA, Tietz BR, Pollak AJ, Bender JA, Guo P, Horomanski AL, Kathman ND; Nieuwoudt C, Brown AE, Quinn RD. Deciding which way to go: how do insects alter movements to negotiate barriers? *Front Neurosci* 6: 97, 2012.

Rosner R, Homberg U. Widespread sensitivity to looming stimuli and small moving objects in the central complex of an insect brain. *J Neurosci* 33: 8122-8133, 2013.

Sakura M, Lambrinos D, Labhart T. Polarized skylight navigation in insects: model and electrophysiology of e-vector coding by neurons in the central complex. *J Neurophysiol* 99: 667-682, 2008.

Sauman I, Briscoe AD, Zhu H, Shi D, Froy O, Stalleicken J, Yuan Q, Casselman A, Reppert SM. Connecting the navigational clock to sun compass input in monarch butterfly brain. *Neuron* 46: 457–467, 2005.

Seelig JD, Jayaraman V. Feature detection and orientation tuning in the *Drosophila* central complex. *Nature* 503: 262-266, 2013.

Skaggs WE, McNaughton BL, Gothard KM, Markus EJ. An information-theoretic approach to deciphering the hippocampal code. *NIPS* 5: 1030-1037, 1993.

Skaggs WE, McNaughton BL, Wilson MA, Barnes, CA. Theta phase precession in hippocampal neuronal populations and the compression of temporal sequences. *Hippocampus* 6: 149-172, 1996.

Srinivasan MV. Honeybees as a model for the study of visually guided flight, navigation, and biologically inspired robotics. *Physiol Rev* 91: 413-460, 2011.

Stalleicken J, Labhart T, Mouritsen H. Physiological characterization of the compound eye in monarch butterflies with focus on the dorsal rim area. *J Comp Physiol A* 192: 321–331, 2006.

Strauss R. The central complex and the genetic dissection of locomotor behaviour. *Curr Opin Neurobiol* 12: 633-638, 2002.

Strauss R, Heisenberg M. A higher control center of locomotor behavior in the *Drosophila* brain. *J Neurosci* 13: 1852-1861, 1993.

Strutt JW. On the light from the sky, its polarization and colour. *Philos Mag* 41: 107-120, 274-279, 1871a.

Strutt JW. On the scattering of light by small particles. *Philos Mag* 41: 447-454, 1871b.

Supèr H, van der Togt C, Spekreijse H, Lamme VAF. Internal state of monkey primary visual cortex (V1) predicts figure–ground perception. *J Neurosci* 23: 3407–3414, 2003.

Taube JS. The head direction signal: origins and sensory-motor integration. *Annu Rev Neurosci* 30: 181-207, 2007.

Träger U, Homberg U. Polarization-sensitive descending neurons in the locust: connecting the brain to thoracic ganglia. *J Neurosci* 31: 2238 –2247, 2011.

Uvarov B. Phase Polymorphism. In: **Uvarov B.** *Grasshoppers and Locusts (Vol. 1)*. Cambridge Univ Press, London, U.K., 1966, p. 332-386.

Vitzthum H, Müller M, Homberg U. Neurons of the central complex of the locust *Schistocerca gregaria* are sensitive to polarized light. *J Neurosci* 22: 1114–1125, 2002.

von Frisch K. Die Polarisation des Himmelslichtes als orientierender Faktor bei den Tänzen der Bienen. *Experientia* 5: 142 – 148, 1949.

von Philipsborn A, Labhart T. A behavioral study of polarization vision in the fly, *Musca domestica*. *J Comp Physiol A* 167: 737-743, 1990.

Wehner R. Astronavigation in insects. *Annu Rev Entomol* 29: 277-298, 1984.

Wehner R. Desert ant navigation: how miniature brains solve complex tasks. *J Comp Physiol A* 189: 579-588, 2003.

Weir PT, Dickinson MH. Flying *Drosophila* orient to sky polarization. *Curr Biol* 22**:** 21-27, 2012.

Weir PT, Schnell B, Dickinson MH. Central complex neurons exhibit behaviorally gated responses to visual motion in *Drosophila. J Neurophysiol* 111: 62-71, 2014.

Wernet MF, Velez MM, Clark DA, Baumann-Klausener F, Brown JR, Klovstad M, Labhart T, Clandinin TR. Genetic dissection reveals two separate retinal substrates for polarization vision in *Drosophila*. *Curr Biol* 22: 12-20, 2012.

Wolf R, Gebhardt B, Gademann R, Heisenberg M. Polarization sensitivity of course control in *Drosophila melanogaster. J Comp Physiol* 139: 177-191, 1980.

CHAPTER I

AMPLITUDE AND DYNAMICS OF POLARIZATION-PLANE SIGNALING IN THE CENTRAL COMPLEX OF THE LOCUST BRAIN

Tobias Bockhorst and Uwe Homberg

AMPLITUDE AND DYNAMICS OF POLARIZATION-PLANE SIGNALING IN THE CENTRAL COMPLEX OF THE LOCUST BRAIN

Tobias Bockhorst and Uwe Homberg

The polarization pattern of skylight provides a compass-cue that various insect species use for allocentric orientation. In the desert locust *Schistocerca gregaria* a network of neurons tuned to the electric field vector (*E*-vector) angle of polarized light is present in the central complex of the brain. Preferred *E*-vector angles vary along slices of neuropils in a compass-like fashion (polarotopy). We studied how the activity in this polarotopic population is modulated in ways suited to control compass-guided locomotion. To this end, we analyzed tuning profiles using measures of correlation between spike rate and *E*-vector angle and, furthermore, tested for adaptation to stationary angles. The results suggest that the polarotopy is stabilized by antagonistic integration across neurons with opponent tuning. Downstream to the input stage of the network, responses to stationary *E*-vector angles adapted quickly which may correlate with a tendency to steer a steady course previously observed in tethered flying locusts. By contrast, rotating *E*-vectors, corresponding to changes in heading direction under a natural sky, elicited non-adapting responses. Yet, response amplitudes were particularly variable at the output stage, co-varying with the level of ongoing activity. Moreover, the responses to rotating *E*-vector angles depended on the direction of rotation in an anticipatory manner. Our observations support a view on the central complex as a substrate of higher-stage processing that could assign contextual meaning to sensory input for motor control in goal-driven behaviors. Parallels to higher-stage processing of sensory information in vertebrates are discussed.

Keywords: insect brain, central complex, *E*-vector signaling, context-dependency

Abbreviations

CBL lower division of the central body
CBU upper division of the central body
CRT cathode ray tube
CS correlation strength
CL1 type 1 columnar (neuron) with arborizations in the PB and CBL
CPU1, CPU2 type 1 and 2 columnar (neuron) with arborizations in the PB and CBU
***E*-vector** electric field vector
IpS information per spike
NGS normal goat serum
OA ongoing activity (background activity)
PB protocerebral bridge
PBS phosphate buffered saline
PBT phosphate buffered saline containing 0.3% Triton X-100
Φ_{max}, Φ_{min} preferred, antipreferred *E*-vector angle
PSTH peri-stimulus time histogram
|r| length of the mean vector
R^2 coefficient of determination
SSA stimulus-specific adaptation
TB1 type 1 tangential neuron of the PB
TL2 type 2 tangential neuron of the CBL
VS vector strength

Journal of Neurophysiology Published 21 January 2015, **DOI: 10.1152/jn.00742.2014**

ALLOCENTRIC ORIENTATION IN SPACE is believed to guide adaptive locomotor behavior both in vertebrates and invertebrates (Mouritsen 2001, Frost and Mouritsen 2006). In particular, a variety of insect central-place foragers and migrants rely on sky-compass signals for spatial learning in local settings or when bridging long distances (Mouritsen 2001, Merlin et al. 2011). A subject´s bearing relative to the Sun provides a straight compass cue if corrected for time of day, but direct view of the sun is often obscured by clouds or objects in the nearby environment. Hence, the benefit of orientation via Sun compass information strongly depends on the capability to conclude on the Sun's position from indirect cues such as the sky polarization pattern. The scattering of direct, unpolarized sunlight in the atmosphere (Rayleigh scattering; Strutt 1871a, 1871b) results in linear polarization of light from the blue sky with a pattern of electric field vector angles (*E*-vector angles) suited to indicate the course of the solar meridian relative to the subject's longitudinal body axis (Fig. 1*A*). Thus, if seen as a pattern of *E*-vectors across the sky (Bech et al. 2014) or integrated with the chromatic or intensity gradient to distinguish between the solar and antisolar sky hemispheres (Pfeiffer and Homberg 2007, Heinze and Reppert 2011), the celestial *E*-vector pattern can signal one's bearing relative to the Sun. If referred to directly, i.e. neither time-compensated nor integrated with additional cues, it can still serve to keep a steady course over moderate timescales.

Evidence from behavioral, anatomical and physiological approaches suggests that the desert locust *Schistocerca gregaria* relies on the polarization pattern of the blue sky during orientation tasks (Homberg 2004, Homberg et al. 2011). When presented with linearly polarized light from a zenith-centered source, tethered flying locusts strive for polarotactic orientation to the *E*-vector angle which would correspond to steering a steady bearing to the Sun (Mappes and Homberg 2004). In line with this, neural substrates for the *E*-vector-dependent reception of polarized skylight and a polarotopic representation of its *E*-vector pattern have been identified in the locust brain (Vitzthum et al. 2002, Heinze and Homberg 2007, 2009; Heinze et al. 2009). Polarization-sensitive dorsal rim areas in both compound eyes connect to pathways of polarization-sensitive interneurons. Some of these neurons show additional tuning to wavelength and azimuthal direction of unpolarized light suited to integrate information from the chromatic gradient to provide an unambiguous compass signal (Pfeiffer and Homberg 2007, el Jundi et al. 2014*B*). These bilateral pathways converge onto a 'polarization vision network' in the central complex, a set of midline-spanning neuropils in the insect brain known to play a role in motor control and visuo-spatial orientation (Neuser et al. 2008, Triphan et al. 2010, Ofstad et al. 2011, Ritzmann et al. 2012, Pfeiffer and Homberg 2014; Fig. 1*B*). Neuropils of the central complex include the lower and upper division of the central body (CBU and CBL, respectively) as well as the protocerebral bridge (PB); polarization-sensitive neurons in the central complex have been categorized according to their branching patterns. Columnar neurons connect distinct slices of the PB to the CBU (CPU-neurons) or CBL (CL-neurons) of the central body and have additional arborizations in the lateral accessory lobes, the presumed main input- and output-relays of the network (Heinze and Homberg 2008). Tangential neurons invade many or all slices within the CBL (TL) or the PB (TB). The putative processing hierarchy is TL-CL-TB-CPU (Heinze et al. 2009). Fig. 1*C* illustrates the subtypes TL2, CL1, TB1, CPU1 and CPU2 relevant here. Investigations into the physiology and anatomy of the polarization-vision network in the central complex revealed polarotopic representations of mean preferred *E*-vector angles that span the width of central-complex neuropils, and cover 180° in *E*-vector angle

within each hemisphere of the PB (Heinze and Homberg 2007).

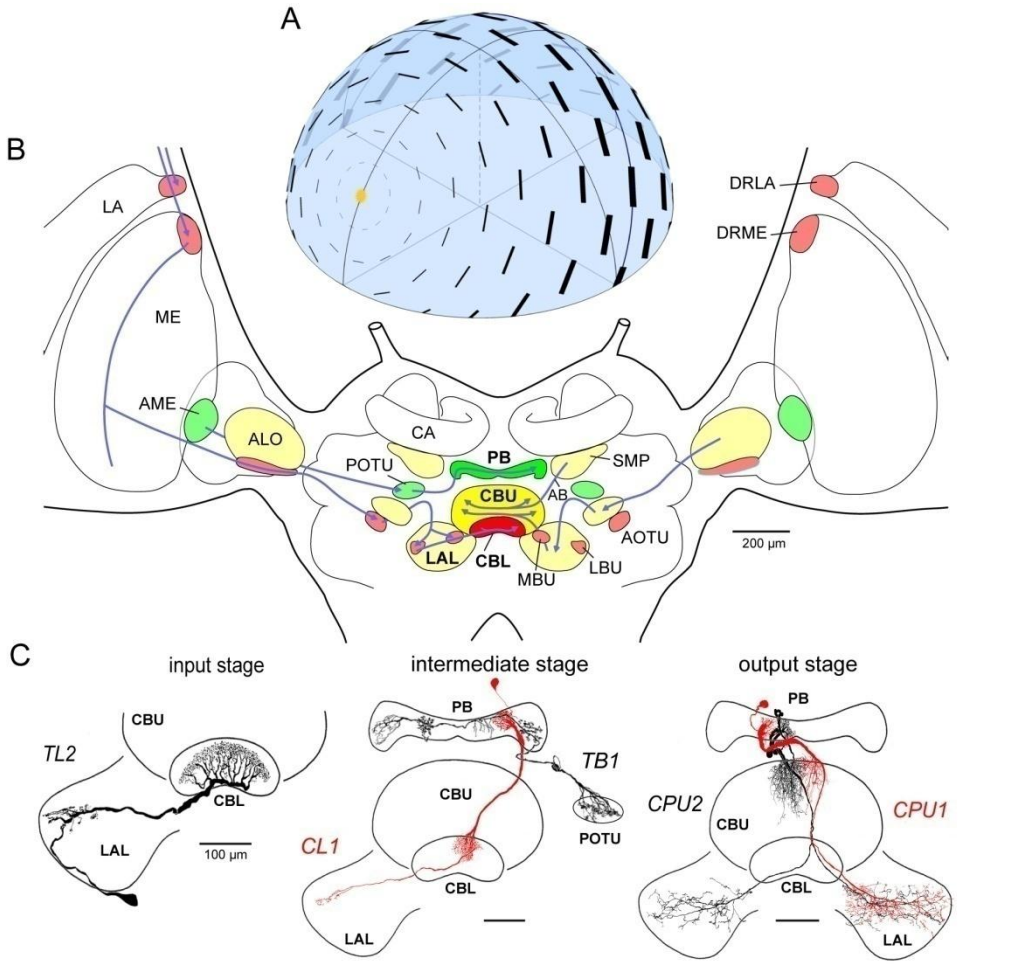

FIG. 1. Celestial compass-cues and neural substrates of polarization-vision in the locust brain. *A:* when the Sun (yellow) is not visible, its position may still be inferred from the intensity gradient of skylight in conjunction with the pattern of polarization. The latter is related to solar position in that the course of the solar meridian represents a line of symmetry for the pattern of electrical field vectors (black bars), which are arranged in concentric circles around the Sun. The degree of polarization (bar thickness) is highest along a circle at 90° angular distance from the Sun. *B:* frontal diagram of the brain of the desert locust. Bilateral pathways of polarization-sensitive (polarization-sensitive) neurons from the optic lobes converge onto a ´polarization-vision network´ in the central complex. An anterior pathway (*red neuropils*) connects the dorsal rim area of the lamina and medulla (DRLA, DRME) via the anterior lobe of the lobula (ALO), the anterior optic tubercle (AOTU), and the medial (MBU) and lateral (LBU) bulb to the lower division of the central body (CBL) of the central complex. A parallel pathway (*yellow neuropils*) originating in the ALO is connected via the AOTU and lateral accessory lobe (LAL) to the upper division of the central body (CBU). The superior medial protocerebrum (SMP) is connected to the CBU via the anterior bundles (AB). Finally, projections from the accessory medulla (AME) extend to the posterior optic tubercle (POTU) and likely target tangential neurons entering the protocerebral bridge (PB; *green*). CA, calyx of mushroom body; LA, lamina; ME, medulla; MBU, medial bulb; LBU, lateral bulb. Together with the LAL, the MBU and LBU make up the lateral complex (LX). *C*: basic types of polarization-sensitive neuron of the central complex. Columnar neurons connect distinct slices of the PB to the CBU (*CPU*-neurons) or CBL (*CL*-neurons) of the central body and have additional arborizations in the lateral complexes. Tangential neurons invade many or all slices within the CBL (*TL*) or the PB (*TB*). *A:* courtesy of Dr. Keram Pfeiffer, *B:* modified from Pfeiffer and Homberg (2014), *C:* modified from Müller et al. (1997), Vitzthum et al. (2002), Heinze and Homberg (2007, 2009).

A standard signal for measurements of *E*-vector tuning is polarized light directed onto the dorsal rim areas, generated by light passing through a steadily rotating polarizer (e.g., Vitzthum et al. 2002; Heinze and Reppert 2011). Under a natural sky, this signal bears an exteroceptive indication of ego-motion: a locust walking or flying under a natural sky will encounter such rapid changes in angle between its longitudinal body axis and the *E*-vector orientation in a patch of the sky only during rotation about its vertical axis. Such yaw movement may serve an initial orientation that could precede ongoing motion on a steady course or re-orientation when drifted off course. In contrast, while on course, i.e. 'aligned´ to the polarization pattern as striven for by tethered flying locusts, the angle between *E*-vector orientation in a patch of the sky and the animal's longitudinal body axis should not vary substantially on moderate timescales.

In the present approach, we measured the responses of polarization-sensitive neurons of the locust central complex to sustained presentation of polarized light with stationary *E*-vector, a condition representing persistent alignment to the celestial *E*-vector pattern. Moreover, we complemented earlier insights into characteristics of *E*-vector tuning by comparing response amplitudes at preferred and anti-preferred *E*-vector angles to levels of ongoing activity and by analysis of the range of polarization sensitivity across cells of a respective type and of the specificity of response profiles for direction of *E*-vector rotation. Cell types studied here cover the putative input, intrinsic, and output neurons of the central-complex polarization vision network. The response characteristics we analyzed in conjunction with the span of processing levels sampled here open a novel perspective on *E*-vector signaling in the polarization vision network of the central complex in the locust brain.

Material and Methods

Experimental animals and preparation. Locusts were reared in crowded indoor cultures at 28 °C under a 11 h : 13 h light-dark regime. Data included in the final analysis covered 45 neurons from 45 adult gregarious animals. Prior to preparation, animals were immobilized by cooling at 4 °C for 15 min. To ease subsequent handling, legs and wings were cut off, and the animals were mounted to a metal holder using dental wax which, along with instant glue (cyanoacrylate), was also used for wound closure. The frontal brain surface was accessed by excision of the frons integument (including antennae and ocelli) and partial removal of the subcuticular fat body and tracheal air sacs. To reduce movements of the brain, muscles connected to the antennae and mouthparts as well as the anteriormost esophagus were transected, the gut was removed through an abdominal incision, and a wire loop waxed to the ventral head capsule was positioned to support the brain from posterior. Finally, the neural sheath was incised and partly removed to ease brain tissue penetration by the recording electrode. During preparation, locust saline (Clements and May 1974) was used to replace fatty hemolymph and keep the brain immersed.

Stimulation. Neural activity was measured in a Faraday cage open to one side. All light sources outside the cage were covered with red filters to prevent interference with controlled stimulation. In addition to polarized light, we presented

object-like patterns of unpolarized light on a CRT screen (Mitsubishi DP2070SB 22" CRT, Mitsubishi, Tokyo, Japan) as well as combinations of both (work in progress). As a result, most responses to polarized light included here (173 out of 214 responses to rotating polarizer, 109 out of 113 responses to stationary polarizer) were recorded under a dim, unilateral wide-field illumination by the CRT (covering -45° to 60° in azimuth and -32° to 28° in elevation within the left latero-frontal visual field), but none of the periods evaluated here coincided with the presentation of visual objects against this uniform grey background.

The wide-field CRT screen emitted $4.3 \cdot 10^{13}$ photons$\cdot cm^{-2} \cdot s^{-1}$, which is within the intensity range of small-field chromatic stimuli considered as unpolarized compass-signals in several studies (e.g., Kinoshita et al. 2007, el Jundi et al. 2011), but had no measurable effect on photon flux within the spectral range of the blue polarized-light signal (see below). All light measurements were performed with a digital spectrometer (USB2000, Ocean Optics, FL, USA) with its detector head at the position of the compound eyes, directed toward the CRT display and source of polarized light, respectively.

The polarized light stimulus was generated from a blue LED (ELJ-465-617, EPIGAP Optoelektronik, Berlin, Germany; 11 mm ID, measured spectral range 421.6 nm – 524.3 nm, peak 461.11 nm, 10^{15} photons$\cdot cm^{-2} \cdot s^{-1}$). It passed a remote-controlled rotatable linear polarizer (HN38S, Polaroid, Cambridge, MA; 20 mm ID) positioned in the zenith of the locusts' head at 60 mm distance (visual angle 19°; common velocity of filter rotation 30°/s).

Intracellular recording and tracer injection. Membrane potentials were recorded with two Ag-AgCl wire interfaces, one being immersed in the saline solution to act as a reference electrode, the other inserted into a sharp micropipette for intracellular measurement. The latter were drawn from borosilicate capillaries (0.75 mm ID, 1.5 mm OD, Hilgenberg, Malsfeld, Germany) with a Flaming/Brown filament puller (P-97 Sutter Instrument Company, Novato, CA), their tips loaded with a solution of Neurobiotin tracer (Vector Laboratories, Burlingame, UK, 4 % in 1 M KCl) and shanks filled with 1 M KCl connected to the Ag-AgCl wire interface. Impedances in tissue ranged from 50 - 200 MΩ. Raw signals were amplified, band-passed (10×, 20 Hz - 20 kHz; SEC 1L/H amplifier, npi electronic, Tamm, Germany), digitized (16 bit / 11.1 kHz; Power1401mkII converter run with Spike2 software, both Cambridge Electronic Devices, Cambridge, UK) and stored for offline analysis in custom-written MATLAB software (MathWorks, Natick, MA, USA). For live monitoring, the amplified signal was fed into an audiomonitor and an oscilloscope (Hameg HM 205-2).

Histology: visualization of cell morphologies. At the end of a respective recording session, Neurobiotin was injected through the recording pipette via application of 0.5-2 nA depolarizing currents for 1-15 min. Brains were dissected out, fixed overnight at 4 °C in a solution of 4 % paraformaldehyde, 0.25 % glutaraldehyde and 0.25 % picric acid in 0.1 M phosphate-buffered saline (PBS), rinsed in PBS (4 x 15 min), and incubated with Cy3-conjugated streptavidin (Dianova, Hamburg, Germany, 1:1000) in 0.1 M PBS with 0.3 % Triton X-100 detergent (PBT) for 3 days at 4 °C in the dark. After rinsing in PBT (2 x 30 min) and PBS (3 x 30 min), preparations were dehydrated in an ascending ethanol series (H_2O, 30%, 50%, 70%, 90%, 95%, and 100% ethanol, 15 min each), cleared in a solution of methyl salicylate in ethanol (1:1, 30 – 45 min), followed by pure methyl salicylate (45 - 60 min), and finally mounted in Permount (Fisher Scientific, Pittsburgh, PA).

For identification of cell morphologies, the wholemount brain preparations were scanned confocally (Leica TCS SP5 confocal laser scanning microscope, Leica Microsystems, Wetzlar, Germany) at 1024 x 1024 pixel resolution and either 10x or 20x magnification (Leica oil immersion objectives HC PL APO 10x/0.40 and

HCX PL APO 20x/0.70, respectively) with Cy3-fluorescence being excited by a DPSS laser at 561 nm. In many cases, autofluorescence of the tissue allowed to contour relevant neuropils as well. Confocal image stacks were then processed in AMIRA 5.3.3 (FEI Visualization Sciences Group, Merignac, France) and COREL Photo-paint (X3 V 13.0.0576, Corel Corporation, Ottawa, ON, Canada) to generate and edit two-dimensional projection views. For detailed analysis of hitherto undescribed morphologies, the respective preparations were rehydrated and sectioned as described by Heinze and Homberg (2008). Briefly, brains were incubated in xylenes (2-4 hours) to remove the embedding medium, and were rehydrated in a decreasing ethanol series (100%, 95%, 90%, 70%, 50% and 30%, 15 min each). After rinsing with 0.1 M PBS (4 × 20 min) they were embedded in albumin-gelatin. The preparations were fixed over night at 4 °C in 8% buffered formaldehyde. On the following day the embedded brains were cut into 130 µm thick sections with a vibrating-blade microtome (LEICA 1200S) and rinsed with 0.1 M PBS (4 × 15 min) before they were preincubated over night in normal goat serum (NGS) (1:20) and 0.1 M PBT. Afterwards the sections were incubated for 5 days with anti-synapsin (1:50, monoclonal, provided by E. Buchner, University of Würzburg, Germany), streptavidin (1:1000) and NGS (1:100) in 0.1 M PBT at 4 °C. Then the sections were washed in 0.1 M PBT (2 × 20 min) and 0.1 M PBS (3 × 20 min) before they were incubated in goat-anti-mouse-Cy5 (1:300) and streptavidin-Cy3 (1:1000) in 1 % NGS in 0,1 M PBT over 3 days at 4 °C in darkness. The sections were rinsed again in 0.1 M PBT (2 × 20 min) and 0.1 M PBS (3 × 20 min), dehydrated in an increasing ethanol series, transferred to a mixture of ethanol (100%) and methyl salicylate (1:1), and finally cleared in pure methyl salicylate and embedded with Permount between two glass coverslips (24 × 60 mm).

The relevant brain sections were scanned with a confocal laser scanning microscope (CLSM, Leica TCS SP5) with a 20× objective (HCX PL APO lambda blue 20×/0.70 Imm UV, working distance: 260 mm, Leica). The Cy3 signal was detected with a DPSS (561 nm) laser while the Cy5-fluorescence was detected with a HeNe (633 nm) laser.

Criteria for inclusion in final data analysis. Physiological data were only included in the final analysis if the recorded neuron was successfully labeled. In some cases, more than one neuronal cell was stained, probably owing to leakage of Neurobiotin into neighboring neurons. In these cases data were included in the analysis if characteristic patterns of ongoing activity (OA) that had previously been determined for distinct cell types could be clearly assigned to one of the labeled morphologies (see Fig. 2 for example traces). To define the spiking patterns of OA typical for a respective cell type, we evaluated experiments that provided both distinct single-cell labeling and several minutes of OA (data not shown). Basic statistics covered the distributions of spike counts (1000 ms bin width, Fig. 2*B*) and inter spike intervals. Along with these numerical measures, action potential waveforms (spike amplitudes and widths, double spikes) and dynamics of subthreshold activity added to the cell-type specific physiological profiles. For instance, the OA of CPU-neurons is marked by alternation between brief states (500-700 ms) of low, intermediate and high spike rates, whereat action potentials are relatively low in amplitude, occasionally occur as doublets and ride upon pronounced dynamics of subthreshold activity marked by fast hyperpolarizations.

Data preprocessing for final analysis. Instantaneous firing rates were estimated by means of Gaussian-smoothed PSTHs (MATLAB implementation as adopted from Jude Mitchell's code (MATLAB function compute_gauss_smooth, accessable at http://www.snl.salk.edu/~jude/sfn2008/index.html) by Kreuz et al. (2011) under avoidance of biasing at the edges of the peristimulus time window. Circular statistics (MATLAB toolbox by Berens; see Berens 2009) were computed to quantify relations between firing rates and *E*-vector angle. For this purpose, corresponding *E*-

vector angles as inferred from orientations of the polarizer were assigned to individual spikes that occurred during rotation of the polarizer, thus obtaining distributions of 'spike angles'. Where necessary for a respective test, transformations from axial to circular scale were performed by doubling spike angles.

Response measures: Polarization-responsiveness. The present study covers a variety of response features, including the principle responsiveness to *E*-vector angle (polarization responsiveness) and the amplitude of the *E*-vector response in terms of the amplitude of spike-rate modulation. We rated polarization responsiveness by correlation strength (CS), i.e., the strength of the association between the *E*-vector angle and spike rate during full (360°) rotations of the polarizer. This association was quantified by means of a circular-linear correlation analysis (Berens 2009) that, analogous to the linear-linear case, provides a circular-linear correlation coefficient and its p-value. The correlation coefficient can be squared to obtain the coefficient of determination (R^2) that ranges from zero to unity and quantifies the proportion of variance shared by the two variables. The size of R^2 can be rated in an objective manner by means of the conventional scale for effect sizes. For instance, an R^2 exceeding 0.25 indicates that more than 25% of the observed variability in spike rate during polarizer rotation can be explained in terms of a dependency on *E*-vector angle which, by convention, corresponds to a strong effect. In other words, R^2 is positively related to the portion of the entire range of *E*-vector angles (i.e., 0°-179°) across which spiking co-varied with *E*-vector angle – it reflects the overall degree to which spiking changed in correlation with the *change* in the *E*-vector angle. The criterion for principle responsiveness to *E*-vectors was the statistical *significance* of R^2 (at α=0.05 and β=0.2). As a measure of polarization responsiveness, correlation strength (CS) as quantified by R^2 is strict but independent from the amplitude of the response. The latter is a desirable feature which is neither met by the commonly applied Rayleigh test for general deviation from circular uniformity nor by tests for significance of the median angle (see Fisher 1995, Zar 1999).

Response measures: Preferred E-vector angle and vector strength. While CS can indicate polarization responsiveness, it does not reflect more specific response features. In particular, (I) R^2 neither indicates the preferred *E*-vector angle, (II) nor distinguishes between actual periods of 180° and 360°, (III) and is insensitive to the amplitude of the spike rate modulation that constitutes the response to a rotating polarizer – a perfect correlation can be observed under minimal or, likewise, under most pronounced deviations from the neuron's ongoing activity. To address (I) and (II), we plotted PSTHs for visual inspection of the *E*-vector tuning and estimated the preferred *E*-vector angle (Φ_{max}, scaled 0° to 179°) as the *angle* of the *mean* (not to be confused with peak spiking) vector of a spike angle distribution pooled across clockwise and counter-clockwise rotations of the polarizer (30°/s). The anti-preferred angle Φ_{min} was defined as the angle perpendicular to Φ_{max}. The *length* of the mean vector |r| quantifies *vector strength* (VS) and ranges from zero to unity (Ashida et al. 2010). It becomes 1 if and only if all the vectors are of the same direction and is closely related to circular variance (S) by S=1-|r|. Here, we refer to it as a measure of response amplitude. It reflects the degree to which spiking was concentrated around the preferred *E*-vector angle (Φ_{max}). Importantly, the same VS may be observed for very different response profiles. For instance, a particular value of |r| could result from a rather silent neuron increasing its spike rate considerably at Φ_{max} or by a neuron with higher ongoing activity that responds with a moderate decrease of spike rate at Φ_{min} *and* a moderate increase at Φ_{max}. If the same modulation amplitude, say, half the difference in spike rate between Φ_{max} and Φ_{min}, is superimposed on different levels of ongoing

spiking activity, |r| is positively related to the resulting amplitude of spike-rate modulation.

Response measures: Information per spike. VS is related to the peakedness of a response to a periodically modulated stimulus. It reflects the degree to which spiking is locked to a certain phase of the stimulus, or here to the preferred *E*-vector angle. Thus, high values of |r| indicate a high level of probability that a single spike observed under rotation of the polarizer coincided with the presentation of Φ_{max}. Skaggs and colleagues have proposed a more straight measure of the information a spike that was observed during periodic stimulation holds over the phase of the stimulus (Skaggs et al. 1993, 1996). This measure of information per spike (IpS) was applied in an analogous manner to quantify the information (in bits per spike) an individual spike observed during the rotation of the polarizer provides over the acute *E*-vector angle. As is the case for VS, IpS may be particularly high for responses of neurons that are effectively 'blind' to virtually each but their preferred *E*-vector angle, i.e. in cases with relatively low CS.

Comparison with ongoing activity: effective response amplitudes. Each response measure described above ignores the degree to which a putative response actually differs from the respective cell´s level and pattern of ongoing activity. Ongoing activity (OA) was defined as the activity recorded under the absence of any controlled stimulation except for wide-field illumination by the CRT display if this was also given during presentation of polarized light. Sections regarded as OA were selected carefully to exclude off-responses to preceding presentation of polarized light as well as effects of other visual stimuli tested. To assess effective response amplitudes, i.e. the degree to which spike rates at Φ_{max} and Φ_{min} effectively differ from OA, we normalized response spike rates to different levels of OA that were observed in the respective neuron. Here, the underlying rationale is to regard a response as robust to the degree to which it stands out against extreme states of the cell's OA – importantly, against states that deviate from the median OA in the same direction as the (putative) response does. Thus, a high effective response amplitude at a respective *E*-vector angle implies that spiking at that angle substantially differs from the particular level of OA that is closest to the putative response. More general analyses were performed on responses normalized to the median OA of the respective neuron.

Types of data plot. Box plots were laid out according to the following: boxes range from the first to the third quartile (Q1 and Q3, respectively); maximum whisker ranges are from Q1-1.5*(Q3-Q1) to Q1 and from Q3 to Q3+1.5*(Q3-Q1), respectively. Plotted whiskers extend to the adjacent value, i.e., the most extreme data value that is not an outlier. Outliers are plotted using cross-shaped markers. Notches indicate the 95 % confidence interval of the median, i.e., two medians are significantly different at the 5 % level if their intervals do not overlap (note that in the Results section, statements on statistic significance of differences between medians rely on this indication). Bubble plots are ´one-dimensional´ scatter plots that use marker size to indicate frequency of observations: the diameters of the circular markers are linearly scaled to the absolute frequency at which a value defined by the center of the marker was observed. Bubble plots were occasionally drawn in addition to box plots to visualize the sampling size and symmetry of individual distributions.

Results

The results are organized according to response features. Within each section, the cell types (see Fig. 1) are addressed with respect to the putative processing hierarchy, TL-CL-TB-CPU. Data from 45 out of 100 recordings from central-complex neurons met the criteria for inclusion in the final analysis. Unless stated otherwise, analyzes of responses to the rotating polarizer were confined to cases with significant correlations between firing and *E*-vector angle. Table 1 provides a brief summary of features of ongoing activity and the most basic response characteristics of central-complex neurons. Fig. 13 schematizes the main findings on responses to polarized light and depicts strongly related aspects of the discussion.

T. 1. Ongoing activity and response characteristics of central-complex neurons

cell type	n	ongoing activity	response, Φ_{min}	response, Φ_{max}	polarization-opponency	adaptation
TL2	4	low, uniform	not robust	strong, robust	no	no
TLU1	1	low, uniform	not robust	strong, robust	no	no
CL1	9	prolonged states	strong, robust	not robust	no	yes
TB1	9	bursts	moderate, robust	moderate, robust	yes	yes
CPU1	12	brief states	variable	variable	yes	yes
CPU2	6	brief states	variable	variable	yes	yes
TL6	1	high, uniform	none	strong	no?	yes

Ongoing activities. The ongoing activity (OA) of polarization-sensitive neurons showed several cell-type specific characteristics. These comprised bursting in TB1-neurons (ca. 50 ms to 100 ms burst duration) and alternation between firing-rate states of higher duration (ca. 500 ms to 1000 ms) and very high duration (up to tens of seconds) in CPU- and CL1-neurons, respectively (Fig. 2*A*). Within the scope of this study, the consideration of OA will be largely restricted to distributions of spike counts at 1000 ms bin width (Fig. 2*B*). These were relatively low and least variable in TL2-neurons at the input stage of the network, except for one in a total of four cells that showed a moderate level of OA and higher variability (Fig. 2*B*). All cell types downstream from TL2-neurons showed substantial variability in spike count both within-cell (over time) and across cells of the same type, including many cases statistically significant at $\alpha = 0.05$ with minimal overlap of interquartile ranges in box plots. Thus, in addition to the cell-type specific complexities in spike pattern, cells of the same type had substantially different median activity levels which persisted throughout the time range of a recording. Along the putative hierarchy of processing (TL-CL-TB-CPU), the lower bounds and ranges of OA spike-count distributions tended to increase. All within-cell spike count histograms differed from normal distribution with statistical significance at $p << 0.01$ as verified by two-tailed Kolmogorov-Smirnov tests. To take this into account, we preferred rank statistics of spike counts (median, 2.5^{th} and 97.5^{th} percentile) for normalization of *E*-vector responses.

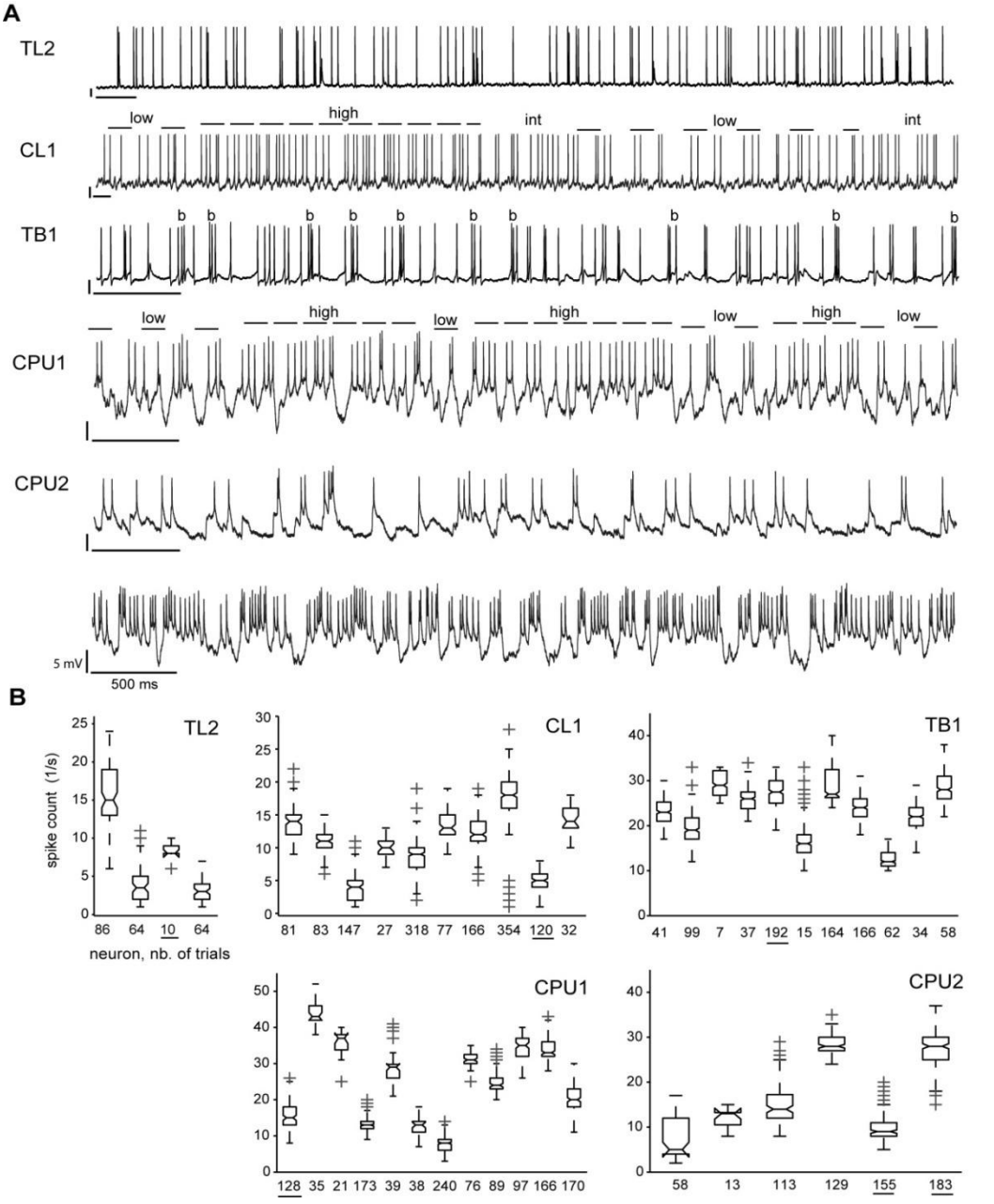

FIG. 2. Complexity and variability of ongoing activity. ***A****:* intracellular recordings revealed cell-type specific levels and dynamics of ongoing activity (OA). OA was comparatively low and rather uniform in TL2-neurons. State-like dynamics were observed in CL1-neurons, with rapid or gradual transitions between states of higher (*high*) and lower (*low*) firing rate (dashed lines) that lasted up to several seconds. Gradual transitions include intermediate states (*int*) in overall rate. TB1-neurons showed moderate average levels of OA marked by bursts (*b*) of 50-100 ms duration. Overall levels of OA were particularly dependent on the individual recording in CPU1-and CPU2-neurons, as illustrated by the two traces recorded from different CPU2-neurons and evident from ranges of box-plots in *B*. In both subtypes, state-like variability of local firing rates (shown for CPU1; same indexing as for CL1) were observed, whereat state durations were substantially lower than in CL1-neurons, commonly between 500 - 1000 ms. Bars: 5 mV, 500 ms. ***B***: box-plots showing the distribution of spike counts in OA for different cells of a respective type. Each box depicts data from an individual neuron. Numbers below the x-axis specify (in seconds) the total duration of OA evaluated. Thus, ranges of box-plots reflect the within-cell dynamics of local spike rate at 1000 ms resolution, as observed over the period of recording sessions. Because the latter varied between 10- 45 min, so does the total duration of OA recorded. Underlined numbers mark data from neurons shown in *A*.

Profiles of E-vector tuning. To capture each cell type's characteristic *E*-vector tuning, we evaluated responses to full rotations of the polarizer. Binned (10°) spike angles were pooled across clockwise and counter-clockwise rotations. Corresponding spike rates were normalized to the median of each respective cell's ongoing activity (OA) and their binned distributions box-plotted against the angular distance to the Φ_{max} – value (Fig. 3*A*) which was calculated for each response individually. Concurrent with the increase in OA along the processing hierarchy, average response amplitudes in terms of vector strength (VS) decreased from the input stage (TL2- , CL1-neurons) over intermediate-stage TB1-neurons to neurons at the output stage (CPU1, 2). This is illustrated by the box plots in Fig. 3*B* as well as by the vertical distances of response rates to the median level of OA (horizontal line) shown in Fig. 3*A*. Notably, a prominent change occurred from CL1- to TB1-neurons: the distribution of |r| values from TB1-cells was less dispersed, more symmetrical and shifted towards lower values as compared to those of CL1-neurons (Fig. 3*B*). While overall spread of |r| is comparable for TB1 and CPU1, its median is significantly lower in the latter than in all other types of polarization-sensitive neuron considered here. By contrast, |r| was substantially more dispersed again in CPU2-neurons. Still, values of individual responses obtained from CPU1-and CPU2-neurons at the output stage matched the enhanced levels observed in TL2-and CL1-neurons near the input stage, as reflected by the overlapping ranges of the box plots in Fig. 3*B*.

In addition to VS, the correlation strength (CS) was calculated for each individual response to quantify the extent to which the firing rate could reflect the acute *E*-vector angle *on average*, i.e. as measured across the response to an entire rotation of the polarizer. Fig. 3*C* shows the respective box plots of R^2 values. Throughout cell types, minimum values of R^2 were well above (in TL2-, CL1-and TB1-neurons) or still very close (in CPU1-and CPU2-neurons) to the conventional lower threshold of 0.25 for large effect size, indicating strong correlations between firing and *E*-vector angle. Highest scores and least inter quartile dispersion were observed in TL2-and TB1-neurons. For these, median values of R^2 were similar and significantly higher than in all other types of neuron considered here, amounting to 79 % and 82 % explained variability, respectively. Thus, the substantial reduction in VS from CL1-neurons to TB1-neurons coincided with a strong and statistically significant increase in CS: tuning profiles became ´flatter´, but spiking became correlated with *E*-vector angle over a wider range of angles. At the output stage variability of CS was increased, whereat the ranges of R^2 were virtually congruent in CPU1-and CPU2-neurons and medians of the data pooled across cells were lower than in upstream cell types.

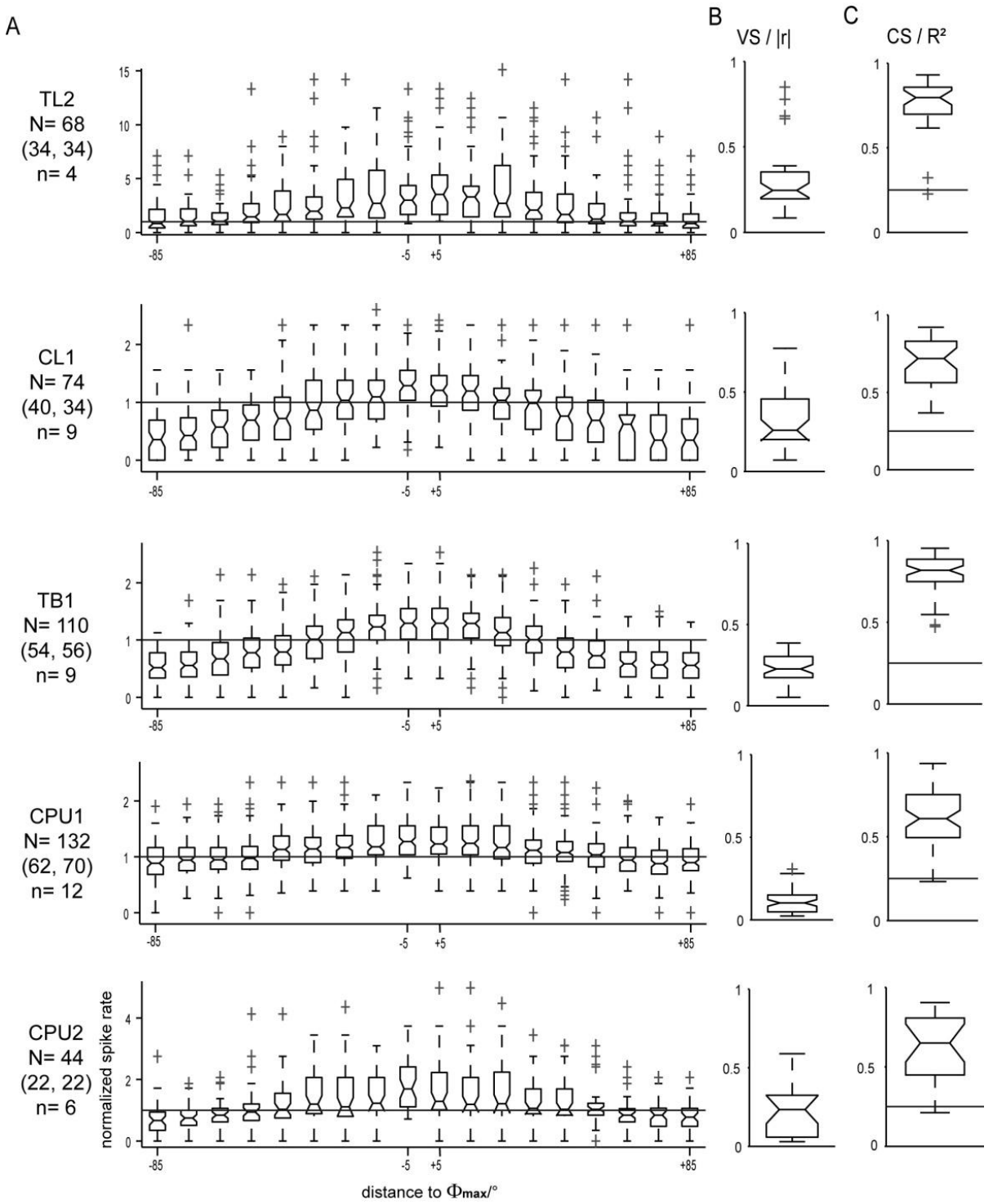

FIG. 3. *E*-vector tuning of central-complex neurons. *A*: tuning profiles were obtained from N responses of n cells to a polarizer rotated at 30°/s. Spike rates in 36 non-overlapping bins spanning the entire period of polarizer rotation were normalized to the median spike rate of ongoing activity and box-plotted against the respective bin's corresponding distance to Φ_{max}. To capture each cell type's profile, data were pooled across responses to clockwise and counter-clockwise polarizer rotation (N-numbers in brackets) that showed significant correlation between spiking and *E*-vector angle. The cell-type specific modulation depth of *E*-vector tuning is reflected by the angle-specific distance of response rates to the horizontal reference line that indicates the median level of ongoing activity. Some outliers that were consistent with the respective tuning profiles are omitted for the sake of appropriate axis scaling. *B*, *C*: the peakedness (vector strength, VS) and overall *E*-vector dependency (correlation strength, CS) of tuning profiles were quantified by calculating |r| and R^2 for each response, respectively. Note that VS decreases from CL1-to TB1-neurons while CS increases. Horizontal lines in *C* indicate the 0.25 threshold level for statistically strong effects.

Amplitudes of E-vector tuning. In the above subsection, we have described the profiles of *E*-vector tuning for different cell types, based on responses to a rotating polarizer that were normalized to the median spike count of each respective cell's ongoing activity (OA). It is important to note that this approach does not suffice to estimate the effective amplitude of the rate-coded responses to *E*-vector angles because the OA of the neurons exhibits substantial dynamics at cell-type specific time scales (Fig. 2). To address this, we have normalized the response spike-rates at Φ_{min} +/- 10°, at intermediate angles (40°-60° distance to both Φ_{max} and Φ_{min}) and at Φ_{max} +/- 10° to very low levels of OA (2.5^{th} percentile of the spike count distributions shown in Fig. 2), median, and very high levels of OA (97.5^{th} percentiles), respectively (Fig. 4). At the input stage, *E*-vector tuning was effectively unidirectional, i.e. responses to the rotating polarizer were only robust at Φ_{max} (in TL2-neurons) or Φ_{min} (in CL1-neurons). The robust responses of TL2-neurons to their preferred *E*-vector angle and of TB1-neurons to their anti-preferred angle constituted the most consistent robust deviations from OA. Thus, the response of an *individual* TL2-neuron to its preferred *E*-vector angle provides a robust and strong input to the polarization-sensitive network of the central complex while the TL2-neurons encountered here were effectively unresponsive to ´anti-preferred´ angles. Their median spike rate near Φ_{min} even exceeded the low states of OA. By contrast, in TB1-neurons, the unidirectional tuning of upstream neurons had apparently been transformed into an ´*E*-vector opponent´ response which is less strong but shows higher overall robustness - though being 'more robust' at Φ_{min} as compared to Φ_{max}, where half of the responses fell below the high-state of OA. Again, CPU2-neurons showed increased variability of response pattern but were still capable of robust opponent responses, as reflected by overlapping ranges of box-plots in Fig. 4. CPU1-neurons showed less robust response opponency than CPU2–cells: the proportion of responses that withstood comparison to extreme states of OA was lower, both at Φ_{min} and Φ_{max}.

In TL2-neurons, median spike rates at ´neutral´ *E*-vector angles were comparable to high-level OA. In all types of neuron downstream from TL2, spike rates at these angles were substantially closer to median than to low- or high-level OA, as expected for stimulus-unrelated spiking. In particular, the average distance to median OA decreases along the putative hierarchy of processing. It shall be noted that the levels of OA that we normalized the responses to were measured in the absence of the additional illumination by polarized light and thus at a lower overall ambient light level than the *E*-vector responses.

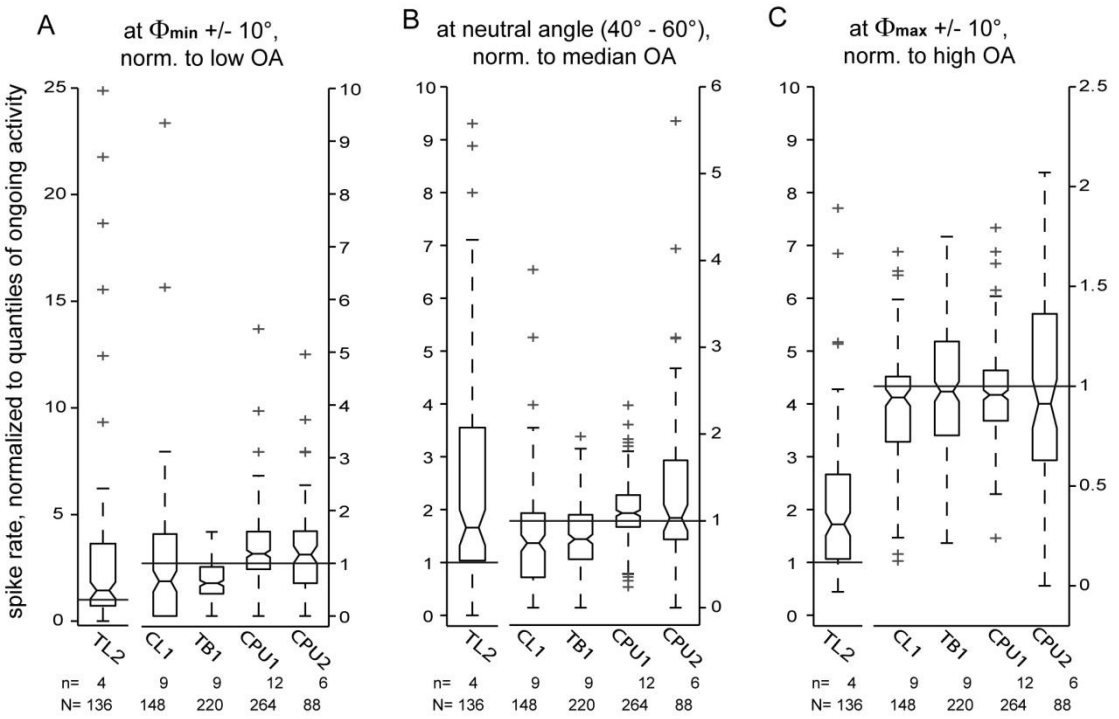

FIG. 4. Effective amplitudes of *E*-vector tuning. To explore how putative *E*-vector responses compare to ongoing activity, we normalized spike rates near Φ_{min} (*A*), intermediate angles (*B*) and Φ_{max} (*C*) to very low (2.5th percentile), median, and very high (97.5th percentile) levels of ongoing activity (horizontal lines), respectively. The underlying spike count samples are the same as for the tuning profiles in Fig. 3 but N numbers of the box plots shown here are doubled as a result of re-binning of the spike counts sampled at 10° to a resolution of 20°. Reference levels of ongoing activity were measured for each individual cell considered here. Some outliers are omitted for the sake of appropriate axis scaling. In all subfigures, the scaling of the Y-axes for TL2-cells (left Y-axes) differs from that of the other cell types (right Y-axes). Responses of TL2- and CL1-neurons are unidirectional: TL2-neurons show robust excitation at Φ_{max} but effectively lack an inhibition at Φ_{min}; In contrast, CL1-neurons show robust inhibition at Φ_{min} but no robust excitation at Φ_{max}. All types of neuron downstream to CL1 appear capable of more robust response opponency, whereas scatter is highest in CPU2-neurons.

Cell-type specific spans of polarization sensitivity. As outlined above, the correlation strength (CS) of responses to the rotating polarizer varied to different degrees in the types of neuron encountered here, with a tendency toward increased spans of R^2 at the output stage of the network (Fig. 3*C*). Spans of vector strength (VS) of these correlation-significant responses appeared less related to processing stage, being comparable between CL1- and CPU2-neurons and between TL2-, TB1- and CPU1-neurons, respectively. To assess the full cell-type specific spans of polarization sensitivity, we re-analyzed the data under inclusion of cases that lacked significant correlation between spiking and *E*-vector angle. All putative responses from a respective cell type were amplitude-ranked according to their vector strength (VS). The sets of ranked data were then split along their medians into their lower and upper halves, corresponding to weaker and stronger responses. Fig. 5 illustrates how tuning profiles (normalized to median OA), VS and CS of both subsets compare to each other within each cell type.

As previously observed for the correlation-significant responses alone, the overall spans of R^2 across weaker and stronger responses tended to increase along the processing hierarchy (TL-CL-TB-CPU) though being lower in TB1 than in

CL1. The tuning profile of stronger responses of TB1-neurons shows the strongest association between spike rate and *E*-vector, resulting in an opponency of responses to Φ_{max} and Φ_{min} unparalleled in consistency by all other cell types (Fig. 5*A*). This is accompanied by high values of R^2 with narrow spans that show small overlap between weaker and stronger responses in TB1-neurons (Fig. 5*C*). Cases that lack significant correlation were not encountered in TB1-neurons, except for a single outlier out of 56 cases. Concurrently, response amplitude in terms of VS was more stable than in upstream neurons and still relatively high for the subset of weaker responses (Fig. 5*B*). Taken together, the differentiated analysis confirmed that TB1-neurons provide a very reliable polarization signaling over the entire range of *E*-vector angles. Moreover, 5 in a total of 9 TB1-neurons contributed both stronger and weaker 'responses', indicating a substantial within-cell component of the low overall variability.

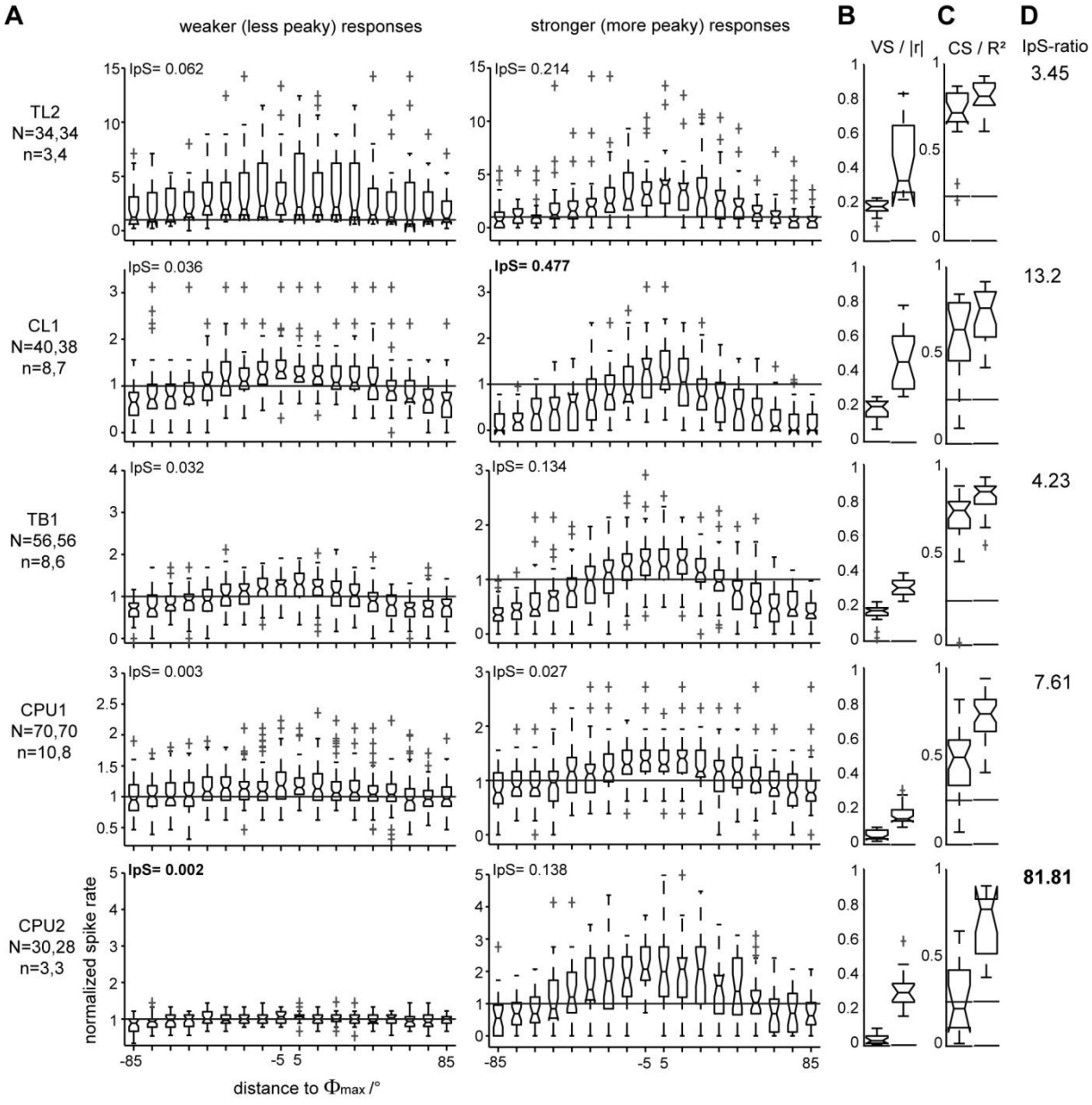

FIG. 5. Cell-type specific spans of sensitivity to *E*-vector angle. To assess spans of sensitivity to *E*-vector angle, we have amplitude-ranked all responses from a respective cell type according to their vector strength (VS). The sets of ranked data were then split into their lower and upper halves, corresponding to

weaker responses (*A*, left column) and stronger responses (*A*, right column), respectively. For compact plotting, rates were box-plotted against the respective bin's corresponding distance to Φ_{max}. Some outliers that were consistent with the respective response profiles are omitted for the sake of appropriate axis scaling. For each subset, information per spike (IpS, bits/spike; see insets in (*A*) as well as the distributions of |r| (*B*) and R^2 (*C*) were calculated. Left and right box plots in *B* and *C* correspond to the data from weaker and stronger responses, respectively. Horizontal lines in box plots of R^2 indicate the 0.25 threshold level for statistically ´strong´ effects. Note that both the difference in steepness of tuning (*A, B*) and in CS (*C*) between weaker and stronger responses increases steadily along the putative hierarchy of processing. In CPU2-neurons, nearly half of the weaker responses lack significant correlation between spiking and *E*-vector angle (p-values of R^2 not shown). Concurrently, the increase in information per spike (IpS-ratio, *D*) from weaker to stronger responses is lowest for TL2-neurons at the input stage and relatively low again in TB1-neurons while being twenty-fold higher in CPU2-neurons.

The spans of CS as well as its separation between weaker and stronger responses were highest in CPU-neurons. Most strikingly, weaker ´responses´ of CPU2-neurons had the flattest response profile (Fig. 5*A*) with a median VS close to zero and lacked significant correlation in 8 out of 15 cases (p-values not shown). Here, cells that provided stronger and weaker responses, respectively, were not identical (14 stronger and 15 weaker responses, both groups covering three cells). Thus a major component of the large overall response variability in CPU2-neurons arises from differences between cells, or from states of responsiveness as prolonged as the duration of a typical recording. Notably, median spike rates of ongoing activity were up to fivefold higher (5 vs. 28 spikes per second) in the less responsive neurons (Fig. 6). For the subsets of stronger responses, median VS and CS were equal for TB1-and CPU2-neurons. To illustrate the range of within-cell (co-) variability of VS and CS, we plotted the individual values of |r| and R^2 from several rotations of the polarizer against the time course of recordings lasting at least 600 s (Fig. 7). These plots show again that variability of CS (i.e. of responsiveness to *E*-vector angles) is small in TB1- and relatively high in CPU2-neurons. As expected, the richness in information per spike (IpS) was positively related to the peakedness of the tuning curves and thus to VS but rather independent from CS (Fig. 5, *A-C*). Lowest values were computed for weak responses of CPU-neurons, accompanied by the lowest median vector strengths. A maximum value of 0.48 bits/ spike was obtained for stronger responses of CL1-neurons, which were also highest in median VS. The increase in information per spike (IpS-ratio, Fig. 5*D*) from weaker to stronger responses is lowest for TL2-neurons at the input stage (x3.45) and still relatively low in TB1-neurons (x4.23) but twenty-fold higher in CPU2-neurons (x81.81). Table 2 provides an overview on responsiveness to polarization-plane in terms of significant correlation between firing and *E*-vector angle during presentations of a rotating polarizer (note that the strength of the effect as measured by R^2 is omitted).

Rotation-direction specificity and anticipatory features of responses to rotating polarizer. All above mentioned analyses (except for plots in Fig. 7) were performed on response data pooled across clockwise rotations (0° to 360°) and counter-clockwise rotations (360° to 0°) of the polarizer. Next, we inspected the responses to the rotating polarizer for rotation-direction specificity and, within each direction, for symmetry of spiking around Φ_{max}. Here, we consider the overall Φ_{max} value for data pooled across directions of rotation ($\Phi_{max,\ pooled}$) an estimator of a neuron's ´actual´ preferred *E*-vector angle.

In all types of neuron, the Φ_{max} values of individual responses differed from $\Phi_{max,\ pooled}$ in a consistent, rotation-direction specific manner (Fig. 8*A*): in the vast majority of cases, individual Φ_{max} values *preceded* the passage of $\Phi_{max,\ pooled}$. Thus, their deviance from $\Phi_{max,\ pooled}$ is not a mere result of latency and is in fact suited to ´anticipate´ future *E*-vector angles. Median

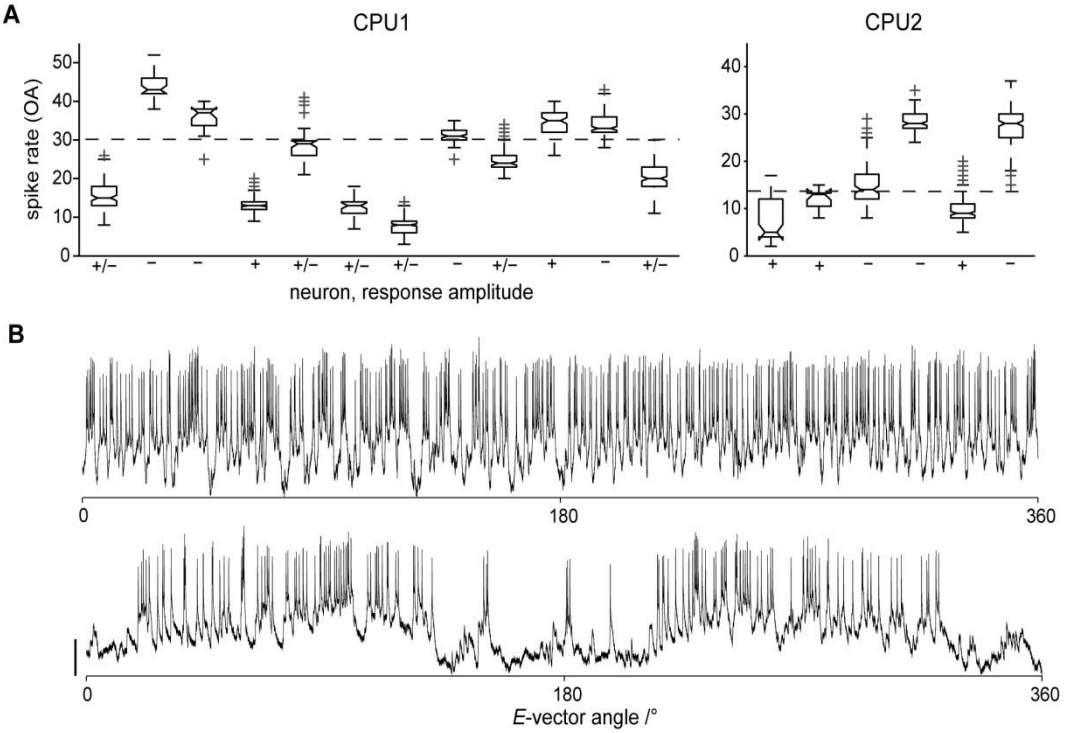

FIG. 6. Sensitivity to *E*-vector angle is related to ongoing activity in CPU-neurons. In CPU-neurons, the average sensitivity to *E*-vector angle co-varied systematically with the individual cell's overall level of ongoing activity. Within-cell distributions of spike rates in ongoing activity shown in Fig. 2 are plotted again in *A*. Here, +, - and +/- mark data from neurons that contributed exclusively stronger (+), exclusively weaker (-) or both stronger and weaker (+/-) responses as rated by vector strength. Horizontal dashed lines indicate approximate threshold levels of ongoing activity that separate the subpopulations of exclusively weakly and exclusively strongly responding cells, set by visual inspection. *B:* traces recorded from a less (upper trace) and a more sensitive CPU2-neuron (corresponding to the two right-most box plots in A) during polarizer rotation at 30°/ s. Bar 5 mV.

T. 2. Polarization-plane responsiveness of central-complex neurons

cell type	n_{total}	$n_{corr.\ sig.}$	$n_{corr.\ n.s.}$	$\%n_{corr.\ sig.}$	N_{total}	$N_{corr.\ sig.}$	$\%N_{corr.\ sig}$
TL2	4	4	0	100	34	34	100
CL1	9	8	0	88.9	39	37	94.9
TB1	9	8	0	88.9	56	55	98.2
CPU1	12	10	0	83.3	70	66	94.2
CPU2	6	4	0	66.7	29	22	75.9

n_{total}: total number of cells; $n_{corr.\ sig.}$($n_{corr.\ n.s}$): number of cells that contributed *exclusively* responses with (non-) significant correlation between *E*-vector and spiking. N_{total}: total number of responses, including those that lacked significant correlation; $N_{corr.\ sig.}$ number of responses with significant correlation. N-values refer to full (360°) rotations of the polarizer. Note that the mere significance of the correlation does not indicate its strength.

deviations from $\Phi_{max,\ pooled}$ amounted to about 10° to 20° in absolute value at 30°/ s rotation velocity, except for a far lower median value for clockwise rotations in CL1-neurons. The difference between median Φ_{max} values of both directions of rotation was highest in CPU1 and CPU2-neurons (about 33° both), pointing at a particularly pronounced anticipation of future *E*-vector angles near the output stage of the network. For the analysis of *symmetry* of spiking

around Φ_{max}, we first grouped responses within each cell type according to direction of rotation and, to avoid bias by brain-side effects, according to soma position in terms of brain hemisphere. Fig. 8, *B* and *C* show bubble plots and medians of normalized response rates for a selected soma position for each cell type. To capture the time course of responses, the spike rates at binned distances to Φ_{max} were additionally normalized to the maximum across cells and trials. In general, spiking in the individual responses was not concentrated symmetrically around Φ_{max} but skewed to peak in advance of its passage, thus further promoting a possible anticipation of future *E*-vector angles. Here, it is important to bear in mind that Φ_{max} values denote the *mean* of a respective distribution of spike angles, which is not necessarily equivalent to the *E*-vector angle of *peak* spiking. In the most prominent cases, again obtained from CPU-neurons, the *E*-vector angle of peak spiking preceded $\Phi_{max,\ pooled}$ by about 45°, being equivalent to 1.5 s at 30°/ s rotation velocity.

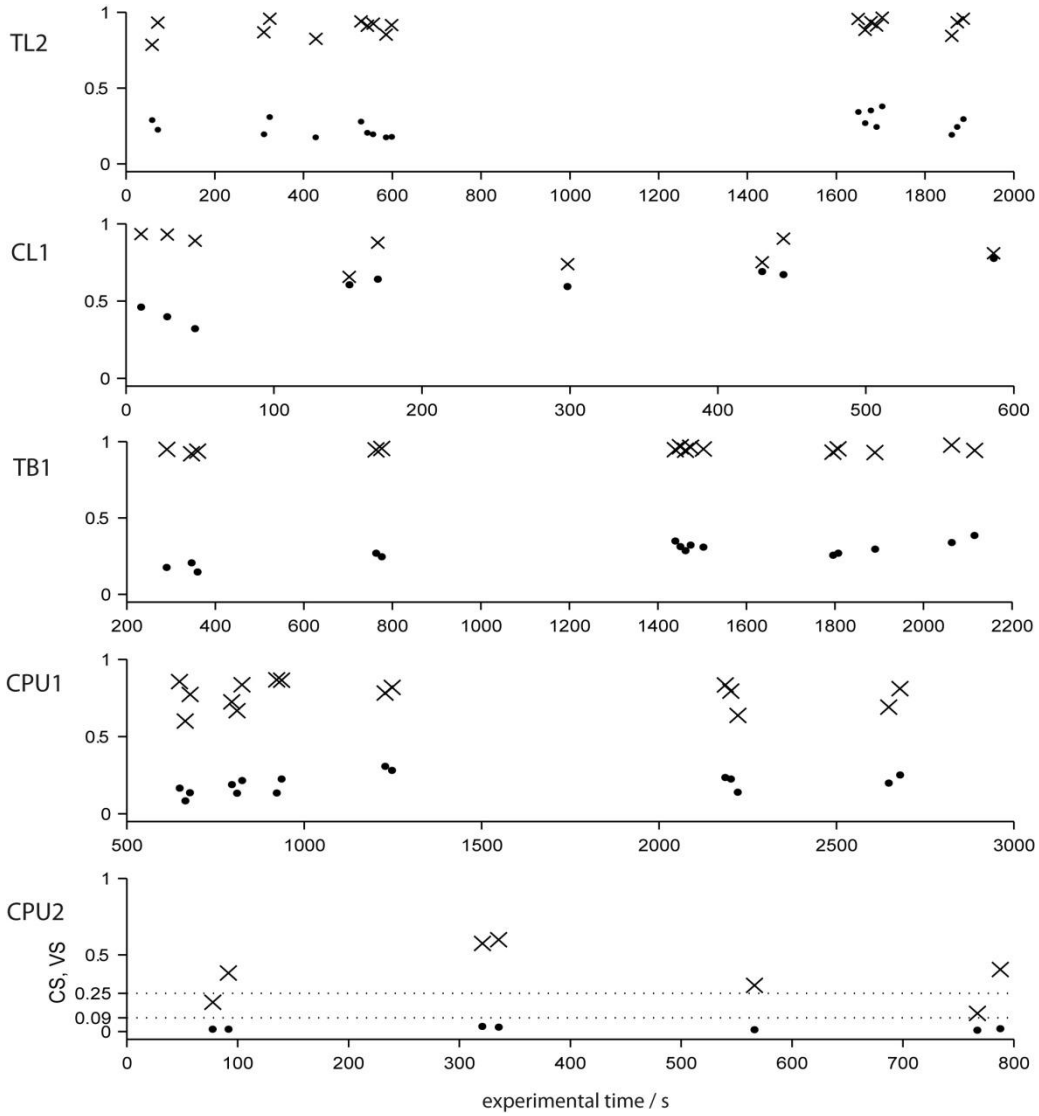

FIG. 7. Within-cell variability of polarization sensitivity. To illustrate within-cell variability of polarization-sensitivity, vector strength (VS; values of |r|, dots) and correlation strength (CS, values of R^2, x-marks) for full rotations of the polarizer (30°/s) were plotted against the time course of exemplary recordings. As a conventional scale for R^2, dotted lines mark the threshold levels for medium and large-sized effects, corresponding to at least 9% and 25% explained variability, respectively. Note that variability of correlation strength, i.e. of principle responsiveness to *E*-vector angles, over time is small in the TL2-and TB1-neuron while relatively high in the two CPU-neurons.

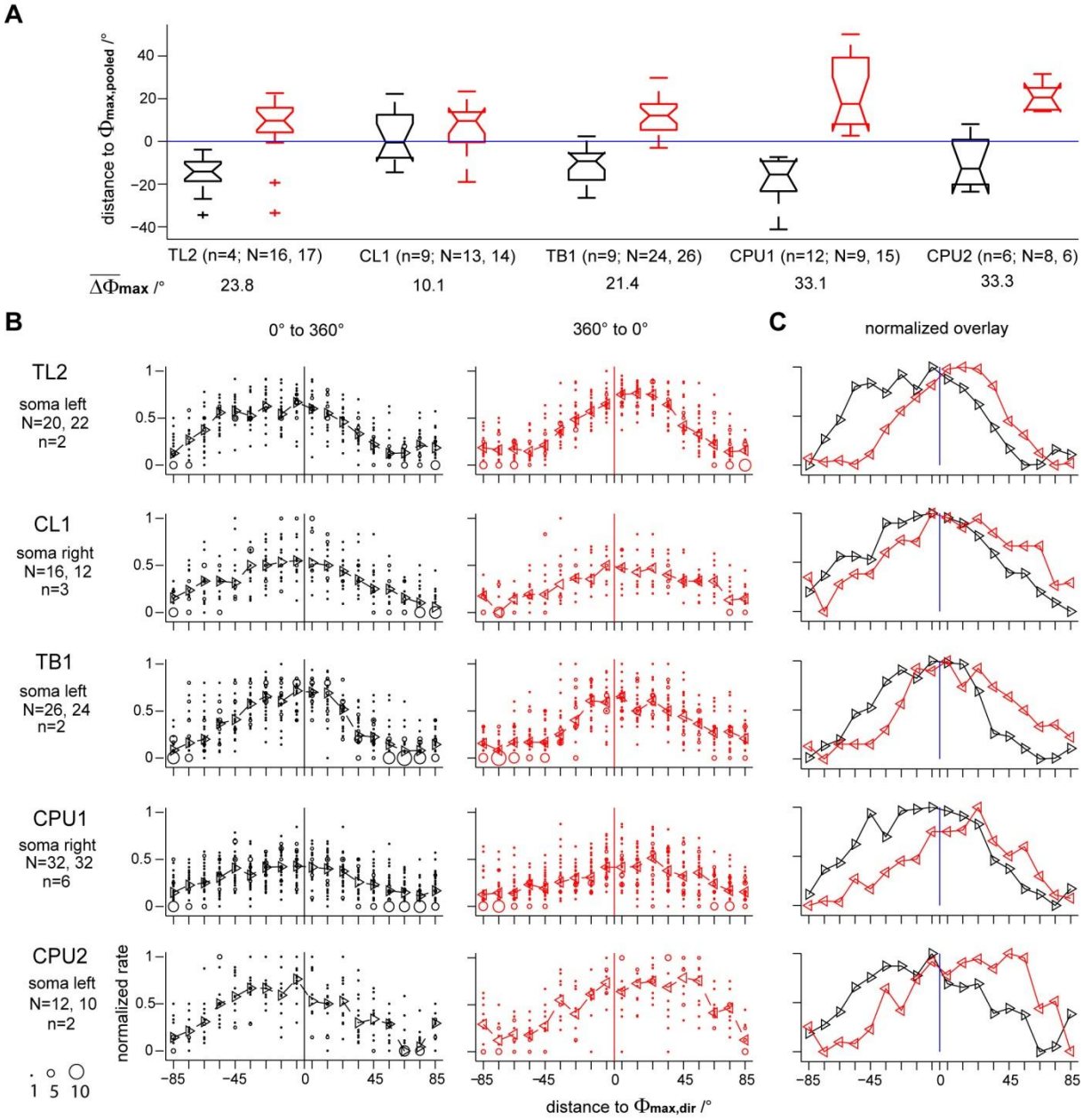

FIG. 8. Responses to rotating polarizer depend on direction of rotation in an anticipatory fashion. In all types of neuron, the preferred *E*-vector angles of individual responses (Φ_{max} values) differed from the overall mean across both directions ($\Phi_{max,\ pooled}$) in a consistent, rotation-direction specific manner. *A:* Distributions of angular distances between $\Phi_{max,\ pooled}$ and Φ_{max} obtained under clockwise (black box plots) and counter-clockwise (red box plots) rotations of a polarizer, respectively. Difference angles ($\Delta\Phi_{max}$) were obtained from N responses of n cells of a given cell type and rescaled to a range of [-90°; 90°] prior to plotting. To include strong responses only, cases with non-significant median spike angle were excluded (Rayleigh-test, α=0.05). In the vast majority of cases, individual Φ_{max} values *preceded* the passage of $\Phi_{max,\ pooled}$. *B*: bubble plots of spike rates at binned (10°) distances to the individual responses' Φ_{max} values ($\Phi_{max,dir}$). Data were obtained from N responses (including weaker responses; significant correlation only) of n cells to clockwise (black, left column) and counter-clockwise (red, middle column) rotation of the polarizer, rescaled to an angular distance range of [-90°; 90°] and normalized to peak rate. Triangles and dashed lines indicate median values. *C*: to ease comparison, median values for both directions were normalized to their maxima and re-plotted together.

Responses to linearly polarized light with stationary E-vector angle. Above, we have provided various characterizations of how spiking in different types of polarization-sensitive neuron is tuned to *E*-vector angle, as rated from responses to continuous rotations of the polarizer. To explore how *E*-vector angles are represented *over time*, we analyzed spiking activity recorded during presentation of polarized light with stationary orientation of the polarizer, lasting for about 20 s to 30 s (Fig. 9*A*). In the majority of cases, we kept presenting the polarized light after tuning measurement and stopped further rotation of the polarizer at positions that evoked a pronounced response. This approach had two advantages over a simple light-on situation: firstly, continuous presentation of polarized light prevented interference by polarization-unrelated lights-on / lights-off responses. Secondly, a directly preceding response to the rotating polarizer indicates that the respective cell was actually in a polarization-sensitive state when the *E*-vector rotation stopped, i.e., when the stationary *E*-vector stimulus began. Due to the anticipatory character of responses to the rotating polarizer, the tested *E*-vector angles that evoked strong responses often differed substantially from the Φ_{min} or Φ_{max} values (see Fig. 8). As a consequence, it would have been misleading to group response data according to the stationary angles´ distances to these. Instead, we grouped recorded activity into putative cases of excitatory response, inhibitory response or 'no' response in a data-driven manner independent from the *E*-vector angle tested. For the tonic responses of TL2-neurons, classification relied on how the median spike rates compared to ongoing activity (OA). If a putative response's median spike count binned at 1 s resolution was equal to or higher than the third quartile of the spike count distribution obtained at the same resolution for OA, it was considered an excitatory response (25 out of 28 cases). Median spike rates equal to or lower than the first quartile of the OA data would have resulted in classification as an inhibitory response, but have not been observed. For all other types of neuron, classification was based on the mere time course of spiking. Here, a simple criterion that was obtained from visual inspection of raw traces sufficed to allocate 89 out of 93 cases to either of two types of response. If the first occurrence of maximum (minimum) spike count in a 5 s-bin PSTH fell within the first 10 seconds after stimulus onset, a sample was rated an excitatory (inhibitory) response. Otherwise, the spiking pattern was classified as neutral. Finally, binned spike rates were normalized to their overall median in case of tonic responses from TL2-neurons or, as for all other types of neuron, rescaled to a common interval of [0, 1].

In CL1-neurons, five out of 23 cases were actually rated excitatory according to the abovementioned criterion (data not shown). We consider these false positive classifications, which might have arisen from the inherent dynamics of OA typical for CL1-neurons (comp. Fig. 2) and could have been promoted by low sample sizes in the later phase of the ´response´ time windows (down to one or two values for 15 s after stimulus onset and later).

Fig. 9*B* illustrates the time courses of responses as captured by normalized spike rates binned at 2 s resolution. With regard to their 'direction' (excitatory vs. inhibitory), responses to stationary *E*-vector angles matched the observations on the effective amplitudes of responses to polarizer rotation. TL2-neurons showed robust excitatory responses but no pronounced inhibitory modulation of spiking was observed, while the opposite was the case in CL1-neurons. By contrast, TB1-and CPU-neurons proved capable of response opponency again, with response courses being more coherent within a respective type of response in TB1-neurons, reflecting the differences in response variability between TB1 and CPU. In terms of time course, the most striking change again occurred at the early-stage transition from TL2- to CL1-neurons: responses to stationary *E*-vector

angles were tonic in TL2-neurons whereas stimulus-specific adaptation was encountered at all downstream stages of *E*-vector signaling. On average, the adapting responses faded to 50 % in normalized amplitude within 6-10 s in CL1 and 8-12 s in TB1 and CPU. Transitions to ongoing-activity-like spiking occurred about 16-20 s after stimulus onset.

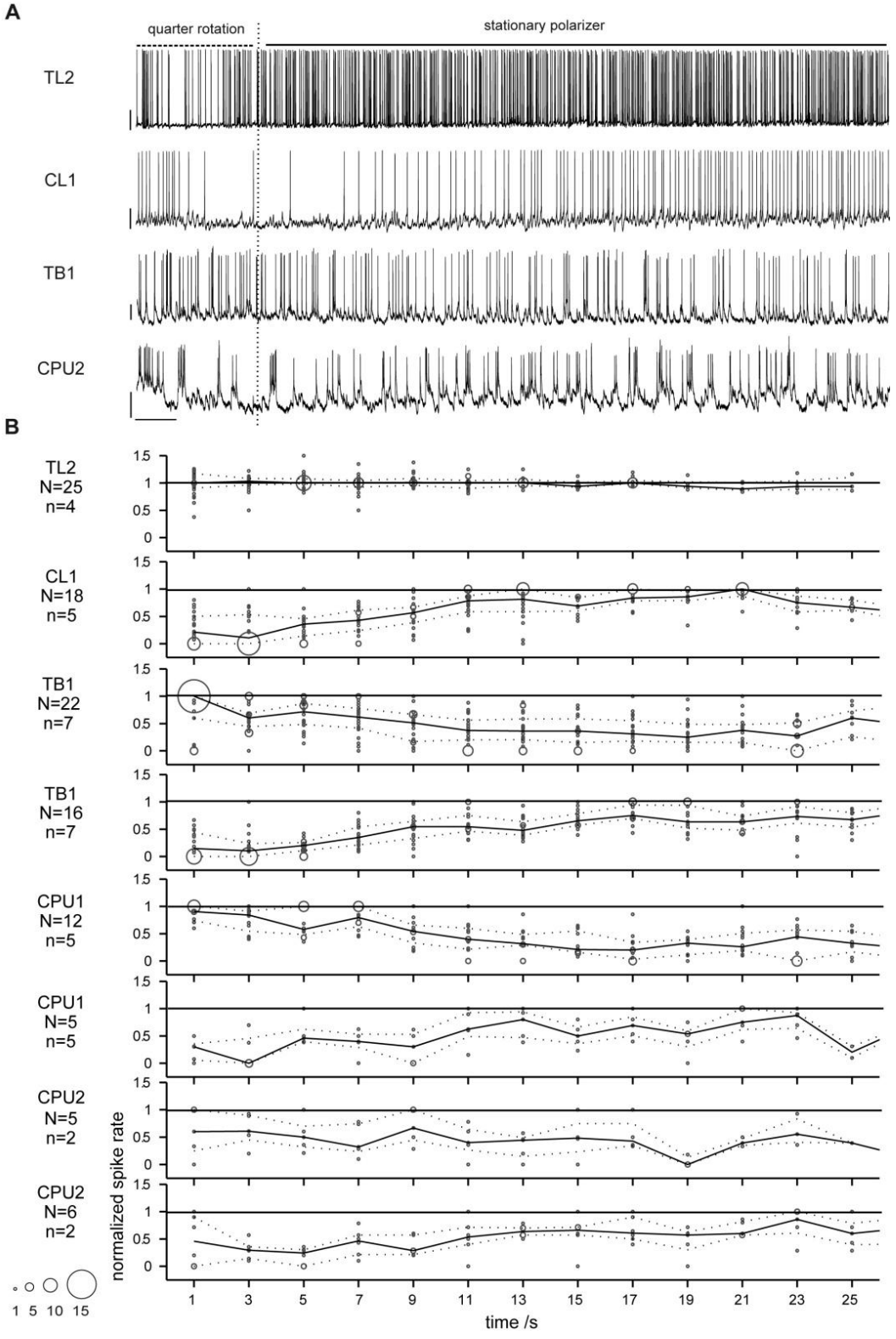

FIG. 9. Responses to presentation of linearly polarized light with stationary *E*-vector angle. *A*: exemplary responses to a stationary polarizer (15 s stimulus duration), preceded

by a quarter rotation (90°, 3 s) of the polarizer. Dashed (solid) horizontal lines: periods with rotating (stationary) polarizer; vertical dashed line: end of polarizer rotation. No response of a CPU1-neuron is shown as spike rates of pronounced responses were too high for resolved plotting. Bars 10 mV, 1s. *B*: time course of responses to a stationary polarizer. Within each cell-type, data were pooled across N responses from n neurons and bubble-plotted for better visualization of scatter. To capture the mere time course of the responses, spike rates were normalized to the within-response median rate for TL2-neurons and to the within-response maximum for all other types of neuron. Solid line plot: median values, dashed line plots: lower and upper quartiles. Note that sampling size generally decreases towards later time bins. As expected from their *E*-vector tuning, responses to stationary angles were exclusively excitatory in TL2-neurons, exclusively inhibitory in CL1-neurons and *E*-vector opponent in TB1-and CPU-neurons. Responses of TL2-neurons were tonic whereas the responses to the specific *E*-vector angle in all other types of neuron quickly adapted.

Novel types of polarization-sensitive neurons of the central complex. Two hitherto undescribed polarization-sensitive neurons of the central complex were termed TLU1 (Fig. 10) and TL6 (Fig. 11). Each of these neurons was recorded and stained only once. Both neurons have wide-field ramifications in several substructures of the central complex and the lateral complexes. TLU1, a tangential neuron of the CBL and CBU, is the first polarization-sensitive neuron with tangential arborizations in the CBU reported so far and might serve an internal feedback role. Putative input regions with fine and smooth neurite endings include a hemisphere of the PB and one of the posterior optic tubercles, both ipsilateral to the cell body in the pars intercerebralis (Fig. 10*A*). Beaded and thus likely presynaptic endings invade the CBL, layers 1 and 2 of the CBU, and both lateral complexes. TL6 is a novel subtype of tangential neuron of the CBL. It has smooth ramifications in the superior medial protocerebrum, the noduli, and the CBL and wide beaded and, thus, presumably presynaptic endings in both lateral complexes (Fig. 11*A*).

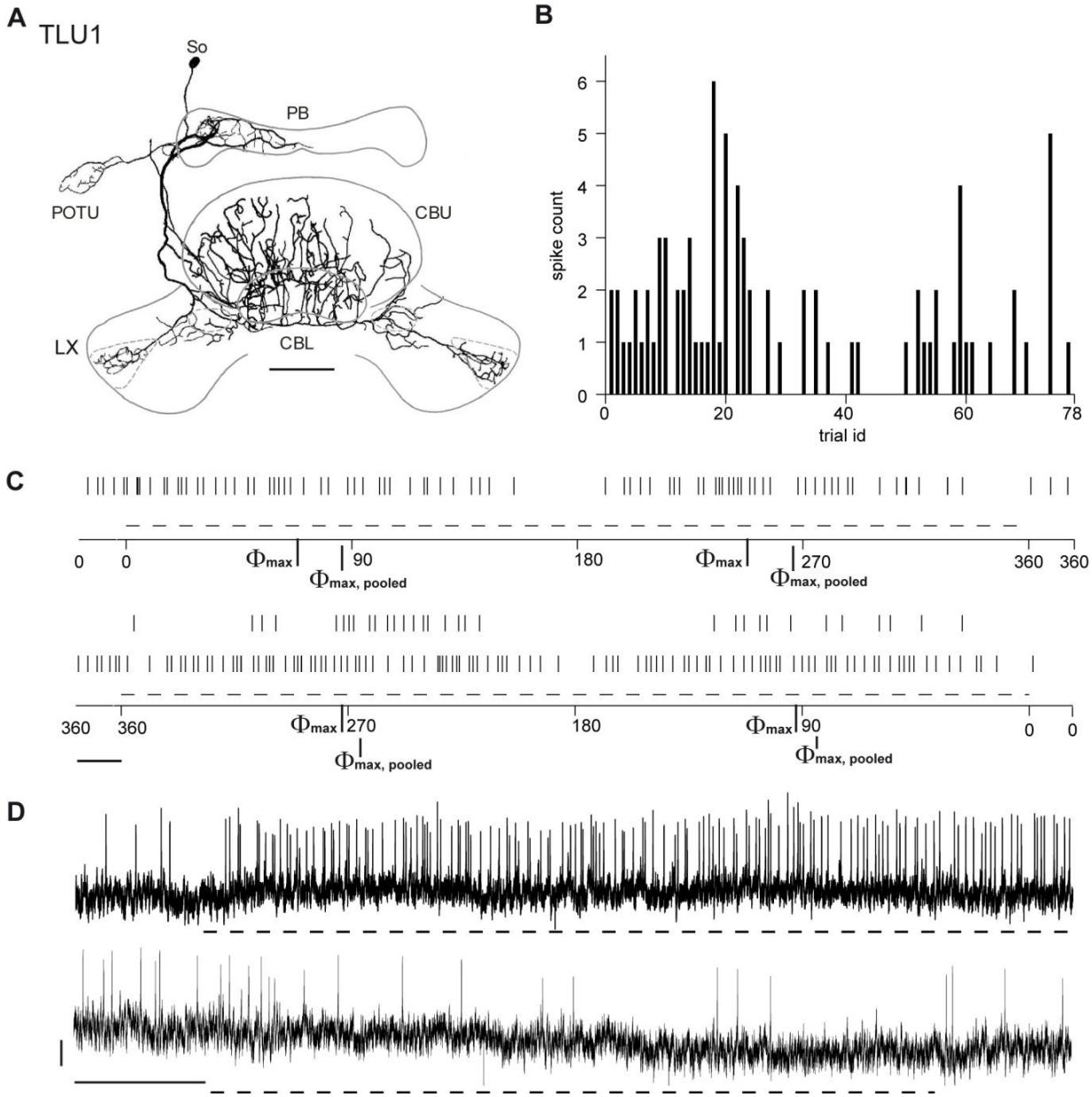

FIG. 10. Morphology, ongoing activity and *E*-vector responses of the TLU1-neuron. *A*: reconstruction of the cell's morphology. Putative input regions with fine and smooth neurite endings include a hemisphere of the protocerebral bridge (PB) and one of the posterior optic tubercles (POTU), both ipsilateral to the soma (So) in the pars intercerebralis. Beaded and thus likely presynaptic endings invade the CBL, layers 1 and 2 of the CBU as well as both lateral complexes (LX). *B*: spike counts in 1000 ms trials of ongoing activity, plotted against trial number and hence the time course of the experiment, whereat trials were not evenly distributed over time. The ongoing activity of TLU1 is low, including several trials with no spiking at all. *C*: Raster plots of spiking responses to clockwise (cw, upper subplot) and counter-clockwise (ccw) rotations of the polarizer at 18°/s. Dashed lines beneath indicate periods of steady polarizer-rotation. Between rotations, presentation of polarized light was preserved. Bars: 1s. Φ_{max} – values for cw / ccw rotations were 68° / 93°; $\Phi_{max,pooled}$ was 86°. *D*: responses to polarized light with stationary *E*-vector angle. Dashed lines beneath the trace mark stimulus time windows. Upper and lower trace show response at 35° and 80° distance to $\Phi_{max\ ,\ pooled}$, respectively. Bars 2 mV / 5s. The response is tonic and more pronounced near $\Phi_{max,\ pooled}$ as expected from the data in *C*.

Physiologically, TLU1 resembled neurons at the input stage, while TL6 shared more properties with intermediate and output stage neurons of the central complex. Similar to TL2-neurons at the input stage, TLU1 showed sparse background spiking and a strong, tonic response to its

preferred *E*-vector angle ($\Phi_{max,pooled}$) while the response amplitude around $\Phi_{min,pooled}$ appeared substantially lower, pointing at a lack of true polarization-opponency (Fig. 10, *B*-*D*). Moreover, responses to a rotating polarizer strongly depended on direction of polarizer rotation in TLU1 and TL6. TL6 spiked more frequently, showed rather moderate, yet polarization-opponent responses to a rotating polarizer and a phasic response at its $\Phi_{max,pooled}$, reminiscent of polarization-sensitive cells at the intermediate (TB1) and output (CPU1, CPU2) stage of the central-complex network. In contrast to TB1-and CPU-neurons, however, TL6 showed no response to stationary presentation of its $\Phi_{min,pooled}$ angle (Fig. 11, *B*-*D*). The processes of TLU1 and TL6 invade neuropils of the central complex and neighboring regions in highly unique patterns. Their complex, wide-spanning arborizations might serve to integrate various inputs or to impose ´operational states´ on the network.

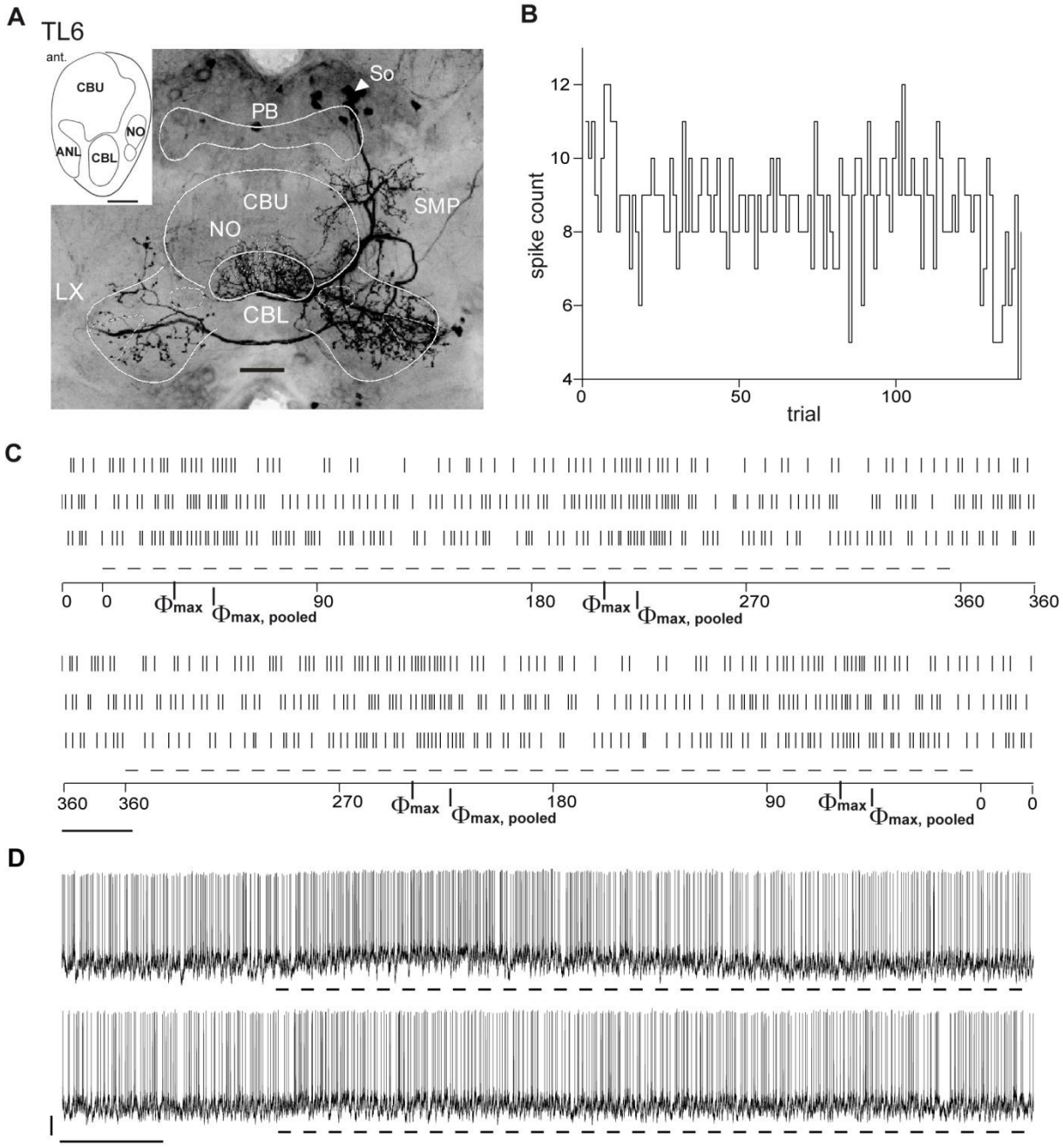

FIG. 11. Morphology, ongoing activity and *E*-vector responses of the TL6-neuron. *A*: projection view of the cell's fluorescent labeling. TL6 has its soma (So) located in the pars intercerebralis and arborizes in the ipsilateral superior medial protocerebrum (SMP), throughout the CBL, the anterior lip (ANL, see inset showing schematic saggital view of the central complex) anterior to the CBL and the paired noduli (NO) posterior to the central body. Endings in the SMP, CBL and the noduli appear smooth, relatively fine and thus presumably constitute input sites. Ramifications with beaded and thus presumably presynaptic endings span both lateral complexes (LX), being more dense in the LX ipsilateral to the soma. *B*: spike counts in 1000 ms trials of ongoing activity, plotted against trial number and hence the time course of the experiment, whereat trials were not evenly distributed over time. *C*: raster plots of spiking responses to clockwise (cw, upper subplot) and counter-clockwise (ccw) rotations of the polarizer at 30°/s. Dashed lines beneath indicate periods of steady polarizer-rotation. Between rotations, presentation of polarized light was preserved. Bars: 1s. Φ_{max} – values for cw / ccw rotations were 31° / 59°; $\Phi_{max,pooled}$ was 46°. TL6 appeared capable of a polarization-opponent response. *D*: responses to polarized light with stationary *E*-vector angle. Dashed lines beneath the trace mark stimulus time windows. Upper and lower traces show responses at response at $\Phi_{max,pooled}$ and $\Phi_{min,pooled}$, respectively. Bars 5mV / 5s. The response at $\Phi_{max,pooled}$ is

transient. Albeit the TL6-neuron appeared capable of polarization-opponent responses as rated from the individual responses shown in *C*, no reduction in spike rate was observed under the presentation of the *E*-vector angle corresponding to the $\Phi_{min,pooled}$.

Discussion

From sensory input to pre-motor output in the locust central-complex polarization-sensitive network: the gross picture. Our study provides novel insights into the dynamics of *E*-vector signaling at different stages of the polarization vision network in the central complex of the locust. In TL2-neurons of the CBL, robust responses to *E*-vector angles are confined to a narrow range around Φ_{max}. Responses are tonic as suggested by earlier recordings using shorter stimuli (Vitzthum et al. 2002), distinct from the rather low and regular ongoing activity (OA) and relatively constant in informational content of the individual spike. This should establish a reliable representation of *E*-vector angles across the population of TL2-neurons at the input stage of the network.

The excitatory responses of TL2-neurons are fed onto ascending subtypes of the CL1-neuron in an inverting manner - probably via GABAergic output of TL2-neurons, as suggested by Homberg et al. (1999). The average level of OA was higher in CL1-neurons than in TL2-neurons and their inhibitory responses adapted rapidly. As a consequence, it appears to be the *absence* of spiking that holds more reliable *E*-vector information in the CL1-neurons encountered here. In line with this notion, their responses to the rotating polarizer were marked by increased variability (and thus by lower reliability) at Φ_{max} as compared to Φ_{min}, particularly within the group of strongly responding neurons. A general increase in response variability from TL2- to CL1-neurons may trace back to superimposition by the more variable, state-like OA typical for CL1-neurons.

At the intermediate stage of the network, tangential neurons of the PB (TB1) responded more robustly to both Φ_{min} and Φ_{max}, which is referred to as polarization opponency. Here, the association between the individual neuron´s spiking and the acute *E*-vector angle was strong and relatively stable for responses to the rotating polarizer. Both phenomena stabilize the compass-like polarotopic mapping of *E*-vector angles across the PB reported by Heinze and Homberg (2007). They may arise from antagonistic integration across CL1-neurons with opponent tuning (Fig. 12). In individual CL1-neurons, the difference between extreme states of OA readily matches the difference in spike rate between *E*-vector responses at Φ_{max} and Φ_{min}. Thus, the mere observation of an individual CL1-neuron's spiking cannot suffice for unambiguous signaling of *E*-vector angles. In theory, this ambiguity could be resolved by inhibitory coupling within pairs of TB1-neurons, with each of two 'paired' TB1-neurons receiving input from a CL1-neuron via non-inverting synapses. If the two CL1-neurons are tuned to Φ_{min} angles 90° apart, their antagonistic integration should result in the polarization opponency found in TB1-neurons (Fig. 12*D*). This antagonistic integration might also smooth out the pronounced state-like variability of OA that interferes with polarization-signaling in CL1-neurons. In addition to explaining how polarization-opponency in TB-neurons arises, the model unravels the redundancy of the polarotopic representation across the width of the PB as a mere ´byproduct´ of the wiring which establishes mutual inhibition among TB-neurons. In other words, the second, from the perspective of compass-signaling demands ´redundant´ representation of another full 180°, consists of those arborizations making up the inhibitory TB-TB´connections.

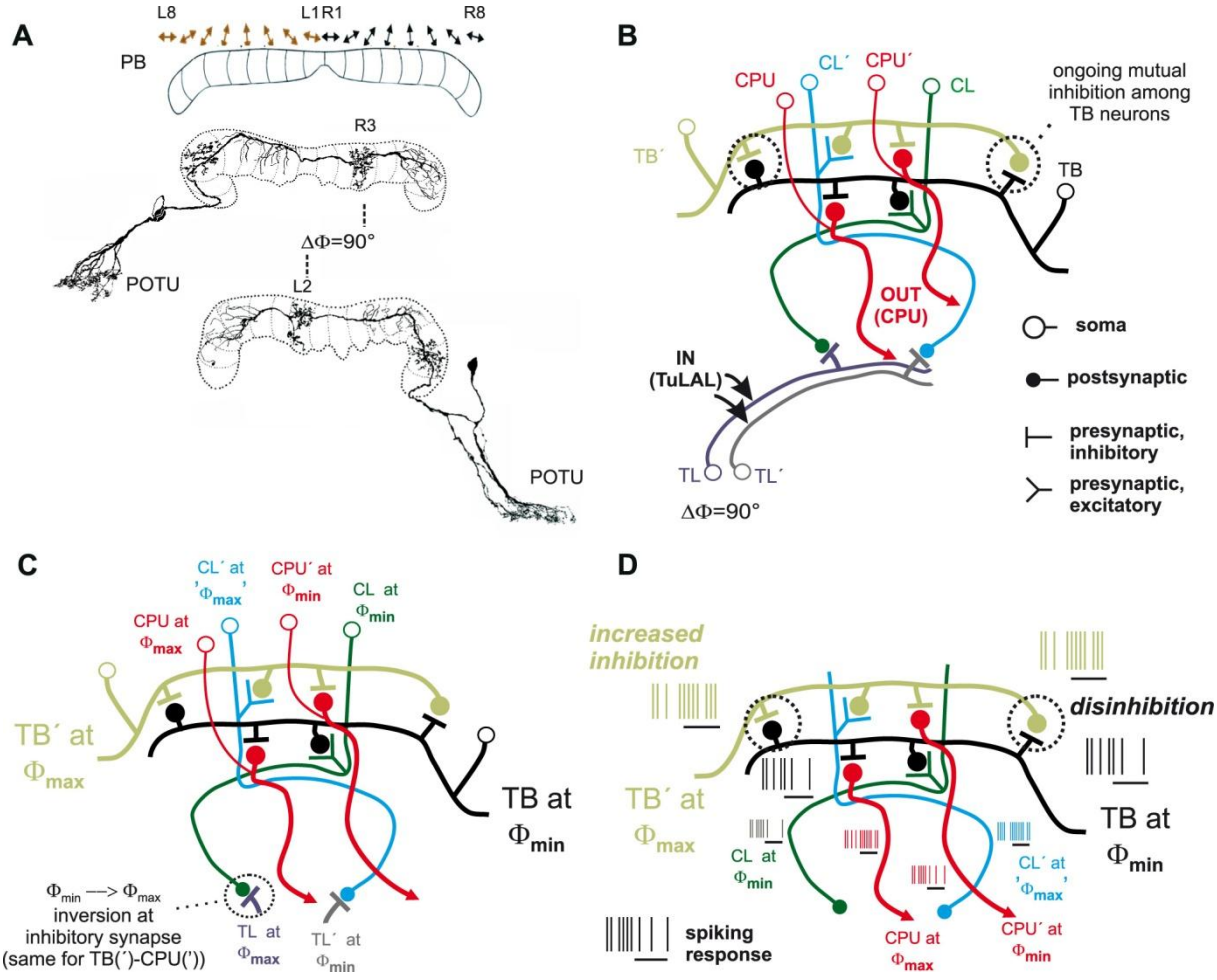

FIG. 12. A mutual inhibition model of polarization-opponent *E*-vector responses in TB1-neurons. Robust polarization-opponency of *E*-vector responses might arise from mutual inhibition among TB1-neurons that receive input from opponently tuned CL1-neurons. *A*: polarotopy in the protocerebral bridge (PB, upper subfigure) and relevant morphological features of TB1-neurons. The PB holds a redundant polarotopic representation of *E*-vector angles, covering 2 x 180° across the 16 vertical slices of the neuropil (corresponding to 180° across 8 slices per hemisphere). Double arrows symbolize the Φ_{max} values of TB-neurons that have varicose and hence putatively presynaptic terminals in the respective slices of the PB sketched beneath. Each TB1-neuron has two distinct columns of presynaptic arborizations lying 8 slices apart from one another and hence in different hemispheres of the PB. Smooth and thus presumably dendritic endings span three neighbouring slices in each hemisphere, with the proximalmost (relative to soma position) of the three lying one slice distal to the respective varicose column. The particular TB1-neurons shown here are tuned to Φ_{max} values 90° apart. According to the general morphology described above, their presynaptic columns lie four slices apart, being congruent with slices that hold dendritic columns of the putative partner TB-neuron. *B*: presumed synaptic wiring among basic types of central-complex neuron involved in the model. Input to the network is provided onto TL-neurons by TuLAL-neurons connecting the anterior optic tubercles to the lateral accessory lobes (see Fig. 1). The model posits inhibitory synapses between TL- and CL-neurons as well as within pairs of TB-neurons and between TB-and CPU-neurons, with synaptic partners being tuned to Φ_{max} values 90° apart as sketched in *C*. *D*: hypothetical network response, as expected from the wiring pattern and resultant tuning relationships depicted in *B* and *C*, to an *E*-vector that matches Φ_{max} for the input TL-neuron to the left in the diagram and Φ_{min} for the second one, labeled TL´. Black horizontal lines beneath the stylized spike trains mark stimulus time windows (adaptation to further ongoing stimulation not shown). In particular, the TB-neuron for which the stimulus *E*-vector angle matches Φ_{min} receives reduced excitatory input from its partner CL-neuron as well as increased inhibitory input from its partner TB-neuron (TB´) for which, in turn, the same stimulus *E*-vector angle corresponds to Φ_{max}. The reduced activity of the TB-neuron at its Φ_{min} releases its partner TB´, from inhibition via the TB-TB´ synapse, thus adding enhancement to the

excitatory input TB´ receives from its partner CL´. Note that the activity of CL´ at its ´Φ_{max}´ is comparatively high but not distinct from higher levels of its ongoing activity whereas the mechanism of mutual inhibition / disinhibition among TB-neurons provides a basis for truly polarization-opponent responses downstream to CL-neurons.

The enhancement in correlation strength (CS) at the transition from CL1- to TB1-neurons is accompanied by both a stabilization of informational content and a *reduction* of response amplitude in terms of overall vector strength (VS; Fig. 13*A*). This is suggestive of a CS-VS trade-off to be a crucial early step to bundle a distributed sensory representation into pooled pre-motor output (of CPU-neurons) which is ´meaningful´ over the entire range of *E*-vectors - even if its overall VS is lower compared to the input stage. Furthermore, this observation speaks against alternative models that could assume a process of ´reading out the compass´ by thresholding the responses of TB1-neurons and comparing the result across slices of the PB, as the thresholding of response rates would be hampered by the reduction in response amplitude.

A second inversion of responses presumably occurs at the transition from TB1- to CPU-neurons near the output stage of the network, as indicated by the near 90° phase shift in the polarotopy between TB1- and CPU-neurons that arborize in the same slice of the PB (Heinze and Homberg 2007; Fig. 13*B*). In CPU-neurons, variability of responses was particularly high with respect to general responsiveness, i.e. correlation strength, response amplitude, and informational content per spike (IpS). At this stage, average response amplitudes are negatively related to the cells´ average levels of OA. This is suggestive of a masking of polarization responses by high-level OA that lasts throughout the 15 – 45 min period of a recording session. In CPU2-neurons, the resultant span of response strength ranges from effective unresponsiveness to a pronounced polarization opponency. This resembles tuning profiles of polarization-sensitive descending neurons (Träger and Homberg 2011) and is in concert with the variability of polarotactic responses to modulations of zenithal *E*-vector angle observed in tethered flying locusts (Mappes and Homberg 2004) and in crickets walking in a treadmill (Brunner and Labhart 1987).

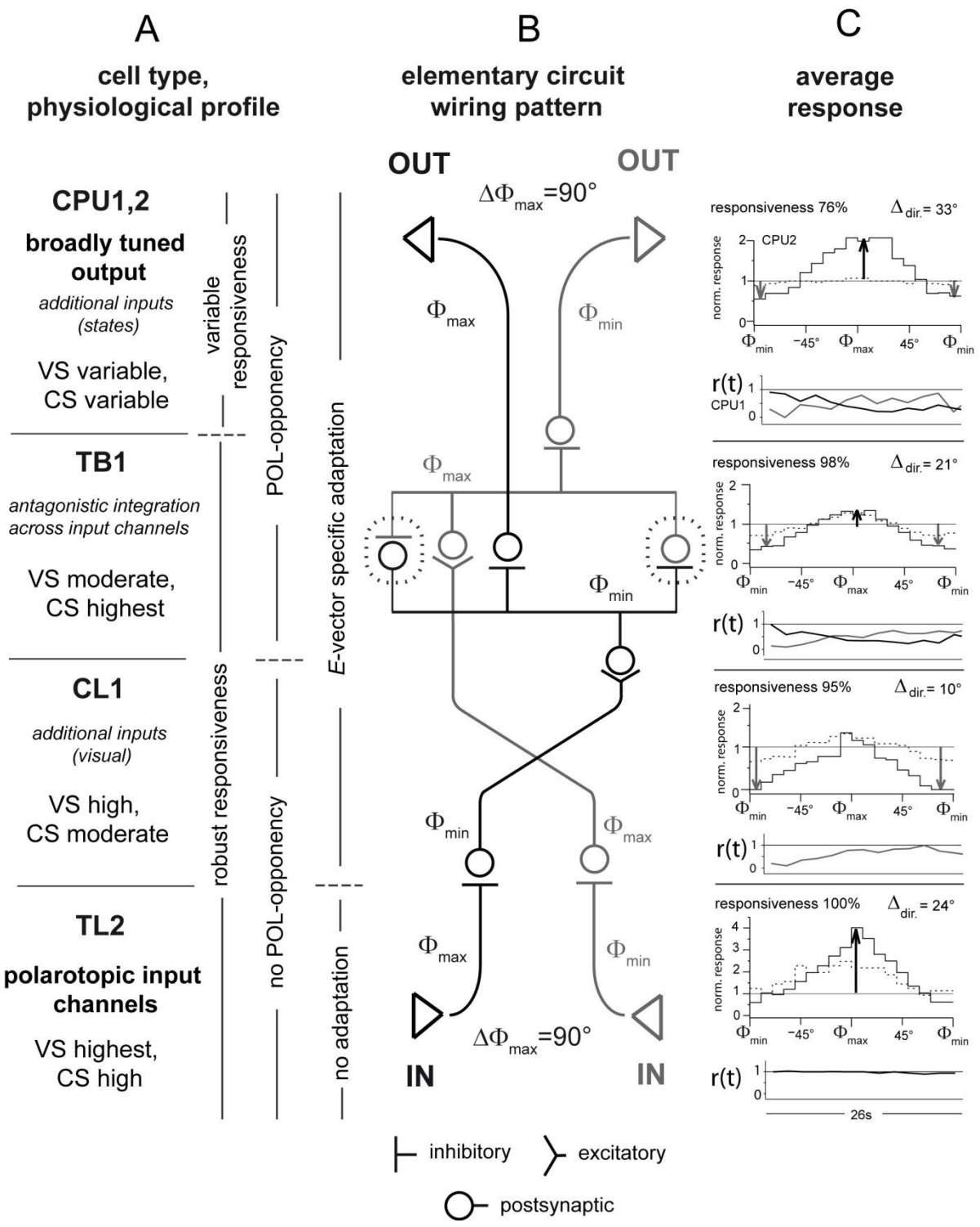

FIG. 13. Summary of main findings. In *A-C*, upwards reading corresponds to going downstream along the presumed hierarchy of processing, TL-CL-TB-CPU. *A:* cell types at consecutive stages of processing, their putative functional relevance and related response features. VS, vector strength; CS, correlation strength. Statements in italics are hypothetical (see Discussion). Statements on CPU-neurons give a summary across CPU1 and CPU2, if not indicated otherwise as in *C*. *B*: simplified scheme of the elementary circuit for the generation of conditional, broadly tuned signaling of the polarization-plane (CPU-neurons) via antagonistic integration (TB1, dashed contours) across opponent, narrowly tuned input channels (TL2, CL1), as proposed in Fig. 12. *C*: tuning to *E*-vector angle and time course of responses to preferred and / or anti-preferred angles. Upper subplots: responses to a rotating polarizer. These tuning plots show medians of binned (10°) spike counts, normalized to median spike count in ongoing activity (OA) and plotted against the angular distance to the mean spike angle (Φ_{max}). Data summarize responses obtained from

clockwise and counter-clockwise rotations but differentiate between stronger (solid line) and weaker (dashed line) responses. At this, responses, including those that lack significant correlation, were ranked according to vector strength; stronger (weaker) responses correspond to the upper (lower) half of the amplitude-ranked dataset. Black (grey) vertical arrows: responses near Φ_{max} (Φ_{min}) that proved robust when compared to very high (very low) levels of OA (these comparisons not shown here). Responsiveness: proportion of responses with significant correlation between spiking and *E*-vector angle; $\Delta_{dir.}$: angular difference between direction-specific Φ_{max} -values. For details on data sets and measures, see Figs. 4, 5, 8 (for robustness of responses near Φ_{max} and Φ_{min} , weaker vs. stronger responses and rotation-of-direction specificity, respectively) and Fig. 9 (for response time courses). Note that the anticipatory effect in direction-of-rotation specific responses is even higher for the *E*-vector angles at peak spike rates, which are not shown here (Fig. 9*D*). Lower subplots: r(t) depicts the average (median) time course of excitatory (black lines) or inhibitory (grey lines) responses to stationary *E*-vector angles over 26 seconds. To capture the mere time course of the responses, binned (2s) spike rates were normalized to the within-response median rate for TL2-neurons and to the within-response maximum for all other types of neuron. As expected from their *E*-vector tuning, responses to stationary angles were exclusively excitatory in TL2-neurons, exclusively inhibitory in CL1-neurons and *E*-vector opponent in TB1-and CPU-neurons. Responses of TL2-neurons were tonic while the responses to the specific *E*-vector angle in all other types of neuron quickly adapted.

A working hypothesis on central-complex function. *E*-vector signaling at the output stage of the central-complex network appears to be governed by variations in responsiveness in terms of lasting ´responsiveness-states´ that are related to the level of ongoing activity (OA). Such modulation of higher-stage responsiveness to exteroceptive cues could assign behavioral ´meaning´ to these cues. Future studies should strive to identify the modulators. These might depend on experience and lifestyle and be related to circadian rhythms, feeding states, and locomotor states such as resting, flying or walking. The indicators of these states could comprise representations of exteroceptive cues, such as airflow or visual flow as well as idiothetic information from proprioceptive feedback or motor-efference copies. First insights into this subject were provided by recordings from tethered flying locusts that revealed flight-correlated activity changes in neurons of the lateral accessory lobes, the main input-output relays of the central-complex network (Homberg 1994). Notably, the neurons that changed activity in a flight-correlated manner included CPU2-neurons. CPU2-neurons arborize in the CBU (see Fig. 1) where they might receive sensory information that signals locomotor state and thus, presumably, the acute behavioral relevance of compass information (el Jundi et al. 2010). The morphological complexities of the newly discovered TLU1- and TL6-neurons are also in line with the notion of the central-complex network as a site for complex integration and modulation (Figs. 10, 11).

In addition to lasting responsiveness-states, we have observed response features suited to link compass signaling to the behavioral goal to stay oriented. Responses to constant stimuli in terms of polarized light with stationary *E*-vector angle were marked by stimulus-specific adaptation (SSA) in all cell types downstream to TL2-neurons (Fig. 13*C*). This may correlate with the tendency to steer a steady course relative to a polarization pattern which was observed in tethered flying locusts (Mappes and Homberg 2004): as long as the locust stays 'on course', the neurons do no longer modulate their firing as a function of *E*-vector angle. Responsiveness to varying *E*-vectors that, under a natural sky, indicate changes in heading direction was generally preserved but more variable at the output stage of the polarization-vision network (Fig. 13). Here, anticipation of near-future *E*-vector angles additionally promotes compass orientation.

Together, the findings outlined above support the concept of the central complex as a substrate of the 'contextualization' of sensory information for locomotor control in goal-driven

behaviors, demonstrated in flies (Strauss 2002, Triphan et al. 2010) and cockroaches (Bender et al. 2010, Guo and Ritzmann 2014). To this end, robust sensory inputs to the network may get ´contextualized´ by certain response features such as SSA as well as via modulation by state indicators, in order to be integrated in the formation of motor programs or not - depending on current behavioral goals. A recent study on the encoding of food odor value in the *Drosophila* brain suggests that this preliminary model on central-complex function might hold across species and sensory modalities (Beshel and Zhong 2013). The activity of neurons that invade the fan-shaped body, the fly's homologue of the CBU, reflected the behaviorally indicated attractiveness of food odors as a function of the animals 'feeding state'. It thus exceeds the role of a mere sensory representation of the odors by adding a context-dependent weighing to it, providing a signaling of the 'acute value' of a respective food odor which is predictive of a locomotor approach response to the odor source.

Parallels to vertebrates. Our findings point at three ways in which polarization-signaling in the locust brain parallels higher sensory processing in vertebrate brains: the co-shaping of responses by ongoing activity (OA), the specific adaptation to constant stimuli, and the ´prediction´ of upcoming stimuli from the recent stimulus history.

In addition to the relation between responsiveness and the level of OA in CPU-neurons, a modulatory role of OA is also suggested by the fact that, during polarizer rotation, spike rates at neutral *E*-vector angles closely matched those of mere OA, in particular in TB1-and CPU-neurons. This may point to the observed response to result from superimposition of an ideal *E*-vector response with acute levels of OA. In vertebrates, an integration of prestimulus OA with an ideal representation of a visual stimulus was shown to explain the large variability in V1 responses (Arieli et al. 1996). Several studies confirmed that variations in prestimulus OA can actually predict stimulus-detection rate in monkey vision (Supèr et al. 2003) as well as perceptual decisions on ambiguous stimuli in both human vision (Hesselmann et al. 2008) and human somatosensation (Boly et al. 2007). In those studies, states of OA were referred to as ´brain states´ related to attention or vigilance.

Responses to constant stimuli, i.e. polarized light with stationary *E*-vector angle, were marked by SSA in all cell types downstream to TL2-neurons. In vertebrates, SSA is a prominent feature of higher-stage auditory processing and a presumed correlate of behavioral habituation (Netser et al. 2011), as we hypothesize here for orientation responses in locusts. Work in progress suggests that SSA in the locust central complex extends to other types of visual stimuli as well.

Previous work (Heinze and Homberg 2007) has drawn an analogy between polarization-sensitive ´compass neurons´ in the locust central complex and vertebrate head direction (HD) cells, discovered in rats by Ranck (1984) and studied in detail by Taube and colleagues (Taube 2007, Clark and Taube 2012). Rat HD cells refer to visual landmarks to signal heading direction in local sceneries; they are low in OA and fire to their preferred stationary head direction ($\Phi_{max,\ stationary}$) with a Gaussian-shaped tuning covering about 90° centered to $\Phi_{max,\ stationary}$. Our current observations extend the analogy between vertebrate HD cells and polarization-sensitive neurons in the locust central complex to anticipatory signaling under rotatory stimulation. Yet, the pronounced asymmetry of spiking around Φ_{max} (i.e., the difference between Φ_{max} and the angle at peak firing) that occurred in polarization-sensitive neurons has not been reported for HD cells. Its presence could be confined to rotation velocities below those applied in the rat studies. In fact, the shift of angular tuning in HD cells is a function of rotation velocity: it is adjusted as to result in an

anticipation of the preferred angle by an invariant, cell-type specific time interval of about 25-75 ms. Future studies should aim to elucidate whether the anticipatory shift in locust polarization-sensitive neurons is also invariant in time period or, alternatively, constant in the angular domain, or a function of rotation velocity in both respects. As for HD cells, anticipation is believed to depend on idiothetic indicators of head motion, such as vestibular signals, proprioceptive signals and motor-efference copies. By contrast, the predictive signaling by polarization-sensitive neurons we observed apparently does not require idiothetic indication of head movements, as locusts were mounted to a holder with their heads immobilized. Rather, it might be controlled by a mechanism which includes information on the velocity and direction of (apparent) rotatory movements inferred from the stimulus history per se, i.e., from the *E*-vector angles encountered in the near past and the corresponding time intervals.

Adaptation to constant head orientation has not been reported for rat HD cells. In fact, they show sustained activity during periods that lack visual cueing, a feature beneficial for tasks of path integration (dead reckoning), such as keeping track of changes in orientation in the dark (see Taube 2007 for review). This holds for HD cells encountered at various processing stages and might point to a difference between the navigational strategies applied by rats and locusts. Rats typically explore their environment by collecting visual cues and turning the head while locomoting about the local scenery. Spatial learning based upon this strategy may strongly depend on exact and ongoing path integration. Locusts could refer to sky compass signals for the simpler purpose of locomotion in a straight direction, independent from how this direction may relate to specific features of the present local scenery (Mappes and Homberg 2004).

Methodological considerations on the interpretation of the novel response measures. We have characterized *E*-vector responses with measures of correlational strength (CS, quantified by R^2) and vector strength (VS, quantified by $|r|$). Below, we provide some reflection on the adequacy and informative value of these measures as a basis for future discussions of *E*-vector responses within this framework. The rationale for which we refer to VS as an *indirect* measure of modulation depth (h) rather than to calculate h directly (as the ratio of modulation amplitude to carrier amplitude) is that estimating a 'carrier amplitude' for the *E*-vector response from activity during rotation of the polarizer is not trivial, albeit the recent results show that one might approximate it in higher-stage neurons by the overall mean or the spike rate at a rather 'neutral' angle such as Φ_{max}. +/- 45°.

While the statistical interpretation of R^2 and $|r|$ alone is straight, their numerical relation is not trivial (see Fig. 7) and their respective relevance may depend on physiological concepts. A perfect correlation between spiking and *E*-vector angle ($R^2=1$) may concur with minimum modulation in spike rate ($|r|<<1$). An increase in $|r|$ does not necessitate an increase in R^2 and may well concur with a *decrease* in it. If different levels of uncorrelated, constant amplitude offsets are superimposed on the same artificial spike-rate signal (i.e., if its ´carrier amplitude´ is varied while its absolute modulation amplitude, peak width and period remain unchanged), $|r|$ behaves positively related to relative modulation depth, while R^2 does not change. For the characterization of responses to a rotating polarizer, the criterion for principle responsiveness to *E*-vectors should be the statistical *significance* of the correlation between spiking and *E*-vector angle (the p-value of R^2 at $\alpha=0.05$ and $\beta=0.2$).

For physiological interpretation, we suggest to consider CS *and* VS in a processing-stage dependent manner. At the *input* level, high VS

may reflect sharp *E*-vector tuning within peripheral polarotopic channels, a prerequisite for enhanced CS in higher-stage responses integrated *across* channels, while within-channel CS may be comparatively low. Near the *output* stage of the central-complex network, enhanced CS could help to bundle the activity of the polarotopic population of neurons into a pre-motor output which is ´meaningful´ over the entire range of *E*-vectors even if its overall VS is lower compared to the input stage, corresponding to the CS-VS tradeoff discussed above. Still, VS may serve to quantify differences in amplitude between higher-stage responses that have equal CS but are superimposed by different levels of uncorrelated ongoing activity. In case of complete masking of an *E*-vector dependency by superimposition of uncorrelated OA, very low VS is accompanied by non-significant and numerically small R^2.

Conclusion. Studies on insect sensory systems and behavior have shown that, and in part how, ´higher´ goal-driven behavior can be controlled by minute brains. For instance, visual processing low on the phylogenetic scale can mediate spatial orientation across a range of scales (obstacle avoidance, navigation) as well as crucial event-related behavior (escape predators, catch prey) most precisely and efficiently despite lacking the ´conscious´ perceptual organization of visual landscapes that we readily experience during comparable tasks (e.g., see Milner and Goodale 1995). We have described dynamics of compass-signaling in an insect brain suited to mediate the control of locomotion in a navigation-like fashion, in particular by relating instantaneous compass-signaling to stimulus history via anticipation and adaptation. Current work addresses the additional modulation of this compass-signaling by events in the visual object-background scenery.

Acknowledgements

We thank Dr. Keram Pfeiffer for feedback on data analyses, Arseny Finkelstein for alluding to the information-theoretic approaches by Skaggs et al., Joss von Hadeln for the reconstruction of the TLU1-neuron, Milosz Krala and Stefan Ries for participation in some experiments, and Dr Erich Buchner for supplying anti-synapsin antibodies.

Grants

This work was supported by grants HO 950/16-3, HO 950/21-1 and HO 950/23-1 from the Deutsche Forschungsgemeinschaft to U. Homberg.

Disclosures

The authors certify that there are no competing financial interests.

References

Arieli A, Sterkin A, Grinvald A, and Aertsen A. Dynamics of ongoing activity: explanation of the large variability in evoked cortical responses. *Science* 273: 1868-1871, 1996.

Ashida G, Wagner H, and Carr CE. Processing of phase-locked spikes and periodic signals. In: *Analysis of Parallel Spike Trains*, edited by Grün S and Rotter S. Springer, 2010. p. 59-74.

Bech M, Homberg U, and Pfeiffer K. Receptive fields of locust brain neurons are matched to polarization patterns of the sky. *Curr Biol* 24: 2124-2129, 2014.

Bender JA, Pollak AJ, and Ritzmann RE. Neural activity in the central complex of the insect brain is linked to locomotor changes. *Curr Biol* 20: 921-926, 2010.

Berens P. CircStat: A MATLAB toolbox for circular statistics. *J Stat Softw* 31, 2009.

Beshel J and Zhong Y. Graded encoding of food odor value in the *Drosophila* brain. *J Neurosci* 33: 15693–15704, 2013.

Boly M, Balteau E, Schnakers C, Degueldre C, Moonen G, Luxen A, Phillips C, Peigneux P, Maquett P, and Laureys S. Baseline brain activity fluctuations predict somatosensory perception in humans. *Proc Natl Acad Sci U.S.A. (PNAS)* 104: 12187-12192, 2007.

Brunner D and Labhart T. Behavioural evidence for polarization vision in crickets. *Physiol Entomol* 12: 1-10, 1987.

Clark BJ and Taube JS. Vestibular and attractor network basis of the head direction cell signal in subcortical circuits. *Front Neural Circuits* 6, 2012.

Clements AN and May TE. Studies on locust neuromuscular physiology in relation to glutamic acid. *J Exp Biol* 60: 673-705, 1974.

Eggers A and Gewecke M. The dorsal rim area of the compound eye and polarization vision in the desert locust (*Schistocerca gregaria*). In: *Sensory Systems of Arthropods*, edited by Wiese K, Gribakin FG, Popov AV, and Renninger G. Birkhäuser, 1993. p. 101-109.

el Jundi B, Heinze S, Lenschow C, Kurylas A, Rohlfing T, and Homberg, U. The locust standard brain: a 3D standard of the central complex as a platform for neural network analysis. *Front Syst Neurosci* 3: 21, 2010.

el Jundi B, Pfeiffer K, Heinze S, and Homberg U. Integration of polarization and chromatic cues in the insect sky compass. *J Comp Physiol A* 200: 575-589, 2014.

el Jundi B, Pfeiffer K, and Homberg U. A distinct layer of the medulla integrates sky compass signals in the brain of an insect. *PLoS ONE* 6: e27855, 2011.

Fisher NI. *Statistical Analysis of Circular Data.* Revised edition. Cambridge University Press, 1995.

Frost BJ and Mouritsen H. The neural mechanisms of long distance animal navigation. *Curr Opin Neurobiol* 16: 481-488, 2006.

Guo P and Ritzmann RE. Neural activity in the central complex of the cockroach brain is linked to turning behaviors. *J Exp Biol* 216: 992-1002, 2013.

Grün S and Rotter S (Eds.). *Analysis of Parallel Spike Trains.* Springer, 2010.

Heinze S and Homberg U. Maplike representation of celestial *E*-vector orientations in the brain of an insect. *Science* 315: 995-997, 2007.

Heinze S and Homberg U. Neuroarchitecture of the central complex of the desert locust: intrinsic and columnar neurons. *J Comp Neurol* 511: 454-478, 2008.

Heinze S and Homberg U. Linking the input to the output: new sets of neurons complement the polarization vision network in the locust central complex. *J Neurosci* 29: 4911–4921, 2009.

Heinze S and Reppert SM. Sun compass integration of skylight cues in migratory monarch butterflies. *Neuron* 69: 345-358, 2011.

Heinze S, Gotthardt S, and Homberg U. Transformation of polarized light information in the central complex of the locust. *J Neurosci* 29: 11783–11793, 2009.

Hesselmann G, Kell CA, Eger E, and Kleinschmidt A. Spontaneous local variations in ongoing neural activity bias perceptual decisions. *Proc Natl Acad Sci U.S.A. (PNAS)* 105: 10984–10989, 2008.

Homberg U. Flight-correlated activity changes in neurons of the lateral accessory lobes in the brain of the locust *Schistocerca gregaria*. *J Comp Physiol A* 175: 597-610, 1994.

Homberg U. In search of the sky compass in the insect brain. *Naturwissenschaften* 91: 199-208, 2004.

Homberg U, Heinze S, Pfeiffer K, Kinoshita M, and el Jundi B. Central neural coding of sky polarization in insects. *Phil Trans R Soc B* 366: 680-687, 2011.

Homberg U, Vitzthum H, Müller M, and Binkle U. Immunocytochemistry of GABA in the central complex of the locust *Schistocerca gregaria*: identification of immunoreactive neurons and colocalization with neuropeptides. J Comp *Neurol* 409: 495–507, 1999.

Kinoshita M, Pfeiffer K, and Homberg U. Spectral properties of identified polarized-light sensitive interneurons in the brain of the desert locust *Schistocerca gregaria*. *J Exp Biol* 210: 1350-1361, 2007.

Kreuz T, Chicharro D, Greschner M, and Andrzejak RG. Time-resolved and time-scale adaptive measures of spike train synchrony. *J Neurosci Methods* 195: 92-106, 2011.

Mappes M and Homberg U. Behavioral analysis of polarization vision in tethered flying locusts. *J Comp Physiol A* 190: 61-68, 2004.

Massey FJ. The Kolmogorov-Smirnov test for goodness of fit. *J Am Stat Assoc* 46: 68-78, 1951.

Merlin C, Heinze S, and Reppert SM. Unraveling navigational strategies in migratory insects. *Curr Opin Neurobiol* 22: 1-9, 2011.

Milner AD and Goodale MA. *The visual brain in action.* Oxford University Press, 1995.

Mouritsen H. Navigation in birds and other animals. *Image Vision Comput* 19: 713-731, 2001.

Müller M, Homberg U, and Kühn A. Neuroarchitecture of the lower division of the central body in the brain of the locust (*Schistocerca gregaria*). *Cell Tissue Res* 288: 159-176, 1997.

Netser S, Zahar Y, and Gutfreund Y. Stimulus-specific adaptation: can it be a neural correlate of behavioral habituation? *J Neurosci* 31: 17811–17820, 2011.

Neuser K, Triphan T, Mronz M, Poeck B, and Strauss R. Analysis of a spatial orientation memory in *Drosophila*. *Nature* 453: 1244-1247, 2008.

Ofstad TA, Zuker CS, and Reiser MB. Visual place learning in *Drosophila melanogaster*. *Nature* 474: 204-207, 2011.

Pfeiffer K and Homberg U. Coding of azimuthal directions via time-compensated combination of celestial compass cues. *Curr Biol* 17: 960–965, 2007.

Pfeiffer K and Homberg U. Organization and functional roles of the central complex in the insect brain. *Annu Rev Entomol* 59: 165–184, 2014.

Ranck JB, Jr. Head-direction cells in the deep cell layers of dorsal presubiculum in freely moving rats. *Soc Neurosci Abstr* 10: 599, 1984.

Ritzmann RE, Harley CM, Daltorio KA, Tietz BR, Pollak AJ, Bender JA, Guo P, Horomanski AL, Kathman ND; Nieuwoudt C, Brown AE, and Quinn RD. Deciding which way to go: how do insects alter movements to negotiate barriers? *Front Neurosci* 6: 97, 2012.

Skaggs WE, McNaughton BL, Gothard, KM and Markus, EJ. An information-theoretic approach to deciphering the hippocampal code. *NIPS* 5: 1030-1037, 1993.

Skaggs WE, McNaughton BL, Wilson MA, and Barnes, CA. Theta phase precession in hippocampal neuronal populations and the compression of temporal sequences. *Hippocampus* 6: 149-172, 1996.

Strauss R. The central complex and the genetic dissection of locomotor behavior. *Curr Opin Neurobiol* 12: 633-638, 2002.

Strutt JW. On the light from the sky, its polarization and colour. *Philos Mag* 41: 107-120, 274-279, 1871a.

Strutt JW. On the scattering of light by small particles. *Philos Mag* 41: 447-454, 1871b.

Supèr H, van der Togt C, Spekreijse H, and Lamme VAF. Internal state of monkey primary visual cortex (V1) predicts figure–ground perception. *J Neurosci* 23: 3407–3414, 2003.

Taube JS. The head direction signal: origins and sensory-motor integration. *Annu Rev Neurosci* 30: 181-207, 2007.

Träger U and Homberg U. Polarization-sensitive descending neurons in the locust: connecting the brain to thoracic ganglia. *J Neurosci* 31: 2238 –2247, 2011.

Triphan T, Poeck B, Neuser K, and Strauss R. Visual targeting of motor actions in climbing *Drosophila*. *Curr Biol* 20: 663-668, 2010.

Vitzthum H, Müller M, and Homberg U. Neurons of the central complex of the locust *Schistocerca gregaria* are sensitive to polarized Light. *J Neurosci* 22: 1114–1125, 2002.

Zar JH. *Biostatistical Analysis.* 4th edition. Prentice Hill, 1999.

C H A P T E R II

HEAD-DIRECTION CELLS IN THE BRAIN OF AN INSECT ARE SENSITIVE TO NOVEL EVENTS IN THE VISUAL WORLD

Tobias Bockhorst and Uwe Homberg

HEAD-DIRECTION CELLS IN THE BRAIN OF AN INSECT ARE SENSITIVE TO NOVEL EVENTS IN THE VISUAL WORLD

Tobias Bockhorst and Uwe Homberg

The central complex (CX) of the insect brain comprises a group of neuropils involved in spatial orientation and memory. In the desert locust, it holds a compass-like representation of head directions, based on the polarization pattern of skylight. Behavioral data and dynamics of neuronal responses suggest that this compass is read to control heading direction when desert locusts migrate. In flies, a lesion study demonstrated that place learning based on visual landmarks depends on the integrity of the CX. Neurons in the lesioned area are tuned to features and egocentric position of visual objects. We investigated whether the locust CX houses a comparable representation of object information suited for landmark-based orientation. Responsiveness to stationary and moving stimuli was measured by intracellular recording from "compass" neurons at different stages of the CX network, followed by dye injection for identification of the recorded cell type. Strongest responses were observed to small moving squares, whereas no topographic representation of object positions was found. Initial responses to individual squares were independent of direction of motion and trajectory. Response amplitudes co-varied with the precedent state of dynamic background activity. Successive stimulation resulted in rapid region-specific adaptation, unaffected by changing the direction of motion. However, a change in moving direction *did* trigger responses if it made the patch pop out against a flow field of coherently moving objects, suggesting exceptionally context-dependent novelty detection. The data show that neurons in the CX of the locust brain are visually bimodal, signaling head direction as well as the novelty character of moving objects. These response properties might serve to attune compass-aided locomotor control to unexpected events in the environment. The difference to data obtained in *Drosophila* may relate to differences in the lifestyle of landmark learners (*Drosophila*) and compass navigators (locust) or point to the existence of parallel networks for the two orientational strategies. Parallels to novelty-based, attention-dependent processing in the vertebrate cortex are discussed.

ANIMAL SURVIVAL critically depends on the ability to orient in space. In comparison to their small brain size, insects have remarkable capacities for spatial orientation, illustrated by the daily foraging of worker bees or the seasonal long-range migration of monarch butterflies. Goal-directed locomotion in these species serves to purposefully and efficiently bridge distances from meters to thousands of kilometers. Depending on goal and setting, spatial cueing is based on salient landmarks or stable, nearly ubiquitous compass-signals such as the position of the Sun at a given time-of-day. While the relevance of either type of cue was studied for various tasks in different insect species, [1-5], investigations on the neural basis of spatial orientation are sparse and largely confined to sky-compass cues [6-8].

The central complex (CX) in the insect brain is a candidate neural substrate controlling spatial orientation. It plays a major role in higher locomotor control [9, 10], visual pattern- and working memory [11-13], sky compass coding [7, 14] and place learning [15]. In locusts, bilateral pathways from specific areas of the visual

system converge onto the CX (Fig. 1A). Its main neuropils are the lower and upper divisions of the central body (CBU and CBL, respectively) and the protocerebral bridge (PB) [16]. These are structured into horizontal layers (CBU, CBL) and vertical slices (PB, CBU, CBL). Heinze and Homberg showed that a compass-like representation of head directions is mapped onto the slices of the PB [14]. This is achieved by neuronal tuning to the polarization pattern of the blue sky, which indicates the position of the Sun even if the latter is not directly visible [7, 17]. Behavioral data [18] and dynamics of neuronal responses [19] suggest that this compass is read to control heading direction when desert locusts migrate.

In flies, place learning based on visual landmarks depends on the integrity of neurons at the input stage to the CX [15]. Seelig and Jayaraman showed that similar neurons are tuned to egocentric position and contour orientation of bar-shaped objects, with a preference for vertical features similar to those that constitute preferred landmarks in flies [20]. We, therefore, investigated whether the compass network in the locust CX houses, in addition, a comparable representation of object-information suited for landmark-based orientation in local settings. To this end, responsiveness to stationary and moving stimuli was measured by intracellular recordings from compass neurons at different stages of the CX network. The respective cells were identified morphologically via fluorescent labelling. Stimuli included small-field and wide-field elements as well as stationary display and simulated translational, rotational and progressive motion.

Material and Methods

Experimental animals and preparation. Male adult locusts were obtained from crowded indoor colonies (28 °C, 11 h : 13 h light-dark regime). To ease handling during preparation, animals were immobilized via cooling (4 °C, 15 min), legs and wings were cut off and the animals waxed to a metal holder. For access to the frontal brain surface, the frons, including antennae and ocelli, was excised and parts of the subcuticular fat body and tracheal air sacs were removed. Several measures were taken to promote stable recording conditions by reducing movements of the brain. Muscles connected to the antennae and mouthparts as well as the esophagus were transected, the gut was removed through an abdominal incision, and a spoon-shaped wire was waxed ventrally to the head capsule with its loop positioned to support the brain from posterior. Finally, the neural sheath was opened to facilitate brain tissue penetration by the intracellular electrode. Locust saline [51] was applied to replace fatty hemolymph and keep the brain immersed during preparation and recording.

Intracellular recording. For intracellular recording, two Ag-AgCl wire interfaces were used, one of which served as reference immersed in saline while the other was inserted into a sharp micropipette. Micropipettes were drawn from borosilicate capillaries (0.75 mm ID, 1.5 mm OD, Hilgenberg, Malsfeld, Germany) with a Flaming/Brown filament puller (P-97 Sutter Instrument Company, Novato, CA), and filled with 1 M KCl for electric conduction. Impedances in tissue ranged from 50 - 200 MΩ. To allow labeling of cells, the tips of the micropipettes were loaded with Neurobiotin tracer (Vector Laboratories, Burlingame, UK, 4 % in 1 M KCl) that could be injected iontophorectically (0.5-2 nA, 1-15 min) after recording. Tapped potentials were amplified and band-passed (10×, 20 Hz - 20 kHz; SEC 1L/H amplifier, npi electronic, Tamm, Germany) prior

to digitization (16 bit / 11.1 kHz; Power1401mkII converter run with Spike2 software, both Cambridge Electronic Devices, Cambridge, UK) and storage. Software for offline analysis was written in MATLAB (MathWorks, Natick, MA, USA).

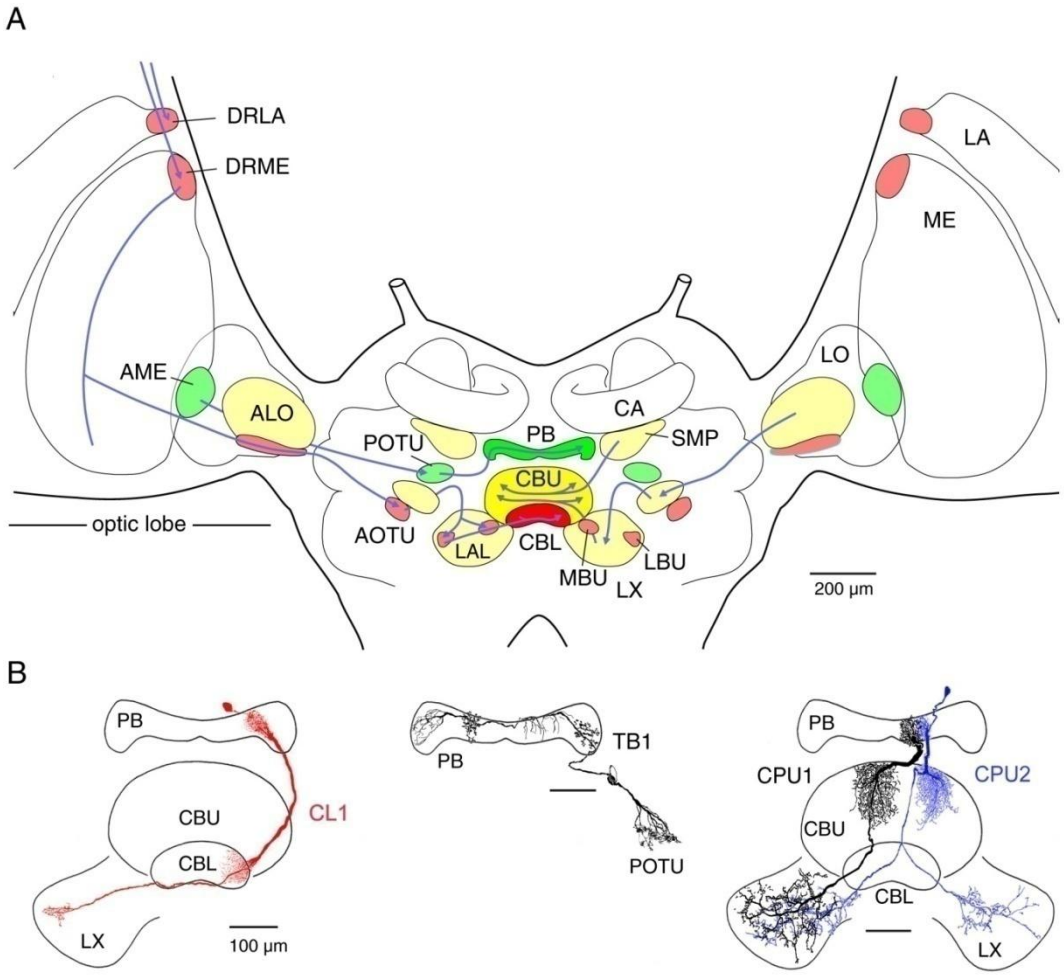

Fig. 1. Gross anatomy of the locust brain, visual pathways, and relevant types of central-complex neurons. A. Bilateral pathways of light-sensitive neurons from the optic lobes converge onto a network in the central complex (frontal view). Stages of early visual processing include the lamina (LA), medulla (ME) and lobula (LO) of the optic lobe. Neuropils shaded red (green) are involved in an anterior (posterior) pathway of interneurons sensitive to sky compass signals. Additional pathways (yellow neuropils) might signal optic flow and / or represent features of the visual object-background scenery. DRLA (DRME), dorsal rim area of the lamina (medulla); (ALO), anterior lobe of the lobula; AME, accessory medulla; AOTU, anterior optic tubercle; POTU, posterior optic tubercle; MBU (LBU) medial (lateral) bulb; LAL, lateral accessory lobe; together with the LAL, the MBU and LBU make up the lateral complex (LX). CBL (CBU) lower (upper) division of the central body; PB, protocerebral bridge; SMP, superior medial protocerebrum; CA, calyx of mushroom body. B. Relevant cell types of the central complex (frontal view). Columnar neurons connect distinct slices of the PB to the CBU (CPU-neurons) or CBL (CL-neurons) of the central body and have additional arborizations in the lateral complexes. Tangential TB-neurons invade slices within the PB and layers in the POTU. Scale bar, 100 μm. A modified from [53], B modified from [14, 43, 54, 55].

Histology. For histological processing, brain preparations were first fixed for 12-24 hrs at 4 °C in a solution of 4 % paraformaldehyde, 0.25 % glutaraldehyde, and 0.25 % picric acid in 0.1 M phosphate-buffered saline (PBS) and rinsed in PBS (4 x 15 min). Subsequently, intracellular

Neurobiotin was coupled to Cy3 fluorophore by means of incubation in a solution of Cy3-conjugated streptavidin (Dianova, Hamburg, Germany, 1:1000) in 0.1 M PBS with 0.3 % Triton X-100 detergent (PBT) for 3 days at 4 °C in the dark. Brains were then rinsed again (PBT, 2 x 30 min and PBS, 3 x 30 min), dehydrated in an ascending ethanol series (H_2O, 30%, 50%, 70%, 90%, 95%, and 100% ethanol, 15 min each) and cleared in a solution of methyl salicylate in ethanol (1:1, 30-45 min) followed by pure methyl salicylate (45-60 min). Finally, preparations were embedded in Permount (Fisher Scientific, Pittsburgh, PA) and scanned confocally (Leica TCS SP5 confocal laser scanning microscope, Leica Microsystems, Wetzlar, Germany) at 1024 x 1024 pixel resolution and either 10x or 20x magnification (Leica oil immersion objectives HC PL APO 10x/0.40 and HCX PL APO 20x/0.70, respectively). Cy3-fluorescence was induced by excitation at 561 nm (DPSS laser). In most cases relevant neuropils could be identified based on their autofluorescence. AMIRA 5.3.3 (FEI Visualization Sciences Group, Merignac, France) and COREL Photo-paint (X3 V 13.0.0576, Corel Corporation, Ottawa, ON, Canada) were used to generate and edit projection views from confocal image stacks.

Visual stimulation. Neural activity was recorded in a Faraday cage open to one side. All light sources outside the cage were covered with red filters to prevent interference with controlled stimulation. Visual stimuli were generated using a ViSaGe device (Cambridge Research Systems, Rochester, Kent, UK) and displayed on a 22" CRT screen (DP2070SB, Mitsubishi, Tokyo, Japan) positioned slightly tilted as to cover -45° to 60° in azimuth and -32° to 28° in elevation within the left antero-lateral visual field (Fig. 2A, B). This visual subfield covered by the CRT is hereafter referred to as the mapping field. With the brightest illumination applied here (RGB 255-255-255), the average luminance of the light emitted from the entire screen was 89.4 cd/m² (900 measurements evenly spaced across the display, using the OPTICAL photometer provided by Cambridge Research Systems; standard deviation 5.14 cd/m²). A 'neutral, grey background' used for measurement of background activity as well as to display the main types of bar- and patch stimuli against was generated by setting the screen to RGB 127-127-127. All visual stimuli were generated by custom-written MATLAB functions using the Cambridge Research Systems toolbox. These also delivered trigger signals for offline analysis of raw data in MATLAB and provided documented pseudo-randomization of order within most stimulus batteries.

Initially, we screened central-complex neurons for responsiveness to basic visual entities, such as object features or egocentric object location. To this end, we designed a variety of visual stimuli, some of which were skipped after a few recordings. Flashes of blue, red, green and white light comparable in photon flux rate (photon flux measured at 710 nm, 520 nm and 450 nm varied from $7 \cdot 10^{13}$ to $9 \cdot 10^{13}$ photons$\cdot s^{-1} cm^{-2}$ at each of the three wavelengths) served to test for general sensitivity to light and spectral tuning. Photon flux was measured with a digital spectrometer (USB2000, Ocean Optics Inc., FL, USA) with the detector head at the position of the compound eye, directed toward the CRT display. Black (white) square patches were displayed against white (black) background at pseudo-randomized positions across the entire mapping field to characterize any spatial tuning within it. Groups of 'random patches' approaching (looming) the locust from the center of the frontal visual field (generated using the built-in function of the Cambridge Research Systems toolbox), as well as translating sine gratings with different spatial frequencies, angular extents, and angular orientations were displayed to simulate both translational and rotational wide-field motion. Stationary displays of these and any other moving stimuli served to control for mere responsiveness to changes in ambient light level

or spatial tuning within the mapping field in case a receptive field mapping had not been performed. These stimuli did not drive any of the cells encountered in a manner tuned to object position or wide-field motion. At most, they evoked transient responses to rapid changes in ambient light level that will, however, not be further characterized in the results section. Additional stimuli designed to mimic black or white bar-shaped objects were displayed individually and varied in vertical extent, contour orientation and combinations thereof. These were presented translating with different velocities along different horizontal (forward or backward motion) or vertical (upward or downward motion) trajectories (Fig. 2B') with stationary controls applied in some experiments. In particular, black, rectangular small-field patches (about 2° visual angle horizontal extent and 1.5° vertical extent) proved an adequate stimulus to the cells considered here. These hence became the building blocks of additional stimulus batteries for deeper characterization of the responses that followed the pre-screening.

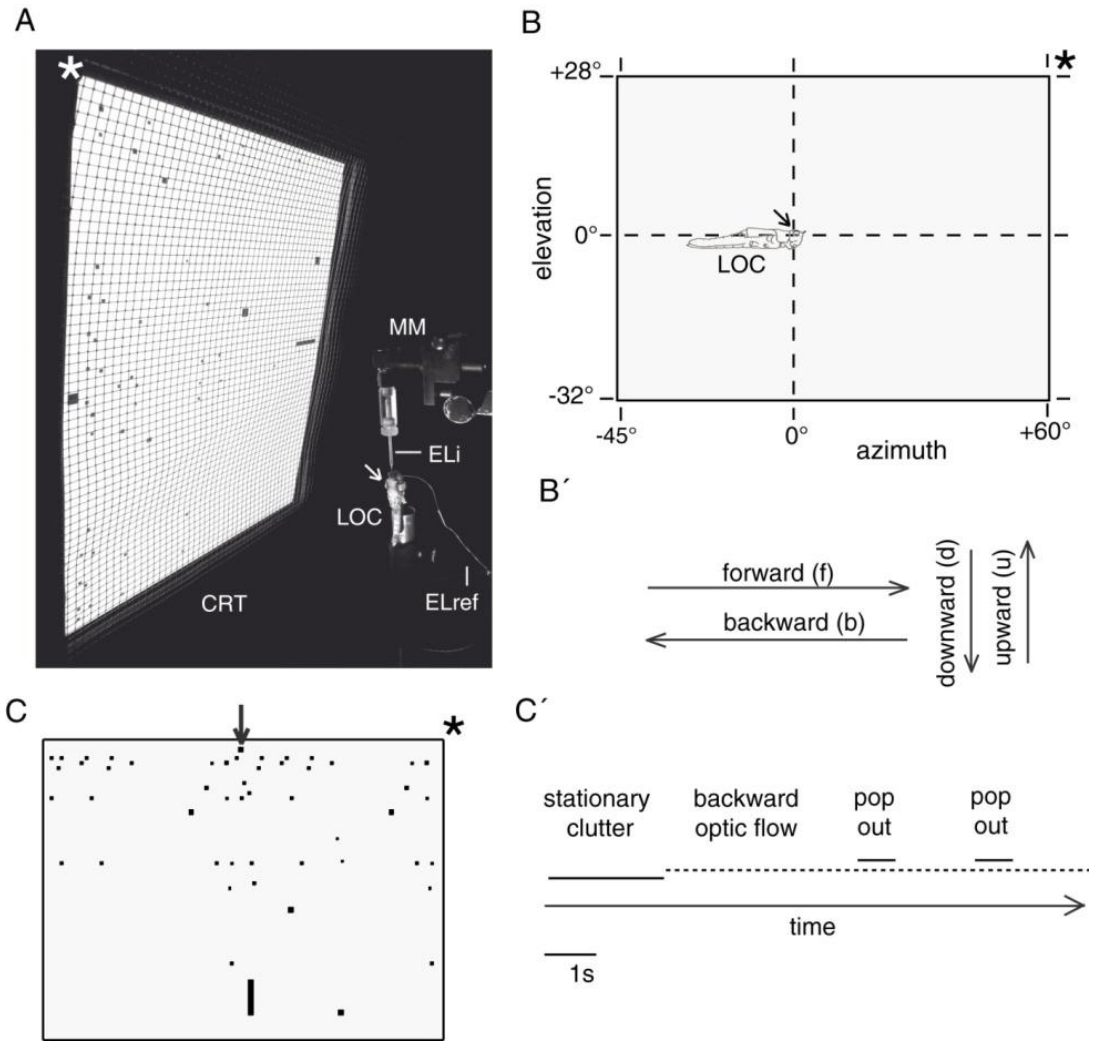

Fig. 2. Experimental setup and visual stimulation. A. Experimental setup (display showing stationary background clutter). CRT, cathode ray tube display; asterisk, fronto-dorsal corner mark of CRT; MM, micromanipulator for positioning of intracellular electrode; ELi, intracellular electrode; ELref, reference electrode; LOC, locust; arrow, stimulated (left) eye. Note the slight tilt of the CRT and the mesh wire shielding which prevented inductive interference between display and measurement circuit. B. Region in the left antero-lateral visual field covered by the stimulus display. Arrow, position of stimulated (left) eye; asterisk, fronto-dorsal corner mark of CRT; LOC, locust (not to scale). B´. Terminology for directions of translational motion, illustrated according to the orientation of the diagram in B.

Abbreviations are given in parentheses. C, C´. Components (C) and time course (C´) of a stimulus sequence designed to mimic sudden forward small-field motion against a backward optic-background flow. The sequence begins with a stationary display of the ´background clutter´ pattern sketched in C, followed by repeated backward translation of the same pattern in an optic-flow like manner at 70°/s (dashed horizontal line in C´). In the late phase of the sequence, an individual object in the background flow (arrow in C) pops out of it twice. Here, the change in behavior of the background-object that constitutes its pop out is a change in direction of motion, i.e. the object suddenly moved forward against the backward background flow (absolute velocity -150°/s; velocity relative to background flow -80°/s). The object, a black, rectangle patch of about 2° visual angle azimuthal extent and 1.5° elevational extent, is identical to the one used in the simple stimulus regimes and moves at the same ´high´ elevation of 25.5° also applied in the latter. For simple stimuli, forward (backward) direction of translation is abbreviated 'f' ('b') and high (low) elevation is abbreviated H (L). Thus, the term 'b, L' (´f, H´) refers to the backward (forward) translation of a 2°x1.5° patch -29.5° (+25.5°) in elevation. For further details on stimuli, see Material and Methods. Asterisk, fronto-dorsal corner mark of CRT.

Features and abbreviations of basic stimuli. Most commonly, forward and / or backward translations of a black, rectangular small-field patch against a grey background at either high elevation (+25.5°) or low elevation (-29.5°) were combined in different sequences. At this, the angular velocity against the blank background was 70°/s (on average, see below), and trajectories spanned the entire width of the display (-45° to + 60° in azimuth). Forward (backward) directions of translation are abbreviated 'f' ('b') and high (low) elevations are abbreviated H (L). Therefore, the term 'b, L' refers to the backward translation of a 2°x1.5° patch at 70°/s, from +60° to -45° in azimuth at -29.5° in elevation. More precisely, the velocity of the moving patch *on the CRT* display was constant. As a consequence of the display's flat geometry, the angular velocity seen by the animal slightly increased (decreased) as the patch moved toward (away) from the animal. As the same holds for angular size, the translating patches also had a mild looming component. However, the response behavior we observed strongly speaks against a role of these minor changes of angular velocity and size. The interval between the individual stimuli usually equaled the stimulus duration (1.35 s and 1.43 s, respectively). In addition to this simple stimulus regime, a more complex stimulus-background scenario was applied in some cases (Fig. 2C, C').

Basic offline data analysis. Spikes were detected by threshold based event detection. An upper threshold as well as an absolute refractory period of 1 ms were applied to prevent false positives. For non-smoothing visualization of spiking dynamics, we applied the instantaneous interspike interval (ISI) method [52] instead of the classical post stimulus time histogram (PSTH) to avoid both arbitrariness of bin placement and the problem of bin width optimization.

Rating responsiveness and response amplitude. Most types of central-complex neuron encountered here exhibited a background activity that was relatively high in average rate and marked by cell-type specific dynamics [19]. Concurrently, putative responses were occasionally subtle, standing out against the complex patterns of background activity rather in terms of their consistency across trials than by high steps in firing rate. Hence, for decision on inclusion of putative responses in meta-analyses, we prioritized consistency across several trials recorded from the same cell or between several cells of the same type. Furthermore, we investigated (I) how responses relate to the local state of background activity that directly precedes the stimulus presentation and (II) how responses compare to different levels of background activity sampled over prolonged periods (commonly several minutes, scattered throughout the course of the experiment). For (I), we performed a linear

regression on the spike counts observed during different peristimulus time windows: the last 700 ms prior to stimulation as opposed to either the first or second 700 ms window during presentation of the standard translating-patch stimulus which had a duration of about 1400 ms in total. This procedure is reminiscent of the first steps in the analysis of evoked activity in V1 neurons reported by Arieli et al. [40]. It was confined to responses pooled across CPU1- and CPU2-neurons, as these comprised a sufficient number of cells and repetitions, and both types of neuron showed pronounced local dynamics of background activity, thus producing a sufficient span of spike counts for a reliable analysis of covariance. For (II), spike counts in stimulus time-windows were compared to different relevant quantiles of the background activity spike count distribution, similar to the procedure described in Bockhorst and Homberg [19].

Criteria for inclusion in final analysis. Physiological data were only included in the final analysis if the recorded neuron was identified. Ideally, this was provided by distinct labeling of an individual cell. If more than one neuronal cell were labeled in the same preparation, recordings were assigned to morphologies based on characteristic patterns of background activity that had previously been determined for distinct cell types (for details, see Bockhorst and Homberg [19]).

Data plots. Raster plots were generated using the MATLAB code kindly provided by Rajiv Narayan, Boston University (rasterplot.m, provided at www.mathworks.com). Plots of spike-count distributions and ISI histograms were based on code kindly provided by Prof. Dr. Sonja Grün (Research Center Jülich, RWTH Aachen University). In box plots, boxes span the inner 50 % of the respective distribution from the first to the third quartile. Box notches give the 95 % confidence interval of the median, i.e. two median values differ significantly (at α=0.05) if the notches of their boxes do not overlap. Whiskers extend to the adjacent values, which are the most extreme data values that are not considered outliers. Outliers are shown in cross-shaped markers. More detailed descriptions of distributions are provided by scatter plots that use marker size to indicate frequency of observation (bubble plots). In these, the diameters of the circular markers are linearly scaled to the absolute frequency at which a value defined by the center of the marker was observed. In contrast to box plots, scatter plots can visualize features such as the actual shape of symmetrical distributions (e.g., to distinguish between unimodal and bimodal cases) and do not involve statistics that should be avoided for low sampling sizes, such as median values or quartile ranges. For visualization of the time course of responses, we used plots of the *normalized* instantaneous ISI. To this end, the ISIs of each individual response were first transformed to the interval [0 1] by element-wise subtraction of the minimum ISI and subsequent division by the maximum of the resultant values. In case of repeated presentation of the same battery, the median normalized ISIs of the individual responses was calculated. As a consequence, average values near zero or unity indicate high consistency of response courses over trials.

Results

Dataset. We screened neurons in the central complex (CX) of the locust brain for responsiveness to various visual entities, including object size, vertical compactness, contour orientation, egocentric object position and rotational / translational motion (see MATERIAL & METHODS for details). Fig. 1B illustrates the morphological cell types encountered in the present study. Columnar neurons connect distinct slices of the PB to the CBU (CPU1- and CPU2-neurons) or CBL (CL1-neurons) and have additional branches in the

lateral complexes, the main input- and output relays of the CX [16]. Tangential neurons invade all slices of the CBL (TL-neurons) or many slices in the PB (TB1-neurons). The putative processing hierarchy is TL-CL-TB-CPU [21]. Data included in the final analysis covered 17 neurons from 17 adult gregarious animals. Of these, 3 recordings were from CL1-neurons, 4 from TB1-neurons, 5 from CPU1-neurons and 5 from CPU2-neurons. Datasets may vary between figures due to the purpose and demands of the respective analyses. Neither topographic mapping of object positions nor narrow tuning to object features was observed, apart from a preference of small-field objects over wide-field bars and visual flow. Yet, CL1-neurons occasionally responded to a single, translating bar in a manner similar to their responses to small-field patches (data not shown). Measurements of polarization sensitivity were performed in the same cells to confirm their role as compass neurons, i.e. head-direction cells [19]. All results described hereafter are based on stimulation by distinct, moving small-field objects (Fig. 2).

Polarization-sensitive neurons of the central complex signal small-field motion in a novelty-dependent manner. As previously reported [19], all cells showed background activity with pronounced cell-type specific dynamics (Fig. 3A-A’’’, B-B’’’). Neurons responded in cell-type specific manners to translational motion of a black small-field patch (about 2°×1.5° in visual angle) against a uniform grey background (Fig. 3C-C’’’, D-D’’’). Within a respective cell-type, responses also varied in latency, duration and amplitude both between cells and over time within a respective cell. In repeated stimulations, responses to the first stimulus were independent of the particular elevation and azimuth of the stimulus trajectory as well as of the direction of motion along that trajectory (Fig. 3D’’, D’’’). In CL1-neurons, responses were inhibitory, often outlasted the first stimulus of a stimulus-battery in duration (about 1.4 s) and tended to be followed by rebound-like states of mildly to substantially increased spiking (Fig. 3A-D). TB1-neurons often responded less prominently by bursting to the onset of motion; an example of more prominent responses that included a moderate, tonic increase in spike rate is shown in Fig. 3 C’ and D’. Similarly, both phasic and prolonged responses were found in CPU1- (Fig. 3A´´-D´´) and CPU2- (Fig. 3A´´´-D´´´) neurons, which responded with inhibition. In these, however, phasic responses were observed more often. In each type of neuron, the background activity included states that resembled the evoked responses (Fig. 3A-A’’’).

Figures 4 and 5 summarize population data on the effects of repeated stimulation, as well as changes in direction of motion, switches of the trajectory, i.e. the region of the visual field, and changing motion against a ‘distracting’ visual background. In all cell types, the repeated presentation of the same stimulus resulted in rapid adaptation, as illustrated by the responses in Fig. 3, and two repetitions of a respective stimulus sufficed for complete adaptation (Fig. 4A). This links responsiveness to stimulus history: responses were strongest for the first presentation of a small-field motion stimulus that had been absent for an extended period (the exact effect of pause duration was not explored), and occasionally responsiveness was confined to these ´novelty´ trials (Fig. 4A).

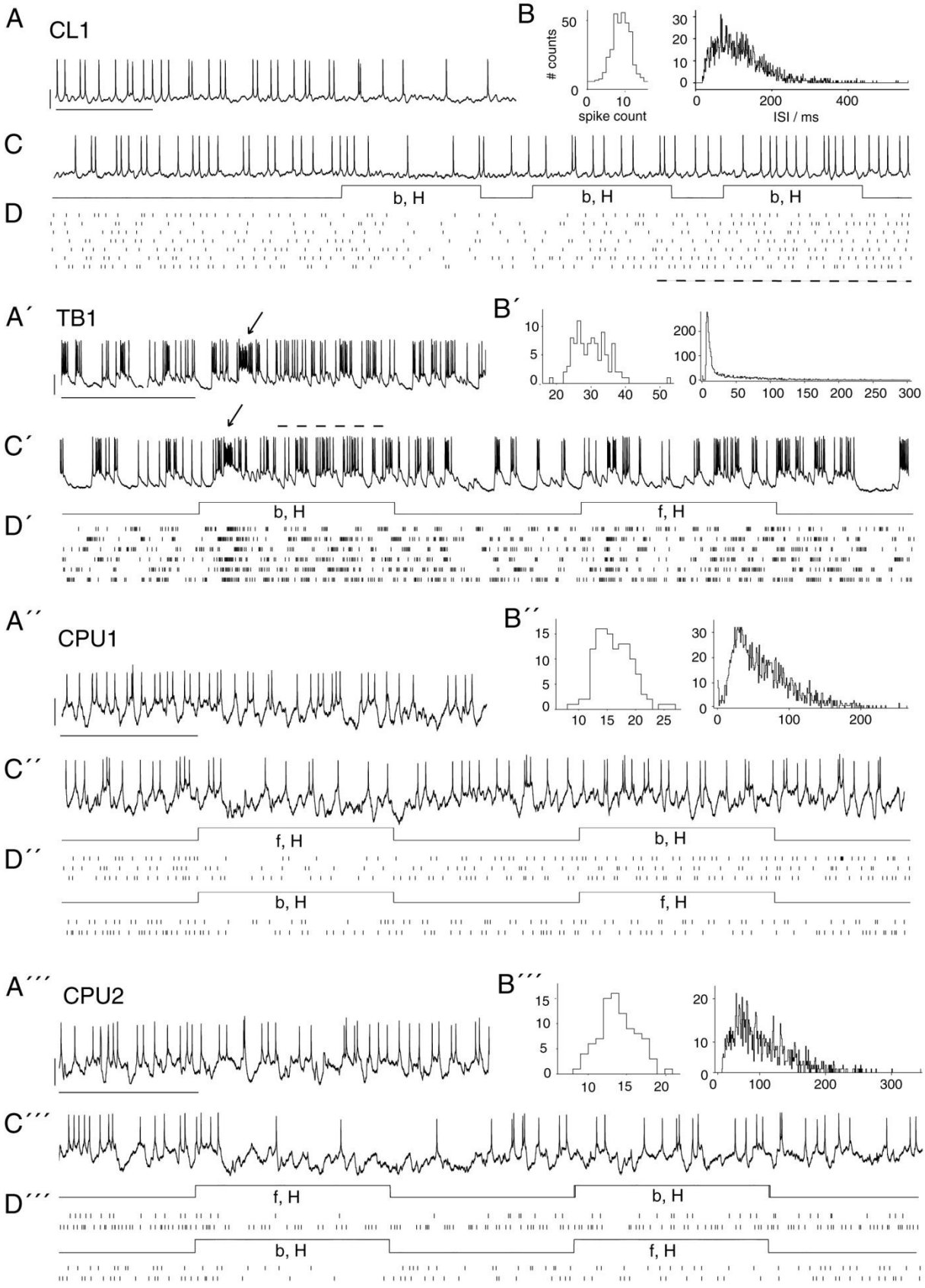

Fig. 3. Background activity and responses to small-field motion in four types of central-complex neuron. Subfigures show data from a CL1-neuron (A-D), TB1-neuron (A'-D'), CPU1-neuron (A''-D'') and CPU2-neuron (A'''-D''') of the central complex. A-A´´´. Traces illustrating background activity. B-B´´´. Spike-count distribution and ISI histogram of background activity (trial duration for spike count 1 s). C-C´´´. Responses to presentations of a translating black, rectangular small-field patch (about 2° visual angle

azimuthal extent and 1.5° elevational extent), illustrating fast adaptation to motion along the same trajectory. Stimulus types and periods, indicated below the recording traces, also hold for raster plots in D-D´´´, unless indicated otherwise. Stimulus abbreviations: f (b), forward (backward) small-field translation; H (L) trajectory with high (low) elevation. D-D´´´. Raster plots of additional responses. Responsiveness is robust across trials shown here, but response amplitudes vary and individual responses resemble motives of background activity. In particular, arrows in A' and C' mark prominent bursts in background activity and in the phasic response-period for the TB-neuron. In the two subtypes of CPU-neuron (D'' and D'''), responses are independent from direction of motion. Dashed lines indicate periods of rebound-like increase in spike rate in D and a period of tonic increase in spike rate in C'. Bars, 1 s; 10 mV.

Context-dependent responses to moving objects. To further elucidate what constitutes the ´stimulus novelty´ that these responses depended on, we applied stimulus batteries that included changes in direction of motion (from forward to backward or vice versa; in few tests from downward to upward or vice versa) or a switch of the trajectory´s elevation (or its azimuth, in few tests with upward / downward motion). Whereas the change in direction of motion was designed to mimic a change in behavior of the *same* object (or an apparent change as a result of rotational ego-motion), the switch of trajectory was designed to signal the appearance of a *novel* object, concurrent with the disappearance of the previously presented one. Interestingly, switching the trajectory of motion broke the adaptation in many cases while mere changes in direction of motion along the same trajectory did not or to a substantially smaller extent (Fig. 3, Fig. 4B, C; Fig. 5A-5A´´´). Figure 5 includes plots of the instantaneous, normalized inter-spike intervals (norm. ISI; Fig. 5). This kind of plot was particularly suited for the inhibitory responses of CL1- and CPU1/2-cells and, as raster plots are, is unaffected by the problem of bin width and bin positioning that complicates conventional peri-stimulus rate histograms. For data pooled across repeated stimulations (N>1 trials) normalized ISI values of 1 (or 0) indicate an inhibitory (or excitatory) response of absolute consistency across trials. Responses of CPU- and TB1-neurons were more variable in amplitude than those of CL1-neurons, as reflected by the population datasets for first-stimulus responses shown in Fig. 4A. In the plots of group data, this reduces the *apparent* strength of the effect of switching elevation (Fig. 4B) and increases the *apparent* strength of the effect of changing direction (Fig. 4C). The substantially stronger effect of switching trajectories as opposed to direction of motion suggests a stimulus-specific adaptation with respect to the region of the visual field that is spanned by the stimulus trajectory. It is consistent with the assumption that these cells signal the novel appearance of a moving small-field object, but not a mere change in the behavior of an object, i.e. here, a change in the direction of motion.

All responses hitherto mentioned were obtained with small-field objects moving against a blank, uniformly grey background. We wondered whether the novelty-detection capacity of these cells extends to more complex object-background scenarios as well. To test this, we introduced a more complex stimulus that included a group of patches and a bar translating backwards along parallel trajectories at a common velocity (70°/s) to simulate visual flow as resultant from ego-motion of the locust (Fig. 2C). After an initial stationary presentation of the background clutter and several repeated translations, the behavior of an individual patch was suddenly altered as to render it a distinct object that suddenly pops out against the uniform visual flow (Fig. 2C'). More precisely, we applied a change in the direction of motion of the individual patch which results in motion relative to the background clutter. All elements of the background clutter had the same contrast as the distinct object patch. Indeed, the sudden transition to an opponent motion against the background clutter (the 'pop out' event)

triggered responses in this object-background regime (Fig. 5B). It is crucial to recall here that changes in direction of motion did *not* break the stimulus-specific adaptation in the simple ´single patch against blank background´ regime (Fig. 5A-5A´´´). Consistent with their responses to simple stimuli, latency was highest in the CL1-neuron. This cell as well as the CPU1/2-neurons responded to the pop out with inhibition, whereas the individual response of the TB1-cell was excitatory. Again, responses were paralleled by motives in background activity, which is particularly evident in the raster plot of the TB1 response. Repeated stimulations (CL1-cell A, CPU2-cell C; both N=7) proved consistent responses to the pop out and low across-trial consistency of background activity at a given point in peri-stimulus time. This is again reflected by the amplitude of the inter-spike intervals normalized across-trials (Fig. 5B). The different response amplitudes of CPU1-cell A and B resemble the relatively high level of response-variability that was previously observed for responses to simple stimuli.

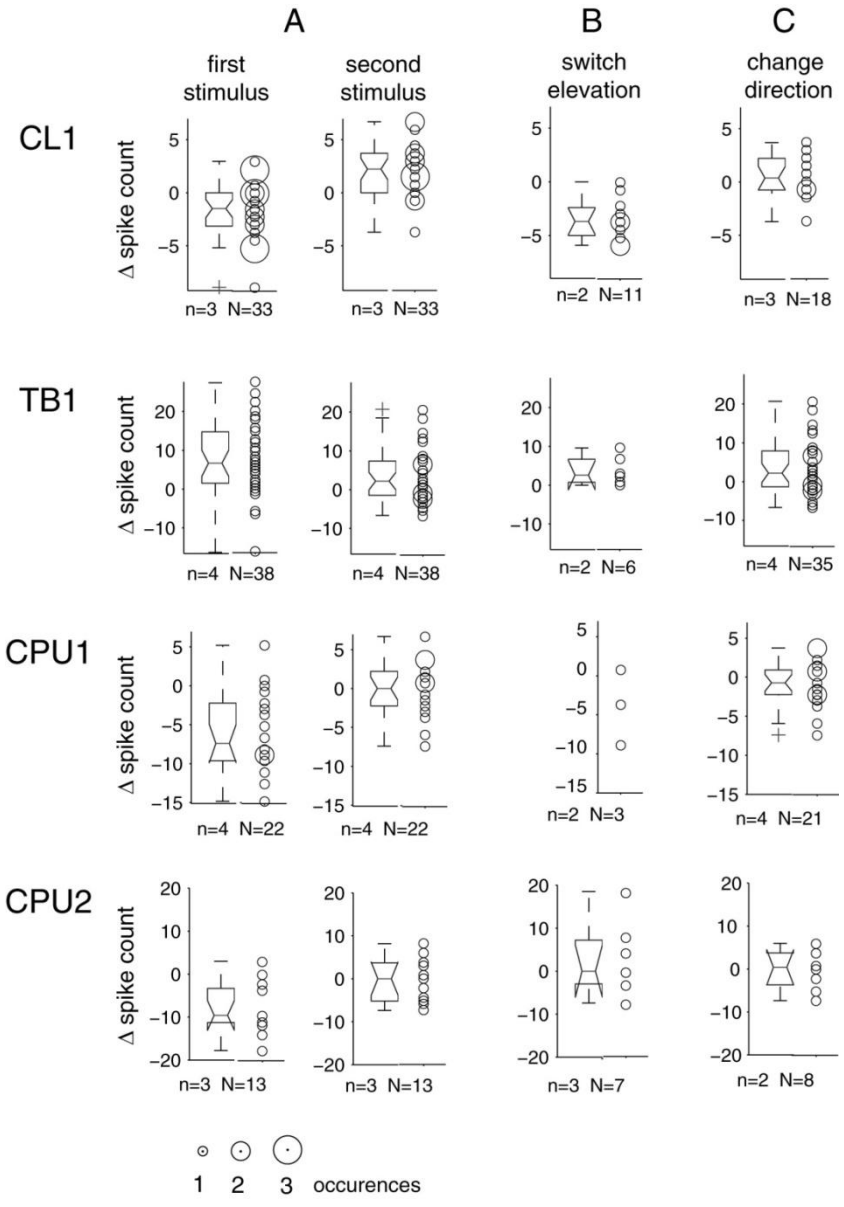

Fig. 4. Stimulus-specific adaptation of responses to small-field motion in CL-, TB- and CPU-neurons. Responses to small-field motion were marked by rapid adaptation (A) that could often be broken by switching the elevation of a horizontal trajectory (B), but not by merely changing the direction of motion along the same elevation (C). A-C. Data show differences in spike count between stimulus time-windows and background activity in a period of 450 ms preceding stimulation, based on N responses obtained from n neurons. Notches in box plots indicate 95% confidence interval of the median and circular plot markers in bubble plots are scaled to the frequency of observations. Some outliers were truncated for the sake of better visualization.

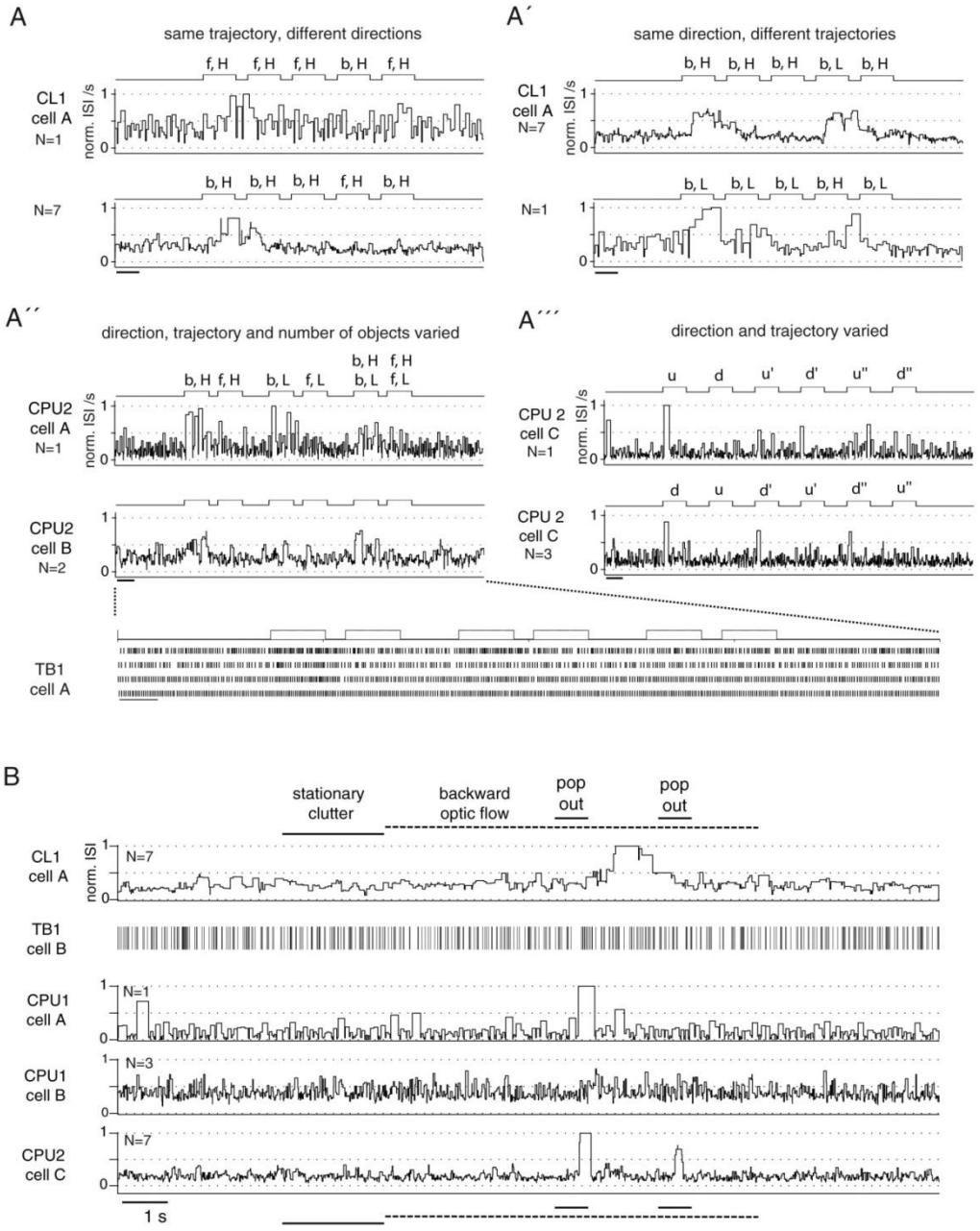

Fig. 5. Context-dependent responses to moving objects. The courses of N responses to a respective stimulus battery are visualized for selected neurons by normalized instantaneous ISIs, averaged across trials when N > 1. For a TB1-neuron, raster plots were preferred. Values of 0 or 1 indicate highest consistency in response course across trials. A-A´´´. Each subplot represents N responses to a specific stimulus battery, obtained from cells identified by capital letters within each cell type (compare to subfigure B). A-A'': Horizontal trajectories; forward (f) or backward (b) motion at high (H) or low (L) elevation. In A'', the third and fourth stimulus consist of two objects that move in the same direction but at different elevations. A'''. Responses to upward (u) and downward (d) motion along vertical trajectories at different azimuths (-38°, 7.5° and 54°). Here, the transitions from d to u' and d' to u'' correspond to switches in the azimuth of the trajectory, whereas the particular sequence of azimuths was randomized in each trial. As a consequence, the lower subplot shows data pooled across 3 different chronological orders of azimuths. For both vertical and horizontal trajectories, it is the switch in trajectory that triggers responses, not the particular position of the trajectory or changes of the direction of motion. Bars, 1 s. B. Responses of the same types of neuron are also suited to detect a distinct object that changes its direction of motion (pop out) against an optic background flow of identical and very similar objects. For detailed description of the stimulus battery, see Fig 2.

Response amplitudes are modulated by states of dynamic background activity. The amplitudes of initial and dis-adapted responses co-varied with preceding states of background activity (Fig. 6A). High-level background activity can mask inhibitory responses (CL1, CPU1) by superimposition and reduce the relative strength of excitatory responses (TB1) via framing of responses by response-like spiking. To characterize their association quantitatively, we tested for correlation between binned spike counts (700 ms windows) during stimulus presentation (first-stimulus responses only) and during the directly preceding stimulus-free period in CPU-neurons. The analysis revealed a highly significant and strong correlation that explains about 70% of the observed overall variability in spike count (Fig. 6B). Yet, the regression line for spike counts obtained from the second half of the stimulus period is slightly closer to the bisecting line of the plot, reflecting the transient course of these responses. The plots illustrate substantial variability in response amplitude, both for the early and the late phase of responses and between recordings as well as across the course of a respective recording. In particular, data points near the bisecting line that represent trials with no pronounced response were often obtained from recordings that included strong responses as well. The results confirm that responses of CPU-neurons were co-shaped by the state of immediately preceding background activity.

We also assessed the degree to which this state-dependency could actually mask responses in all cell types considered here. To this end, we compared spike counts and response-related inter-spike intervals to those from different states of long-term background activity, also corresponding to different points in time throughout an experiment, i.e. on a more ´global´ scale than the directly preceding background activity (see MATERIAL & METHODS). The results imply that the background activity includes states suited to completely mask even the most pronounced responses observed here, in each of the cell types encountered (Fig. 6C). For instance, the relatively strong responses of CL1-neurons appeared rather neutral when compared against the lower quartile of the background activity´s spike count distribution and even corresponded to an *increase* in spike rate relative to the lower extreme (2.5^{th} percentile) of background activity.

Discussion

We characterized how central-complex (CX) neurons of the locust brain, known for their role as head-direction cells, respond to small-field objects that translate rapidly through a unilateral part of the visual field. In sequential translations of single objects, initial responses were independent of direction of motion and trajectory whilst subject to strong region-specific adaptation. Adaptation was unaffected by changing the direction of motion along an unchanged trajectory. Yet, changing the direction of motion *did* trigger responses if it made a single object pop out against a flow field of coherently moving objects of similar size and shape and identical contrast. Responses in both the simple and the complex stimulus regime were always inhibitory in CL1- and CPU1/2-neurons, but excitatory in TB1-cells.

In addition to modulation by stimulus-specific adaptation, response amplitudes co-varied with precedent background activity, and the cell-specific ranges of background activity (i.e. variability over time) imply that this effect could mask even the most pronounced responses observed here. This highly context- and state-dependent response behavior allows these insect head-direction cells to signal novel, i.e. unexpected events in the visual scenery. At this,

novelty is 'defined' in a highly dynamic manner that preserves sensitivity even in the presence of 'distracting' background flow. Furthermore, the observed context-dependency appears reasonable for higher-stage generalization as the very same entity, e.g., a change in the direction of motion, might signal a mere change in the behavior of the same object (in the ´blank-background regime´) or the sudden emergence of a novel object (in the ´complex object-background regime´). A variety of other object-vision stimuli, in particular wide-field motion alone, failed to drive these cells.

Methodological considerations. Our conclusions on the event-related character of responses are corroborated by consequent variation of the critical parameters, direction and trajectory of translation, as well as by randomization of stimulus order within the test batteries. Findings for horizontal trajectories are furthermore validated by those for vertical translations. Moreover, the robustness of responses was strictly evaluated by a differential comparison of response amplitudes to relevant levels (quantiles of the spike-count distribution) of each cells' highly variable background activity. While sampling size varied between individual groups of data, the principle findings are confirmed by consistency across experiments and hence experimental animals as well as cell types. As we showed that trial-to-trial-variability mainly traces back to co-variation with variable background activity, we consider this inter-individual consistency a statistical factor at least as powerful as consistency across trials in an experiment.

Comparison to early-stage motion detecting neurons in the insect brain. Early-stage interneurons of insect visual systems, tuned to the (apparent) motion of distinct objects against a visual background, have been identified in several insect species [hawkmoth: 22, 23; locust: 24- 28; blowflies: 29, 30; dragonfly: 31, 32; hoverfly: 33, 34]. In particular, small-target (1°-2°) motion detectors (STMD) in the dragonfly show response properties that range from simple selectivity for target size and direction of motion [31] to a putative correlate of selective attention to either of two simultaneously presented targets [35]. In both the dragon- and hoverfly, STMDs proved capable of detecting a small, high-contrast target against a background clutter of strikingly different elements, whereas some responded whether or not there was a relative motion between the two [36, 38]. Their response behavior can be explained in terms of extreme selectivity for small-field objects that contrast strongly against neighboring patches of background clutter.

Such strict tuning to target size and contrast does not suffice to explain the object-detection performance we observed in the locust CX neurons. In the object-background discrimination task we applied, the background clutter consisted (apart from a single bar in the ventral part) of small-field objects identical or very similar to the 'target', all of which shared the same level of contrast against the grey display. This task requires a substantially more contextual, dynamic identification of background vs. target-like objects by the direction-unselective CL-, TB- and CPU-neurons. It may follow the Gestalt principle [36] of common fate (here: common direction of motion) rather than common size or common contrast. Gestalt principles describe the laws of how physical objects and events in the outside world are grouped into perceptual objects, and in the present case, the principle of common fate predicts that objects moving in the same direction will be grouped together, thus distinguishing background flow from distinct target objects. One might argue that motion of the individual patch in a direction opposite to the optic flow results in an increased relative velocity of the target-like object compared to the simple blank background scenario. However, a mere increase in relative velocity by faster translation in the same direction as the optic-background flow, that was applied as a control-

condition in the same CL1-neuron included in Fig. 5B, did not trigger comparable responses (Fig. 7).

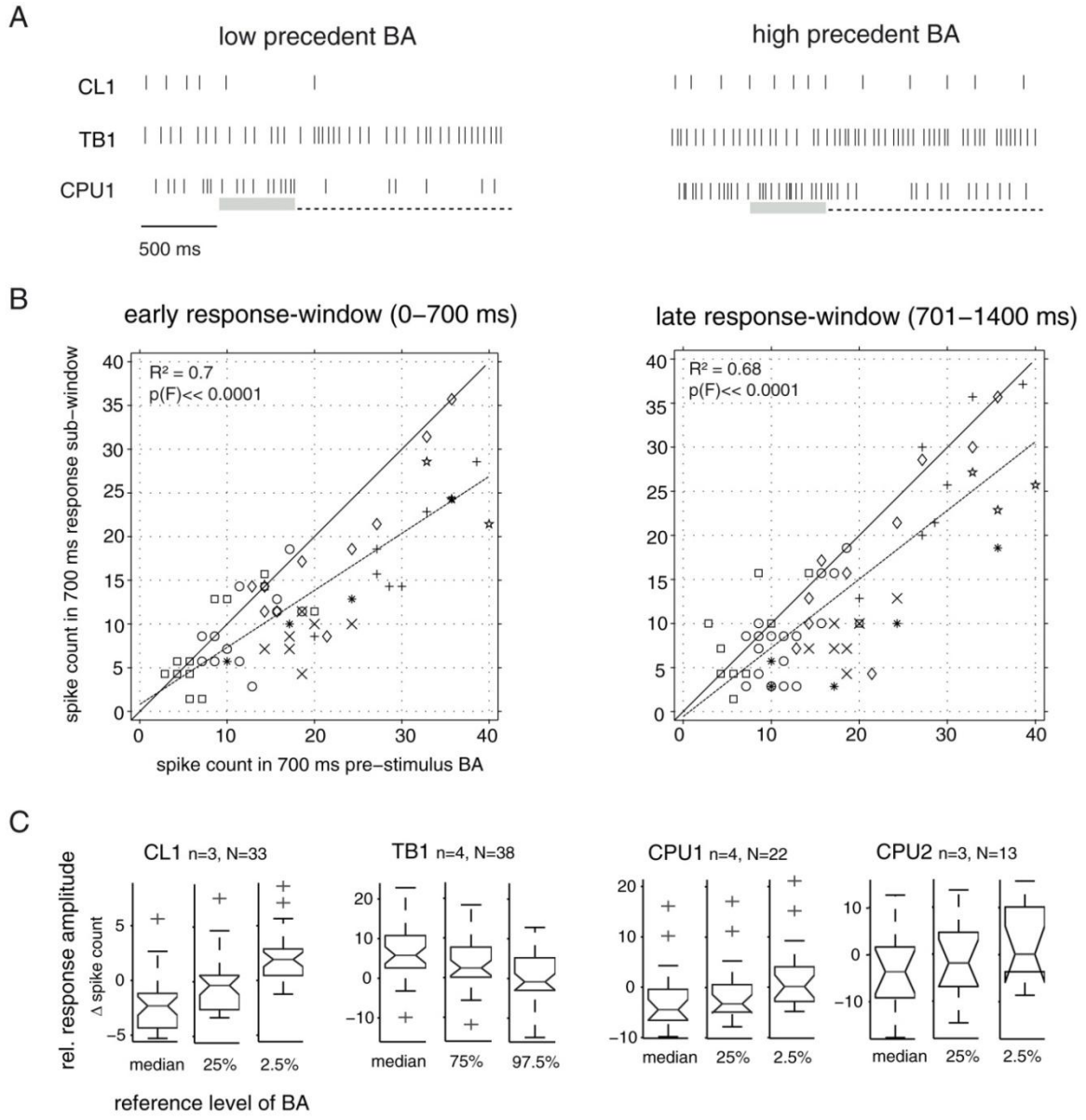

Fig. 6. Modulation of responses to moving small-field objects by variable background activity. A. Raster plots show selected responses to a translating small-field patch (dashed line: stimulus window) which are modulated by relatively low states (left subplot) and relatively high states (right subplot) of precedent background activity (BA). The relevant period of background activity may roughly cover the last 500 ms (grey shading) preceding the stimulus. B. Correlation analysis in CPU-neurons. Spike counts within the first (second) 700 ms-window during stimulus presentation were plotted against those in the 700 ms-window of background activity directly preceding the stimulus. Data points close to or above the bisecting line correspond to trials that lacked the inhibitory response typical for CPU-neurons; strongest responses are reflected by data points closest to the x-axis. Data were obtained from 3 CPU1-and 4 CPU2-neurons and cover 62 responses to the first stimulus in batteries of single small-field patches translating against a blank background; different plot markers correspond to different neurons. Plot markers are not scaled to the frequency of observations, thus identical values from the same experiment appear as a single data point. Dotted lines show linear regressions. C. Response amplitudes compared to different states of background activity. Box plots show distributions of relative response amplitudes (changes in spike rate relative to different levels of background activity). These were calculated for responses to the first stimulus in a respective battery of small-field patches translating against a blank background (N responses from n neurons). For estimation of relative response amplitudes, we subtracted the spike rates of different levels of background activity, obtained from the very same respective cell. These levels include

the median and to two additional quantiles of the background activity's spike count distribution that lie beyond the median in the same side of the distribution as expected for responses. In case of the inhibitory responses in CL- and CPU-neurons, the 25% and 2.5% quantile of the spike rate distribution were used. For the excitatory responses of TB-neurons, the 75% and 97.5% quantile provide relevant normalization. While responses are relatively robust compared to the median levels of background activity (left columns of subplots), the additional response-type specific normalizations (middle and right columns) reveal that more extreme levels of background activity may result in masking of responses. Notches in box plots indicate 95% confidence interval of the median. Some outliers were truncated for the sake of better visualization.

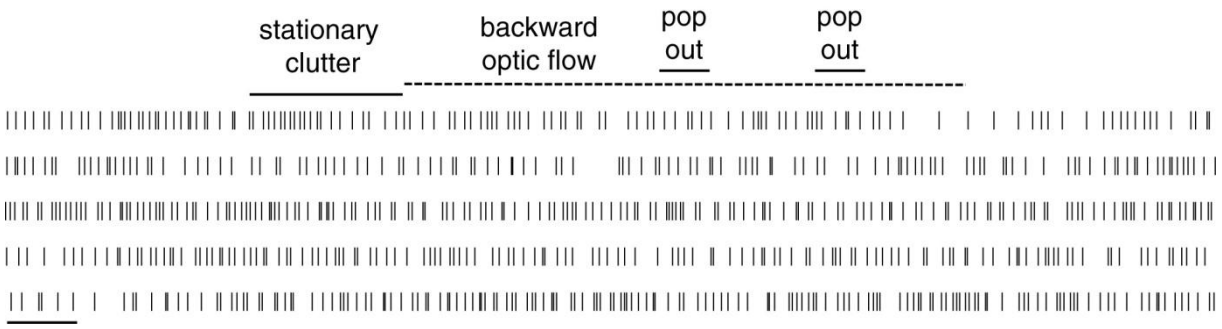

Fig. 7. Mere increase in relative object-velocity does not trigger pop-out responses in a CL1-neuron. The raster plot depicts five traces of peri-stimulus activity recorded from the same CL1-neuron (cell A) included in Fig. 5. The cell responded to object-novelty in terms of switches in trajectory (Fig. 5A, A') as well as pop out by motion in a direction opposite to the optic-background flow (Fig. 5B, resulting in a relative object-background velocity of -80°/s). The latter is likely not explainable in terms of responding to the step increase in relative object-velocity, as illustrated by the trials shown here, in which the pop out consisted of a backward translation at 140°/s, corresponding to 70°/s relative to the optic-background flow at 70°/s. Bar, 1 s.

Role of response dynamics at peripheral and central stages of processing. A variety of studies analyzed responses to looming and translating objects in descending neurons postsynaptic to a motion detector neuron in the locust optic lobe [24-28]. In particular, region-specific and object-size-specific adaptation has been observed [25]. Combined physiological and behavioral work in the crab has confirmed that the adaptation of responses from optic lobe neurons is correlated with the plasticity of avoidance behavior [37, 38]. These studies provide strong evidence that early-stage (optic lobe) neurons mediate the escape behavior triggered by looming or moving (translating) objects. In the locust, the identification of the associated descending premotor-neuron underlines that the pathways controlling these fast locomotor responses do not involve central processing-stages of the locust brain. Yet, Rosner and Homberg [39] showed that neurons of the locust CX are sensitive to looming stimuli as well, and the authors provided some initial observations of responses to small-field objects. Here, we show that the latter constitute the preferred type of non-looming object stimulus in polarization-sensitive compass neurons of the locust CX. We systematically explored the dynamics of the neuronal responses in these multimodal cells and found enhanced context-dependency. The observed stimulus-specific adaptation might trace back to input from the unimodal early-stage neurons. Yet, responses at the CX stage were further modulated by dynamics of background activity, as previously shown in vertebrate cortical cells [40]. This further modulated response to object motion might serve to integrate novelty-event information in the control of compass-guided locomotion. Such an interaction could mediate between the acute necessity to escape from a threat and the higher goal to locomote along a certain compass

course. Any effect of such an interaction on locomotor behavior is likely to occur substantially later than the fast escape-behavior controlled by peripheral motion-detector pathways.

Higher-stage responses to distinct objects may reflect navigational strategies. Lesion studies in flies have demonstrated a role of CX neurons in visual pattern memory [11, 12], spatial working memory [13], and visual place learning promoted by oriented patterns of bar-shaped objects in the visual panorama [15]. Yet, reports on responsiveness of CX neurons to distinct visual objects (as opposed to mere illumination or wide-field background-motion) are sparse [flies: 20, 41]. Most thoroughly, a study in *Drosophila* revealed that cells presumably involved in the observed place learning are responsive to the orientation, egocentric location and movement-direction of bar-shaped objects [20]. Neurons we encountered in the locust CX lacked such tuning to object features, spatial- or spatial-temporal tuning. They signaled events but did not precisely represent the objects involved. This difference to data obtained in *Drosophila* might relate to lifestyle differences between the two species. Although *Drosophila* can navigate using the sky polarization pattern [42], it largely lives in local, visually rich environments suited for landmark learning. In contrast, the desert locust is a long-range migrating species that might perferentially rely on compass navigation. It should finally be noted, that Seelig and Jayaraman studied ring neurons of the central body of *Drosophila* [20]; these correspond to TL-neurons in the locust [43] which were not included in the present study.

Parallels to novelty- and attention-dependent processing in vertebrates. Higher visual interneurons tuned to absolute and relative motion of small-field targets have been described in vertebrates, e.g. in the monkey [44] and pigeon [45]. Cells in the pigeon optic tectum were maximally driven by bright small-field targets when these moved in the opposite direction to a moving wide-field background-pattern, comparable to the stimulus regime in the complex object-background task we applied here (Figs. 2C, C' and 5B). It was argued that this response pattern might arise from integration across directionally selective input neurons with antagonistic center-surround organization, and the same might hold for the cells we encountered in the locust brain.

All CX neurons encountered here showed rapid stimulus-specific adaptation of responses to small-field motion stimuli. In vertebrates, stimulus-specific adaptation is a prominent feature of higher sensory processing, a presumed correlate of behavioral habituation to frequent sensory input and closely related to the capacity of novelty detection in the sensory scene [46]. Netser et al. [47] demonstrated that stimulus-specific adaptation can provide a correlate of behavioral habituation to sequential acoustic stimuli in the owl. They reported that the response to an odd stimulus in a sequence was not smaller than the response to the same stimulus when it was the first in a sequence, which parallels our current observations.

Responses of CX neurons furthermore co-varied with the level of background activity that directly preceded them. Similarly, the large variability of visual responses in cat V1 neurons has been explained in terms of an integration of prestimulus background activity with an ideal (trial-averaged) representation of a visual stimulus [40]. Modulations of sensory responses by prestimulus background activity correlate with stimulus-detection rate in monkey vision [48] as well as perceptual decisions on ambiguous stimuli in both human vision [49] and human somatosensation [50]. In the studies mentioned above, states of background activity were commonly referred to as ´brain states´ related to attention or vigilance. In case of the CX neurons we encountered in the locust brain, these states might reflect operational network states related to the function of this brain area

as a higher integration site. With respect to sky-compass signaling based on polarization planes, the best-studied function of these multimodal CX cells in the locust brain, we recently showed that increased background activity in output neurons of the network can mask polarization-plane signaling [19]. This might serve to exclude the information represented in the masked responses from locomotor control promoted by the output of the CX. A similar function may be fulfilled by the effect of highly dynamical background activity on the amplitude of responses to object motion, a feature not present in the well-studied early-stage neurons of the visual system.

Acknowledgements

We are grateful to Dr. Sonja Grün and Rajiv Narayan for providing some MATLAB code. Furthermore we thank Dr. Ronny Rosner for helpful comments on the manuscript and Milosz Krala and Stefan Ries for assistance in one experiment.

Author Contributions

T. B. and U.H. conceived the research topic and wrote the paper. T.B. designed the stimuli and physiological experimental procedures, carried out the experiments, and conceptualized and performed data analysis.

Financial Disclosure

This work was supported by Deutsche Forschungsgemeinschaft (http://www.dfg.de/) grants HO 950/21-1 and HO 950/23-1. The funders had no role in study design, data collection and analysis, decision to publish, or preparation of the manuscript.

Competing Interest

The authors declare no competing financial, personal, or professional interest.

References

1. **Srinivasan MV.** Honeybees as a model for the study of visually guided flight, navigation, and biologically inspired robotics. Physiol Rev. 2011; 91: 413-460.
2. **Merlin C, Heinze S, Reppert SM.** Unraveling navigational strategies in migratory insects. Curr Opin Neurobiol. 2011; 22: 1-9.
3. **Cheng K, Middleton EJT, Wehner R.** Vector-based and landmark-guided navigation in desert ants of the same species inhabitating landmark-free and landmark-rich environments. J Exp Biol. 2012; 215: 3169-3174.
4. **Collett M, Chittka L, Collett TS.** Spatial memory in insect navigation. Curr Biol. 2013; 23: R789-R800.
5. **Chapman JW, Reynolds DR, Wilson K.** Long-range seasonal migration in insects: mechanisms, evolutionary drivers and ecological consequences. Ecology Letters. 2015; 18: 287-302.
6. **Sakura M, Lambrinos D, Labhart T.** Polarized skylight navigation in insects: model and electrophysiology of e-vector coding by neurons in the central complex. J Neurophysiol. 2008; 99: 667-682.
7. **Homberg U, Heinze S, Pfeiffer K, Kinoshita M, el Jundi B.** Central neural coding of sky polarization in insects. Philos Trans R Soc B. 2011; 366: 680-687.
8. **Heinze S, Reppert SM.** Sun compass integration of skylight cues in migratory monarch butterflies. Neuron. 2011; 69: 345-358.
9. **Strauss R.** The central complex and the genetic dissection of locomotor behaviour. Curr Opin Neurobiol. 2002; 12: 633–638.
10. **Ritzmann RE, Harley CM, Daltorio KA, Tietz BR, Pollack AJ, Bender JA, et al.** Deciding which way to go: how do insects alter movements to negotiate barriers? Front Neurosci. 2012; 6: 97
11. **Liu G, Seiler H, Wen A, Zars T, Ito K, Wolf R, Heisenberg M, Liu L.** Distinct memory traces for two visual features in the *Drosophila* brain. Nature. 2006; 439: 551–56.
12. **Pan Y, Zhou Y, Guo C, Gong H, Gong Z, Liu L.** Differential roles of the fan-shaped body and the ellipsoid body in *Drosophila* visual pattern memory. Learn Mem. 2009; 5: 289–295.
13. **Neuser K, Triphan T, Mronz M, Poeck B, Strauss R.** Analysis of a spatial orientation memory in *Drosophila*. Nature. 2008; 453: 1244–1247.
14. **Heinze S, Homberg U.** Maplike representation of celestial *E*-vector orientations in the brain of an insect. Science. 2007; 315: 995-997.
15. **Ofstad TA, Zuker CS, Reiser MB.** Visual place learning in *Drosophila melanogaster*. Nature. 2011; 447: 204–207.
16. **Heinze S, Homberg U.** Neuroarchitecture of the central complex of the desert locust: intrinsic and columnar neurons. J Comp Neurol. 2008; 511: 454-478.
17. **Bech M, Homberg U, Pfeiffer K.** Receptive fields of locust brain neurons are matched to

polarization patterns of the sky. Curr Biol. 2014; 24: 1-6.

18. **Mappes M and Homberg U.** Behavioral analysis of polarization vision in tethered flying locusts. J Comp Physiol A. 2004; 190: 61-68.
19. **Bockhorst T Homberg U.** Amplitude and dynamics of polarization-plane signaling in the central complex of the locust brain. J Neurophysiol. 2015. *In press* doi:10.1152/jn.00742.2014.
20. **Seelig JD, Jayaraman V.** Feature detection and orientation tuning in the *Drosophila* central complex. Nature. 2013; 503: 262-266.
21. **Heinze S, Gotthardt S, Homberg U.** Transformation of polarized light information in the central complex of the locust. J Neurosci. 2009; 29: 11783–11793.
22. **Collett TS.** Visual neurones for tracking moving targets. Nature. 1971; 232: 127-130.
23. **Collett TS.** Visual neurones in the anterior optic tract of the pivet hawk moth. J Comp Physiol. 1972; 78: 396-433.
24. **O'Shea M, Rowell CHF.** Protection from habituation by lateral inhibition. Nature. 1975; 254: 53-55.
25. **Gray JR.** Habituated visual neurons in locusts remain sensitive to novel looming objects. J Exp Biol. 2005; 208: 2515-2532.
26. **Rowell CHF, O'Shea M, Williams JLD.** The neuronal basis of a sensory analyser, the acridid movement detector system. IV. The preference for small field stimuli. J Exp Biol. 1977; 68: 157-185.
27. **Gewecke M, Kirschfeld K, Feiler R.** Identification of optic lobe neurons of locusts by video films. Biol Cybern. 1990; 63: 411-420.
28. **Gewecke M, Hou T.** Visual brain neurons in *Locusta migratoria*. In: Wiese K, Gribakin FG, Popov AV, Renninger G, editors. Sensory Systems of Arthropods. Basel: Birkhäuser; 1993. pp. 119-144.
29. **Egelhaaf M.** On the neuronal basis of figure-ground discrimination by relative motion in the visual system of the fly. II. Figure-detection cells, a new class of visual interneurones. Biol Cybern. 1985; 52: 195-209.
30. **Gilbert C, Strausfeld NJ.** The functional organization of male-specific visual neurons in flies. J Comp Physiol A. 1991; 169: 395-411.
31. **O'Carroll D.** Feature-detecting neurons in dragonflies. Nature. 1993; 362: 541- 543.
32. **Wiederman SD, O'Carroll DC.** Discrimination of features in natural scenes by a dragonfly neuron. J Neurosci. 2011; 31: 7141-7144.
33. **Collett TS, King AJ.** Vision during flight. In: Horridge GA, editor. The Compound Eye and Vision of Insects. Oxford: Clarendon Press; 1975. pp. 437-466.
34. **Nordström K, Barnett PD, O'Carroll DC.** Insect detection of small targets moving in visual clutter. PLoS Biol. 2006; 4: 379-386.
35. **Wiederman SD, O'Carroll DC.** Selective attention in an insect visual neuron. Curr Biol. 2013; 23: 156-161.
36. **Goldstein EB.** Perceiving objects. In: Goldstein EB, editor. Sensation and Perception (7th edition). Belmont, CA: Thomson-Wadsworth; 2007. pp. 93-119.
37. **Tomsic D, de Astrada MB, Sztarker J.** Identification of individual neurons reflecting short- and long-term visual memory in an arthropod. J Neurosci. 2003; 23: 8539–8546.
38. **de Astrada MB, Bengochea M, Sztarker J, Delorenzi A, Tomsic D.** Behaviorally related neural plasticity in the arthropod optic lobes. Curr Biol. 2013; 23: 1389–1398.
39. **Rosner R, Homberg U.** Widespread sensitivity to looming stimuli and small moving objects in the central complex of an insect brain. J Neurosci. 2013; 33: 8122-8133.
40. **Arieli A, Sterkin A, Grinvald A, Aertsen A.** Dynamics of ongoing activity: explanation of the large variability in evoked cortical responses. Science. 1996; 273: 1868-1871.
41. **Phillips-Portillo J.** The central complex of the flesh fly, *Neobellieria bullata*: recordings and morphologies of protocerebral inputs and small-field neurons. J Comp Neurol. 2012; 520: 3088-3104.
42. **Weir PT, Dickinson MH.** Flying *Drosophila* orient to sky polarization. Curr Biol. 2012; 22: 21-27.
43. **Müller M, Homberg U, Kühn A.** Neuroarchitecture of the lower division of the central body in the brain of the locust (*Schistocerca gregaria*). Cell Tissue Res. 1997; 288: 159-176.
44. **Bridgeman B.** Visual receptive fields sensitive to absolute and relative motion during tracking. Science. 1972; 178: 1106-1108.
45. **Frost BJ Nakayama K.** Single visual neurons code opposing motion independent of direction. Science. 1983; 220: 744-745.
46. **Gutfreund Y.** Stimulus-specific adaptation, habituation and change detection in the gaze control system. Biol Cybern. 2012; 106: 657-668.
47. **Netser S, Zahar Y, Gutfreund Y.** Stimulus-specific adaptation: can it be a neural correlate of behavioral habituation? J Neurosci. 2011; 31: 17811–17820.
48. **Supèr H, van der Togt C, Spekreijse H, Lamme VAF.** Internal state of monkey primary visual

cortex (V1) predicts figure-ground perception. J Neurosci. 2003; 23: 3407–3414.

49. **Hesselmann G, Kell CA, Eger E, Kleinschmidt A.** Spontaneous local variations in ongoing neural activity bias perceptual decisions. Proc Natl Acad Sci USA (PNAS). 2008; 105: 10984–10989.
50. **Boly M, Balteau E, Schnakers C, Degueldre C, Moonen G, Luxen A, Phillips C, Peigneux P, Maquett P, Laureys S.** Baseline brain activity fluctuations predict somatosensory perception in humans. Proc Natl Acad Sci USA (PNAS). 2007; 104: 12187-12192.
51. **Clements AN, May TE.** Studies on locust neuromuscular physiology in relation to glutamic acid. J Exp Biol. 1974; 60: 673-705.
52. **Kreuz T, Haas JS, Morelli A, Abarbanel HDI, Politi A.** Measuring spike train synchrony. J Neurosci Methods. 2007; 165: 151–161.
53. **Pfeiffer K, Homberg U.** Organization and functional roles of the central complex in the insect brain. Annu Rev Entomol. 2014; 59: 165–184.
54. **Vitzthum H, Müller M, Homberg U.** Neurons of the central complex of the locust *Schistocerca gregaria* are sensitive to polarized light. J Neurosci. 2002; 22: 1114–1125.
55. **Heinze S, Homberg U.** Linking the input to the output: new sets of neurons complement the polarization vision network in the locust central complex. J Neurosci. 2009; 29: 4911– 4921.

CHAPTER III

GAIN MODULATION OF COMPASS SIGNALING BY SALIENT OBJECT MOTION IN AN INSECT BRAIN

Tobias Bockhorst and Uwe Homberg

GAIN MODULATION OF COMPASS SIGNALING BY SALIENT OBJECT MOTION IN AN INSECT BRAIN

Tobias Bockhorst and Uwe Homberg

Goal-directed animal behavior is often interfered with by unpredictable events, such as the appearance of a predator during locomotion in a planned direction. This can require maneuvers contrary to the objective pursued, e.g. evasive glides that deflect a flying insect from its route. In the desert locust, oriented flight is believed to be promoted by sky-compass neurons which adapt to constant bearings. We wondered whether these neurons modulate their compass-signaling in response to salient object motion and observed two types of response to combined stimulation in immobilized locusts: 1.) a linear integration to the disadvantage of compass-signaling and 2.) non-linear gain modulation that re-increases the declined compass-response. Because the small-field motion stimuli we applied are likely to trigger escape in flying locusts, we conclude that 2.) is suited to prepare for spatially directed escape or for subsequent memory-based reorientation that gets the locust back on route.

ANIMAL SURVIVAL critically depends on spatial orientation for goal-directed locomotion (*1*) as well as on the ability to respond to unexpected events. As for insects, a role in goal-directed locomotion has been assigned to the central complex (CX), a higher integration center in the brain (Fig. 1D, 2A) (*1, 2*). In the desert locust the CX is innervated by neurons sensitive to the polarization plane of skylight, a sky-compass cue (Fig. 1, A-C). At this, preferred angles of the electric field vector (*E*-vector) are mapped onto a neural axis (Fig. 1D) (*3, 4*). These ´sky-compass neurons´, comparable to vertebrate head direction cells (*5, 6*), are believed to mediate goal-directed locomotion along courses relative to the Sun's azimuth (Fig. 1C) (*7*). In nature, such planned behavior is frequently interfered with by unpredictable events such as the sudden appearance of prey, imminent collision with a conspecific in a swarm, or approach of a predator. Small-field motion stimuli that mimic object motion were shown to excite neurons of the locust optic lobes (OL, Fig. 2A) which trigger evasive glides in response to looming stimuli (*8-11*). Such escape responses will most often deflect a flying locust away from its compass-route, and it is an open question how this is compensated for. Here, we present an effort to address this topic in asking whether the compass-signaling of higher neurons in the CX in itself is modulated in response to salient events of visual motion.

We recently showed that several types of compass-cell in the CX respond to moving targets in a novelty-detecting manner, when there is no concurrent presentation of polarized light. More precisely, they signal the appearance of a small-field object (2° visual angle azimuthal extent and 1.5° elevational extent) that rapidly moves through the visual field (translation at 70°/s) by responses that are subject to region-specific adaptation but lack positional and directional information (*12*). Responses to polarized light with unmodulated *E*-vector angle are marked by *E*-vector specific adaptation, resulting in a phasic or, less frequently, in a phasic-tonic response course (*5*). To study possible interactions between compass-signaling and novelty detection, we performed intracellular recordings, followed by tracer injection, from male adult desert locusts in gregarious phase with wings and legs removed.

Moving small-field objects were presented under the absence of compass stimulation as well as during concurrent compass stimulation, after responses to polarized light had ceased or declined by *E*-vector specific adaptation as previously demonstrated (*5*) (see Material and Methods for details). The latter scenario mimics the unexpected appearance of a moving object while the animal is flying aligned to a steady compass course.

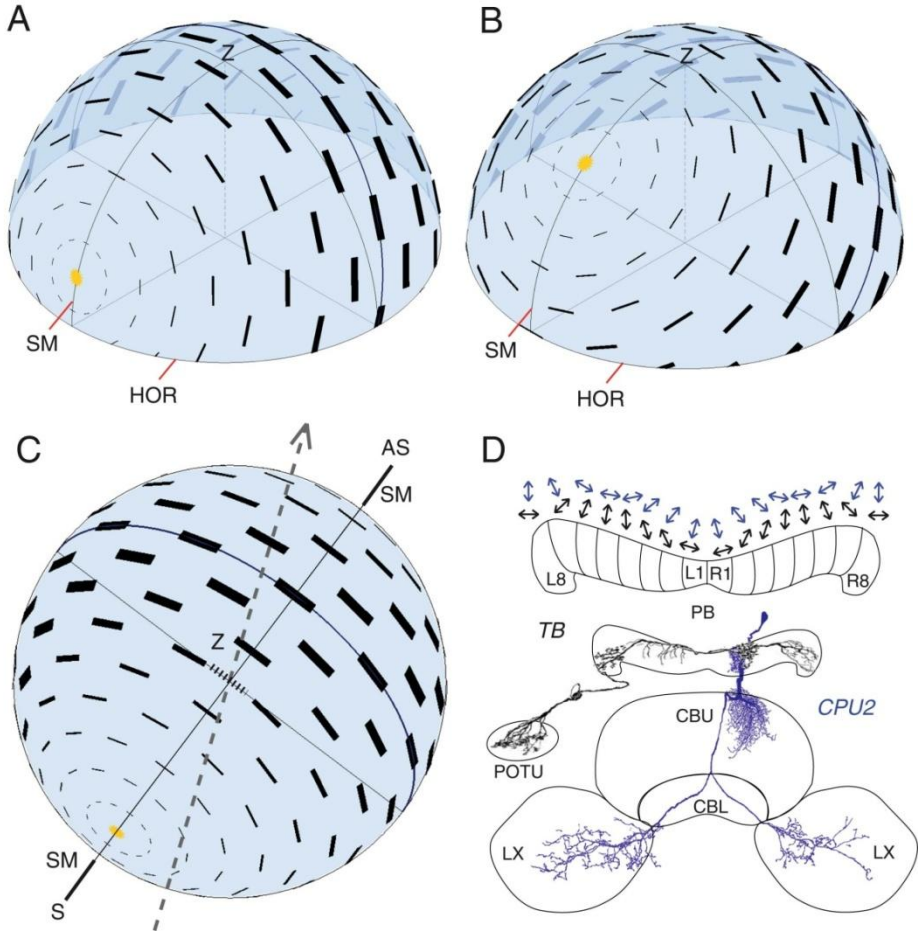

Fig. 1. Skylight polarization as a compass cue and its representation in the central complex of the locust brain. (A) Light from the Sun (yellow) gets linearly polarized when scattered at particles in the atmosphere, which results in a pattern of *E*-vector angles (black bars) mirror-symmetric to the solar meridian (SM). The degree of polarization (bar thickness) is highest along a circle at 90° angular distance to the Sun's elevation. HOR, geometrical horizon (elevation 0°). While a fixed-perspective view of the *E*-vector pattern changes with solar elevation throughout the day **(A,B)**, *E*-vector angles along the SM, and hence in the zenith (Z) remain perpendicular to the SM. (**C**) This robust relationship may serve to align the direction of locomotion (grey, dashed arrow) relative to the SM, as illustrated in top-down view (dashed black line: approximation of the *E*-vector angle in the zenith). Yet, to obtain true compass information it is mandatory to distinguish between the solar (S) and anti-solar (AS) hemisphere, which requires additional cues such as a gradient in light intensity or a comparison with *E*-vector angles at locations off the solar meridian. (**D**) In case of polarized light from the zenith, preferred *E*-vector angles (arrows) of TB-cells (morphology and preferred angles shown in black) and CPU-cells (blue) vary systematically along the slices of the protocerebral bridge (PB). Across the entirety of the PB, this polarotopic axis spans 360° in *E*-vector angle, roughly binned into steps of 22.5° according to the 16 vertical slices. Note that preferred angles of TB- and CPU-cells differ by roughly 90°, probably due to inhibitory synapses between these cells. PB, protocerebral bridge; POTU, posterior optic tubercle; CBU (CBL), upper (lower) division of the central body; LX, lateral complex; L1-L8 (R1-R8) slices that subdivide the left (right) hemisphere of the PB. Polarization pattern in A-C calculated and plotted with scripts provided by Dr. Keram Pfeiffer.

Results

A total of 10 cells were accepted for final analysis (see Material and Methods for inclusion criteria). These included tangential neurons of the protocerebral bridge that represent an intermediate processing stage (TB1-cells, Fig. 2A) as well as output neurons of the network that invade the upper division of the central body in a columnar fashion (CPU1-and CPU2-cells) (*3*). In addition to these 10 cells, some recordings were obtained from columnar neurons of the lower division of the central body (CL1-neurons, supplemental fig. S1), those most likely provide input to TB-cells (*3, 5*). Experiments lasted for 10 to 45 minutes. Two fundamentally different types of response behavior were observed. All CL1-neurons, two TB1-neurons and one CPU1-neuron showed compass-signaling and typical novelty-dependent responses to the moving object alone, as previously described (*5, 12*). Their responses to *combined* stimulation were similar to those to the moving objects alone, hence not reflecting the respective concurrent compass stimulus (Fig. 2, B-D; fig. S1). In the CL1-cells responses to combined stimulation were always inhibitory, even if the concurrently presented *E*-vector angle was maximally different (i.e.by 90°) from the inhibitory *E*-vector angle (Φ_{min}) of the respective cell. In the latter case, the combined responses were thus ´paradox´ in terms of compass-signaling. Analogously, responses were paradox in terms of compass signaling for excitatory *E*-vector angles in CPU-cells (inhibitory responses to combined stimulation) and for inhibitory *E*-vector angles in TB-cells (excitatory responses to combined stimulation). We consider this ´destructive interference´ a *linear integration* of the novelty-event response with a declined response to the compass-stimulus.

By contrast, six neurons (three TB1-neurons, one CPU1-neuron and two CPU2-cells) were unresponsive to the moving object alone and showed compass-responses that were phasic-tonic rather than merely phasic in time course. They responded to combined stimulation in a *nonlinear* manner that re-increased the gain of the residual compass-response during the events of small-field motion (Fig. 2, B'-D'). Importantly, the very same events brought back a respective cell's excitatory response to its preferred *E*-vector angle and its inhibitory response to the anti-preferred *E*-vector, while no effect was observed at neutral, intermediate *E*-vector angles. We consider this response behavior as context-dependent compass-signaling and termed it 'gain modulation'. Noteworthy, these effects surpassed the duration of novelty-dependent responses to object motion that marked the abovementioned linear integration behavior.

To quantify gain-modulation, we performed correlation analyzes on data sets of individual experiments as well as on pooled data (Fig. 3A). These measured the degree to which the response to combined stimulation covaried with the initial, phasic compass-response. Both responses were quantified by difference in spike rate relative to the declined compass-response (see supplementary material). The results proved positive correlations significant at the 5% level, with values of R^2 ranging from 0.33 to 0.85, except for one of the CPU2-neurons in which, nevertheless, a positive trend in line with the observed phenomenon was found. The analysis of pooled data was restricted to the five cells that showed a significant correlation (three TB1-neurons, one CPU1-, and one CPU2-neuron), covering 101 measurements with a highly significant positive correlation ($F(99,1)=50.55$, $p(F)<<0.0001$) and a strong associated effect that explained about 34 % of the observed variability, as quantified by R^2. Peri-stimulus time histograms (Fig. 3B) confirmed, as suggested by the traces in Figure 2D', that modulated compass-responses can match the pronounced early response in duration. Wide-field motion mimicking a unilateral, progressive optic flow

was occasionally applied as well but failed to elicit gain modulation (data not shown). Also, the response behavior did not co-vary systematically with time of day or time of year (data not shown).

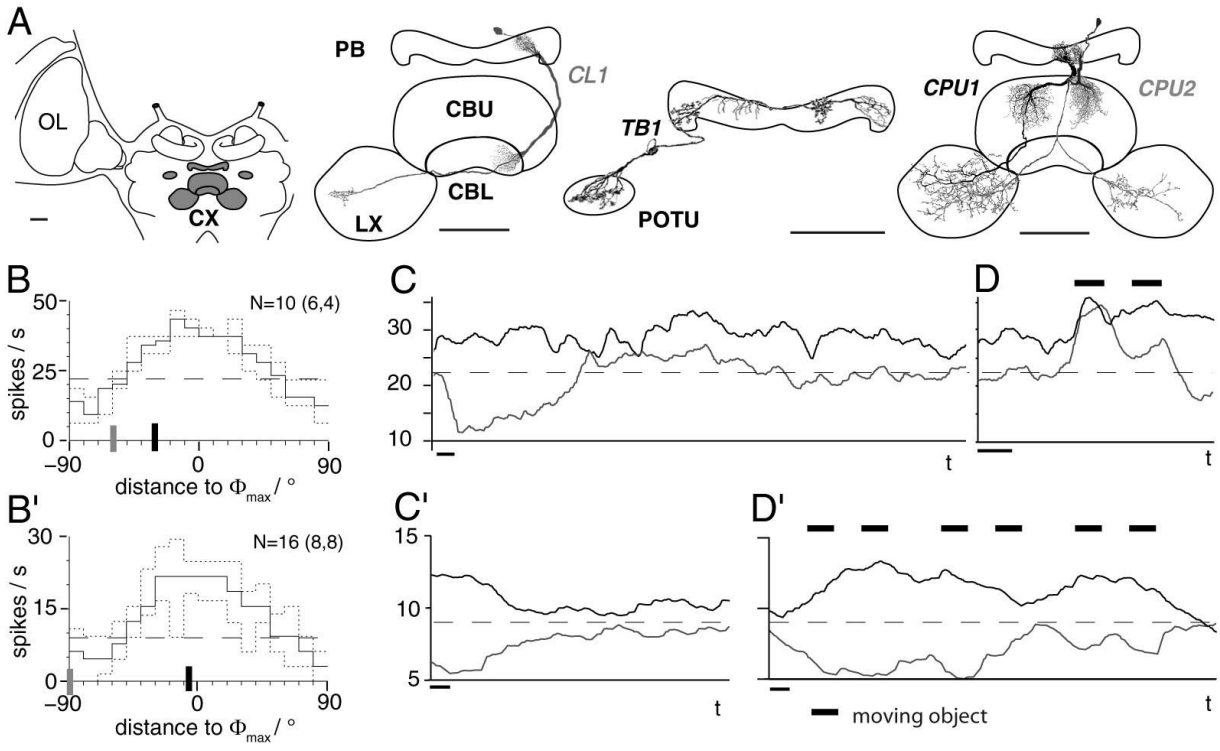

Fig. 2. Morphology and response profiles of polarization-sensitive cell types of the central complex. **(A)** Frontal diagrams illustrating the location of the central complex (CX), associated neuropils (grey shading) and the morphology of selected polarization-sensitive neurons. OL, optic lobe; LX, lateral complex; CBL (CBU), lower (upper) division of the central body; PB, protocerebral bridge; POTU, posterior optic tubercle. CL, columnar neuron of the CBL; TB, tangential neuron of the PB; CPU, columnar neuron of the CBU. Numbers indicate cellular subtypes. Modified from (*2*, 4, 20-22). Scale bars, 200 µm. **(B, B')** Polarization-plane tuning, based on N (clockwise, counter-clockwise) half-rotations (30°/s) of a linear polarizer. Quartiles (solid line: median) of spike rate are plotted as a function of binned (10°) distance to the respective cell's preferred *E*-vector angle, Φ_{max}. Horizontal dashed lines in **(B)** to **(D')** give median levels of background activity for reference. Grey (black) tags at X-axes indicate angles of stimuli underlying the response plots in **(C, C')** and **(D, D')**. **(C, C')** and **(D, D')** show selected responses to constant *E*-vector angle and to combined stimulation, respectively. Time bars, 1s. **(B)** to **(D):** data from a TB1-cell responding with linear integration of responses to compass- and object-motion stimuli. At the avoided *E*-vector angle (grey line), this results in a combined response **(D)** contrary to the phasic compass-response **(C)**. The excitatory response (black line) was rather tonic, concurrent with a prolonged excitatory response to combined stimulation. **(B') to (D'):** data from a CPU2-neuron that responds to combined stimulation in a gain-modulating manner, re-increasing the declined responses to both excitatory and inhibitory *E*-vector angles. Note that responses to polarized light alone include a tonic component in the gain-modulating case.

Discussion

As rated from its strength and duration, the gain-modulating effect should provide suitable compass-signaling that could serve the planning of directed evasive maneuvers. Bringing back a brief representation of the original compass bearing – right before an escape maneuver – might provide a memory template for subsequent re-orientation to get re-aligned to

this ‘desired’ compass-course. This would be in line with previous implications on a role of the central complex for visuo-spatial working memory (see below). The actual execution of an escape maneuver would result in an apparent drift or rotation of the skylight polarization pattern across the polarization-sensitive parts of the compound eyes. As responsiveness to changes in *E*-vector orientation was preserved throughout the entire course of experiments, this effect should provide compass signaling after the initiation of escape. Acute heading direction could then be compared to the abovementioned hypothetical memory template of the original compass course for controlling corrective yaw.

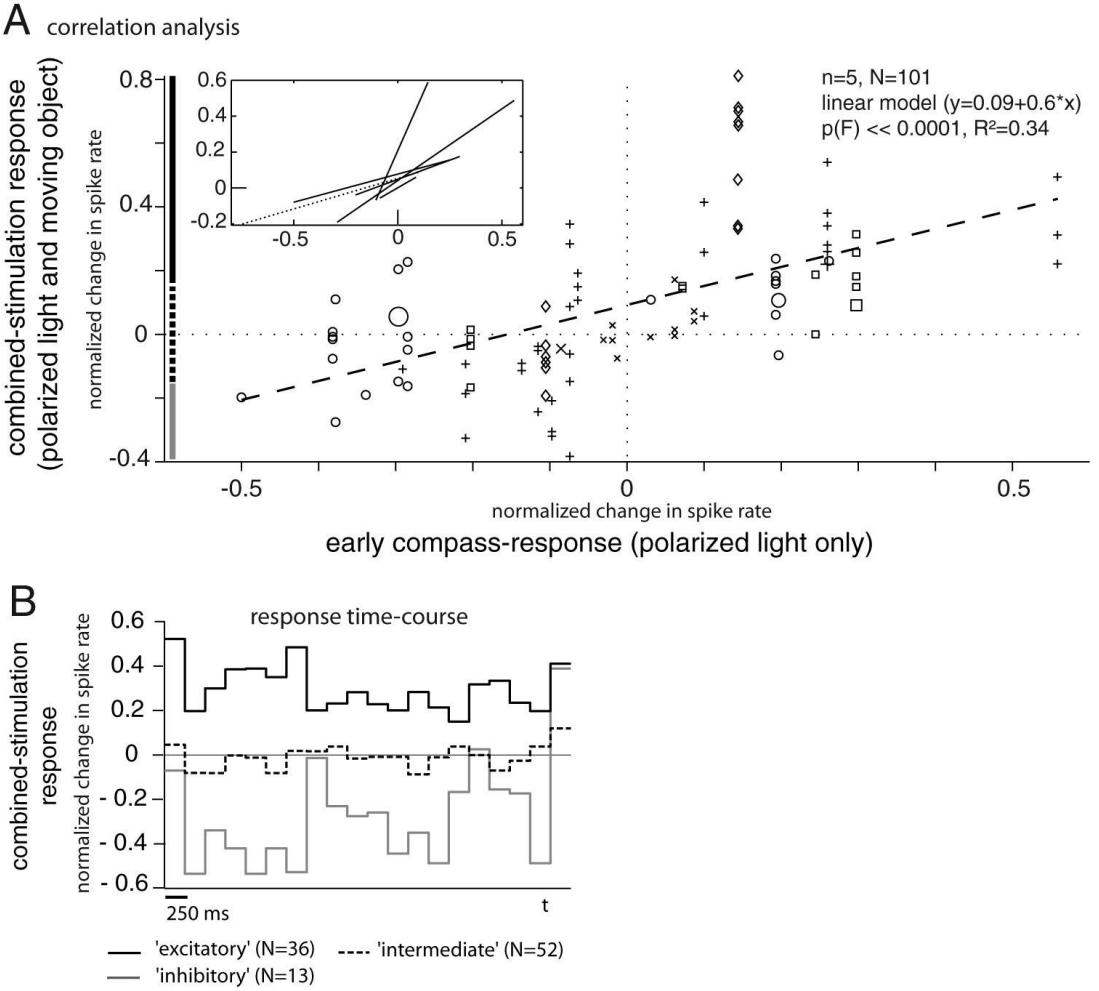

Fig. 3. Correlation strength and time course of gain-modulating effects. (A) Under gain-modulation, early compass-responses and associated responses to subsequent combined stimulation go in the same direction. This is reflected by a significant and strong positive correlation (dashed grey line). Plot markers identify data from the same respective cell, marker size is scaled to frequency of observations. Inset: regression lines from individual neurons, including a case lacking significance (dashed line). Grey, dashed black and solid black parallels to the vertical axis distinguish ranges of combined-stimulation responses that were considered inhibitory (decrease of average spike rate by 15%), intermediate and excitatory (increase of average spike rate by 15%), respectively. **(B)** Peri-stimulus time histograms (250 ms bins) of excitatory, intermediate, and inhibitory responses to combined stimulation; based on 5 s analysis windows in different stimulus sequences (see Material and Methods).

While gain modulation most likely promotes compass-guidance, linear integration does not necessarily have to hinder the same. Any *E*-vector unrelated response to object motion could be cancelled out by lateral inhibition between output channels of the compass network (i.e., neurons downstream to CPU-cells), and the same might hold for coincident background activity in the channels.

With respect to the underlying mechanisms, we presume that the two types of response behavior represent different operational states of the CX network rather than two functionally distinct cellular populations. A network wiring scheme (Fig. 4) that accounts for dynamics of responses to polarized light alone (*5*) is suited explain the functional dualism of compass cells if extended by a simple assumption, a conditional transition from phasic responses to polarized light to phasic-tonic responses (Fig. 2C') that concurred with gain modulation.

In the experiments presented here, gain modulation integrates input from two different exteroceptive domains, as distinguished from previously demonstrated effects of locomotor state on visual responsiveness in CX neurons of the fly (*13, 14*). An integration of internal state (level of satiation) and complex exteroceptive input (quantity and quality of food odors) by cells that invade the CX was shown to play a role in the graded encoding of food odor value in the fly brain (*15*). In concert with evidence for a role in visual pattern memory (*16, 17*), visuo-spatial working memory (*18*) and place learning (*19*), converging evidence suggests a role of the CX as a higher processing site in the insect brain that integrates goals, internal states and exteroceptive input to control goal-driven locomotion.

Material and Methods

Locusts were reared in crowded indoor colonies under an 11 h : 13 h light-dark regime at 28°C. Male subjects were preferred over females for lower content of fat in hemolymph which eases preparation. Details on preparation, intracellular recordings, and histological processing are provided in (*5*). After removal of antennae, wings and legs, the frontal brain surface was accessed via an excision from the frontal cuticle of the head. To stabilize recordings, muscles in the vicinity of the brain were transected, a spoon-shaped wire loop was used to support the brain from posterior, and the gut was removed to stop peristaltic pumping. Electrode insertion was facilitated by an incision of the neural sheath of the brain. During preparation and recording, the brain was kept immersed in locust saline (*23*). Sharp micropipettes (50 - 200 MΩ) filled with 1 M KCl were used for intracellular recording and cell labeling, their tips loaded with Neurobiotin tracer (Vector Laboratories, Burlingame, UK, 4 % in 1 M KCl) for iontophoretic injection (0.5-2 nA, 1-15 min) after recording. Connectors, and likewise reference electrodes immersed in the saline outside the brain, were made from Ag-AgCl wire. Digitized signals were analyzed offline using software written in MATLAB (MathWorks, Natick, MA, USA).

For visualization of neural morphologies, wholemount preparations were fixed chemically and incubated in a solution of streptavidin-conjugated Cy3 fluorophore (Dianova, Hamburg, Germany) that targets the Neurobiotin tracer. Subsequently, brains were dehydrated in an ethanol series, cleared using methyl salicylate, embedded in Permount (Fisher Scientific, Pittsburgh, PA), and scanned confocally (Leica TCS SP5 confocal laser scanning microscope, Leica Microsystems, Wetzlar, Germany) at either 10x or 20x magnification. Cy3-fluorescence was induced by excitation at 561 nm (DPSS laser). Relevant neuropils could usually be identified based on their autofluorescence.

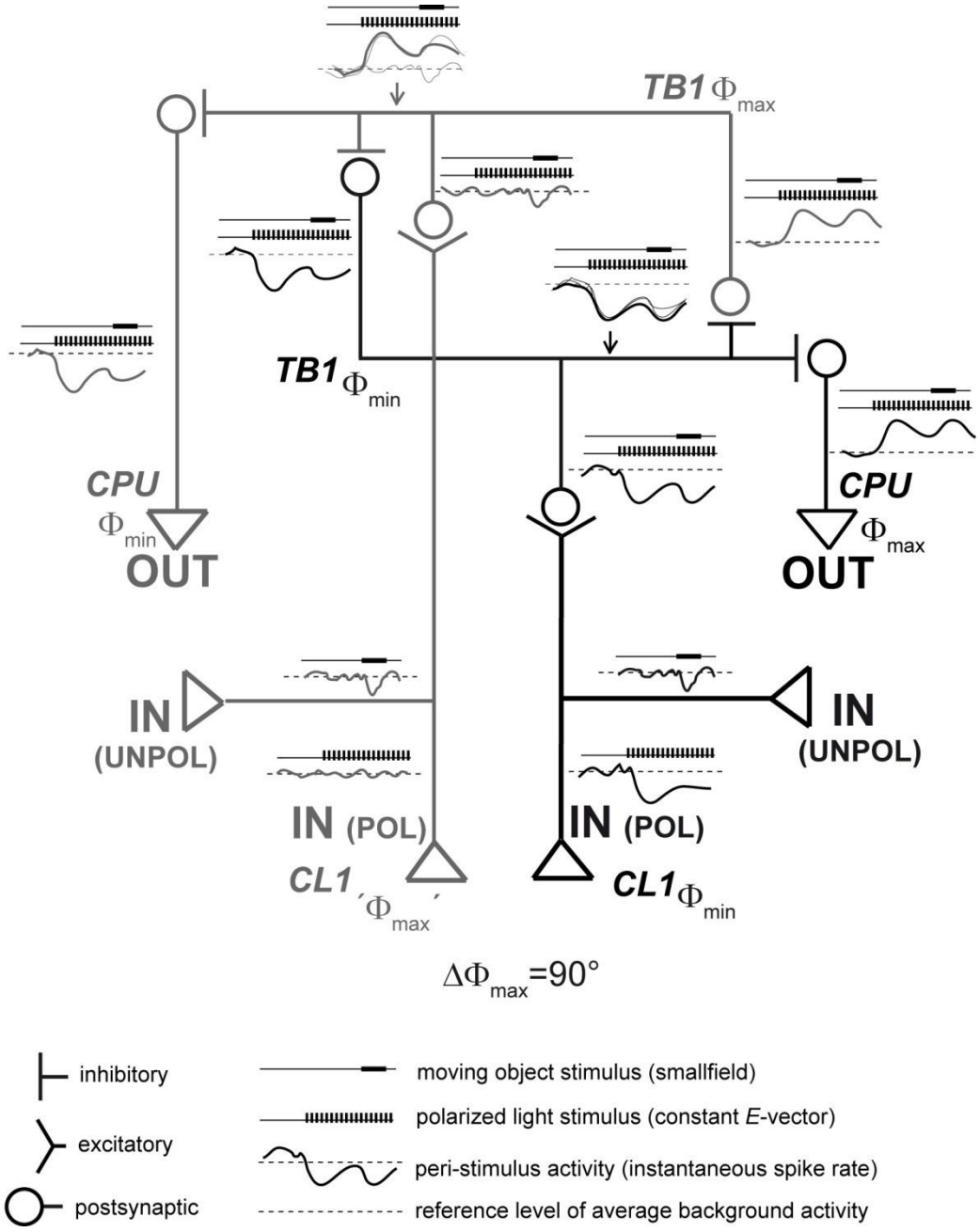

Fig. 4. A wiring model of the CX explains both types of response behavior. The scheme illustrates how CL-, TB- and CPU-cells are presumably connected and responding in the elementary circuit of the polarization-vision network (*12*). The key element is mutual (dis-)inhibition between two TB-cells that receive input from oppenently tuned CL-cells (Φ_{max}=90°). This 'antagonistic integration' also explains how TB-and CPU-neurons can respond to preferred (Φ_{max}) *and* anti-preferred *E*-vector angles (Φ_{min}), while CL1-cells solely respond to their Φ_{min}. All responses of CL-cells to presentations of moving objects alone as well as to combinations with polarized light are inhibitory. A phasic-tonic response of CL at Φ_{min} (black path) should cause a stronger response to combined stimulation as compared to the partner CL-cell (grey path) which 'responds' neutrally to its 'Φ_{max}' –angle. Due to the mutual (dis-) inhibition among the TB-cells, this difference in amplitude of responses to combined stimulation results in the gain modulation observed in TB- and CPU-cells, concurrent with phasic-tonic compass-responses. Thin (thick) lines indicate responses to separate (combined) stimulation by compass- and motion stimuli, 'tapped' at the positions indicated by arrows. IN, OUT: input to and output of the circuit, respectively; (UN)POL: responses to presentation of (un)polarized-light stimuli. Otherwise (not illustrated), a pure phasic response to polarized light would, once declined to the level of background activity, result in equal amplitudes of combined responses in CL. This in turn would cause linear integration for combined

stimuli by TB- and CPU-cells. Variability of the gain-modulating effect (at the same *E*-vector) might trace back to dynamics of background activity in upstream neurons (CL1) that most likely provide input (*3, 5*) to TB1-cells.

Figure 5 provides an overview on the experimental setup, stimuli and response analysis. Compass-stimulation was applied by means of blue light (range 421.6 nm – 524.3 nm, peak 461.11 nm, 10^{15} photons·cm^{-2}·s^{-1}) from an LED source (ELJ-465-617, EPIGAP Optoelektronik, Berlin, Germany), passing a rotatable linear polarizer (HN38S, Polaroid, Cambridge, MA; 20 mm ID) positioned zenithal to the head at 60 mm distance (visual angle 19°). Neuronal activity was recorded under dim, unilateral wide-field illumination ($4.3 \cdot 10^{13}$ photons·cm^{-2}·s^{-1}) by a cathode-ray tube display (CRT; Mitsubishi DP2070SB 22”, Mitsubishi, Tokyo, Japan) that was used for the presentation of moving virtual objects. Photon flux was measured with a digital spectrometer (USB2000, Ocean Optics Inc., FL, USA). The display was positioned slightly tilted in the left latero-frontal visual field, covering -45° to 60° in azimuth and -32° to 28° in elevation. Virtual objects were generated by MATLAB software (based on the CRS toolbox provided by Cambridge Research Systems, Rochester, Kent, UK) and displayed against the abovementioned dim (‘grey’) background using a ViSaGe stimulus device (Cambridge Research Systems). Neuronal responses shown in Figures 2 and 3 were triggered by sequential translations (70°/s) of a single black, rectangular small-field patch (about 2° visual angle azimuthal extent and 1.5° elevational extent) in either forward or backward direction along a horizontal trajectory (Fig. 5, B-C’). The latter spanned the entire width of the display (-45° to + 60° in azimuth) at either high elevation (+25.5°) or low elevation (-29.5°). As the gain modulation appeared to occur independently from direction of motion and trajectory elevation, data were pooled across stimulus batteries. Experiments began with measurements of tuning to *E*-vector angle by means of clockwise and anti-clockwise rotations of the polarizer. Tuning curves (Fig. 2, B and B’) were calculated offline using the circular statistics toolbox for MATLAB (*25*). Subsequent to tuning measurement, the polarizer was rotated to orientations that elicited prominent inhibitory and excitatory responses, respectively. Details on these procedures were described earlier (*5*). Once the response to the stationary *E*-vector had declined, moving objects were presented concurrent with the ongoing presentation of polarized light (Fig. 5D).

Physiological data were accepted for further evaluation if the recorded cell was identified unambiguously. Ideally, this was provided by its distinct labeling. In case of more than one neuron being labeled in the same specimen, measurements were assigned to morphologies by means of cell-type specific features of background activity (*5*). In final analyzes, solely those experiments were included that yielded at least 10 measurements of 5 s peri-stimulus activity during concurrent presentation of compass- and object stimuli, whereat measurements at both excitatory and inhibitory *E*-vector angles within the same experiment were mandatory. Table S1 provides an overview on the final dataset underlying Figures 2 and 3. Spike times were determined via threshold-based event detection and false positives excluded by an upper threshold for spike amplitude as well as an absolute refractory period of 1 ms. Rasterplots were generated using a MATLAB function (rasterplot.m) kindly provided by Rajiv Narayan (Boston University), available at http://www.mathworks.com/MATLABcentral/fileexchange/10000-rasterplot.

To estimate the instantaneous firing rate in an objective manner, we applied the nonparametric empirical Bayes method, optimized using the maximized-likelihood principle (*24*). This tool gives a robust estimate independent from assumptions concerning the true underlying rate function. To quantify phasic responses to

polarized light as well as responses to combined stimulation, we compared spike rates in peri-stimulus time windows to a sample of the declined response to polarized light alone (Fig. 5, C and D).

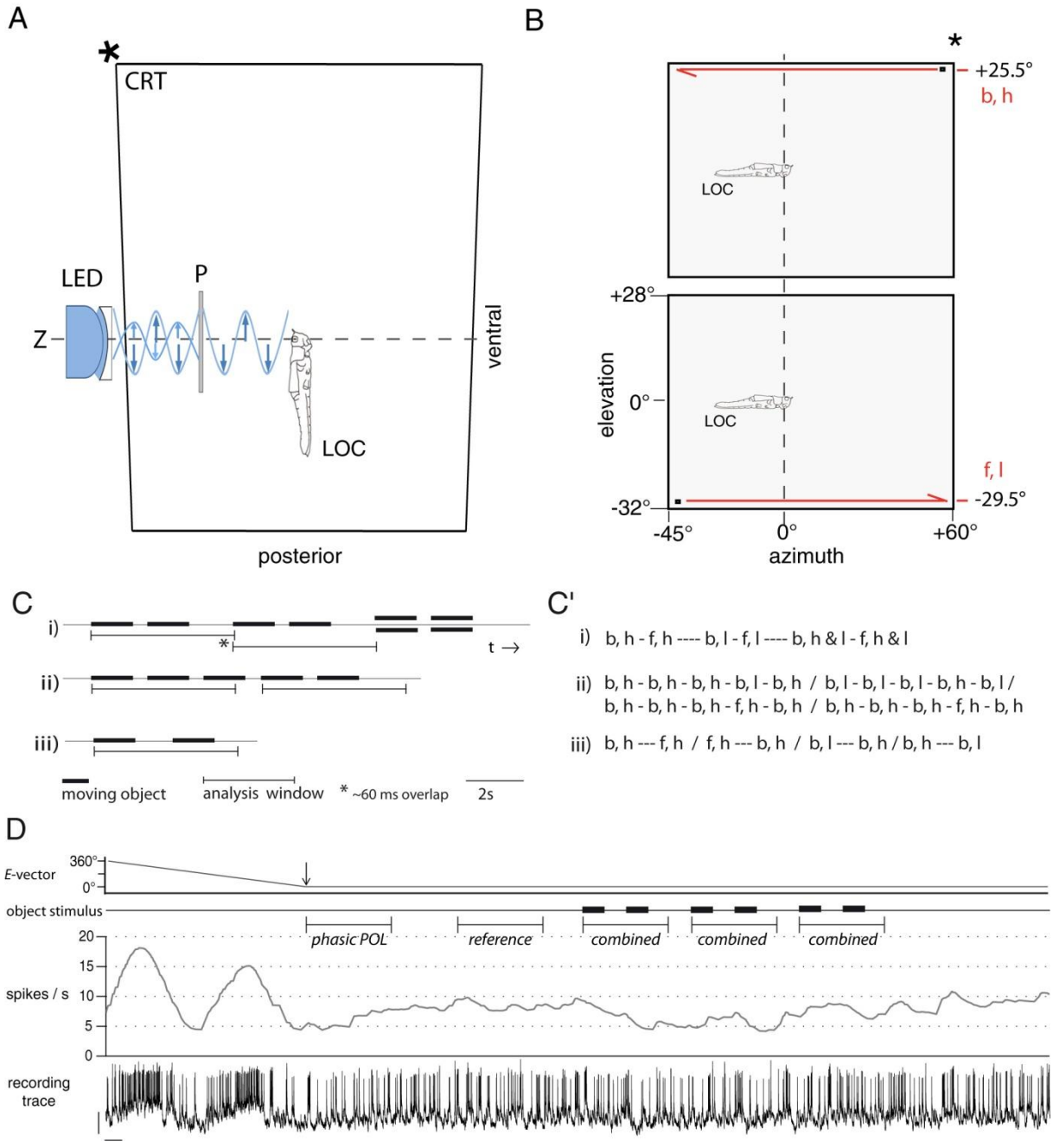

Fig. 5. Visual stimulation and evaluation of neuronal activity. (A) Experimental setup for presentation of virtual objects and polarized light during intracellular recording (the latter not illustrated). For compass-stimulation, blue light emitted from an LED in the zenith (Z) was directed through a rotatable linear polarizer (P) onto the locust (LOC) eyes. Blue arrows symbolize electric field vectors of unpolarized and polarized light. Virtual objects were presented on a cathode ray tube display (CRT) positioned slightly tilted into the left antero-lateral visual field. The asterisk in (**A**) and (**B**) marks the antero-dorsal edge of the CRT; dashed lines represent a vertical (dorso-ventral) plane that passes the eyes. Locust not to scale. **(B)** The CRT display covered about -45° to +60° in azimuth and -32 to +28° in the left visual field. The building block for object-stimuli was a single black, rectangular small-field patch, about 2° visual angle azimuthal extent and 1.5° elevational extent. This was displayed translating at 70°/s along horizontal

trajectories (red arrows) at high elevation (25.5°, h) or low elevation (-29.5° , l). The direction of translation was either forward (f) or backward (b). The four possible stimuli (f,h; b,h; f,l and b,l) were combined into three types of battery (i-iii) that differed in time course **(C)** and composition **(C')**. Note that the number of time windows for response evaluation, the number of stimuli covered by the window(s), as well as the inter-stimulus-intervals varied between the batteries as illustrated in C. **(D)** Evaluation of neuronal activity. Tuning to *E*-vector angle was measured with clockwise and anti-clockwise rotations of the polarizer. Subsequently, the polarizer was rotated to an orientation that elicited a prominent response, such as the pronounced inhibition near 0° *E*-vector angle in this illustration (vertical arrow in uppermost trace marks stop of polarizer rotation at 0°). Once the *E*-vector response had declined, moving objects were presented concurrent with the ongoing presentation of polarized light with stationary *E*-vector. Offline analyses included an estimation (Bayes) of the instantaneous firing rate as well as comparisons of spike counts in analysis windows (5 s duration) set to capture the early response to polarized light (*phasic POL*), the response(s) to combined stimulation(s) (*combined*) and a common reference sample of the declined response to polarized light (*reference*). To obtain a normalized measure of the compass-response and possible gain-modulation effects, differences in spike rate between the respective response window and the common reference window were calculated and divided by the reference spike count. Bars 10 mV, 1s.

At this, normalized changes in spike rate (Fig. 3) were obtained via division of the respective change in spike rate by the spike rate in the reference sample.In few cases in which combined stimulation was started earlier, reference windows shorter than 5 s or located subsequent to combined stimulation were tolerated. Occasional presentations of optic flow in the form of many patches moving together failed to cause gain modulation in cells that showed gain modulation in response to salient single-patch motion (data not shown).

Acknowledgments

This work was supported by Deutsche Forschungsgemeinschaft grants HO 950/16-3 and HO 950/23-1. The authors declare no conflict of interest. Tobias Bockhorst and Uwe Homberg conceived the research topic and wrote the paper. Tobias Bockhorst designed the stimuli and physiological experimental procedures, carried out the experiments and conceptualized as well as performed data analysis. The authors are grateful to Dr. Keram Pfeiffer for MATLAB scripts used to calculate and plot polarization patterns in Figure 1.

References

1. **B.J. Frost, H. Mouritsen**, *Curr. Opin. Neurobiol.* **16**, 481-488 (2006).
2. **K. Pfeiffer, U. Homberg**, *Annu. Rev. Entomol.* **59**, 165–184 (2014).
3. **U. Homberg, S. Heinze, K. Pfeiffer, M. Kinoshita, B. el Jundi**, *Philos. Trans. R. Soc. London Ser. B* **366**, 680-687 (2011).
4. **S. Heinze, U. Homberg**, *Science* **315**, 995-997 (2007).
5. **T. Bockhorst, U. Homberg**, *J. Neurophysiol.*, in press (doi:10.1152/jn.00742.2014)
6. **J.S. Taube**, *Annu. Rev. Neurosci.* **30**, 181-207 (2007).
7. **M. Mappes, U. Homberg**, *J. Comp. Physiol. A* **190**, 61-68 (2004).
8. **M. O'Shea, C.H.F. Rowell**, *Nature* **254**, 53-55 (1975).
9. **M. Gewecke, K. Kirschfeld, R. Feiler**, *Biol. Cybern.* **63**, 411-420 (1990).
10. **F.C. Rind, R.D. Santer, G.A.Wright**, *J. Neurophysiol.* **100**, 670-680 (2008).
11. **H. Fotowat, F. Gabbiani**, *Annu. Rev. Neurosci.* **34**, 1-19 (2011).
12. **T. Bockhorst, U. Homberg**, *PLOSBiol*. submitted
13. **P.T. Weir, B. Schnell, M.H. Dickinson**, *J. Neurophysiol.* **111**, 62-71 (2014).
14. **J.D. Seelig, V. Jayaraman**, *Nature* **503**, 262-266 (2013).
15. **J. Beshel, Y. Zhong**, *J. Neurosci.* **33**, 15693-15704 (2013).
16. **G. Liu et al.**, *Nature* **439**, 551-556 (2006).
17. **Y. Pan et al.**, *Learn. Mem.* **5**, 289-295 (2009).
18. **K. Neuser, T. Triphan, M. Mronz, B. Poeck, R. Strauss**, *Nature* **453**, 1244–1247 (2008).
19. **T.A. Ofstad, C.S. Zuker, M.B. Reiser**, *Nature* **447**, 204-207 (2011).
20. **M. Müller, U. Homberg, A. Kühn**, *Cell Tissue Res.* **288**, 159-176 (1997).
21. **H. Vitzthum, M. Müller, U. Homberg**, *J. Neurosci.* **22**, 1114-1125 (2002).
22. **S. Heinze, U. Homberg**, *J. Neurosci.* **29**, 4911-4921 (2009).
23. **A.N. Clements, T.E. May**, *J. Exp. Biol.* **60**, 673-705 (1974).
24. **T. Shimokawa, S. Shinomoto**, *Neural Comput.* **21,** 1931-1951 (2009).
25. **P. Berens**, *J. Stat. Softw.* **31** (2009).

Supplemental Information

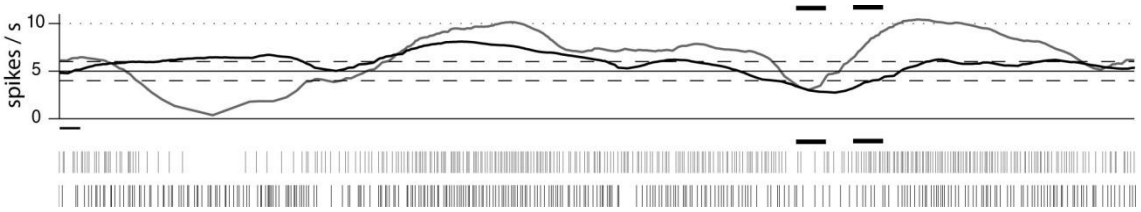

fig. S1. Responses of a CL1-neuron. CL1-cells respond prominently and phasic to an anti-preferred *E*-vector angle (grey line and raster plot) whilst presentation of an opponent angle (black line and raster plot) does not cause excitation beyond levels frequently observed in background activity (horizontal lines indicate quartiles of background activity). Traces shown here were obtained from stimulations with no directly preceding visible rotation of the *E*-vector, i.e. the polarizer was rotated to the respective position before the polarized light was switched on. This procedure was applied in piloting experiments and often resulted in an increased (apparent) latency of the response (see grey line), possibly due to an early lights-on-component. Responses to presentations of moving objects alone (not shown here) as well as to concurrent presentation of polarized light and moving objects (thick horizontal black bars) were always inhibitory and mostly confined to the first stimulus in a sequence. This corresponds to linear integration of compass- and object responses. Yet the amplitude of combined responses may co-vary with the level of directly precedent spiking. Time bar 1 s.

T. S1. Sample composition: responses to combined stimulation.

battery	# trials	# measurements	# cells
i	1	2	1
ii	12	24	2
iii	75	75	4

A total of 101 measurements of 5s peri-stimulus activity during combined stimulation were obtained from 5 cells (cell numbers in column 4 are not additive) with significant correlation between responses to combined stimulation and responses to compass-stimulation only. Stimulus batteries i-iii as well as the evaluation of combined stimulation are illustrated in Figure 5.

A P P E N D I X

ADDENDA TO CHAPTER I

Cell-type specificity of background-activity in central-complex neurons

In Chapter I, we described cell-type specific patterns of background activity (termed 'ongoing activity' in Chapter I) in locust central-complex neurons by means of recording traces and spike-count distributions (Chapter I, figure 2). These were exploited to identify cell-types in the rare cases of faint cell-staining or ambiguous labeling of more than one cell in the same preparation. Figure A1 provides some additional statistics on the rate and temporal pattern of background activity in TL2-, CL1-, TB1-, and CPU1/2-neurons. Furthermore, the profiles of action potentials (peri-spike potential profiles, PSPP) are illustrated. These may vary between recordings from the same type of neuron as they probably depend on the particular position of the recording electrode, but the examples shown here are representative for the recordings included in this thesis. Most likely, they represent the case encountered when the electrode penetrates the most easy-to-hit part of main neurites.

These simple evaluations of background activity are manageable during the recording and could be extended by tools such as comparisons between encountered distributions of a metric (e.g. spike count or inter-spike-interval) to reference templates already obtained in experiments with distinct labeling of the neuron recorded from. They hence provide a basis for morphological on-the-fly typification of a neuron recorded from, which sets the stage for a variety of novel approaches. They ease the targeted investigation of specific cell types and allow recording from several cells (of different types) in the same preparation, without depending on the use of different cell-tracers for unambiguous allocation of recordings to labeled cells.

In addition to increasing yield, the recording from several identified cells in the same preparation provides a means to identify features of neuronal activity that depend on the subject or recording condition rather than on cell type (i.e., feature that vary stronger between cells of the same type encountered in different subjects than between cells of different type encountered in the same subject), or vice versa. For instance, it would be simple and informative to investigate whether the average level of background activity tends to be collectively increased or decreased (still considering its cell-type specific range) in cells that were encountered in the same preparation, across a relatively small period (30-60 mins). This would support the idea of prolonged network-states that could modulate neuronal responses to certain stimuli as a function of internal states of the subject, such as satiation or an urge to migrate.

Detailed knowledge of properties of background activity will also promote the quantitative modeling of activity in the compass network of the locust central complex, on the basis of the refined wiring scheme we introduced in Chapter I and referenced to explain phenomena reported in Chapter III.

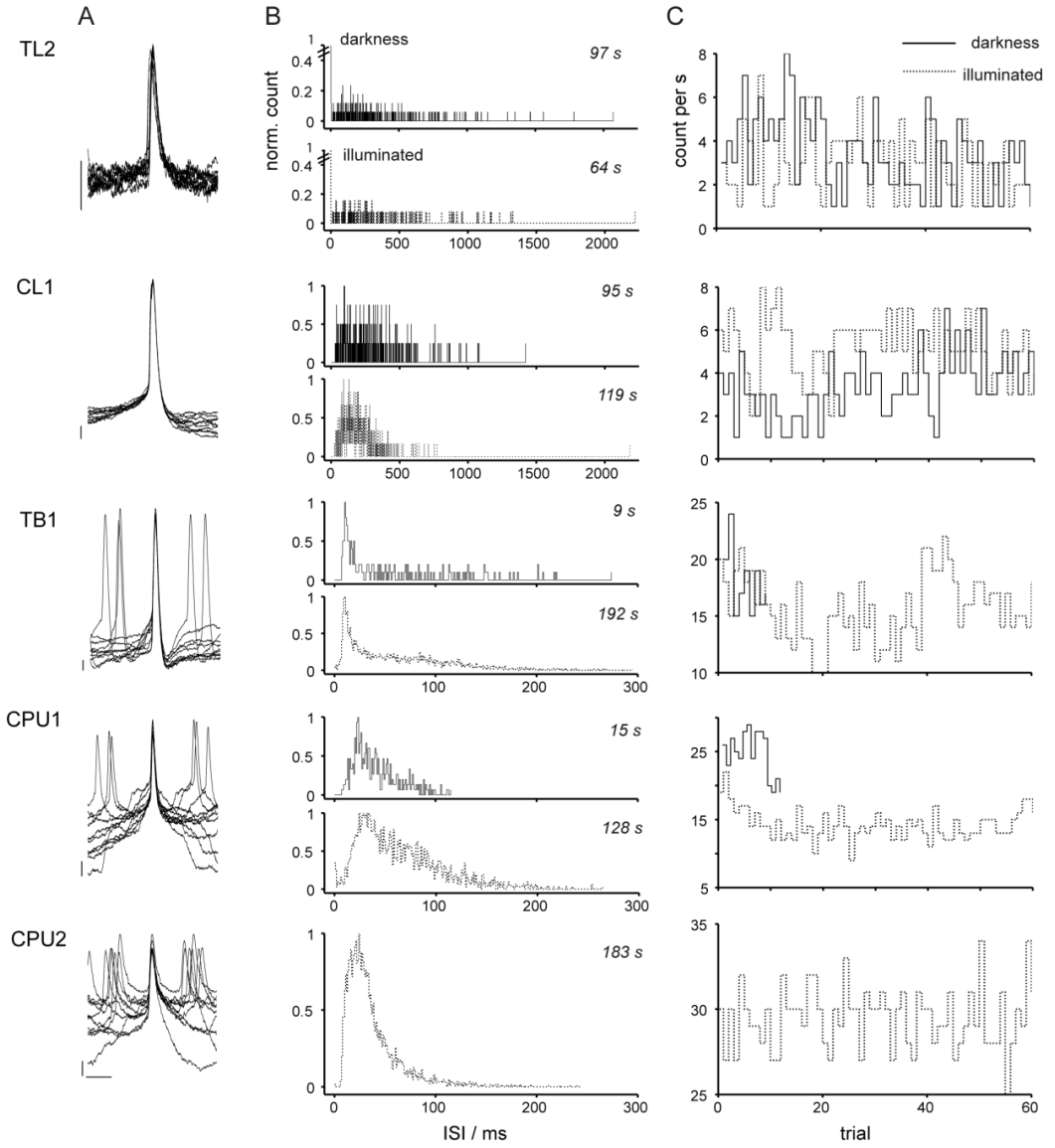

Fig. A1. Further features of background activity in central-complex neurons. ***A*** and ***B*** illustrate features of background activity that were used as additional hints to identify a recorded cell type in the rare case of ambiguous staining. ***A*** 50 ms peri-spike potential profiles (PSPP), i.e., superimposed plots of 50ms membrane potential waveforms, centered to the peaks of ten randomly selected action potentials. Bars 2 mV, 10 ms. In particular, these profiles illustrate the (ir-) regularity of subthreshold activity. As electrode impedances and placement for recordings from a respective cell type were quite comparable, even the gross amplitude of action potentials could provide an additional cue (low in TL, intermediate in CPU- and high in CL- and TB-cells). Note that profiles of the ´triggering´ spike in the center are more blurred in the TL-neuron and in the two CPU-cells than in CL- and TB-cells. This might reflect that spikes in these types of neuron occasionally occur as 'doublets' with two peaks very close in time. ***B*** Normalized inter-spike interval histograms (ISIHs) of background activity recorded in darkness (upper subplots; not available for the CPU2-cell included here) and under wide-field illumination by the CRT display in the recording setup ('illuminated'). The sample duration in seconds is shown in italics. As for the TL-cell shown here, a peak near zero ms probably reflects the spike-doublets mentioned above (y-axis truncated; the absolute counts amounted to 17 and 13 in darkness and under wide-field illumination, respectively). Both conditions provided very similar distributions, indicating that the background activity does not merely represent the ambient light level (mind the difference in sampling sizes of both conditions in TB and CPU1). ISIHs of TL- and CL-cells were marked by relatively wide ranges and less distinct clustering as compared to TB- and CPU-cells. While concentrations around short intra-burst-intervals produce a prominent peak in the

ISIH of TB-neurons, those of CPU-cells often have a tendency towards bimodality which might trace back to the alternation between brief states of increased and decreased firing. Data shown here were obtained from the same cells included in Fig. 2A of Chapter I (CPU2: less sensitive cell, lowermost trace in Chapter I, Fig. 2A). To allocate recorded background activity to a particular of several labeled cells, PSPPs and normalized ISIHs were compared to reference patterns obtained from prolonged periods of background activity in preparations with strong and distinct labeling of a single cell. ***C*** Binned (1s) spike counts measured scattered throughout the course of a respective experiment. Where available, counts from background activity recorded in darkness (solid lines) were added to the plot of counts from 60 measurements under wide-field-illumination (dashed lines). As expected from the ISIHs, spike rates under both conditions are comparable, with a possible trend towards slightly increased activity of the CPU1-cell in darkness.

Methodological considerations on the interpretation of the novel response measures

In Chapter I, we have characterized *E*-vector responses with measures of correlational strength (CS, quantified by R^2) and vector strength (VS, quantified by |r|) and proposed the following framework for application of these novel response measures: (I) the criterion for principle responsiveness to *E*-vectors is the statistical *significance* of the correlation between spiking and *E*-vector angle (the p-value of R^2 at α=0.05 and β=0.2), (II) correlational *strength* (CS, the particular *size* of the effect of *E*-vector on spike rate as quantified by R^2) may be particularly helpful to characterize variable correlation strength of higher-stage responses and (III) vector strength (VS, quantified by |r|, the length of the mean resultant spike angle vector) can reflect (IIIa) tuning sharpness within polarotopic input channels or (IIIb) the amplitude modulation of higher-stage responses by states of superimposed background activity, respectively.

In the following, the methodological discussion in Chapter I will be extended by some illustrations and results from tests with artificial data. In addition, an alternative measure of response amplitude suggested by Labhart (1996) is discussed.

Vector strength and response amplitude. The rationale for which we refer to VS as an *indirect* measure of modulation depth (h) rather than to calculate h directly (as the ratio of modulation amplitude to carrier amplitude) is that estimating a 'carrier amplitude' for the *E*-vector-response from activity during rotation of the polarizer is not trivial, albeit the recent results show that one might approximate it in higher-stage neurons by the overall mean or the spike rate at a rather 'neutral' angle such as Φ_{max}. +/- 45°. However, simply referencing a 'mean background activity' observed in-between stimulations is misleading considering the dynamics of background activity in higher-stage polarization-plane sensitive neurons. Besides, measures of amplitude modulation depth such as h are conceptually linked to modulations with ´symmetrical´ (e.g. sinusoidal) dynamics while higher-stage responses to a rotating polarizer may exhibit pronounced asymmetry in spike-rate modulation as observed in rotation-direction specific responses of CPU2-neurons.

An alternative measure of response amplitude: Labhart's R. Labhart (1996) suggested a measure of response strength to compare the performance of polarization-plane sensitive interneurons in the cricket at different degrees of polarization. This measure, denoted (Labhart's) *R* has since been applied in various studies, where analyzes were typically confined to pronounced responses with a significant value of the Rayleigh-statistic (see SYNOPSIS, Chapter I).

To obtain *R*, spike counts of the activity during a full rotation of a polarizer are binned (18 adjacent, non-overlapping bins; bin width hence corresponding to 20° change in polarizer orientation). Then, the sum of the 18 absolute differences between these spike counts and their mean is calculated. Labhart considered the resultant *R*-value a *„(…)measure of the amplitude of spike frequency modulation during a 360 ° e-vector rotation"*. Yet, this is exactly what *R* alone does *not* provide if modulation depth is to be measured *relative to the amplitude of the ´carrier signal´* (the mean spike frequency during polarizer rotation), as usual by convention (see above subsection). *R* alone quantifies some kind of *absolute* modulation amplitude while being blind to relative modulation depth, i.e. not taking into account the relation (ratio) to background firing rate, an entity probably relevant to neural coding.

To better assess coding strength, Labhart tested for statistically significance difference between a respective *R*-value and a reference value R_0, obtained from a section of background activity that directly preceded the stimulation. This was considered to identify cases with "significant e-vector-evoked modulation of spike frequency". Yet, Labhart states that *„(...) even with a response value R that significantly exceeds the baseline value R_0, the e-vector response function may be too noisy for coding useful directional information*" and suggests that coding reliability be quantified by the scatter of preferred *E*-vector angles observed in repeated stimulation. This however requires a huge number of repetitions to provide a statistically relevant measure of scatter – especially in the light of the direction-of-rotation dependency of the preferred *E*-vector angle (Φ_{max}) which we report in Chapter I.

Moreover, I suggest that statistical significance of a difference in mean values of absolute modulation amplitude (or, likewise, the ratio of Labhart's *R* to Labhart's R_0) should not be considered an adequate criterion of coding strength here. Instead, the measure of correlation strength should be used – in particular, as the size of Labhart's *R* does not reflect whether the change in spike is linked to the 180° periodicity of *E*- vector angles.

Besides, the numerical value of Labhart's *R* can vary between 0 and any upper value corresponding to the highest spike frequency measured. This complicates the interpretation of differences between *R*-values obtained from different types of neuron differing in their ranges of spiking frequency.

In sum, these aspects motivated me to conceptualize the novel method of response analysis to provide a means to rate responsiveness and response amplitude independently as well as in ways better suited to reflect physiologically relevant features and to ease comparisons.

Validation of the correlation analysis. The physiological significance of correlation analyzes for the identification of stimulus-responses is undisputed. Still, it remains crucial to assure that a respective measure behaves is a manner suited to prevent false positives (i.e., reports of a response were there actually is none) as well as false negatives (i.e. the failure to detect an actually existing response).

Figure A2 shows responses of a CPU1-cell to clockwise (0° to 360°) and counterclockwise rotation of a polarizer. Visual inspection of the recording traces (Fig. A2*A*) reveals a 180° periodicity in both; yet the response to clockwise rotation is less pronounced and as rated from the circular spike-count histograms (Fig. A2*B*) biased by additional, most likely *E*-vector unrelated activity peaks around 0° (180°). Here, the Rayleigh-based classification produced a false negative, rejecting the biased but evident response. The novel, correlation-based approach succeeds to detect the responsiveness to *E*-vector angle. Numerical values of the relevant test statistics are provided in Table A1.

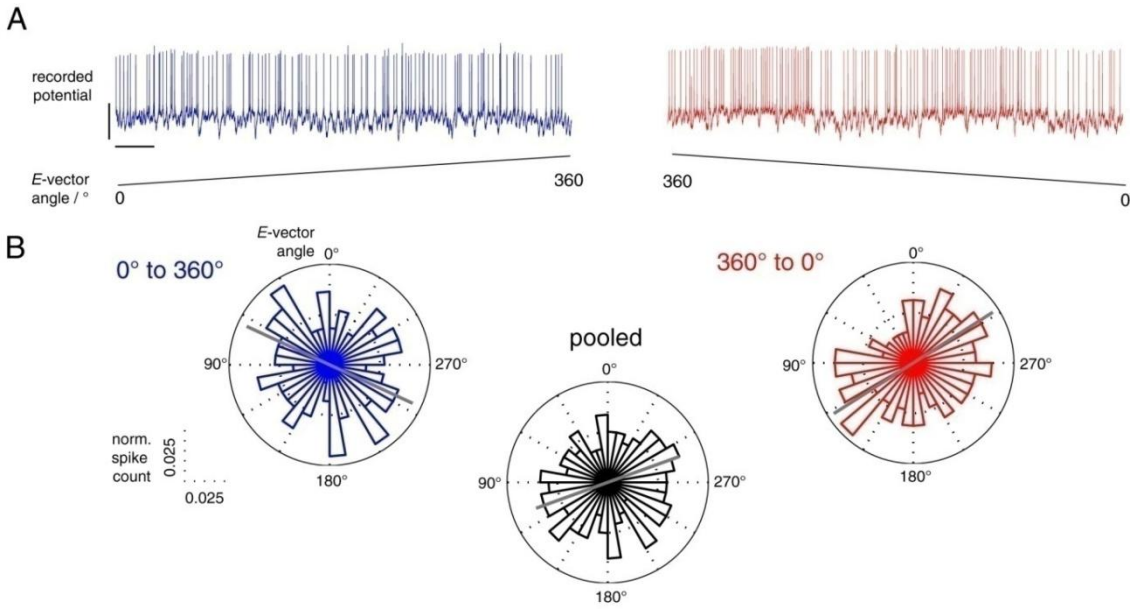

Fig. A2. Correlation analysis surpasses Rayleigh-based distribution tests in detecting noisy responses. ***A*** Intracellularly recorded spiking responses of a CPU1-cell to clockwise (0° to 360°, blue trace) and counterclockwise (360° to 0°, red trace) rotation of a polarizer. Both bear a 180° periodicity as expected for *E*-vector related responses to a full rotation of a polarizer. Yet, the response to clockwise rotation is less coherent, in particular due to some spikes 'missing' in the excitatory part and other spikes 'reducing' the inhibitory component. Bars, 10 mV, 1 s. ***B*** Circular 'peri-stimulus time histograms' illustrate the directional tuning of the individual responses (blue, red) and the pooled data. Grey axes indicate the mean spike-angles, i.e. the two direction-of-rotation specific Φ_{max}-values and the direction-averaged one, respectively. While the Rayleigh test yields no significant deviation from a uniform circular distribution except for the more pronounced counterclockwise response, the correlation analysis reveals *E*-vector angle related spiking in all three cases. See Table A1 for numerical data.

T. A1. Circular statistics of the responses to polarizer-rotation shown in Figure A2.

statistic	response, clockwise rotation (0° to 360°)	pooled data (direction-averaged)	response, counter-clockwise rotation (360° to 0°)
Φ_{max}	65°	110°	122°
VS (|r|)	0.082	0.08	0.165
Rayleigh-*p*	0.479	0.213	**0.03**
Correlation-*p*	**0.038**	**<< 0.0001**	**<< 0.0001**
CS (R^2)	0.43	0.75	0.85

Preferred angles differ substantially between directions of rotation. The lower amplitude of the response to clockwise rotation is reflected in the smaller value of |r|. While the Rayleigh test (Rayleigh-*p*) yields no significant deviation from a uniform circular distribution except for the more pronounced counterclockwise response, the correlation analysis (Correlation-*p*) reveals *E*-vector angle related spiking in all three cases. Even for the response to clockwise rotation, the associated effect size (R^2) is high, explaining 43% of the observed variability.

To explore the validity of the analysis in a systematical manner, several test signals were designed (using MATLAB) to simulate 'responses' to a rotating polarizer that either lack any periodicity or have a 'false' (other than 180°)

period. In addition, the effect of non-sine² response functions on the test statistic was explored to address saw tooth-like courses of responses with pronounced anticipation of the preferred angle. The correlation analysis passed these tests (Fig. A3), correctly rejecting random noise and a false periodicity while correctly recognizing both a noisy response as well as saw-tooth shaped response courses with 'correct' periodicities. In case of the latter, the calculated size of the correlation (R^2) was higher for a peak-to-peak period of 180° (Fig. A3C) as opposed to 90° and 270° (Fig. A3C').

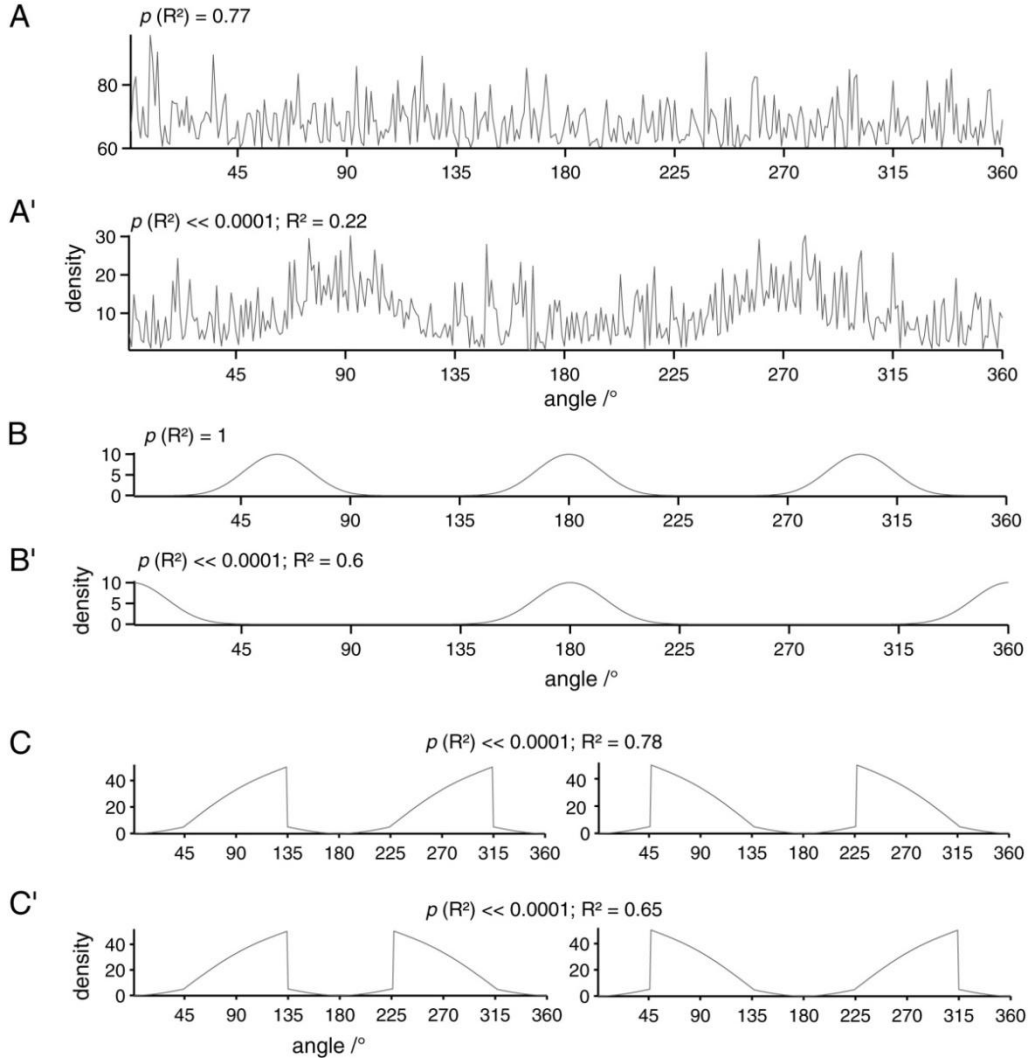

Fig. A3. Exploration of test validity by means of simulated responses to polarizer-rotation. ***A-C'*** show signals designed to mimic the instantaneous rate of spiking activity during a full rotation of a polarizer. Here, *angle* corresponds to *E*-vector angle (orientation of the polarizer) and *density* is analogous to the spike rate. To explore the validity of the novel approach, these signals were used as input for the linear-circular correlation analysis to see if they are correctly rejected or recognized as 'correct responses' respectively. For each case, R^2 and $p(R^2)$ denote the value of the coefficient of determination, R^2, and its associated *p*-value. Hence, $p(R^2)<0.05$ identifies those cases with significant correlation between 'spike rate' and '*E*-vector angle' and R^2 indicates the strength of the association. ***A*** noise (correctly rejected), ***A'*** noisy sine² (correctly recognized), ***B*** sine²-like, false period (correctly rejected); ***B'*** sine²-like (correctly recognized), ***C*** saw-tooth shape, 180° peak-to-peak period (correctly recognized) ***C'*** saw-tooth shape, peak-to-peak period of 90° / 270° (correctly recognized). Note that for the saw-tooth profiles, R^2 is reduced in the mirror-symmetric case that concurs with a peak-to-peak period other than 180°.

Dependency of correlation strength and vector strength on physiologically relevant parameters. While the statistical interpretation of R^2 and |r| alone is straight, their numerical relation is not trivial (see within-experiment plots in Figure 7 of Chapter I) and their respective relevance may depend on physiological concepts. For instance, a perfect correlation between spiking and *E*-vector angle (R^2=1) may concur with minimum modulation in spike rate (|r|<<1). Which of them is considered more relevant may depend on the respective network stage: narrow but steep tuning may be beneficial for polarotopic input channels, while output neurons should encode the entire range of the compass directions (0° - 180° in *E*-vector angle) via enhanced correlation between spike rate and *E*-vector angle (a decrease in modulation depth may then be compensated for via lateral inhibition between downstream neurons, which could cancel out the *E*-vector-uncorrelated 'amplitude offset' of the response).

The following subsection describes in which ways values of R^2 (the coefficient of determination, quantifying correlation strength and not to be confused with a square of Labhart's measure) and |r| (quantifying vector strength) depend on physiologically relevant properties of a modified sine² input-signal that mimics the instantaneous spike rate of a response to polarizer rotation. Here, the peak width of the signal, its absolute modulation depth and constant amplitude offset are considered analogous to tuning width (dynamic range), tuning slope and the level of persistent background activity, respectively. Explorations of how R^2 and |r| 'respond' to variation of these parameters are shown in Figure A4.

An increase in |r| does not necessitate an increase in R^2 and may well concur with a *decrease* in it. This can be retraced when varying the ´peak width´ of a sine^(2*n) signal (n Ɛ **N**) that models spike rate while observing |r| and R^2 (Fig. A4A-A''). Importantly, this type of signal is indeed suited to model *E*-vector signaling in many cases, particularly upstream to the central complex, as well as in higher-stage responses in which spike rates near Φ_{min} readily approach zero. With increasing n, the signal becomes more peaky which is reflected by an increase in |r| as probability density accumulates more ´tightly´ around Φ_{max} (while modulation depth remains constant, which also results in steeper tuning). Concurrently, R^2 decreases as the ´spike rate´ mimicked by the more peaky signal is constant over a wider range of *E*-vector angles.

If solely the peak amplitude ('response amplitude') increases but the dynamic range is kept constant, |r| increases while R^2 does not vary (Fig. A4B-B''). If different levels of uncorrelated, constant amplitude offsets are superimposed on the same artificial spike-rate signal (i.e., if its ´carrier amplitude´ is varied while its absolute modulation amplitude, peak width and period remain unchanged), |r| behaves positively related to relative modulation depth, while R^2 does not change (Fig. A4C-C'').

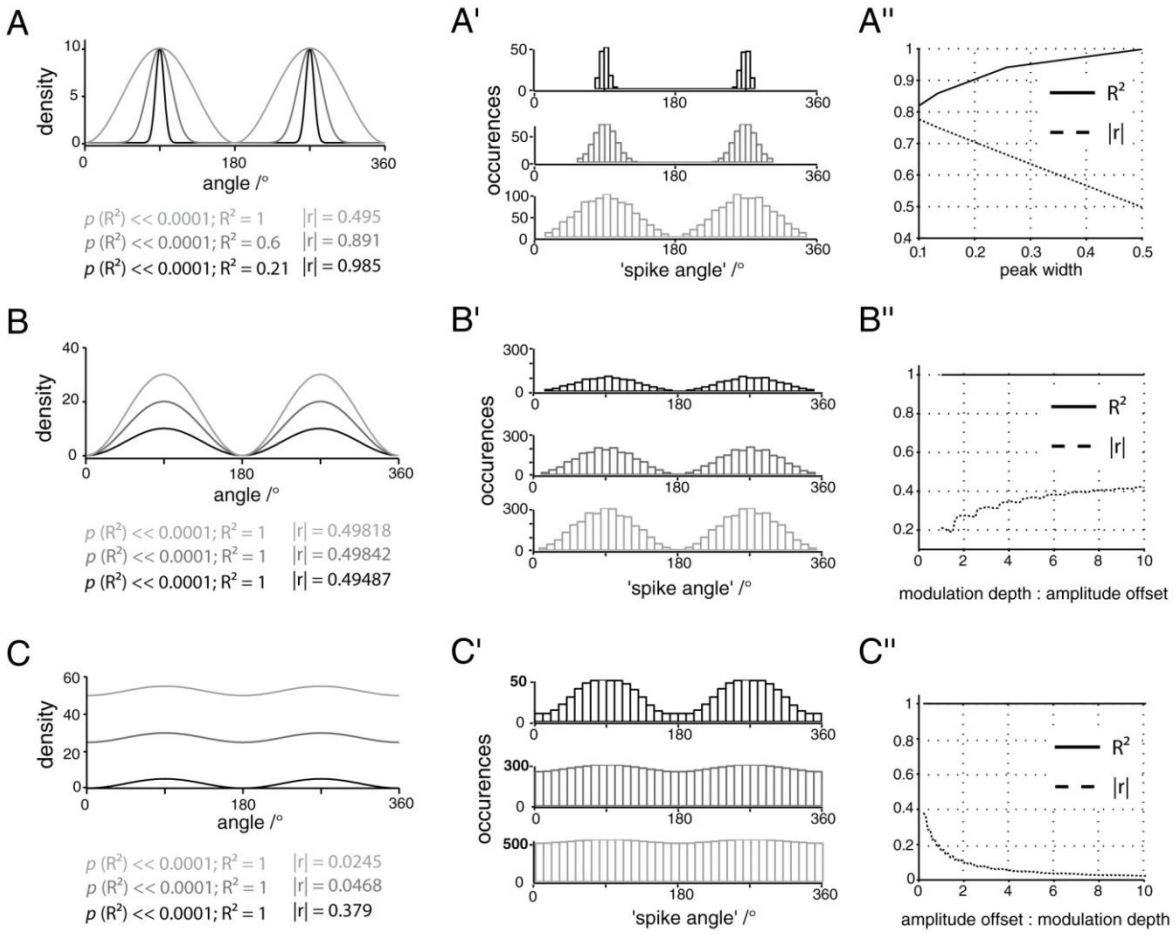

Fig. A4. Dependency of R^2 and |r| on features of simulated responses to polarizer-rotation. ***A,B,C*** plots of simulated responses to polarizer rotation with associated values of $p(R^2)$ and R^2 denoted below (see Figure A3 for further explanation). ***A',B',C'*** 'spike-count' (occurences) histograms for artificial raw data generated from the response profiles co-plotted in *A,B,C*. These were used to calculate values of |r|. ***A'',B'',C''*** R^2 and |r| as a function of the respective 'response' features varied. Peak width = (density at Φ_{max} +45°/density at Φ_{max}); modulation depth = peak-to-peak amplitude of the density (constant in C''); amplitude offset = density at 'Φ_{min}' (constant in B'').

References

Labhart T. How polarization-sensitive interneurones of crickets perform at low degrees of polarization. J Exp Bio 199: 1467-1475, 1996.

Suggested stimulation protocol for measurement of responses to polarizer rotation

Some types of neuron (e.g., CL-neurons; data not shown) respond to the increase in ambient light level that results from switching on the polarized-light stimulus. Obviously, such a stereotypical light-response would strongly affect the measurement of an *E*-vector specific response. As a result, the experimenter should wait for the *E*-vector unrelated light-response to decline before measuring responses to polarizer rotation. Yet, it is crucial to note that simply waiting before turning on polarizer-rotation will

cause a decline of the compass response as well, due to the *E*-vector specific adaptation (except in TL-cells). Hence, the measurement of responses to polarizer rotation should be performed as follows: 1.) after switching on the polarized light, wait for several (3-5) seconds until the stereotypical light-response has declined; 2.) then rotate the polarizer for the first time to break or counteract *E*-vector specific adaptation – concurrently, the residual stereotypical light-response will fade; 3.) and present subsequent polarizer-rotations in sufficiently rapid succession to prevent *E*-vector specific adaptation. When analyzing the data, make sure to exclude the response to the first polarizer-rotation.

ADDENDUM TO CHAPTER III

An extended wiring model for polarotactic sensory-motor transformation

In Chapter III, we report:

All CL1-neurons, two TB1-neurons and one CPU1-neuron showed compass-signaling and typical novelty-dependent responses to the moving object alone (…). Their responses to combined stimulation were similar to those to the moving objects alone, hence not reflecting the respective concurrent compass stimulus (…). (…) We consider this ´destructive interference´ a linear integration of the novelty-event response with a declined response to the compass-stimulus.

In the Discussion, we address this result, saying:

While gain modulation most likely promotes compass-guidance, linear integration does not necessarily have to hinder the same. Any E-vector unrelated response to object motion could be cancelled out by lateral inhibition between output channels of the compass network (i.e., neurons downstream to CPU-cells), and the same might hold for coincident background activity in the channels.

The latter is illustrated in Figure A5 by a downstream-extended version of the wiring model introduced in Chapter I. Situated between the output of the central complex and the final stage of sensory-motor transformation, this lateral inhibition could sharpen compass signaling by cancellation of noise, i.e. *E*-vector unrelated activity that is identical in both channels, be it coincident background activity or not spatially tuned, stereotypic responses to moving objects. The output is thus optimized for polarotactic steering, e.g. by controlling wing beat frequencies in flight.

In addition to this post-processing, the control of maneuvers such as turning in the 'correct' ('faster') direction towards a desired compass-bearing could rely on the direction-of-turning specificity of responses to perceived *E*-vector rotation. To find the direction of turning that aligns the animal to the desired compass course faster than the opposite direction of turning, the animal could perform rotatory scanning movements while the network 'looks at the derivative of the instantaneous spike rates´ in a pair of two particular opponently tuned channels - one of which has a Φ_{max} corresponding to the desired compass course.

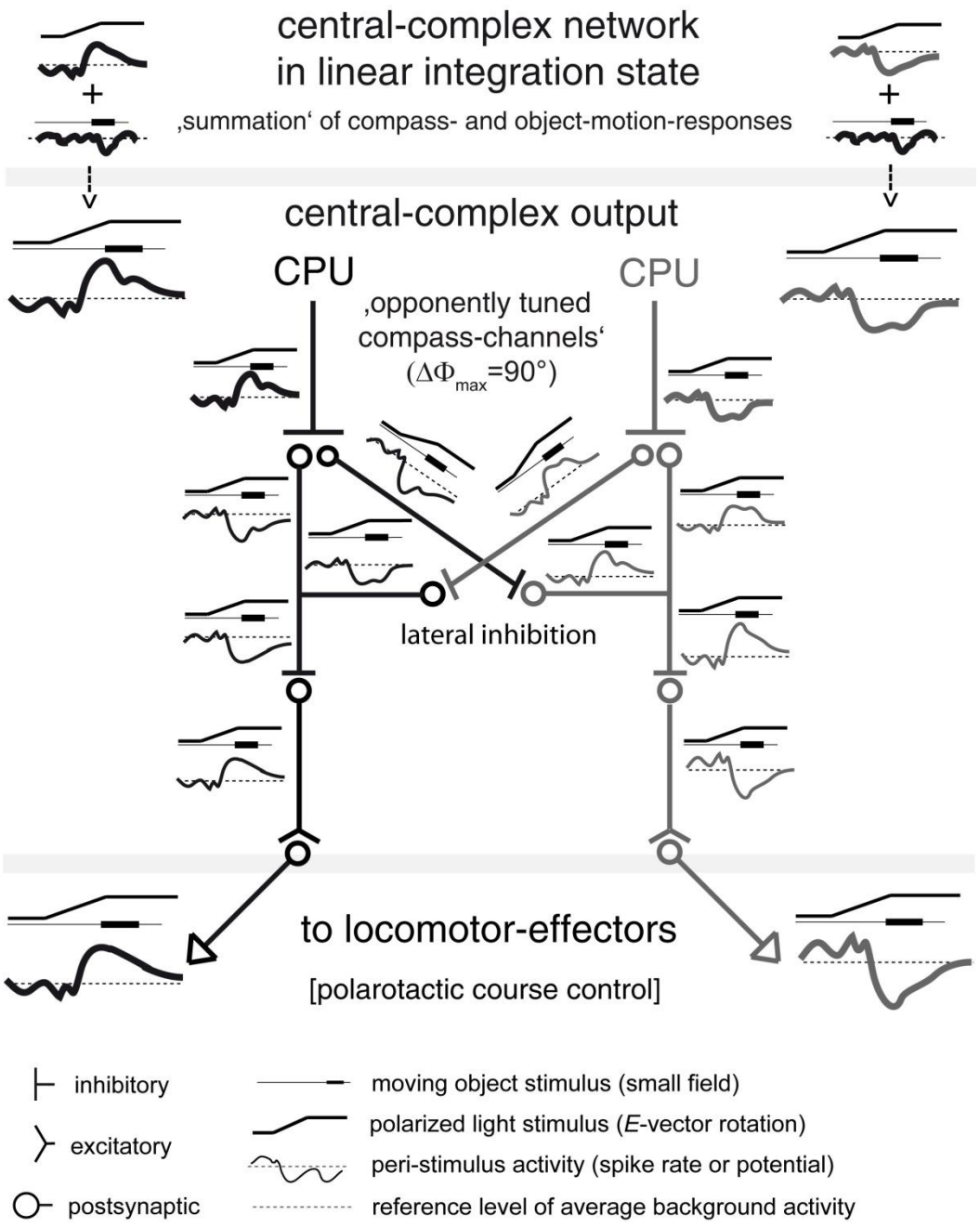

Fig. A5. A lateral-inhibition model of post-processing of central-complex output for polarotactic behavior. The model illustrates that a linear integration of responses to moving objects and to *E*-vectors by central-complex neurons does not necessarily hamper polarotactic control of turning direction. By inhibitory connections between channels tuned to opponent *E*-vector angles, each channel's *E*-vector response could be preserved and possibly even amplified, while 'destructive interference' by linearly integrated responses to object motion might get reduced.

ADDENDUM TO CHAPTERS II AND III

Responses of a TL6-neuron to virtual objects and combined stimulation

In addition to the datasets presented in Chapter II and III, the two previously undescribed polarization-sensitive neurons TLU1 and TL6 were tested for responsiveness to virtual objects and combined stimulation by the latter and polarized-light. TLU1 showed no responses to virtual objects and no effect of their presentation together with polarized light (data not shown). As illustrated in Figure A6 below, TL6 responded to small-field motion in a variable, inhibitory manner comparable to CPU-neurons (Fig. A6*C*,*D*); possibly including the breakage of region-specific adaptation by a switch in trajectory (single-trial data, Fig. A6*D*). Under combined stimulation, the cell showed the same object-motion related responses, irrespective of the concurrently presented *E*-Vector angle (Fig. A6*E*) .

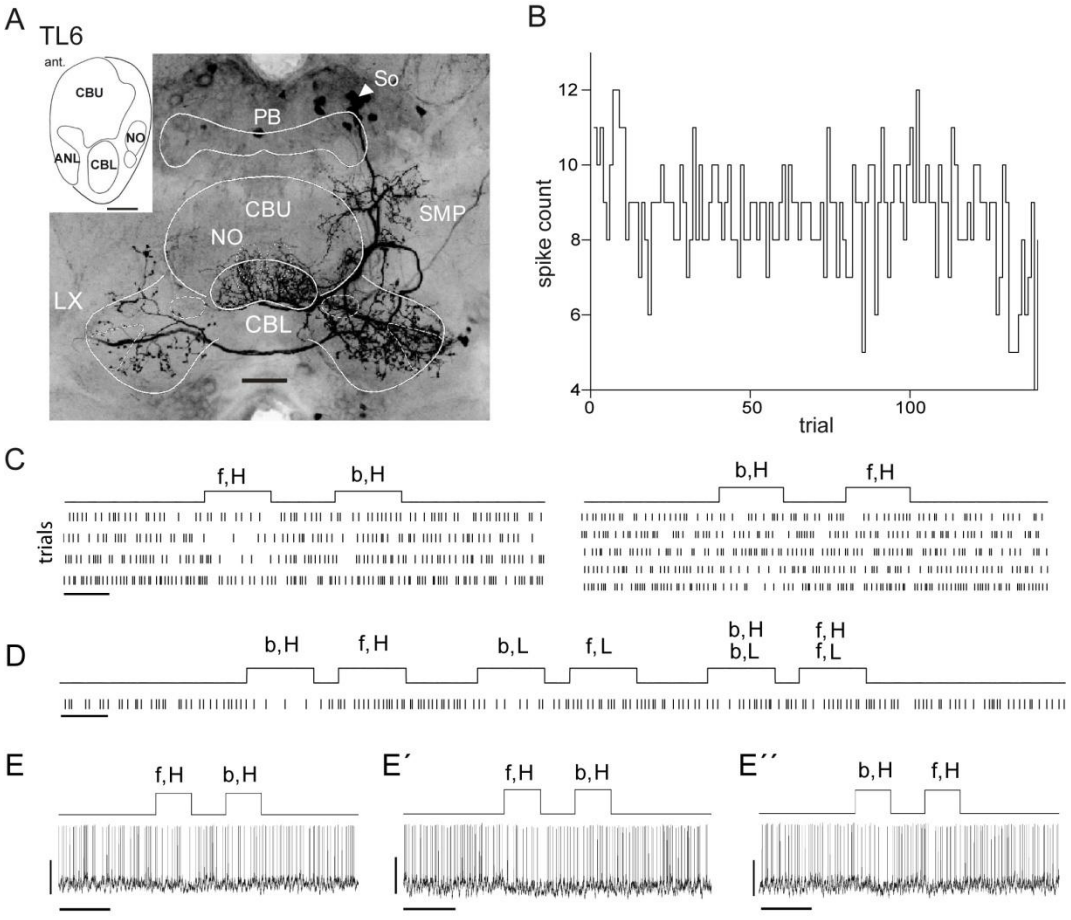

Fig. A6. Responses of a TL6-neuron to virtual objects and combined stimulation by those and polarized light. ***A*** Morphology as visualized by an inverted, frontal maximum intensity projection of confocal image stacks. So, soma; PB, protocerebral bridge; CBU (CBL), upper (lower) division of the central body; NO, noduli; LX, lateral complexes; SMP, superior medial protocerebrum. Inset shows schematic saggital view of the central complex and the anterior lip (ANL). Bars 100 µm. ***B*** Spike counts in 140 trials of background activity (1s per trial), plotted against trial number and hence the time course of the experiment, although trials were not evenly distributed over time. ***C***, ***D*** Responses to batteries of simple stimuli that include changes in direction of motion (*C*) or both changes in direction of motion and

switches of trajectory (*D*), respectively. ´f, H´ and ´b, L´ denote forward (f) and backward (b) translations (70°/s) of a small-field object along a horizontal trajectory at high (H) and low (L) elevation, respectively. For further specification of stimuli see Chapter II. ***E*-*E*´´** Responses to combined stimulation with polarized light and a moving object. The stationary *E*-Vector of the polarized light corresponds to the cell´s direction-of-rotation-averaged Φ_{max} in *E*, to an intermediate angle (Φ_{max} + 45°) in *E´* and to Φ_{min} in *E´´*. Note that TL6 responded to polarized light with stationary *E*-vector in a phasic manner and traces shown here include the adapted state of the *E*-Vector responses, which was independent from *E*-vector angle. Procedures of stimulation by visual objects and of combined stimulation as described in Chapters II and III, respectively. Bars 10 mV, 2 s. *A*, *B* reproduced from Chapter I, Figure 11.

CHARACTERIZATION AND CALIBRATION OF STIMULUS DEVICES

Polarized-light source

In case of the polarized-light stimulus, *E*-vector angle as determined by polarizer orientation was intended the only stimulus property varied; other features such as light intensity or spectral composition were required not to change – in particular not as a function of polarizer orientation.

The wide-field LED emitted a signal stable in spectral composition and intensity (Fig. A7), as measured at the position of the locust head with a digital spectrometer (USB2000, Ocean Optics Inc., FL, USA). Illumination the CRT display had no measurable effect on the spectrum when the detector head was positioned towards the polarized-light source.

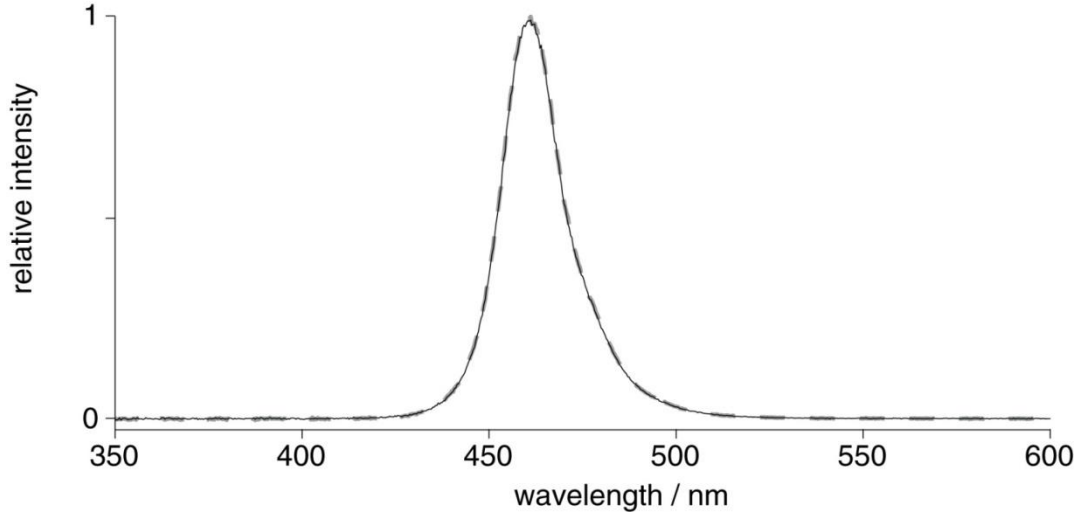

Fig. A7. Wavelength spectrum of the polarized-light stimulus. Relative intensity as a function of wavelength was measured with the CRT display set to black (black plot) and set to grey (grey plot), respectively. As both spectra are virtually congruent, unilateral wide-field illumination by the CRT appeared not to have an effect on the spectrum measured with the detector directed towards the polarizer.

To exclude any effect of polarizer rotation on the intensity of the polarized light, the absolute luminance of the signal was measured at the position of the locust's head using an OPTICAL photometer (SN 141 / 60780, Cambridge Research Systems, Rochester, Kent, UK). Surprisingly, operating the stepper motor that rotated the polarizer did have an effect in terms of a quasi-sinusoidal modulation of light intensity (Fig. A8). Yet, the modulation depth was as low as 5 cd/m², corresponding to about 1% of the luminance measured with the motor being switched off, and modulation period (about 0.4 s) was substantially lower than the periodicity of the *E*-vector (180°, corresponding to 6 s at 30°/s rotation velocity). This artifact was hence considered negligible. *E*-vector dependent reflection of polarized light at surfaces inside the Faraday booth was excluded by visual inspection.

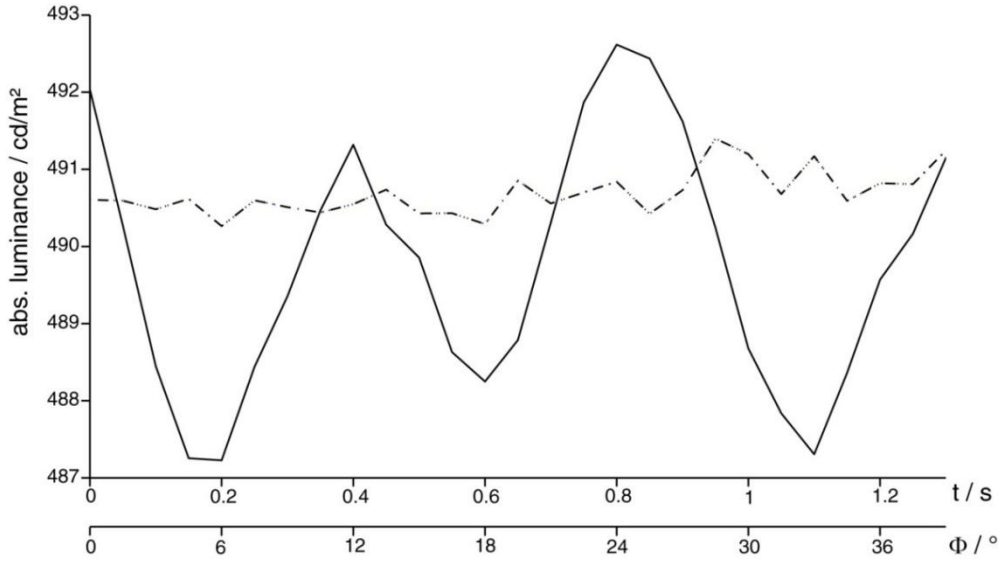

Fig. A8. Stability of the intensity of the polarized light stimulus. To assess whether the polarized-light stimulus is sufficiently stable in intensity, its absolute luminance was measured with the polarizer stationary (dashed line) and rotated at 30 degrees per second (solid line), respectively. The two X-axes indicate time since onset of rotation (t) and the corresponding orientation angle of the polarizer (Φ). The detector head was positioned where the head of the animal would be, i.e. at a distance to the light source of 15 cm.

In addition to the measures denoted above, a simple ´monopolat´ (a term suggested by Dr. Thomas Labhart in a poster contribution to the 3rd International Conference on Invertebrate Vision, Bäckaskog Castle, Sweden, August 2013) analyzer was built and positioned in the beam path of the polarized light, right ´behind´ the locust head and slightly to the side of it. This device, based on a piece of the polarizer material glued to a photoresistor, generates an output voltage that varies as a function of the *E*-vector angle. It hence provided a means to exclude possible malfunction of the stepper motor that rotated the polarizer as well as to calibrate polarizer orientation to the null direction (an *E*-vector angle congruent to the longitudinal body axis).

Cathode-ray-tube (CRT) display

Work presented in Chapter II began with an extensive screening of central-complex neurons for responsiveness to a variety of visual stimuli, including spectral composition of wide-field illumination as well as the position or movement direction of virtual objects. Photoreceptor-responses are a function of photon flux density which, for monochromatic light of a specific intensity, is linked to wavelength. As a result, spectral tuning can only be characterized by co-varying the wavelength and intensity of (nearly) monochromatic light in a manner that results in a constant photon flux density across the wavelengths used. To this end, a spectral calibration was performed using the OPTICAL photometer (SN 141 / 60780, Cambridge Research Systems, Rochester, Kent, UK) and an automated protocol embedded in the operating software of the visual stimulus device VISAGE (Cambridge Research Systems, Rochester, Kent, UK). Resultant photon flux densities for red-, green- and blue light are listed in Table T. A2. Corresponding wavelength spectra are shown in Figure A9 (measured using a digital spectrometer (USB2000, Ocean Optics ., FL, USA).

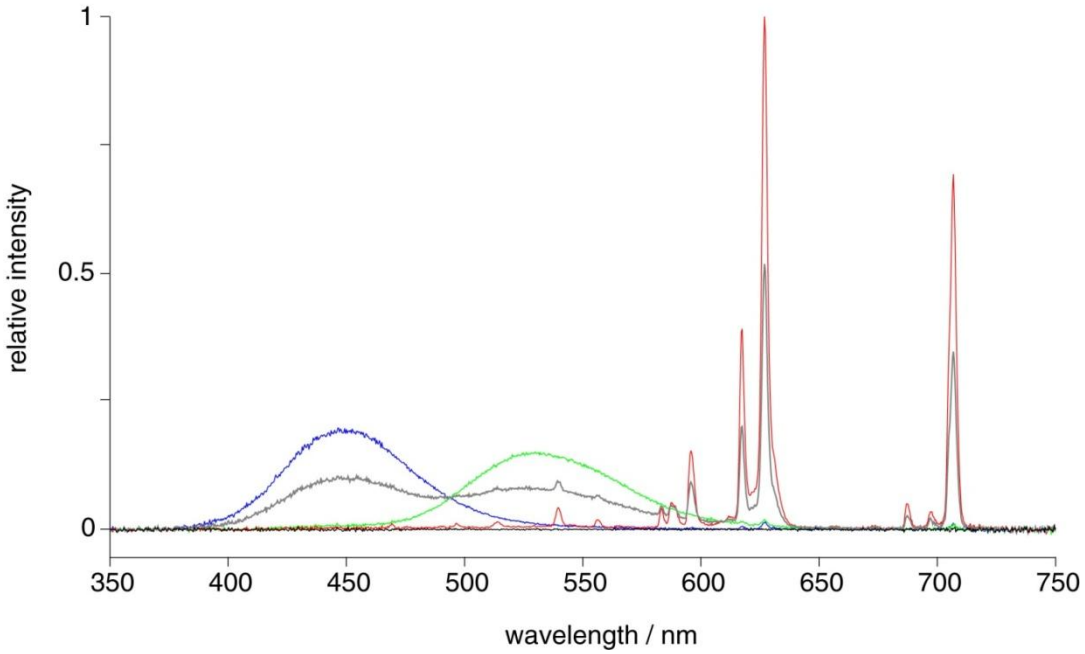

Fig. A9. Wavelength spectra of unpolarized blue, red and green light emitted by the CRT display. Each spectrum is plotted in a color corresponding to light color. Also shown are spectra measured with the CRT set to 'black' and 'grey' (plotted in black and grey).

T. A2. Ranges of photon-flux density for flashes of red-, green- and blue light after spectral calibration of the CRT display.

color	λ / nm	photon-flux / (photons * s^{-1}*cm^{-2})/ 10^13	
		minimum	maximum
red	710	7.1484	8.5781
green	520	7.5914	8.9663
blue	450	7.0226	8.1553

For each wavelength, values give the minimum (maximum) from a total of 12 measurements along a 'grid' of 12 equidistant positions spanning the CRT display (the centers of the sectors specified in the next subsection).

For measurement of tuning to object position or direction of motion, inhomogenity in luminance across the display area need to be reasonably small. Otherwise, tuning to position or to movement-direction (i.e., effectively, a sequence of object positions) cannot be distinguished from tuning to light intensity (which might occur in the same cell as well). To measure inhomogenity, the area of the CRT display (800 x 600 pixels) was divided into 12 non-overlapping sectors (200 x 200 pixels each) within which absolute luminance of a filled white patch (covering the entire sector) was measured repeatedly at three evenly spaced positions (25 measurements per position, i.e. 75 per sector and 900 measurements in total). The results are depicted in Figure A10.

In fact, sector identity had a significant ($p<0.05$; non-parametric Kruskal-Wallis one-way ANOVA for independent samples) and in several cases strong effect ($p<0.05$ and $R^2>0.25$; pairwise comparison of luminances by Wilcoxon signed-

rank tests) on luminance, indicating inhomogeneous illumination of the CRT. Across positions, luminance ranged from 82 to 98 cd/m² with a mean of 89 cd/m² (N=900; standard deviation 5 cd/m²). Though being significant and strong in statistical terms, I considered this inhomogenity acceptable for physiological measurements and simply compared the results of receptive-field mappings to the ´inhomogenity map´. In central-complex neurons, I have not observed response behaviors likely to be susceptible to or even explainable in terms of this luminance artifact.

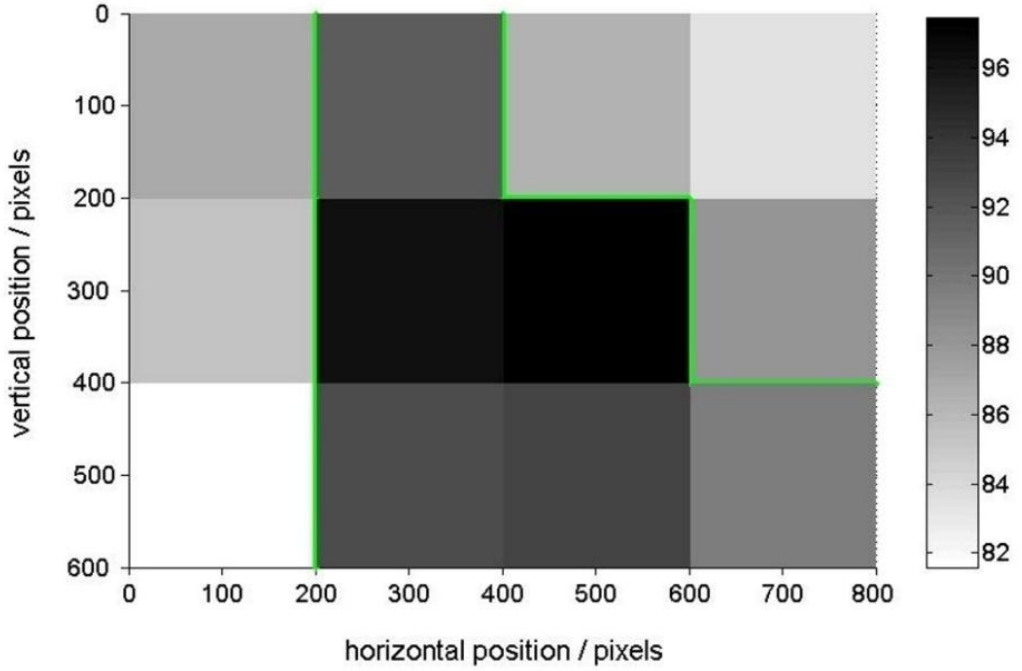

Fig. A10. Luminance map of the CRT display. Shades of grey indicate the average luminance (cd/m^2) of a white square patch (200 pixels edge length) as a function of position on the display. Each value is based on 75 measurements within the respective sector (see text). Standard deviations ranged from 0.5 to 3.1. Green line: interpolated crossing of the overall mean (89.408; N=900; overall standard deviation 5.14).

C U R R I C U L U M V I T A E

D A N K S A G U N G

V E R S I C H E R U N G

ANGABEN ZU EIGENEN BEITRÄGEN UND HILFSMITTELN

Hiermit versichere ich, Tobias Bockhorst, die vorliegende Dissertation " Novelty detection and context dependent processing of sky-compass cues in the brain of the desert locust *Schistocerca gregaria "* ("Novelty detection und die kontextabhängige Prozessierung von Himmelskompasssignalen im Gehirn der Wüstenheuschrecke *Schistocerca gregaria"*) selbstständig, ohne unerlaubte Hilfe angefertigt zu haben und mich keiner anderen als der von mir ausdrücklich bezeichneten Quellen und Hilfen bedient zu haben (siehe ERKLÄRUNG: EIGENE BEITRÄGE UND VERÖFFENTLICHTE TEILE DER ARBEIT).

Die Dissertation wurde weder in der vorliegenden noch in anderer Form an einer anderen Hochschule eingereicht und hat bisher auch keinen sonstigen Prüfungszwecken gedient.

Marburg, _____

_____

Tobias Bockhorst